frontiers | Research Topics

Modelling and numerical simulations with differential equations in mathematical biology, medicine and the environment

Edited by
Appanah Rao Appadu, Ramoshweu Solomon Lebelo, Hagos Hailu Gidey and Bilge Inan

Published in
Frontiers in Applied Mathematics and Statistics

ISSN 1664-8714
ISBN 978-2-83251-825-0
DOI 10.3389/978-2-83251-825-0

About Frontiers

Frontiers is more than just an open access publisher of scholarly articles: it is a pioneering approach to the world of academia, radically improving the way scholarly research is managed. The grand vision of Frontiers is a world where all people have an equal opportunity to seek, share and generate knowledge. Frontiers provides immediate and permanent online open access to all its publications, but this alone is not enough to realize our grand goals.

Frontiers journal series

The Frontiers journal series is a multi-tier and interdisciplinary set of open-access, online journals, promising a paradigm shift from the current review, selection and dissemination processes in academic publishing. All Frontiers journals are driven by researchers for researchers; therefore, they constitute a service to the scholarly community. At the same time, the *Frontiers journal series* operates on a revolutionary invention, the tiered publishing system, initially addressing specific communities of scholars, and gradually climbing up to broader public understanding, thus serving the interests of the lay society, too.

Dedication to quality

Each Frontiers article is a landmark of the highest quality, thanks to genuinely collaborative interactions between authors and review editors, who include some of the world's best academicians. Research must be certified by peers before entering a stream of knowledge that may eventually reach the public - and shape society; therefore, Frontiers only applies the most rigorous and unbiased reviews. Frontiers revolutionizes research publishing by freely delivering the most outstanding research, evaluated with no bias from both the academic and social point of view. By applying the most advanced information technologies, Frontiers is catapulting scholarly publishing into a new generation.

What are Frontiers Research Topics?

Frontiers Research Topics are very popular trademarks of the *Frontiers journals series*: they are collections of at least ten articles, all centered on a particular subject. With their unique mix of varied contributions from Original Research to Review Articles, Frontiers Research Topics unify the most influential researchers, the latest key findings and historical advances in a hot research area.

Find out more on how to host your own Frontiers Research Topic or contribute to one as an author by contacting the Frontiers editorial office: frontiersin.org/about/contact

Modelling and numerical simulations with differential equations in mathematical biology, medicine and the environment

Topic editors

Appanah Rao Appadu — Nelson Mandela University, South Africa
Ramoshweu Solomon Lebelo — Vaal University of Technology, South Africa
Hagos Hailu Gidey — Botswana International University of Science and Technology, Botswana
Bilge Inan — Iskenderun Technical University, Türkiye

Citation

Appadu, A. R., Lebelo, R. S., Gidey, H. H., Inan, B., eds. (2023). *Modelling and numerical simulations with differential equations in mathematical biology, medicine and the environment*. Lausanne: Frontiers Media SA.
doi: 10.3389/978-2-83251-825-0

Table of contents

frontiers | Frontiers in Applied Mathematics and Statistics

TYPE Editorial
PUBLISHED 20 February 2023
DOI 10.3389/fams.2023.1150552

OPEN ACCESS

EDITED AND REVIEWED BY
Raluca Eftimie,
University of Franche-Comté, France

*CORRESPONDENCE
Appanah R. Appadu
✉ Rao.Appadu@mandela.ac.za

SPECIALTY SECTION
This article was submitted to Mathematical Biology, a section of the journal Frontiers in Applied Mathematics and Statistics

RECEIVED 24 January 2023
ACCEPTED 31 January 2023
PUBLISHED 20 February 2023

CITATION
Appadu AR, Lebelo RS, Gidey HH and Inan B (2023) Editorial: Modeling and numerical simulations with differential equations in mathematical biology, medicine, and the environment.
Front. Appl. Math. Stat. 9:1150552.
doi: 10.3389/fams.2023.1150552

Editorial: Modeling and numerical simulations with differential equations in mathematical biology, medicine, and the environment

Appanah R. Appadu[1]*, Ramoshweu S. Lebelo[2], Hagos H. Gidey[3] and Bilge Inan[4]

[1]Department of Mathematics and Applied Mathematics, Nelson Mandela University, Gqeberha, South Africa, [2]Education Department, Faculty of Human Sciences, Vaal University of Technology, Vanderbiljpark, South Africa, [3]Department of Mathematics and Statistical Sciences, Faculty of Sciences, Botswana International University of Science and Technology, Palapye, Botswana, [4]Engineering Basic Sciences, Iskenderun Technical University, Iskenderun, Hatay, Türkiye

KEYWORDS

modeling, differential equations, mathematical biology, medicine, environment, simulation

Editorial on the Research Topic
Modeling and numerical simulations with differential equations in mathematical biology, medicine, and the environment

The main objective of this Research Topic has been to bring academics, engineers, researchers and scientists to share recent ideas, methods, trends, problems and solutions in mathematical biology, medicine and the environment. There were four topic editors and the issue was open from August 2021 to May 2022 with a further extension of 6 months until November 2022 to submit papers. Fifteen papers were submitted, out of which ten were accepted and published. A total of 22 authors contributed papers in that Research Topic.

Manuscripts in this Research Topic were requested through a general call on the website https://www.frontiersin.org/research-topics/25070/modeling-and-numerical-simulations-with-differential-equations-in-mathematical-biology-medicine-and and invitation was sent by email to about 200 academics. All submissions were subjected to rigorous peer-review process following the well-known policies and standards of Frontiers in Applied Mathematics and Statistics. Every submission was reviewed by two or three experts in the field.

In the following paragraphs, we give a short summary of the 10 published papers in that Research Topic.

Appadu and Tijani obtain the numerical solution of a 1D generalized Burgers-Huxley equation under specified initial and boundary conditions using Forward Time Central Space and a non-standard finite difference scheme. There are two proposed solutions and they show that only one is correct. Error analysis and convergence tests are performed.

Attia (A) models the progression of the non-alcoholic fatty liver disease (NAFLD) process by continuous time Markov chains with nine states. Maximum likelihood is used to estimate the transition intensities among the states.

Mhlanga and Rundora look at the existence and uniqueness of strong solutions to the Cauchy problem of stochastic equations. Sufficient and necessary conditions for existence

of a global positive solution of non-homogeneous stochastic differential equations with a non-Lipschitzian diffusion coefficient are obtained.

Oukouomi Noutchie et al. extends on the work of Jia and Qin on sexually transmitted disease models with a novel class of non-linear incidence. The existence, uniqueness, boundedness and positivity of solutions are established.

Kehinde et al. solve a two-dimensional semilinear singularly perturbed convection-diffusion problem. The approach requires linearization of the continuous semilinear problem using quasi linearization technique and nonstandard finite difference methods. Convergence tests are performed.

Kinyili et al. address the question of whether to drop or to continue wearing face masks especially after being vaccinated among the public. A deterministic mathematical model that takes into account vaccination program and wearing of face masks as intervention strategies is developed for COVID-19.

Attia (B) looks at the deleterious effects of obesity type II diabetes and insulin resistance, systolic and diastolic hypertension on the rate of progression of fibrosis in patients with non-alcoholic fatty liver disease (NAFLD).

Agbavon et al. obtain numerical solution for Fisher's equation using a numerical experiment with three different cases. The three cases correspond to different coefficients for the reaction term. The three methods are Forward Time Central Space, nonstandard and explicit exponential finite difference schemes. They determine if the optimal time step size is influenced by choice of the numerical methods or the coefficient of reaction term. Convergence tests are performed.

Anwar et al. construct mathematical model to understand viral dynamics within plants. They analyse the dynamics of two models of virus transmission in plants.

Kwofie et al. formulate a mathematical model to study crime dynamics and incorporate educational programs as a tool to assess the population-level impact on the spread of crime. The least square method is used.

Author contributions

All authors listed have made a substantial, direct, and intellectual contribution to the work and approved it for publication.

Funding

ARA is grateful to Nelson Mandela University which enabled the work to be done.

Acknowledgments

The guest-editors for this Research Topic would like to appreciate and thank the editorial technical team for their guidance and support rendered throughout the session.

Conflict of interest

The authors declare that the research was conducted in the absence of any commercial or financial relationships that could be construed as a potential conflict of interest.

Publisher's note

frontiers in Applied Mathematics and Statistics

REVIEW
published: 14 January 2022
doi: 10.3389/fams.2021.773733

1D Generalised Burgers-Huxley: Proposed Solutions Revisited and Numerical Solution Using FTCS and NSFD Methods

Appanah R. Appadu and Yusuf O. Tijani*

Department of Mathematics and Applied Mathematics, Nelson Mandela University, Gqeberha, South Africa

In this paper, we obtain the numerical solution of a 1-D generalised Burgers-Huxley equation under specified initial and boundary conditions, considered in three different regimes. The methods are Forward Time Central Space (FTCS) and a non-standard finite difference scheme (NSFD). We showed the schemes satisfy the generic requirements of the finite difference method in solving a particular problem. There are two proposed solutions for this problem and we show that one of the proposed solutions contains a minor error. We present results using FTCS, NSFD, and exact solution as well as show how the profiles differ when the two proposed solutions are used. In this problem, the boundary conditions are obtained from the proposed solutions. Error analysis and convergence tests are performed.

Keywords: Burgers-Huxley equation, three different regimes, FTCS, NSFD, proposed solutions, error analysis, convergence tests

OPEN ACCESS

Edited by:
Daihai He,
Hong Kong Polytechnic University,
Hong Kong SAR, China

Reviewed by:
Paola Lecca,
Free University of Bozen-Bolzano, Italy
Agisilaos Athanasoulis,
University of Dundee, United Kingdom

****Correspondence:***
Appanah R. Appadu
rao.appadu@mandela.ac.za;
rao.appadu31@gmail.com

Specialty section:
This article was submitted to Mathematical Biology, a section of the journal Frontiers in Applied Mathematics and Statistics

Received: *10 September 2021*
Accepted: *06 December 2021*
Published: *14 January 2022*

Citation:
Appadu AR and Tijani YO (2022) 1D Generalised Burgers-Huxley: Proposed Solutions Revisited and Numerical Solution Using FTCS and NSFD Methods. Front. Appl. Math. Stat. 7:773733. doi: 10.3389/fams.2021.773733

1. INTRODUCTION

The study of nonlinear partial differential equation continues to fascinate many researchers due to their ubiquitous application in every area of science and technology. Because of their complexity, many of these nonlinear partial differential equations do not always have explicit solutions using a known finite combination of elementary functions [1]. Some non linear partial differential equations, on the other hand, become integrable following a symbolic transformation. The analytical solution becomes available in this instance. Some analyses of most numerical and semi-analytical methods are studied using the heat equation. The linearity of this differential equation makes it a test case for many problems, it takes the form

$$\frac{\partial u}{\partial t} = D\frac{\partial^2 u}{\partial x^2}\,, \tag{1}$$

where D is the diffusivity term or coefficient of diffusion. Burgers [2] while studying turbulence in flow resulted in the investigation of a non linear partial differential equation that contains an advective term in addition to the diffusion term and it may be regarded as a prototype in the theory of nonlinear diffusive waves. The equation takes the form

$$\frac{\partial u}{\partial t} = -\alpha u\frac{\partial u}{\partial x} + D\frac{\partial^2 u}{\partial x^2}\,. \tag{2}$$

Many approximate solutions have been documented for Equation (2) subject to different initial and boundary conditions, we mention the works of Abazari and Borhanifar [3] and Mukundan and Awasthi [4].

The FitzHugh-Nagumo model is a well-known reaction-diffusion system proposed by Hodgkin and Huxley [5] for the conduction of electrical impulses through a nerve fibre. A decade later, FitzHugh [6] and Nagumo et al. [7] solved the challenge by reducing the original four-variable system to a simplified model with only two variables. The differential equation is expressed as

$$\frac{\partial u}{\partial t} = D\frac{\partial^2 u}{\partial x^2} + \beta u\,(1-u)\,(u-\gamma)\,. \tag{3}$$

The Newell-Whitehead-Segel equation is applicable in nonlinear systems that describe the emergence of stripe patterns. This equation, on the other hand, is used as a mathematical model in a variety of systems, including Rayleigh-Benard convection, chemical reactions, and Faraday instability, and is given by

$$\frac{\partial u}{\partial t} = D\frac{\partial^2 u}{\partial x^2} + \beta u\,(1-u)\,(u+1)\,. \tag{4}$$

The generalised Huxley equation which models the propagation of neural pulses, the motion of liquid crystal walls, and the dynamics of nerve fibres is expressed as

$$\frac{\partial u}{\partial t} = D\frac{\partial^2 u}{\partial x^2} + \beta u\left(1-u^{\delta}\right)\left(u^{\delta}-\gamma\right). \tag{5}$$

We note here that δ is an arbitrary constant. The nonlinear partial differential equation which generalises (Equations 1–5) and can be thought of as an archetypal equation for explaining the interplay between reaction mechanisms, convection effects, and diffusion transport is called the generalised Burgers-Huxley which takes the form

$$\frac{\partial u}{\partial t} = D\frac{\partial^2 u}{\partial x^2} - \alpha u^{\delta}\frac{\partial u}{\partial x} + \beta u\left(1-u^{\delta}\right)\left(u^{\delta}-\gamma\right). \tag{6}$$

Equation (6) can as well be thought of as a combination of Burger's equation with advective term and Huxley's equation with non linear reaction term with diffusion, hence the name. It is worth noting that, for $\delta = 1$, Equation (6) yields the Burgers-Huxley equation. Wang et al. [8] obtained a closed form solution for Equation (6) and all of its variances. There have been many semi-analytical and numerical methods used in obtaining an approximate solution to the generalised Burgers-Huxley equation, many authors have compared some numerical solutions to the exact solution obtained in Wang et al. [8] and these works are [9–18], among many others. However, there is a minor discrepancy between the closed form solution obtained by Wang et al. [8] and the one obtained by Deng [19] using the first-integral approach. To the best of our knowledge, few researchers have compared their methods with the exact solution in [19], these include [20] using the modified exponential finite difference method, Ervin et al. [21], and Nourazar et al. [22] using the homotopy perturbation method.

Many drawbacks of the approximation analytical approaches include slow convergence at long propagation t, expensive computer memory usage, and difficulty in finding a closed form formula for the resulting series expression ([9, 10]). To this end, we cannot overemphasise the need for analysing the two proposed solutions from Wang et al. [8] and Deng [19]. In this study, we will obtain solution of the generalised Burgers-Huxley equation using the classical finite difference scheme (FTCS) and non-standard finite difference scheme (NSFD).

2. ORGANISATION OF THE PAPER

The structure of the paper is as follows. In section 3, we present the numerical experiment and describe some estimation tools. Section 4 is devoted to the analysis of the two proposed solutions. In section 5, we present the two numerical methods (FTCS and NSFD) and study some of their properties. We present the numerical results from FTCS and NSFD schemes using the reference solution of Wang et al. [8] as a benchmark in section 6 and the proposed solution of Deng [19] as a measure in section 7. Section 8 contains the dynamics of the travelling wave phenomenon of the Burgers-Huxley equation. Conclusion and final remarks of this study are given in section 9.

3. NUMERICAL EXPERIMENT

We solve the generalised 1-D Burgers-Huxley Equation (6) which is given by

$$\frac{\partial u}{\partial t} = D\frac{\partial^2 u}{\partial x^2} - \alpha u^{\delta}\frac{\partial u}{\partial x} + \beta(1+\gamma)u^{1+\delta} - \beta\gamma u - \beta u^{2\delta+1}, \tag{7}$$

subject to the following initial conditions

$$u(x,0) = \left[\frac{\gamma}{2} + \frac{\gamma}{2}\tanh\{\sigma\gamma x\}\right]^{\frac{1}{\delta}}, \tag{8}$$

where $\alpha > 0$, $\beta > 0, 0 < \gamma < 1$, and $\delta > 0$ is a positive constant, $x \in [0,1]$ and $t \geq 0$. The boundary conditions are obtained from exact solution.

Wang et al. [8] used the non linear transformation to obtain a closed form solution for Equation (6) given as

$$u_1(x,t) = \left[\frac{\gamma}{2} + \frac{\gamma}{2}\tanh\left\{\sigma\gamma\left(x - \left\{\frac{(\alpha+\rho)\gamma + (1+\delta)(\alpha-\rho)}{2(1+\delta)}\right\}t\right)\right\}\right]^{\frac{1}{\delta}}, \tag{9}$$

where $\sigma = \dfrac{\delta(\rho-\alpha)}{4(1+\delta)}$ and $\rho = \sqrt{\alpha^2 + 4\beta(1+\delta)}$.

Deng [19] claimed there is a minor error in the proposed solution given by Wang et al. [8] using the first-integral approach,

which is based on the ring theory of commutative algebra. Deng [19] presented a new proposed solution given as

$$u_2(x,t) = \left[\frac{\gamma}{2}+\frac{\gamma}{2}\tanh\left\{\sigma\gamma\left(x-\left\{\frac{(\alpha-\rho)\gamma+(1+\delta)(\alpha+\rho)}{2(1+\delta)}\right\}t\right)\right\}\right]^{\frac{1}{\delta}}, \quad (10)$$

where $\sigma = \dfrac{\delta(\rho-\alpha)}{4(1+\delta)}$ and $\rho = \sqrt{\alpha^2+4\beta(1+\delta)}$.

The closed-form expressions are given in Equations (9) and (10) both lie in the interval $(0, \gamma^{\frac{1}{\delta}})$, refer to the work of Ervin et al. [21]. We fix the coefficient of diffusion to be equal to one and we obtain the solution of generalised Burgers-Huxley equation in three distinct regimes using two finite difference methods. In this study, we consider three different cases as follows:

(1) $\alpha = 1.0,\ \beta = 1.0,\ \gamma = 0.01,\ \delta = 4.0.$
(2) $\alpha = 1.0,\ \beta = 5.0\ (\beta > \alpha),\ \gamma = 0.01,\ \delta = 4.0.$
(3) $\alpha = 5.0\ (\alpha > \beta),\ \beta = 1.0,\ \gamma = 0.01,\ \delta = 4.0.$

We used finite difference technique; Forward time central space (FTCS) and non-standard approaches in obtaining numerical solutions for the numerical experiment. The solution domains are discretised into cells as (x_j, t_n), where $x_j = jh, ; (j = 1, 2, ..., N)$ and $t_n = nk, ; (n = 1, 2, ...)$, where $h = \frac{1-0}{N-1}$ is the spatial mesh size and the values of h selected for computations are explicitly specified for each instance. The temporal step size is denoted by k. The following estimation techniques were used to assess the accuracy of the schemes as well as to check the exact solution with oversight

$$\text{Absolute Error} = \left|u(x,t) - U\left(x_j, t_n\right), \right|$$

$$L_1 = h\sum_{j=1}^{N}\left|u(x,t) - U\left(x_j,t_n\right)\right|, \quad (11)$$

and

$$L_\infty = \max\left|u(x,t) - U\left(x_j,t_n\right)\right|.$$

where $u(x,t)$ and $U(x_j,t_n)$ are the exact and numerical solutions, respectively.

The rate of convergence in space and time are computed using

$$R^T = \frac{\ln\left(\frac{E_k}{E_{\frac{k}{2}}}\right)}{\ln\left(\frac{k}{0.5k}\right)}, \quad (12)$$

where $E_k = \left|\left|L_\infty\right|\right|$ stands for maximum norm errors at grid point k. All numerical simulations are done in MATLAB computing platform on an Intel Core-i5, 2.50 GHz PC with 5GB RAM. We use the two different proposed solutions from Wang et al. [8] and Deng [19] in order to test the performances of our two finite difference methods.

4. ANALYSIS OF THE PROPOSED SOLUTIONS

Before we begin solving a differential equation, we must first answer three basic questions which are due to Hadamard [23]. However, we keep in mind that non linear partial differential equations may have multiple solutions in different space functions. For example, a problem may have multiple solutions, only one of which is bounded. We would argue the uniqueness of the solution in the space of bounded functions. This is the case of the closed form solution provided in Wang et al. [8] and Deng [19]. The question of well-posedness, existence, and uniqueness of the solution to the Burgers-Huxley Equation (7) has been recently reported by Mohan and Khan [24]. One classic test for possible closed form solution to any differential equation is the *Painleve* test, which informs us about the possible integrability of the differential equation.

In this section, we will subject the two proposed solutions in Equations (9) and (10) to test using the ansatz technique on the Burgers-Huxley equation. We consider the case where $D = \beta = \delta = 1$ and $\gamma = 1$, we have our equation now as

$$\frac{\partial u}{\partial t} - \frac{\partial^2 u}{\partial x^2} + \alpha u\frac{\partial u}{\partial x} - 2u^2 + u + u^3 = 0. \quad (13)$$

Using the closed form expression of Wang et al. [8], we assume the solution of Equation (13) to be

$$u_1(x,t) = \left[\frac{1}{2}+\frac{1}{2}\tanh\left\{\sigma\left(x-\left\{\frac{3\alpha-\rho}{4}\right\}t\right)\right\}\right], \quad (14)$$

where $\sigma = \dfrac{\rho-\alpha}{8}$ and $\rho = \sqrt{\alpha^2+8}$. By substituting Equation (14) into Equation (13) and using the Maple symbolic package in differentiating term by term before simplification, we obtain

$$\frac{\partial u}{\partial t} - \frac{\partial^2 u}{\partial x^2} + \alpha u\frac{\partial u}{\partial x} - 2u^2 + u + u^3 = \frac{8-\rho\alpha+\alpha^2}{32\cosh\left[\left(\frac{\rho}{8}-\frac{\alpha}{8}\right)\left(x-\frac{3\alpha t}{4}+\frac{\rho t}{4}\right)\right]^2}. \quad (15)$$

By using the closed form expression of Deng [19], we assume the solution of Equation (13) in the form

$$u_2(x,t) = \left[\frac{1}{2}+\frac{1}{2}\tanh\left\{\sigma\left(x-\left\{\frac{3\alpha+\rho)}{4}\right\}t\right)\right\}\right], \quad (16)$$

we substitute the assumed solution Equation (16) into Equation (13) and using the Maple symbolic package to differentiate before simplification of terms, we obtain

$$\frac{\partial u}{\partial t} - \frac{\partial^2 u}{\partial x^2} + \alpha u\frac{\partial u}{\partial x} - 2u^2 + u + u^3 = 0. \quad (17)$$

REMARK 1. *The supposed solution using Deng [19] closed-form expression satisfy Equation (13). However, the assumed solution utilising the closed-form expression of Wang et al. [8] does not satisfy Equation (13). We expect the remainder to be zero but obtained some terms on the right hand side of Equation (15).*

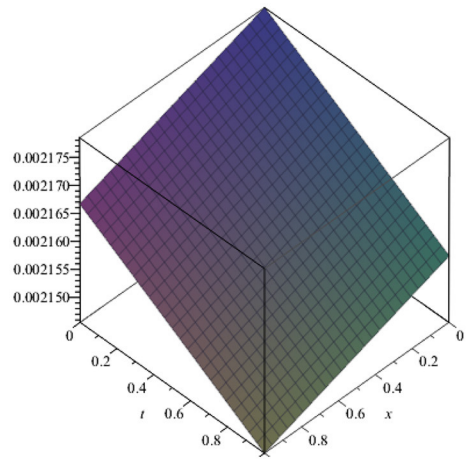

CASE 1. [Wang et al., 1990] remainder

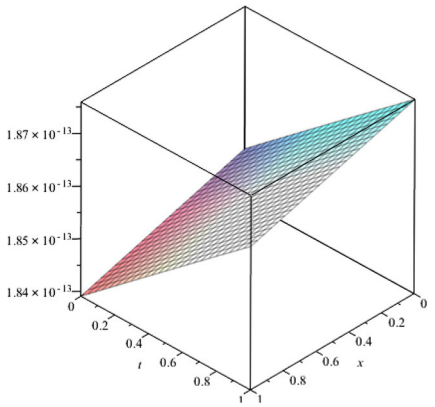

CASE 1. [Deng, 2008] remainder

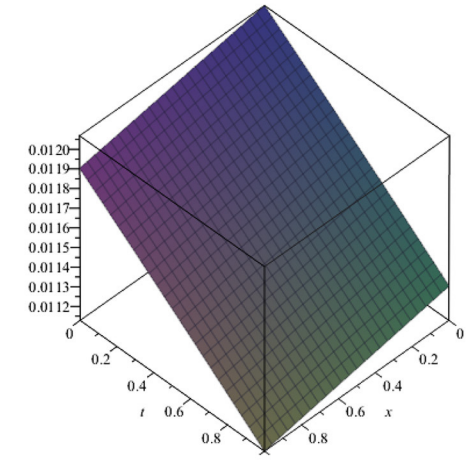

CASE 2. [Wang et al., 1990] remainder

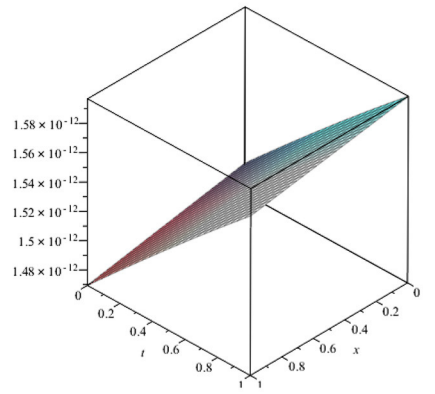

CASE 2. [Deng, 2008] remainder

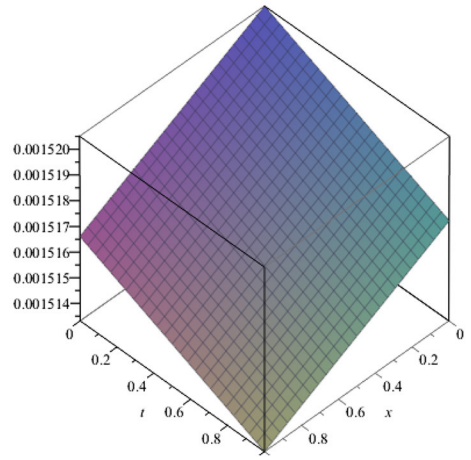

CASE 3. [Wang et al., 1990] remainder

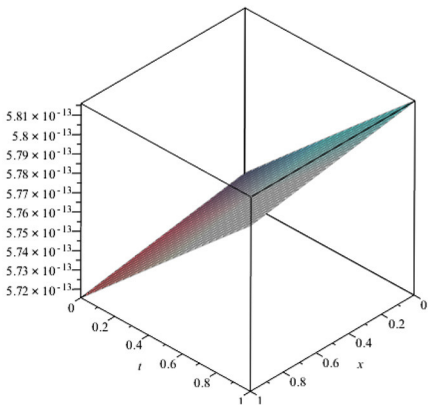

CASE 3. [Deng, 2008] remainder

FIGURE 1 | 3D plots of the remainder for the two proposed solutions of Wang et al. [8] and Deng [19] for the three cases using $x \in [0, 1]$ and $t \in [0, 1]$.

Figure 1 gives the plots of the remainder from the two proposed solutions using the three test cases. We observed that remainder becomes extremely small, around (10^{-13}) in case of Deng [19] but this is not the case for [8] proposed solution.

5. NUMERICAL METHODS

The study of stability, consistency, positivity, and boundedness of NSFD for the case $\delta = 4$ was done in Appadu et al. [25], we have reproduced some of the main analyses.

5.1. FTCS Scheme

Using the FTCS scheme for Equation (7), we have

$$\frac{U_j^{n+1}-U_j^n}{k} = \left(\frac{U_{j+1}^n - 2U_j^n + U_{j-1}^n}{h^2}\right) - \alpha (U_j^n)^\delta \frac{U_{j+1}^n - U_{j-1}^n}{2h} + \beta(1+\gamma)(U_j^n)^{\delta+1} - \beta\gamma U_j^n - \beta (U_j^n)^{2\delta+1}. \tag{18}$$

By making U_j^{n+1} the subject, we have

$$U_j^{n+1} = U_j^n + \frac{k}{h^2}\left(U_{j+1}^n - 2U_j^n + U_{j-1}^n\right) - \frac{k\alpha}{2h}(U_j^n)^\delta \left(U_{j+1}^n - U_{j-1}^n\right) + k\beta(1+\gamma)(U_j^n)^{\delta+1} - k\beta\gamma U_j^n - k\beta (U_j^n)^{2\delta+1}. \tag{19}$$

By using the freezing coefficient method and Von-Neumann stability analysis, we obtain the amplification factor as

$$\xi = 1 - I\frac{k\alpha}{h} U_{max} \sin w + \frac{k}{h^2}(2\cos w - 2) + k\beta (U_{max})^4 (1+\gamma) - k\beta\gamma - k\beta (U_{max})^8. \tag{20}$$

Since $0 \leq U(x_j, t_n) \leq \gamma^{1/\delta}$, it follows that $U_{max} = \gamma^{1/4}$. On simplification, we obtain

$$|\xi| = \sqrt{\left(1 - \frac{4k}{h^2}\sin^2\frac{w}{2}\right)^2 + \left(\frac{k\alpha}{h}\sin w\right)^2}. \tag{21}$$

Stability is guaranteed when $0 \leq |\xi| \leq 1$ for $w = [-\pi, \pi]$. Region of stability is $k \leq 0.005$. We next study the consistency.

We expand using Taylor's series expansion around (t_n, x_j) using Equation (19) and obtain

$$U + kU_t + \frac{k^2}{2}U_{tt} + \frac{k^3}{6}U_{ttt} + \mathcal{O}(k^4) = U + \frac{k}{h^2}\left(h^2 U_{xx} + \frac{h^4}{12}U_{xxxx} + \mathcal{O}(h^6)\right) - \frac{k\alpha}{2h}U^\delta \left(2hU_x + \frac{1}{3}h^3 U_{xxx} + \mathcal{O}(h^5)\right) + k\beta(1+\gamma)U^{\delta+1} - k\beta\gamma U - k\beta U^{2\delta+1}. \tag{22}$$

Dividing throughout by k and simplifying, we have

$$U_t - U_{xx} + \alpha U^\delta U_x - \beta(1+\gamma)U^{\delta+1} + \beta\gamma U + \beta U^{2\delta+1} = -\frac{k}{2}U_{tt} - \frac{k^2}{6}U_{ttt} - \alpha\frac{h^2}{6}U^\delta U_{xxx} + \frac{h^2}{12}U_{xxxx} + \mathcal{O}(k^3) + \mathcal{O}(h^4), \tag{23}$$

and as $k, h \to 0$, we recover the generalised Burgers-Huxley equation. We note that the FTCS scheme is first-order accurate in time and second-order accurate in space.

REMARK 2. *The generalisation of Equation (18) to a higher dimension is quite straight-forward. In $\mathbb{R}^m$, the approximate solution in the reaction term becomes $U^n_{\{j_1,j_2,\cdots,m\}}$. The diffusion term $\triangle U$ and advection term takes the form of the generalised finite difference, refer to Prieto et al. [26].*

5.2. Non-standard Finite Difference

The use and popularity of the NSFD scheme are due to anomalous behaviour of the traditional finite difference scheme when used in discretisation of some continuous differential equation. In particular, some partial differential equations are of practical importance. The idea of NSFD scheme gained the popular attention from many researchers after the work of Mickens [27]. Some noteworthy failure of standard finite difference methods is the lack of preservation of physical properties like positivity and boundedness for equations arising in mathematical biology [27]. The derivations are primarily based on the notion of dynamical consistency, which includes features like special solutions with predetermined stability. There are certain guidelines to follow while developing such techniques. They are as follows:

- Linear or non linear terms are modelled non-locally on the computational grid.
  e.g. $u_n^3 \approx 3u_{n+1}(u_n)^2 - 2(u_n)^3$.
- Use of non-classical denominator functions.
- The order of the difference equation should be the same as the order of the differential equation. In general, spurious solutions arise when the order of the difference equation is greater than the order of the differential Equation [27].
- The discrete approximation should preserve some important properties of the corresponding differential equation.

We discretise the 1-D generalised Burgers-Huxley equation i.e.

$$u_t = u_{xx} - \alpha u^\delta u_x + \beta(1+\gamma)u^{1+\delta} - \beta\gamma u - \beta u^{2\delta+1},$$

using the forward Euler in time and the usual second order approximation in the diffusion term. We employed the non-local discretisation in the advection and reaction terms as employed in Appadu et al. [25, 28].

To this end, we propose the following non standard finite difference scheme for Equation (7):

$$\frac{U_j^{n+1}-U_j^n}{\phi(k)} = \left[\frac{U_{j+1}^n - 2U_j^n + U_{j-1}^n}{[\psi(h)]^2}\right] - \alpha U_j^{n+1}(U_j^n)^{\delta-1}\left(\frac{U_j^n - U_{j-1}^n}{\psi(h)}\right) + \beta(1+\gamma)\left[2(U_j^n)^{\delta+1} - (U_j^n)^\delta U_j^{n+1}\right] - \beta\gamma U_j^{n+1}$$

$$-\beta U_j^{n+1}(U_j^n)^{2\delta}. \tag{24}$$

where $\phi(k)=\dfrac{e^{\beta k}-1}{\beta}$ and $\psi(h)=\dfrac{e^{h}-1}{h}$. To restate in a more concise form, we have

$$U_j^{n+1}=\frac{\begin{array}{c}(1-2R)U_j^n+R(U_{j+1}^n+U_{j-1}^n)\\ +2\phi(k)\beta(1+\gamma)(U_j^n)^{\delta+1}\end{array}}{\begin{array}{c}1+\alpha r(U_j^n)^{\delta-1}(U_j^n-U_{j-1}^n)+\phi(k)\beta\gamma\\ +\phi(k)\beta(1+\gamma)(U_j^n)^{\delta}+\phi(k)\beta(U_j^n)^{2\delta}\end{array}}. \tag{25}$$

The denominator functions are defined as $R=\dfrac{\phi(k)}{[\psi(h)]^2}$ and $r=\dfrac{\phi(k)}{\psi(h)}$.

5.2.1. Positivity

If $1-2R\geq 0$ and $1-\alpha r\gamma\geq 0$ the numerical solution from NSFD obeys

$$0\leq U_j^n\leq \gamma^{\frac{1}{\delta}},\ \implies\ 0\leq U_j^{n+1}\leq \gamma^{\frac{1}{\delta}},$$

for all considered values of n and j.

PROOF: Since $\alpha,\beta\in\mathbb{R}^+$, and $\gamma\in(0,1)$. For positivity, we require $1-2R\geq 0$ and $1-\alpha r\gamma\geq 0$. Substituting R and using $1-2R>0$, we obtain

$$\left(\frac{e^{\beta k}-1}{\beta}\right)\left(\frac{\beta}{e^{\beta h}-1}\right)^2\leq\frac{1}{2}, \tag{26}$$

which gives

$$k\leq\frac{1}{\beta}\ln\left(1+\frac{(e^{\beta h}-1)^2}{2\beta}\right). \tag{27}$$

Simplifying $1-\alpha r\gamma\geq 0$ and after some manipulation, we have

$$k\leq\frac{1}{\beta}\ln\left(1+\frac{(e^{\beta h}-1)}{\alpha\gamma}\right). \tag{28}$$

Thus, the positivity condition rests on the following conditions:

$$k\leq\begin{cases}\dfrac{1}{\beta}\ln\left(1+\dfrac{(e^{\beta h}-1)^2}{2\beta}\right),\\ \dfrac{1}{\beta}\ln\left(1+\dfrac{(e^{\beta h}-1)}{\alpha\gamma}\right).\end{cases} \tag{29}$$

On substituting $h=0.1$, and evaluating for different values of α, β, and γ we obtain

(a) $k\leq 5.515\times10^{-3}$ and $k\leq 2.4438$ for $\alpha=\beta=1.0$.
(b) $k\leq 8.244\times10^{-3}$ and $k\leq 8.375\times10^{-1}$ for $\alpha=1.0,\ \beta=5.0$.
(c) $k\leq 5.515\times10^{-3}$ and $k\leq 1.1325$ for $\alpha=5.0,\ \beta=1.0$.

We chose the time of the experiment to be $t=1.0$. For positivity, we require $k\leq 5.515\times10^{-3}$ for all the three cases.

5.2.2. Boundedness

We assume $0\leq U_j^n\leq\gamma^{\frac{1}{\delta}}$ for all considered values of n and j. Therefore,

$$\begin{aligned}&(U_j^{n+1}-\gamma^{\frac{1}{\delta}})\Big[1+\alpha r(U_j^n)^{\delta-1}(U_j^n-U_{j-1}^n)+\phi(k)\beta\gamma\\ &\qquad+\phi(k)\beta(1+\gamma)(U_j^n)^{\delta}+\phi(k)\beta(U_j^n)^{2\delta}\Big]\\ &=(1-2R)U_j^n+R(U_{j+1}^n+U_{j-1}^n)+\ 2\phi(k)\beta(1+\gamma)(U_j^n)^{\delta+1}\\ &-\gamma^{\frac{1}{\delta}}-\alpha r\gamma^{\frac{1}{\delta}}(U_j^n)^{\delta-1}(U_j^n-U_{j-1}^n)-\ \phi(k)\beta\gamma^{1+\frac{1}{\delta}}\\ &-\phi(k)\beta\gamma^{\frac{1}{\delta}}(1+\gamma)(U_j^n)^{\delta}-\phi(k)\beta\gamma^{\frac{1}{\delta}}(U_j^n)^{2\delta}\leq(1-2R)\gamma^{\frac{1}{\delta}}\\ &+2R\gamma^{\frac{1}{\delta}}+2\phi(k)\beta(1+\gamma)(U_j^n)^{\delta+1}-\gamma^{\frac{1}{\delta}}\\ &-\alpha r\gamma^{\frac{1}{\delta}}(U_j^n)^{\delta-1}(U_j^n-U_{j-1}^n)-\phi(k)\beta\gamma^{1+\frac{1}{\delta}}\\ &-\phi(k)\beta\gamma^{\frac{1}{\delta}}(U_j^n)^{2\delta}\leq 2\phi(k)\beta(1+\gamma)(U_j^n)^{\delta+1}\\ &-\alpha r\gamma^{\frac{1}{\delta}}(U_j^n)^{\delta-1}(U_j^n-U_{j-1}^n)-\phi(k)\beta\gamma^{1+\frac{1}{\delta}}\\ &-\phi(k)\beta\gamma^{\frac{1}{\delta}}(1+\gamma)(U_j^n)^{\delta}-\phi(k)\beta\gamma^{\frac{1}{\delta}}(U_j^n)^{2\delta}\\ &\leq\phi(k)\beta(1+\gamma)(U_j^n)^{\delta+1}-\alpha r\gamma^{\frac{1}{\delta}}(U_j^n)^{\delta-1}(U_j^n-U_{j-1}^n)\\ &-\phi(k)\beta\gamma^{1+\frac{1}{\delta}}-\phi(k)\beta\gamma^{\frac{1}{\delta}}(U_j^n)^{2\delta}\\ &\leq-\alpha r(U_j^n)^{\delta-1}(U_j^n-U_{j-1}^n)\leq 0.\end{aligned} \tag{30}$$

This implies that $0\leq U_j^{n+1}\leq\gamma^{\frac{1}{\delta}}$. Hence, boundedness property is satisfied.

5.2.3. Consistency

We consider Equation (25) and using the Taylor's series expansion around (nk, jh), we obtain

$$\begin{aligned}&U+kU_t+\frac{k^2}{2}U_{tt}+\frac{k^3}{6}U_{ttt}+\mathcal{O}(k^4)\\ &\Big(1-2R\Big)U+R\Big(2U+h^2U_{xx}+\frac{h^4}{12}U_{xxxx}+\mathcal{O}(h^6)\Big)\\ &=\frac{\begin{array}{c}+2k\beta(1+\gamma)U^{\delta+1}\end{array}}{\begin{array}{c}1+\alpha rU^{\delta-1}\Big(hU_x-\dfrac{h^2}{2}U_{xx}+\mathcal{O}(h^3)\Big)\\ +k\beta\gamma+k\beta(1+\gamma)U^{\delta}+k\beta U^{2\delta}\end{array}}.\end{aligned} \tag{31}$$

Since $R=\dfrac{\phi(k)}{[\psi(h)]^2}$, $r=\dfrac{\phi(k)}{\psi(h)}$ and $\phi(k)\approx k$, $\psi(h)\approx h$, we therefore approximate R as $\dfrac{k}{h^2}$ and r as $\dfrac{k}{h}$.

Equation (31) after some simplification can be rewritten as

$$\begin{aligned}&\Big(U+kU_t+\frac{k^2}{2}U_{tt}+\frac{k^3}{6}U_{ttt}+\mathcal{O}(k^4)\Big)\Gamma_\omega\\ &=U+kU_{xx}+\frac{kh^2}{12}U_{xxxx}+2k\beta(1+\gamma)U^{\delta+1},\end{aligned} \tag{32}$$

where $\Gamma_\omega = \left[1+\alpha k U^{\delta-1}\left(U_x - \frac{h}{2}U_{xx} + \mathcal{O}(h^2)\right) + k\beta\gamma + k\beta(1+\gamma)U^{\delta} + k\beta U^{2\delta}\right]$.

Expanding, simplifying, and dividing throughout by k, gives

$$\alpha U^{\delta}U_x - \frac{h}{2}\alpha U^{\delta}U_{xx} + \alpha\frac{h^2}{6}U^{\delta}U_{xxx} + \beta\gamma U + \beta(1+\gamma)U^{\delta+1} + \beta U^{2\delta+1} + \left(U_t + \frac{k}{2}U_{tt} + \frac{k^2}{6}U_{ttt} + \mathcal{O}(k^3)\right)\Gamma_\omega = U_{xx} + \frac{h^2}{12}U_{xxxx} + 2\beta(1+\gamma)U^{\delta+1}. \quad (33)$$

As $k, h \to 0$, we recover the generalised Burgers-Huxley equation which is given by Equation (7).

5.2.4. Accuracy

Using Equation (33), we have

$$\begin{aligned} U_t - U_{xx} + \alpha U^{\delta}U_x - \beta(1+\gamma)U^{\delta+1} + \beta\gamma U + \beta U^{2\delta+1} &= -\left[\alpha k U^{\delta-1}\left(U_x - \frac{h}{2}U_{xx} + \frac{h^2}{6}U_{xxx}\right) + k\beta\gamma + k\beta(1+\gamma)U^{\delta} + k\beta U^{2\delta}\right]U_t \\ &- \left(\frac{k}{2}U_{tt} + \frac{k^2}{6}U_{ttt}\right)\left[1 + \alpha k U^{\delta-1}\left(U_x - \frac{h}{2}U_{xx} + \frac{h^2}{6}U_{xxx}\right) + k\beta\gamma + k\beta(1+\gamma)U^{\delta} + k\beta U^{2\delta}\right] \quad (34) \\ &+ \frac{h}{2}\alpha U^{\delta}U_{xx} - \frac{h^2}{6}\alpha U^{\delta}U_{xxx} + \frac{h^2}{12}U_{xxxx} + \mathcal{O}(k^4) + \mathcal{O}(h^3). \end{aligned}$$

We deduce that NSFD has first-order accuracy in time and second order in space.

5.2.5. Stability

We consider Equation 24, using the freezing coefficient technique, we obtain

$$\begin{aligned} &U_j^{n+1} - U_j^n \\ &= R\left[U_{j+1}^n - 2U_j^n + U_{j-1}^n\right] - r\alpha(U_{max})^{\delta}\left(U_j^n - U_{j-1}^n\right) \\ &+\phi(k)\beta(1+\gamma)\left[2(U_j^n)(U_{max})^{\delta} - (U_{max})^{\delta}U_j^{n+1}\right] \\ &- \phi(k)\beta\gamma U_j^{n+1} - \phi(k)\beta U_j^{n+1}(U_{max})^{2\delta}, \end{aligned} \quad (35)$$

where $U_{max} = \gamma^{\frac{1}{\delta}}$. We use the ansatz $U_j^n = \xi^n e^{Ijw}$ where w is the phase angle and obtain

$$\begin{aligned} \xi^{n+1}e^{Ijw} &= \xi^n e^{Ijw} + R\left[\xi^n e^{I(j+1)w} - 2\xi^n e^{Ijw} + \xi^n e^{I(j-1)w}\right] \\ &-r\alpha\gamma\left(\xi^n e^{Ijw} - \xi^n e^{I(j-1)w}\right) \\ &+ \phi(k)\beta(1+\gamma)\gamma\left[2\xi^n e^{Ijw} - \xi^{n+1}e^{Ijw}\right] \\ &-\phi(k)\beta\gamma\xi^{n+1}e^{Ijw} - \phi(k)\beta\gamma^2\xi^{n+1}e^{Ijw}. \end{aligned} \quad (36)$$

The amplification factor, ξ in Equation (36) takes the form

$$\xi = \frac{1 - 2R + R(e^{Iw} + e^{-Iw}) + 2\phi(k)\beta\gamma(1+\gamma) - \alpha r\gamma(1 - e^{-Iw})}{1 + \phi(k)\beta\gamma^2 + \phi(k)\beta\gamma + \phi(k)\beta\gamma(1+\gamma)}, \quad (37)$$

TABLE 1 | A comparison between the exact and numerical solutions at some values of x for $\alpha = 1.0$, $\beta = 1.0$, and $\gamma = 0.01$ at time $t = 1.0$.

t	x	Exact	FTCS	Abs Error (FTCS)	NSFD	Abs Error (NSFD)
1	0.1	2.66808×10^{-1}	2.66711×10^{-1}	9.70955×10^{-5}	2.66701×10^{-1}	1.07217×10^{-4}
	0.5	2.66997×10^{-1}	2.66727×10^{-1}	2.69371×10^{-4}	2.66699×10^{-1}	2.97924×10^{-4}
	0.9	2.67185×10^{-1}	2.67088×10^{-1}	9.68712×10^{-5}	2.67077×10^{-1}	1.07212×10^{-4}

TABLE 2 | A comparison between the exact and numerical solutions at some values of x for $\alpha = 1.0$, $\beta = 5.0$, and $\gamma = 0.01$ at time $t = 1.0$.

t	x	Exact	FTCS	Abs Error (FTCS)	NSFD	Abs Error (NSFD)
1	0.1	2.71286×10^{-1}	2.70774×10^{-1}	5.12597×10^{-4}	2.70423×10^{-1}	8.62784×10^{-4}
	0.5	2.71735×10^{-1}	2.70311×10^{-1}	1.42389×10^{-3}	2.69334×10^{-1}	2.40108×10^{-3}
	0.9	2.72181×10^{-1}	2.71670×10^{-1}	5.10520×10^{-4}	2.71320×10^{-1}	8.60918×10^{-4}

TABLE 3 | A comparison between the exact and numerical solutions at some values of x for $\alpha = 1.0$, $\beta = 5.0$, and $\gamma = 0.01$ at time $t = 1.0$.

t	x	Exact	FTCS	Abs Error (FTCS)	NSFD	Abs Error (NSFD)
1	0.1	2.66130×10^{-1}	2.66062×10^{-1}	6.81536×10^{-5}	2.66055×10^{-1}	7.52697×10^{-5}
	0.5	2.66221×10^{-1}	2.66031×10^{-1}	1.89299×10^{-4}	2.66011×10^{-1}	2.09794×10^{-4}
	0.9	2.66311×10^{-1}	2.66243×10^{-1}	6.81112×10^{-5}	2.66235×10^{-1}	7.57484×10^{-5}

$$= \frac{1 - 2R + R(2\cos w) + 2\phi(k)\beta\gamma(1+\gamma) \\ -\alpha r\gamma(1 - \cos w + I\sin w)}{1 + 2\phi(k)\beta\gamma(1+\gamma)}. \quad (38)$$

$$= \frac{1 - 2R + R(2\cos w) + 2\phi(k)\beta\gamma(1+\gamma) - \alpha r\gamma(1-\cos w)}{1 + 2\phi(k)\beta\gamma(1+\gamma)} \\ -I\frac{\alpha r\gamma \sin w}{1 + 2\phi(k)\beta\gamma(1+\gamma)}. \quad (39)$$

The scheme is stable whenever the Von-Neumann condition, $|\xi| \leq 1$ is satisfied. The modulus of amplification factor is given by

$$|\xi| = \sqrt{(\mathcal{R}(\xi))^2 + (\mathcal{I}(\xi))^2},$$

where $\mathcal{R}(\xi)$ and $\mathcal{I}(\xi)$ are the real and imaginary parts of ξ, respectively. From Equation (39), we get

$$|\xi| = \sqrt{\frac{\left(1 - 2R + R(2\cos w) + 2\phi(k)\beta\gamma(1+\gamma) \right.\\ \left. -\alpha r\gamma(1-\cos w)\right)^2 + \left(\alpha r\gamma \sin w\right)^2}{\left(1 + 2\phi(k)\beta\gamma(1+\gamma)\right)^2}}, \quad (40)$$

where $w \in [-\pi, \pi]$. On differentiation and solving for w, we obtain $w = 0, \pi$, and $-\pi$. We note for $w = 0$, we get $|\xi| = 1$.

Substituting $w = \pi$ or $-\pi$ in Equation (40) yields

$$|\xi| = \frac{1 + 2\phi(k)\beta\gamma(1+\gamma) - 4R - 2\alpha\gamma r}{1 + 2\phi(k)\beta\gamma(1+\gamma)}. \quad (41)$$

which is

$$-1 \leq \frac{1 + 2\phi(k)\beta\gamma(1+\gamma) - 4R - 2\alpha\gamma r}{1 + 2\phi(k)\beta\gamma(1+\gamma)} \leq 1. \quad (42)$$

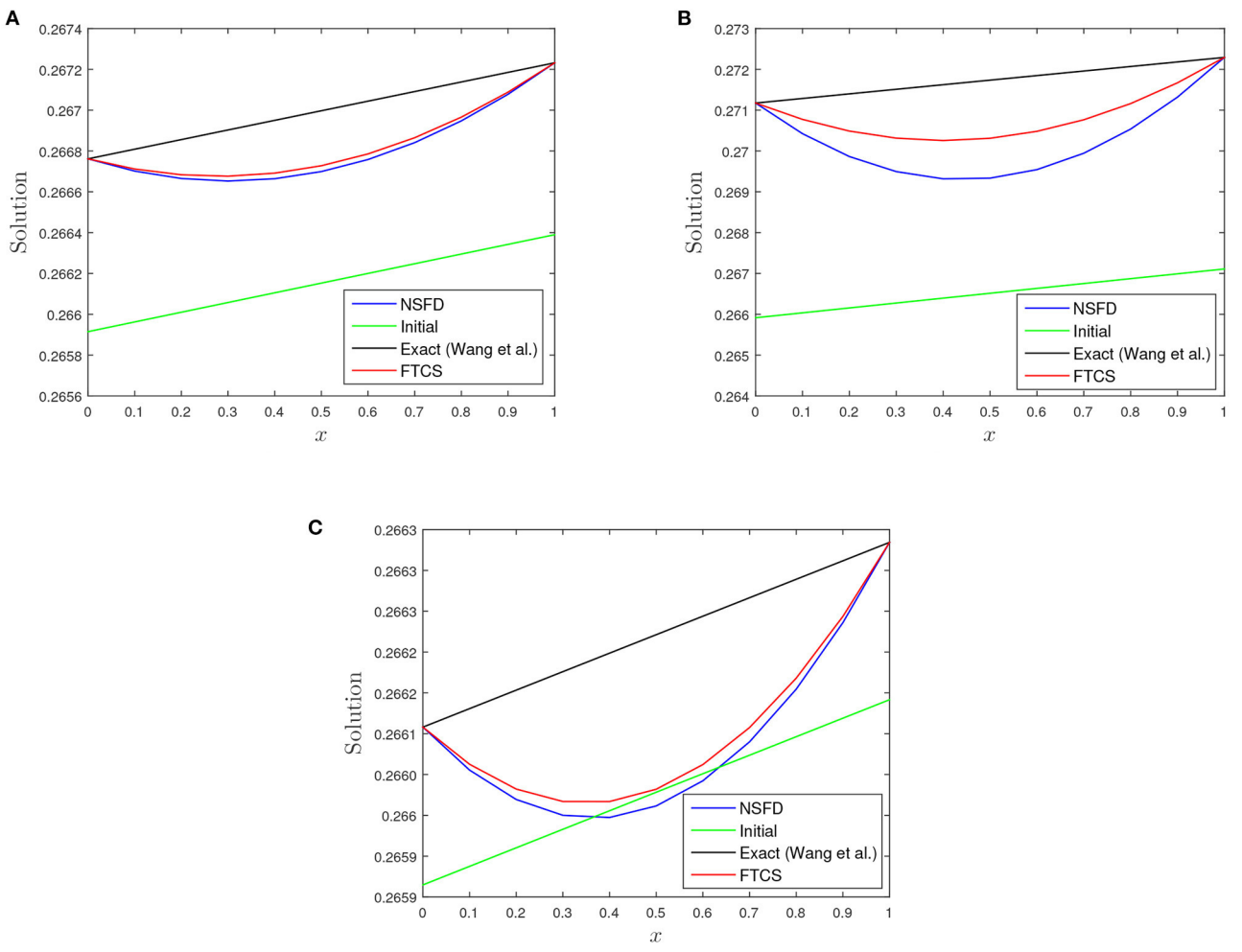

FIGURE 2 | A plot of initial, numerical profiles, and profile from proposed solution [8] vs. x for the three test cases using FTCS and NSFD at $t = 1.0$ using $h = 0.1$ and $k = 0.00125$. **(A)** $\alpha = 1.0$, $\beta = 1.0$, and $\gamma = 0.01$. **(B)** $\alpha = 1.0$, $\beta = 5.0$, and $\gamma = 0.01$. **(C)** $\alpha = 5.0$, $\beta = 1.0$, and $\gamma = 0.01$.

After some simplification,

$$2R + \alpha\gamma r \leq 1 + 2\phi(k)\beta\gamma(1+\gamma). \tag{43}$$

We note from Equation (43) that

$$2R \leq 1 \implies 1 - 2R \geq 0 \text{ and } \alpha\gamma r \leq 1 \implies 1 - \alpha\gamma r \geq 0,$$

which are the conditions for positivity.

The inequalities

$$\alpha\gamma r \leq 2\phi(k)\beta\gamma(1+\gamma) \text{ and } 2R \leq 2\phi(k)\beta\gamma(1+\gamma)$$

are $2\phi(k)\beta\gamma(1+\gamma) - \alpha\gamma r \geq 0$ and $2\phi(k)\beta\gamma(1+\gamma) - 2R \geq 0$.

Thus, the conditions for stability are

$$1 - 2R \geq 0,\ 1 - \alpha\gamma r \geq 0,\ 2\phi(k)\beta\gamma(1+\gamma) - 2R \geq 0,$$
$$\text{and } 2\phi(k)\beta\gamma(1+\gamma) - \alpha\gamma r \geq 0. \tag{44}$$

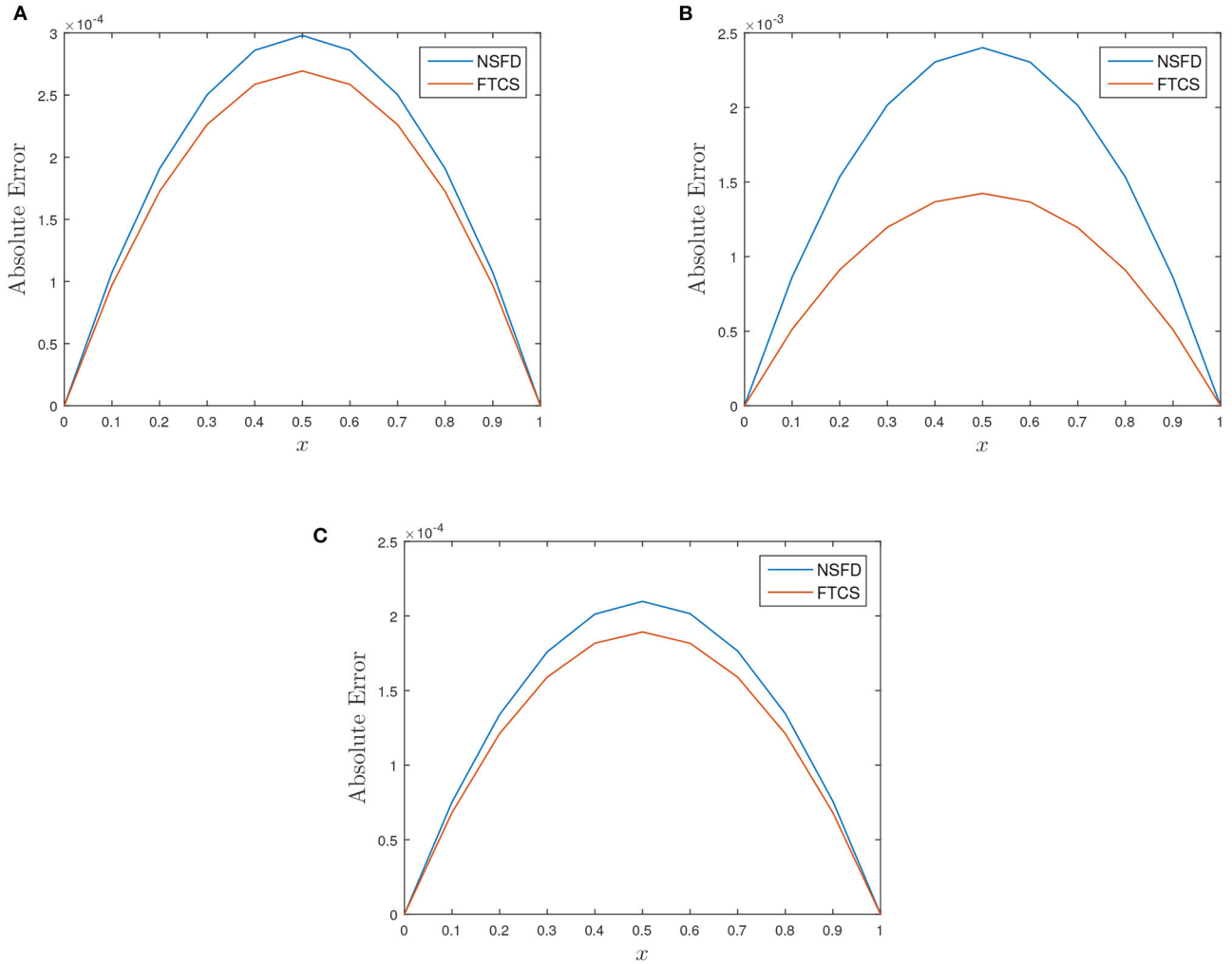

FIGURE 3 | Plot of absolute error vs. x for the three test cases at $t = 1.0$ using $h = 0.1$ and $k = 0.00125$. **(A)** $\alpha = 1.0$, $\beta = 1.0$, and $\gamma = 0.01$. **(B)** $\alpha = 1.0$, $\beta = 5.0$, and $\gamma = 0.01$. **(C)** $\alpha = 5.0$, $\beta = 1.0$, and $\gamma = 0.01$.

TABLE 4 | A comparison between the exact and numerical solutions at some values of x for $\alpha = 1.0$, $\beta = 1.0$, and $\gamma = 0.01$ at time $t = 1.0$.

t	x	Exact	FTCS	Abs Error (FTCS)	NSFD	Abs Error (NSFD)
1	0.1	2.64625×10^{-1}	2.64625×10^{-1}	1.08007×10^{-7}	2.64625×10^{-1}	1.41772×10^{-7}
	0.5	2.64818×10^{-1}	2.64818×10^{-1}	3.00189×10^{-7}	2.64818×10^{-1}	3.93692×10^{-7}
	0.9	2.65011×10^{-1}	2.65010×10^{-1}	1.08071×10^{-7}	2.65010×10^{-1}	1.41709×10^{-7}

We would like to point out that we have obtained the conditions of positivity for stability.

REMARK 3. *The generalisation of Equation (24) to a higher dimension rests on the fact that terms (reaction and advection) with non-standard approximation U^{n+1} should have a minus sign. In $\mathbb{R}^m$, the approximate solution in the reaction term becomes $U^n_{\{j_1,j_2,\cdots,m\}}$. The diffusion term $\triangle U$ and advection term takes the form of the generalised finite difference, refer to Prieto et al. [26]. In Appadu et al. [25], we have constructed a few versions of NSFD methods to solve a 2D generalised Burgers-Huxley equation.*

6. NUMERICAL RESULTS AND ERROR ANALYSIS USING PROPOSED SOLUTION FROM WANG ET AL.

In this section, we have reproduced some results obtained by Appadu et al. [29]

Case 1: $\alpha = \beta = 1.0$ and $\gamma = 0.01$.
Case 2: $\alpha = 1.0$, $\beta = 5.0$, and $\gamma = 0.01$.
Case 3: $\alpha = 5.0$, $\beta = 1.0$, and $\gamma = 0.01$.

In **Table 1**, we observed the absolute error of the FTCS scheme to be of order $10^{-4} - 10^{-5}$ while that from NSFD scheme is of the order 10^{-4}. The relative error of both schemes is of order $10^{-3} - 10^{-4}$. When the reaction coefficient β dominates the advection coefficient α, we noticed a decline in the accuracy of both schemes as the absolute and relative errors increase to magnitude of order $10^{-3} - 10^{-4}$ and 10^{-3}, respectively, as shown in **Table 2**. Absolute and relative errors decrease to $10^{-4} - 10^{-5}$ and 10^{-4} when $\alpha > \beta$, we refer to **Table 3**. **Figures 2**, **3** shed more light on the behaviour and performance of the FTCS and NSFD scheme with respect to the exact solution of Wang et al. [8].

REMARK 4. *There is always deviation in the numerical profiles (FTCS and NSFD) with the profile from proposed solution of*

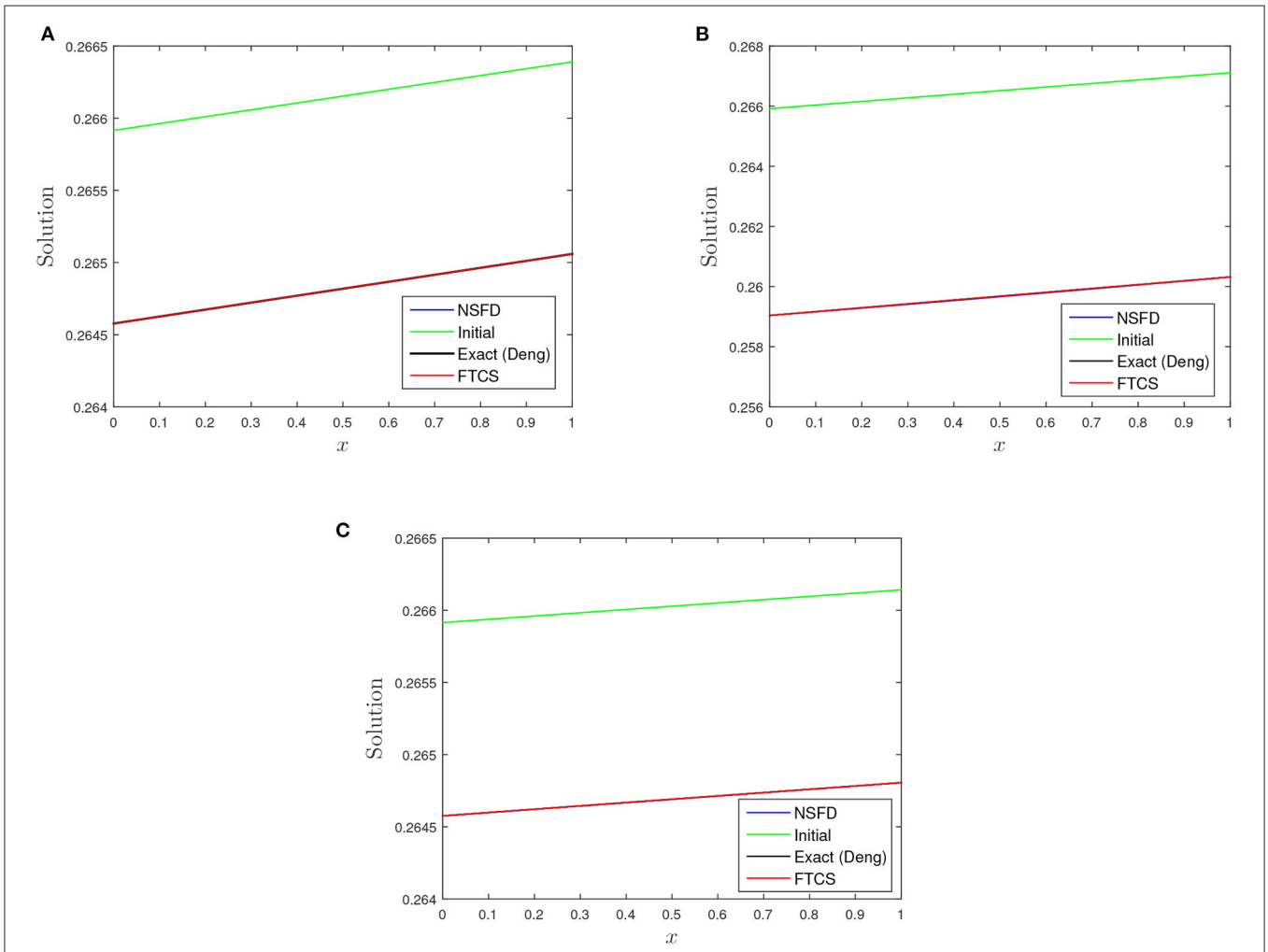

FIGURE 4 | A plot of initial, numerical profiles, and profile from proposed solution [19] vs. x for the three test cases using FTCS and NSFD at $t = 1.0$ using $h = 0.1$ and $k = 0.00125$. **(A)** $\alpha = 1.0$, $\beta = 1.0$, and $\gamma = 0.01$. **(B)** $\alpha = 1.0$, $\beta = 5.0$, and $\gamma = 0{:}01$. **(C)** $\alpha = 5.0$, $\beta = 1.0$, and $\gamma = 0.01$.

Wang et al. [8] as depicted in ***Figure 1****, despite performing grid refinement i.e.,* $k \to 0$.

7. NUMERICAL RESULTS AND ERROR ANALYSIS USING PROPOSED SOLUTION FROM DENG

The results in this section are novel and are not taken from any reference.

Case 1: $\alpha = \beta = 1.0$ and $\gamma = 0.01$.

Case 2: $\alpha = 1.0$, $\beta = 5.0$, and $\gamma = 0.01$.

Case 3: $\alpha = 5.0$, $\beta = 1.0$, and $\gamma = 0.01$.

Table 4 show the absolute error of the FTCS and NSFD schemes to be of order 10^{-7} while the relative error of both schemes is of order $10^{-6} - 10^{-7}$. When the reaction coefficient β dominates the advection coefficient α, we noticed a decline in the accuracy of both schemes (FTCS and NSFD) as the absolute errors increase to magnitude of order $10^{-5} - 10^{-7}$ and relative error to 10^{-6} and 10^{-5}, respectively, as shown in **Table 6**. In **Tables 5**, **7**, **9** show the rate of convergence as we perform grid refinement in time. **Figures 4**, **5** shed more light on the behaviour and performance

TABLE 5 | L_1, L_∞ errors and rate of convergence (in time) for $\alpha = 1.0$, $\beta = 1.0$, and $\gamma = 0.01$ (Case 1) at some different time-step size k with spatial mesh size $h = 0.1$ using FTCS and NSFD at $t = 1.0$.

Scheme	k	L_1 Error	L_∞ Error	R_t
FTCS	0.005	1.9810×10^{-6}	3.0018×10^{-7}	–
	0.0025	1.9608×10^{-6}	2.9711×10^{-7}	1.484×10^{-2}
	0.00125	1.9506×10^{-6}	2.9558×10^{-7}	7.479×10^{-3}
NSFD	0.005	2.5984×10^{-6}	3.9369×10^{-7}	–
	0.0025	1.1361×10^{-6}	1.7213×10^{-7}	1.193
	0.00125	4.0451×10^{-7}	6.1282×10^{-8}	1.489

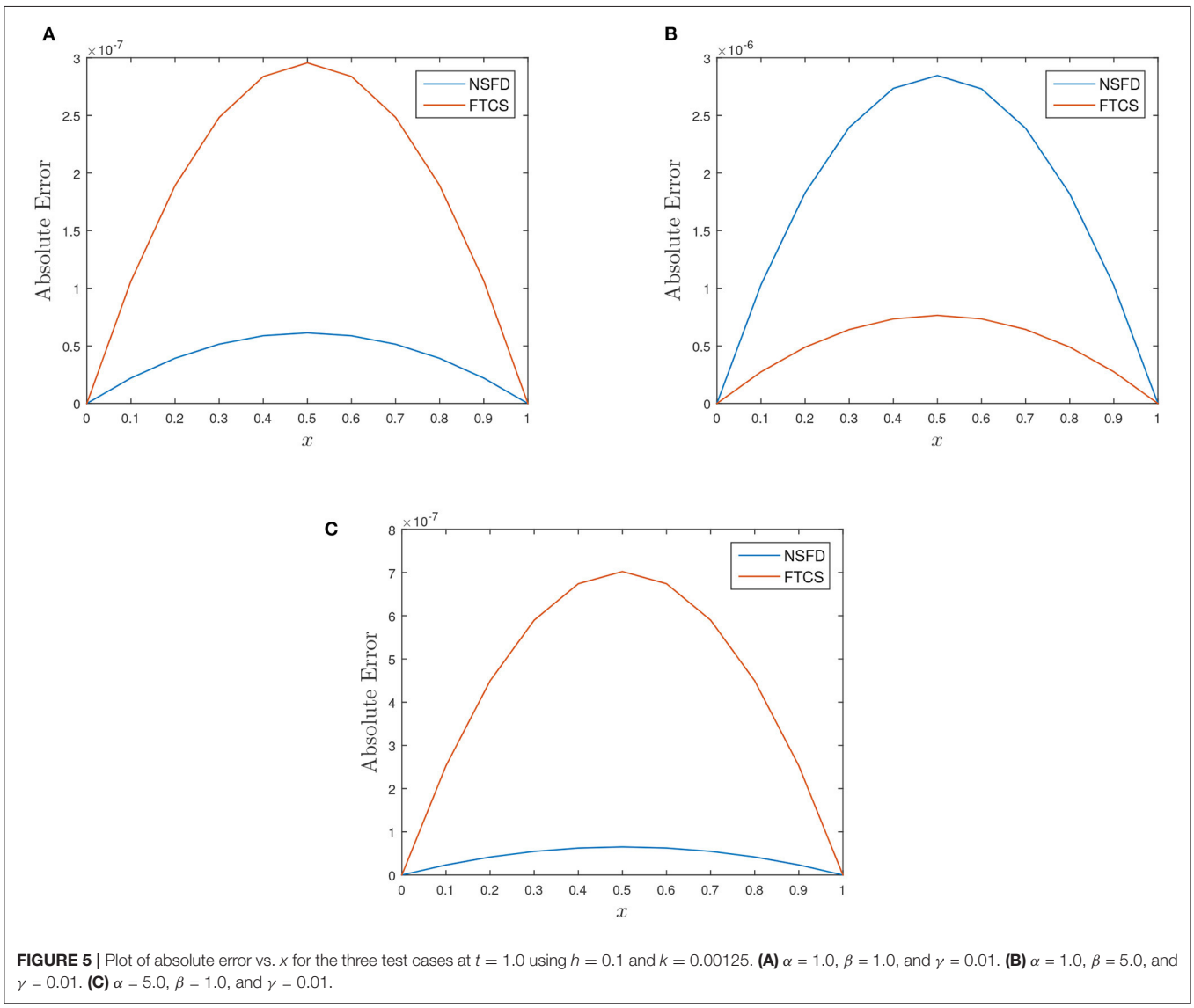

FIGURE 5 | Plot of absolute error vs. x for the three test cases at $t = 1.0$ using $h = 0.1$ and $k = 0.00125$. **(A)** $\alpha = 1.0$, $\beta = 1.0$, and $\gamma = 0.01$. **(B)** $\alpha = 1.0$, $\beta = 5.0$, and $\gamma = 0.01$. **(C)** $\alpha = 5.0$, $\beta = 1.0$, and $\gamma = 0.01$.

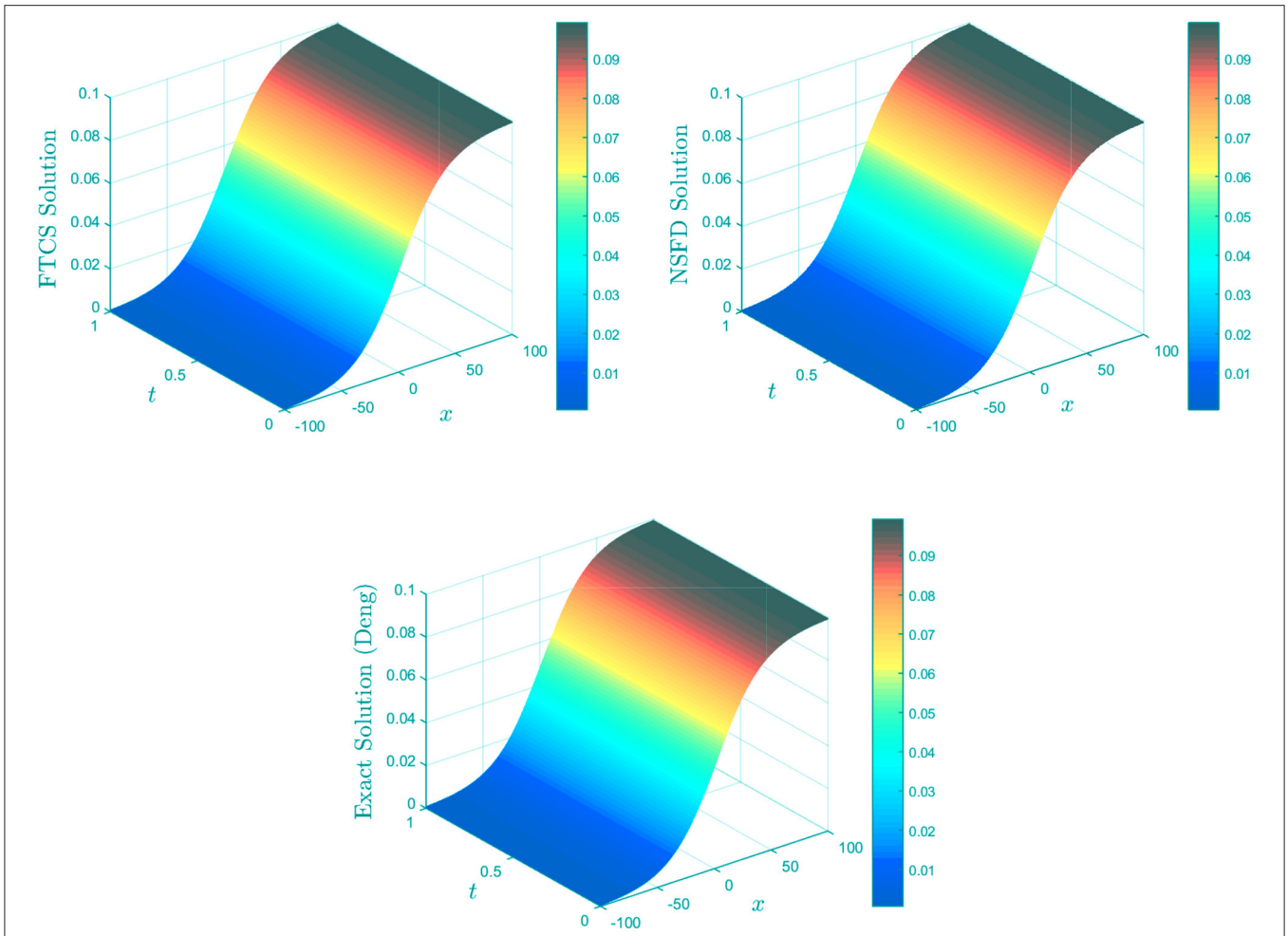

FIGURE 6 | 3D plots of solution vs. t vs. x using FTCS, NSFD, and proposed solution [19] for $\alpha = 1$, $\beta = 1$, $\delta = 1.0$, and $\gamma = 0.1$ using $k = 0.005$ and $h = 0.1$.

TABLE 6 | A comparison between the exact and numerical solutions at some values of x for $\alpha = 1.0$, $\beta = 1.0$, and $\gamma = 0.01$ at time $t = 1.0$.

t	x	Exact	FTCS	Abs Error (FTCS)	NSFD	Abs Error (NSFD)
1	0.1	2.59166×10^{-1}	2.59166×10^{-1}	3.13176×10^{-7}	2.59160×10^{-1}	5.80488×10^{-6}
	0.5	2.59680×10^{-1}	2.59680×10^{-1}	8.72601×10^{-7}	2.59664×10^{-1}	1.60915×10^{-5}
	0.9	2.60191×10^{-1}	2.60191×10^{-1}	3.14074×10^{-7}	2.60185×10^{-1}	5.79044×10^{-6}

TABLE 7 | L_1, L_∞ errors and rate of convergence (in time) for $\alpha = 1.0$, $\beta = 1.0$, and $\gamma = 0.01$ (Case 2) at some different time-step size k with spatial mesh size $h = 0.1$ using FTCS and NSFD at $t = 1.0$.

Scheme	k	L_1 Error	L_∞ Error	R_t
FTCS	0.005	5.75636×10^{-6}	8.72601×10^{-7}	–
	0.0025	5.28394×10^{-6}	8.00967×10^{-7}	1.235×10^{-1}
	0.00125	5.04769×10^{-6}	7.65145×10^{-7}	6.601×10^{-2}
NSFD	0.005	1.0623×10^{-4}	1.6091×10^{-5}	–
	0.0025	4.7996×10^{-5}	7.2693×10^{-6}	1.146
	0.00125	1.8799×10^{-5}	2.8461×10^{-6}	1.352

of the FTCS and NSFD schemes with respect to the proposed solution of Deng [19].

8. THE DYNAMICS OF A TRAVELLING WAVE BY THE BURGERS-HUXLEY EQUATION

The Burgers-Huxley equation is a non linear PDE that exhibits many complex phenomena among which is the wave phenomenon. The proposed solutions are given in Equations

TABLE 8 | A comparison between the exact and numerical solutions at some values of x for $\alpha = 1.0$, $\beta = 1.0$, and $\gamma = 0.01$ at time $t = 1.0$.

t	x	Exact	FTCS	Abs Error (FTCS)	NSFD	Abs Error (NSFD)
1	0.1	2.64598×10^{-1}	2.64598×10^{-1}	2.54332×10^{-7}	2.64598×10^{-1}	1.42838×10^{-7}
	0.5	2.64690×10^{-1}	2.64691×10^{-1}	7.06786×10^{-7}	2.64691×10^{-1}	3.97948×10^{-7}
	0.9	2.64782×10^{-1}	2.64783×10^{-1}	2.54418×10^{-7}	2.64783×10^{-1}	1.43706×10^{-7}

TABLE 9 | L_1, L_∞ errors and rate of convergence (in time) for $\alpha = 1.0$, $\beta = 1.0$, and $\gamma = 0.01$ (Case 3) at some different time-step size k with spatial mesh size $h = 0.1$ using FTCS and NSFD at $t = 1.0$.

Scheme	k	L_1 Error	L_∞ Error	R_t
FTCS	0.005	4.6644×10^{-6}	7.0678×10^{-7}	–
	0.0025	4.6441×10^{-6}	7.0371×10^{-7}	6.291×10^{-3}
	0.00125	4.6339×10^{-6}	7.0217×10^{-7}	3.156×10^{-3}
NSFD	0.005	2.6265×10^{-6}	3.9794×10^{-7}	–
	0.0025	1.1622×10^{-6}	1.7608×10^{-7}	1.176
	0.00125	4.2962×10^{-7}	6.5089×10^{-8}	1.435

(9) and (10) both exhibit the dynamics of a travelling wave. A travelling wave is a wave that moves in a certain direction while maintaining a stable form. In this section, we show the travelling wave dynamics of the Burgers-Huxley equation using the proposed solution by Deng [19] and behaviour of the approximate solutions by looking at Equation (7) in an extended domain for the spatial variable $x \in [-100, 100]$ and $t \in [0, 1]$. The plots are displayed in **Figure 6**.

9. CONCLUSION

In this work, we examined the two proposed solutions provided by Wang et al. [8] and Deng [19] for the generalised Burgers-Huxley equation. The FTCS and NSFD schemes are designed to approximate the solution of the generalised Burgers-Huxley equation. The numerical estimation tools of absolute error, relative error, and rate of convergence serve as the means of benchmarking the two proposed solutions. We observed that despite the consistency of the two (FTCS and NSFD) finite difference schemes and working within their region of stability, the results deviate from the proposed solution from Wang et al. [8] upon grid refinements. This directly has a greater impact on its error analysis as shown in **Figure 1** and **Tables 1**–**3**. This anomalous behaviour was not experienced using the proposed solution of Deng [19] as seen in **Figure 3** and **Tables 4**–**9**. In conclusion, the proposed solution of Wang et al. [8] indeed contains a minor error while the solution provided by Deng [19] is the true exact solution for the generalised Burgers-Huxley equation for the initial conditions given by Equation (8). In our future work, we will consider an application in microfluidic, microfluidics deals with the flow of fluids and suspensions in channels of sub-millimetre-sized cross-sections under the influence of external forces. In these instances, viscosity dominates over inertia, ensuring the absence of turbulence and the appearance of regular and predictable laminar flow streams, which implies an exceptional spatial and temporal control of solutes. The equation modelling microfluidics is as follows [30]:

$$\begin{cases} \nabla \cdot u = 0, \\ \rho\left(\dfrac{\partial u}{\partial t} + (u \cdot \nabla)u\right) = -\nabla P + \eta \nabla^2 u + \rho g \end{cases} \tag{45}$$

we will approach the set of partial differential equations given in Equation (45) using FTCS, NSFD, and possibly other methods.

AUTHOR CONTRIBUTIONS

The plan of the paper was sent by AA, writing up was done by both authors. YT carried out the computations and analysis of the methods under the supervision of AA. AA and YT agree to be accountable for the content of the work.

FUNDING

YT acknowledges the support received from the Department of Mathematics and Applied Mathematics of the Nelson Mandela University which ensured that the author is registered for his Ph.D. study at the University for three years.

ACKNOWLEDGMENTS

The authors are grateful to the two reviewers who provided feedback which allowed us to improve content and presentation of the paper considerably.

REFERENCES

1. Adekanye O. *The Construction of Nonstandard Finite Difference Schemes for dynamiCal Systems*. Washington, DC: Howard University; (2017).
2. Burgers JM. A mathematical model illustrating the theory of turbulence. *Adv Appl Mech*. (1948) 1:171–99. doi: 10.1016/S0065-2156(08)70100-5
3. Abazari R, Borhanifar A. Numerical study of the solution of the Burgers and coupled Burgers equations by a differential transformation method. *Comput Math Appl*. (2010) 59:2711–22. doi: 10.1016/j.camwa.2010.01.039
4. Mukundan V, Awasthi A. Linearized implicit numerical method for burgers' equation. *Nonlinear Eng*. (2016) 5:0031. doi: 10.1515/nleng-2016-0031
5. Hodgkin AL, Huxley AF. A quantitative description of membrane current and its application to conduction and excitation in nerve. *J Physiol*. (1952) 117:500–44. doi: 10.1113/jphysiol.1952.sp004764

6. FitzHugh R. Impulses and physiological states in theoretical models of nerve membrane. *Biophys J*. (1961) 1:445–66. doi: 10.1016/S0006-3495(61)86902-6
7. Nagumo J, Arimoto S, Yoshizawa S. An active pulse transmission line simulating nerve axon. Proc IRE. (1962) 50:2061–70. doi: 10.1109/JRPROC.1962.288235
8. Wang XY, Zhu ZS, Lu YK. Solitary wave solutions of the generalized Burgers-Huxley equation. *J Phys A*. (1990) 23:271–4. doi: 10.1088/0305-4470/23/3/011
9. Ismail HNA, Raslan K, Abd Rabboh AA. Adomian decomposition method for Burgers-Huxley and Burgers–Fisher equations. *Appl Math Comput*. (2004) 1:291–301. doi: 10.1016/j.amc.2003.10.050
10. Batiha B, Noorani MSM, Hashim I. Application of variational iteration method to the generalized Burgers-Huxley equation. *Chaos Solitons Fractals*. (2008) 36:660–3. doi: 10.1016/j.chaos.2006.06.080
11. Sari M, Gurarslan G. Numerical solutions of the generalized burgers-huxley equation by a differential quadrature method. *Math Problems Eng*. (2009) 2009:370765. doi: 10.1155/2009/370765
12. Biazar J, Mohammadi F. Application of differential transform method to the generalized Burgers-Huxley Equation. *Appl Appl Math*. (2010) 5:629–43.
13. Bratsos AG. A fourth order improved numerical scheme for the generalized burgers-Huxley Equation. *Am J Comput Math*. (2011) 1:660–3. doi: 10.4236/ajcm.2011.13017
14. Ray SS, Gupta AK. Comparative analysis of variational iteration method and Haar wavelet method for the numerical solutions of Burgers-Huxley and Huxley equations. *J Math Chem*. (2014) 52:1066–80. doi: 10.1007/s10910-014-0327-z
15. Singh BK, Arora G, Singh MK. A numerical scheme for the generalized Burgers-Huxley equation. *J Egypt Math Soc*. (2016) 24:629–837. doi: 10.1016/j.joems.2015.11.003
16. Zibaei M, Zeinadini S, Namjoo M. Numerical solutions of Burgers-Huxley equation by exact finite difference and NSFD schemes. *J Diff Equat Appl*. (2016) 22:1098–113. doi: 10.1080/10236198.2016.1173687
17. Verma KA, Kayenat S. An efficient Mickens' type NSFD scheme for the generalized Burgers Huxley equation. *J Diff Equat Appl*. (2020) 26:1213–46. doi: 10.1080/10236198.2020.1812594
18. Cicek Y, Korkut S. Numerical solution of generalized burgers-huxley equation by lie-trotter splitting method. *Numer Anal Appl*. (2021) 14:90–102. doi: 10.1134/S1995423921010080
19. Deng X. Travelling wave solutions for the generalized Burgers-Huxley equation. *Appl Math Comput*. (2008) 204:733–7. doi: 10.1016/j.amc.2008.07.020
20. Macías-Díaz JE. A modified exponential method that preserves structural properties of the solutions of the Burgers-Huxley equation. *Int J Comput Math*. (2018) 95:3–19. doi: 10.1080/00207160.2017.1377339
21. Ervin VJ, Macías-Díaz JE, Ruiz-Ramírez J. A positive and bounded finite element approximation of the generalized Burgers-Huxley equation. *J Math Anal Appl*. (2015) 424:1143–60. doi: 10.1016/j.jmaa.2014.11.047
22. Nourazar SS, Soori M, Nazari-Golshan A. On the exact solution of burgers-huxley equation using the homotopy perturbation method. *J Appl Math Phys*. (2015) 95:285–94. doi: 10.4236/jamp.2015.33042
23. Hadamard J. Sur les problèmes aux dérivées partielles et leur signification physique. *Bull Univ Princeton*. (1902) 13:49–52.
24. Mohan MT, Khan A. On the generalized Burgers-Huxley equation: existence, uniqueness, regularity, global attractors and numerical studies. *Discrete Continuous Dyn Syst B*. (2021) 26:3943–88. doi: 10.3934/dcdsb.2020270
25. Appadu AR, Tijani YO, Aderogba AA. On the performance of some NSFD methods for a 2-D generalized Burgers-Huxley equation. *J Diff Equat Appl*. (2021) 27:1537–73. doi: 10.1080/10236198.2021.1999433
26. Prieto FU, Muñoz JJB, Corvinos LG. Application of the generalized finite difference method to solve the advection–diffusion equation. *J Comput Appl Math*. (2011) 235:1849–55. doi: 10.1016/j.cam.2010.05.026
27. Mickens RE. *Application of Nonstandard Finite Difference Scheme*. Singapore: World Scientific (2000).
28. Appadu AR, İnan B, Tijani YO. Comparative study of some numerical methods for the Burgers-Huxley equation. *Symmetry*. (2019) 11:1333. doi: 10.3390/sym11111333
29. Appadu AR, Tijani YO, Munyakazi J. Computational study of some numerical methods for the generalized Burgers-Huxley equation. In: Awasthi A, John SJ, Panda S, editors. *Computational Sciences-Modelling, Computing and Soft Computing. CSMCS Communications in Computer and Information Science, Vol. 1345*. Singapore: Springer (2020).
30. Bruus H. Governing equations in microfluidics. *Microscale Acoustofluidics*. (2014) 1–28. doi: 10.1039/9781849737067-00001

Conflict of Interest: The authors declare that the research was conducted in the absence of any commercial or financial relationships that could be construed as a potential conflict of interest.

Publisher's Note: All claims expressed in this article are solely those of the authors and do not necessarily represent those of their affiliated organizations, or those of the publisher, the editors and the reviewers. Any product that may be evaluated in this article, or claim that may be made by its manufacturer, is not guaranteed or endorsed by the publisher.

frontiers in Applied Mathematics and Statistics

REVIEW
published: 14 February 2022
doi: 10.3389/fams.2021.766085

Novel Approach of Multistate Markov Chains to Evaluate Progression in the Expanded Model of Non-alcoholic Fatty Liver Disease

*Iman M. Attia**

Department of Mathematical Statistics, Faculty of Graduate Studies for Statistical Research, Cairo University, Giza, Egypt

A global increase in the prevalence of obesity and type 2 diabetes is strongly connected to an increased prevalence of non-alcoholic fatty liver disease (NAFLD) worldwide. In this article, the progression of the NAFLD process is modeled by continuous time Markov chains (CTMCs) with nine states. Maximum likelihood is used to estimate the transition intensities among the states. Once the transition intensities are obtained, the mean sojourn time and its variance are estimated, and the state probability distribution and its asymptotic covariance matrix are also estimated. A hypothetical example based on a longitudinal study assessing patients with NAFLD in various stages is discussed. The mean time to absorption is estimated, and the other abovementioned statistical indices are examined. In this article, the maximum likelihood estimation (MLE) function is utilized in a new approach to compensate for the missing values in the follow-up period of patients evaluated in longitudinal studies. A MATLAB code link is provided, at the end of the article, for the estimation of the transition rate matrix and transition probability matrix.

Keywords: multistate Markov chains, non-alcoholic fatty liver disease, continuous time Markov chains, maximum likelihood estimation, mean sojourn time, longitudinal study, mean time to absorption

OPEN ACCESS

Edited by:
Hagos Hailu Gidey, Botswana International University of Science and Technology, Botswana

Reviewed by:
Saheed Ojo Akindeinde, Botswana International University of Science and Technology, Botswana
Ashish Awasthi, NITc, India

***Correspondence:**
Iman M. Attia
imanattiathesis1972@gmail.com; imanattia1972@gmail.com

Specialty section:
This article was submitted to Mathematical Biology, a section of the journal Frontiers in Applied Mathematics and Statistics

Received: *28 August 2021*
Accepted: *28 December 2021*
Published: *14 February 2022*

Citation:
Attia IM (2022) Novel Approach of Multistate Markov Chains to Evaluate Progression in the Expanded Model of Non-alcoholic Fatty Liver Disease. Front. Appl. Math. Stat. 7:766085. doi: 10.3389/fams.2021.766085

INTRODUCTION

Continuous time Markov chain (CTMC) is commonly used to model data obtained from longitudinal studies in medical research and to investigate the evolution and progression of diseases over time. Estes et al. [1] used multistate Markov chains to model the epidemic of non-alcoholic fatty liver disease (NAFLD). Younossi et al. [2] used multistate Markov chains to demonstrate the economic and clinical burden of NAFLD in the United States and Europe.

According to the American Association for Study of Liver Disease, American College of Gastroenterology, and the American Gastroenterological Association, NAFLD to be defined requires (a) evidence of hepatic steatosis (HS) either by imaging or by histology and (b) no causes of secondary hepatic fat accumulation, such as significant alcohol consumption, use of steatogenic medications, or hereditary disorders [3]. This is the same definition established by the European Association for the Study of the Liver (EASL), the European Association for the Study of Diabetes (EASD), and the European Association for the Study of Obesity (EASO) [4]. NAFLD can be categorized histologically into the non-alcoholic fatty liver (NAFL) or non-alcoholic steatohepatitis (NASH). NAFL is defined as the presence of $\geq$ 5% HS without evidence of hepatocellular injury in the form of hepatocyte ballooning. NASH is defined as the presence of $\geq$ 5% HS and inflammation with hepatocyte injury (ballooning), with or without any fibrosis.

In Attia [5], non-alcoholic fatty liver disease (NAFLD) can be modeled by the simplest form of a multistate model for the health-illness-death process as illustrated in **Figure 1**. The system is composed of 4 states. State 1 represents the individuals with high risk factors such as type 2 diabetes, hypercholesterolemia, obesity, and hypertension. State 2 represents patients suffering from NAFLD with all possible substates that are explained and clarified in a more elaborate manner in this paper. The death state is represented by two states highlightening the competing risk factors for death: state 3 represents the death state as a complication of NAFLD and state 4 represents the death state from other causes than the complications of NAFLD. For this general and abstract system, 5 rates of transitions among states are estimated using the maximum likelihood estimation (MLE) function and quasi-Newton. Once the transition rate matrix is obtained, exponentiation of this rate matrix will yield the transition probability matrix to estimate the eight probability density functions (PDFs). All diseases can be modeled by this abstract form (health-illness-death process), what makes each disease unique from the other is the detailed substages of the illness state: how many substates that encompass the illness state, how the movements among these states can take place, and the definitions specified for each of these substates. In this article; the system is composed of nine unique different states. Each state defines specific biological changes in the whole journey of the disease, and from each state, the patient can be in the death state without specifying the cause of death for simplicity. This more complicated system of the NAFLD process is composed of 22 rates in addition to 49 PDFs to be estimated. The transition rate matrix differs from the simple model as the number and movement among the states are more specified and complicated; consequently, the PDFs are different.

A MATLAB code illustrating all the calculations is published in the code Ocean site at the URL: https://codeocean.com/capsule/8641183/tree/v2 with doi: 10.24433/CO.6022979.v2.

A full detailed description of a simple form of the model to enhance understanding of the difference between the two forms of the model is illustrated in a thorough explanation in the **Supplementary Materials** for the simple model (refer to **Supplementary Material**).

In this article, NAFLD is modeled as a multistage disease process consisting of nine stages, as depicted in **Figure 2** [2]. As shown in **Figure 2**, the patient can move across the stages of the disease process. Whereas, remission rates are allowed from stage 4 (compensated liver cirrhosis) to earlier stages, the patient progresses to HCC and liver transplantation once he arrives at stage 5 (decompensated liver cirrhosis), and remission rates are not allowed. Death state can be reached from any state. The patient can move from the first 5 stages to stage 8 (HCC) with a higher rate of progression from stage 4 (CC) or stage 5 (DCC) to stage 8 (HCC) compared to the first 3 stages. A brief definition of each stage is illustrated below the figure.

NAFLD stages are modeled as time-homogenous CTMCs, that is, $P_{ij}(\Delta t)$ depends on Δt and not on t, with constant transition intensities λ_{ij} over time, exponentially distributed time spent within each state and patient events following a Poisson distribution. The states are finite and can be defined or identified based on various aspects, such as clinical symptoms and invasive

Abbreviations: CC, compensated cirrhosis (stage 4); CTMCs, continuous time Markov chains; CVS, cardiovascular disease; DCC, decompensated cirrhosis (stage 5); EASD, European Association for the Study of Diabetes; EASL, European Association for the Study of Liver; EASO, European Association for the Study of Obesity; EM, extramortality (stage 9); HCC, hepatocellular carcinoma (stage 8); HS, hepatic steatosis; LT, liver transplant (stage 6); NAFLD, non-alcoholic fatty liver disease; NAFL-NO FB, non-alcoholic fatty liver with no fibrosis (stage 1); NASH, non-alcoholic steatohepatitis; NASH-NO FB, non-alcoholic steatohepatitis with no fibrosis (stage 2); NASH-FB, non-alcoholic steatohepatitis with fibrosis (stage 3); PLT, postliver transplant (stage 7); PNPLA-3, patatin-like phospholipase domain containing protein 3 gene variants; TE, transient elastography; T2DM, type 2 diabetes mellitus.

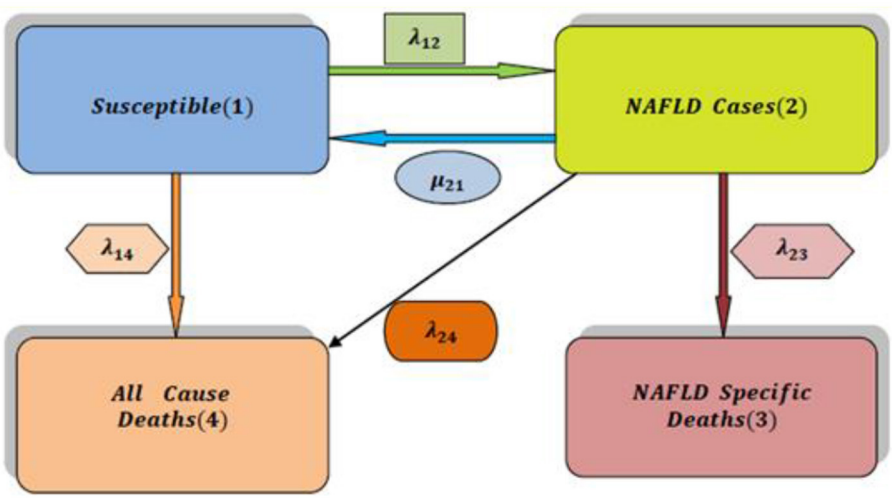

FIGURE 1 | The simplest multistate model for analysis of NAFLD (health-illness-death process) [2].

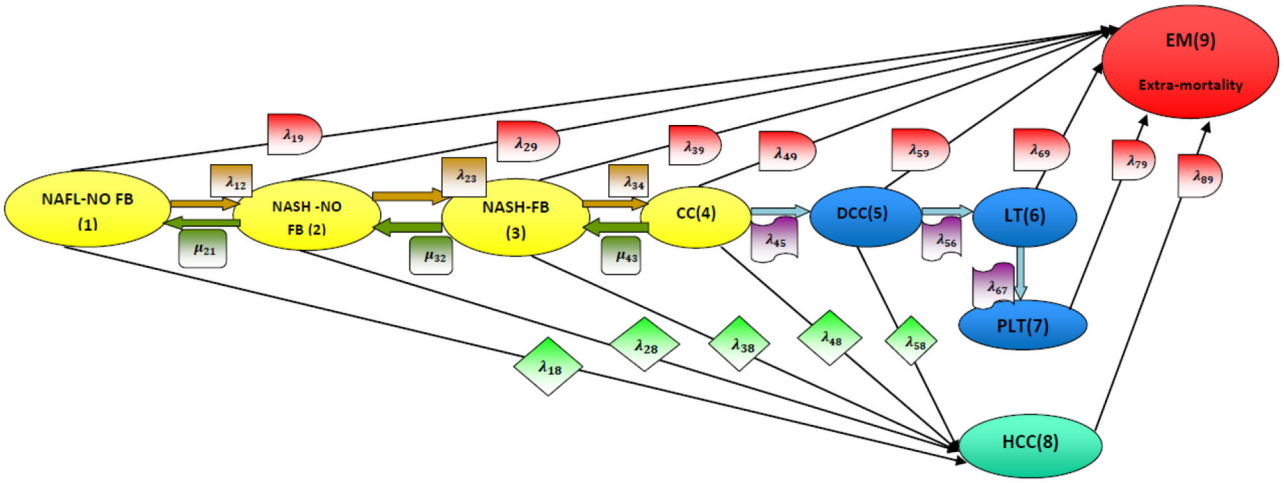

FIGURE 2 | Disease model structure. NAFL-NO FB, non-alcoholic fatty liver with no fibrosis (stage 1); NASH-NO FB, non-alcoholic steatohepatitis with no fibrosis (stage 2); NASH-FB, non-alcoholic steatohepatitis with fibrosis (stage 3); CC, compensated cirrhosis (stage 4); DCC, decompensated cirrhosis (stage 5); LT, liver transplant (stage 6); PLT, post liver transplant (stage 7); HCC, hepatocellular carcinoma (stage 8); EM, extramortality (stage 9). [2].

or non-invasive investigations. The gold-standard method for the classification of histopathological changes in the liver is invasive liver biopsy. It is presently the most trustworthy procedure for diagnosing the presence of steatohepatitis and fibrosis in patients with NAFLD [6]. The limitations of this procedure are cost, sampling error, and procedure-related morbidity and mortality. MR imaging, by spectroscopy [7] or by proton density fat fraction [8], is an excellent non-invasive technique for quantifying HS and is being widely used in NAFLD clinical trials [9]. The use of transient elastography (TE) to obtain continuous attenuation parameters is a promising tool for quantifying hepatic fat in an ambulatory setting [10]. However, non-invasive quantification of HS in patients with NAFLD is limited in routine clinical care. Additionally, one of the most recent biological markers is the keratin (K18) and its caspase-cleaved fragments (cK18). There are many scoring systems that can identify the stages of the disease process [11]. NAFLD has a higher prevalence rate in individuals with risk factors such as visceral obesity, type 2 diabetes mellitus (T2DM), dyslipidemia, hypertension, older age, male sex, and Hispanic ethnicity [12].

For simplicity, all individuals are assumed to enter the disease process at stage one, and they are all followed up with the same length of the time interval between measurements.

The article is divided into eight sections. In Section 1, the transition probabilities are thoroughly discussed. In Section 2, transition rates are clarified. In Section 3, the mean sojourn time and its variance are reviewed. In Section 4, the state probability distribution and its covariance matrix are discussed. In Section 5, the life expectancy of the patients is considered. In Section 6, the expected numbers of patients in each state are obtained. A hypothetical numerical example is used in Section 7 to illustrate the above concepts. Finally, a brief summary is comprehended in Section 8. A link to the MATLAB code is provided at the end of the article (refer to **Supplementary Material**, Appendix A & B).

1. TRANSITION PROBABILITIES

NAFLD is modeled by multistate Markov chains that define a stochastic process:

$$\left[(\mathrm{X(t),\ t} \in \mathrm{\ T})\right] \text{ over a finite state space } \mathrm{S} = \{1, 2, \ldots, 9\} \text{ and } \mathrm{T} = [0, \mathrm{t}] \text{ and } \mathrm{t} < \infty.$$

The transitions can occur at any point in time and, hence, are called continuous time Markov chains, in contrast to the discrete time Markov chains in which transitions occur at fixed points in time. The rates at which these transitions occur are constant over time and, thus, are independent of t; that is, the transition of the patient from *state i at time* $= t$ *to state j at* $t = t + s$ *where* $s = \Delta t$ depends on the difference between two consecutive time points. In addition, it is defined as $\theta_{ij}\ (t) = \lim_{\Delta t \to 0} \frac{P_{ij}(\Delta t) - I}{\Delta t}$ or the Q matrix; while, the I matrix is the identity matrix, the thetas are the transition rates among states (in this model, they are 22 rates).

For the above multistate Markov model demonstrating the NAFLD process, the forward Kolmogorov differential Equations (1) are as follows:

$$\frac{d}{dt}P\,(t) = PQ =$$

$$\begin{bmatrix} P_{11} & P_{12} & P_{13} & P_{14} & P_{15} & P_{16} & P_{17} & P_{18} & P_{19} \\ P_{21} & P_{22} & P_{23} & P_{24} & P_{25} & P_{26} & P_{27} & P_{28} & P_{29} \\ P_{31} & P_{32} & P_{33} & P_{34} & P_{35} & P_{36} & P_{37} & P_{38} & P_{39} \\ P_{41} & P_{42} & P_{43} & P_{44} & P_{45} & P_{46} & P_{47} & P_{48} & P_{49} \\ 0 & 0 & 0 & 0 & P_{55} & P_{56} & P_{57} & P_{58} & P_{59} \\ 0 & 0 & 0 & 0 & 0 & P_{66} & P_{67} & 0 & P_{69} \\ 0 & 0 & 0 & 0 & 0 & 0 & P_{77} & 0 & P_{79} \\ 0 & 0 & 0 & 0 & 0 & 0 & 0 & P_{88} & P_{89} \\ 0 & 0 & 0 & 0 & 0 & 0 & 0 & 0 & P_{99} \end{bmatrix}$$

$$\begin{bmatrix} -\gamma_1 & \lambda_{12} & 0 & 0 & 0 & 0 & 0 & \lambda_{18} & \lambda_{19} \\ \mu_{21} & -\gamma_2 & \lambda_{23} & 0 & 0 & 0 & 0 & \lambda_{28} & \lambda_{29} \\ 0 & \mu_{32} & -\gamma_3 & \lambda_{34} & 0 & 0 & 0 & \lambda_{38} & \lambda_{39} \\ 0 & 0 & \mu_{43} & -\gamma_4 & \lambda_{45} & 0 & 0 & \lambda_{48} & \lambda_{49} \\ 0 & 0 & 0 & 0 & -\gamma_5 & \lambda_{56} & 0 & \lambda_{58} & \lambda_{59} \\ 0 & 0 & 0 & 0 & 0 & -\gamma_6 & \lambda_{67} & 0 & \lambda_{69} \\ 0 & 0 & 0 & 0 & 0 & 0 & -\lambda_{79} & 0 & \lambda_{79} \\ 0 & 0 & 0 & 0 & 0 & 0 & 0 & -\lambda_{89} & \lambda_{89} \\ 0 & 0 & 0 & 0 & 0 & 0 & 0 & 0 & 0 \end{bmatrix} \quad (1)$$

Solving the Kolmogorov differential equations will give the transition probability matrix $P_{ij}(t)$ (refer to **Supplementary Material Section 1**).

$P_{ij}(t)$ satisfies the following properties:

1. $P_{ij}(t+s) = \sum_{i.j.l \in S} P_{il}(t) P_{lj}(s), \quad \forall\ t \geq 0,\ s \geq 0,\ i,j,l \in S$; *obeying kolmogrov equations*.
2. $\sum_S P_{ij}(t) = 1$.
3. $P_{ij}(t) \geq 0, \quad \forall\ t \geq 0 \quad$ *and* $\quad i,j \in S$.

The Q matrix satisfies the following conditions:

1. $\sum_S q_{ij}(t) = 0$.
2. $q_{ij}(t) \geq 0 \quad i \neq j$.
3. $-\sum_S q_{ij}(t) = q_{ii} \quad i = j$.

where q_{ij} is the (i,j) *th* entry in the Q matrix emphasizing that P_{ij} depends only on the interval between t_1 and t_2 and not on t_1.

2. MAXIMUM LIKELIHOOD ESTIMATION OF THE Q TRANSITION RATE MATRIX

Let n_{ijr} be the number of individuals in state i at t_{r-1} and in state j at time t_r. Conditioning on the distribution of individuals among states at t_0, the likelihood function for θ is (2):

$$L(\theta) = \prod_{r=1}^{\tau} \left\{ \prod_{i,j=1}^{k=9} \left[P_{ij}(t_{r-1}, t_r) \right]^{n_{ijr}} \right\} \quad (2)$$

where k is the index of the number of states

$$\log L(\theta) = \sum_{r=1}^{\tau} \sum_{i.j=1}^{k=9} n_{ijr} \ \log\ P_{ij}(t_{r-1}, t_r) \ \ where\ \ \tau = (t_r - t_{r-1}).$$

According to Kalbfleisch and Lawless [13], applying the quasi-Newton method to estimate the rates mandates calculating the score function $S(\theta)$ (3), which is a vector–valued function for the required rates and is the first derivative of the log likelihood function. The second derivative of the probability transition function with respect to theta is assumed to be zero.

$$S(\theta) = \frac{\partial}{\partial \theta_h} \log L\ (\theta) = \sum_{r=1}^{\tau} \sum_{i,j=1}^{k} n_{ijr} \frac{\partial P_{ij}(\tau) / \partial \theta_h}{P_{ij}(\tau)}\ ,$$

$$h = 1, \ldots, 22 \ \ while\ P_{ij}(\tau) = \frac{n_{ijr}}{n_{i+}},\ such\ that\ \ n_{i+} = \sum_{j=1}^{k} n_{ijr}.$$

$$S(\theta) = \tau\ e^{\Lambda \tau} d\Lambda \quad (3)$$

where $S(\theta)$ *is the score function.*

Λ is the eigenvalue for each Q matrix in each τ (refer to **Supplementary Material Section 2**). Taking the second derivative of $\log L\ (\theta)$ (4):

$$\frac{\partial^2}{\partial \theta_g \partial \theta_h} \log L(\theta)$$

$$= \sum_{r=1}^{\tau} \sum_{i,j=1}^{k} n_{ijr} \left\{ \frac{\partial^2 P_{ij}(\tau) / \partial \theta_g \partial \theta_h}{P_{ij}(\tau)} - \frac{\partial P_{ij}(\tau) / \partial \theta_g \partial P_{ij}(\tau) / \partial \theta_h}{P_{ij}^2(\tau)} \right\} \quad (4)$$

Assuming the second derivative is zero and $\frac{n_{ijr}}{P_{ij}(\tau)} = n_{i+}$ where $n_{i+} = \sum_{j=1}^{9} n_{ij}$ then:

$$M_{ij}\ (\theta) = \frac{\partial^2}{\partial \theta_g \partial \theta_h} \log L(\theta)\ =$$

$$-\sum_{r=1}^{\tau} \sum_{i,j=1}^{k} n_{i+} \frac{\partial P_{ij}(\tau) / \partial \theta_g \partial P_{ij}(\tau) / \partial \theta_h}{P_{ij}(\tau)}.$$

The quasi-Newton formula is (5).

$$\theta_1 = \theta_0 + [M(\theta_0)]^{-1} S(\theta_0) \quad (5)$$

According to Klotz and Sharples [14], the initial $\theta_0 = \frac{n_{ijr}}{n_{i+}}$ *for* $\Delta t = 1$.

For this NAFLD process (refer to **Supplementary Material Section 2**).

3. MEAN SOJOURN TIME

It is the mean time spent by a patient in a given state i of the process. It is calculated in relation to transition rates $\hat{\theta}$. These times are independent and exponentially distributed random variables with mean $\frac{1}{\lambda_i}$ where $\lambda_i = -\lambda_{ii};\ \ i = 1, \ldots, 8$.

According to Kalbfleisch and Lawless [13], the asymptotic variance of this time is calculated by applying the multivariate delta method (6):

$$var(s_i) = \left[\left(q_{ii}\left(\hat{\theta}\right) \right)^{-2} \right]^2 \sum_{h=1}^{22} \sum_{g=1}^{22} \frac{\partial q_{ii}}{\partial \theta_g} \frac{\partial q_{ii}}{\partial \theta_h}\ [M(\theta)]^{-1}\big|_{\theta=\hat{\theta}} \quad (6)$$

where s_i *is the mean sojourn time.*

For this NAFLD process (refer to **Supplementary Material Section 3**).

4. STATE PROBABILITY DISTRIBUTION

According to Cassandras and Lafortune [15], it is the probability distribution for each state at a specific time point given the initial probability distribution. Thus, using the rule of total probability, a solution describing the transient behavior of a chain characterized by Q and an initial condition $\pi\ (0)$ is obtained by direct substitution to solve (7):

$$\pi\ (t) = \pi\ (0)\, P\,(t)\,. \tag{7}$$

The stationary probability distribution when t goes to infinity or, in other words, when the process does not depend on time is obtained by differentiating both sides of the following Equation (8):

$$\pi\ (t) = \pi\ (0)\, P\,(t) = \pi\ (0)\, e^{Qt} \tag{8}$$

differentiate both sides to obtain $\left.\frac{d}{dt}\pi\ (t)\right|_{t=0} = \pi\ (0)\, Q.$

$$\left.\frac{d}{dt}\pi_i\,(t)\right|_{t=0}$$

$$= \begin{bmatrix}\pi_{0(1)} & \pi_{0(2)} & \pi_{0(3)} & \pi_{0(4)} & \pi_{0(5)} & \pi_{0(6)} & \pi_{0(7)} & \pi_{0(8)} & \pi_{0(9)}\end{bmatrix} \times$$

$$\begin{bmatrix} -\gamma_1 & \lambda_{12} & 0 & 0 & 0 & 0 & 0 & \lambda_{18} & \lambda_{19} \\ \mu_{21} & -\gamma_2 & \lambda_{23} & 0 & 0 & 0 & 0 & \lambda_{28} & \lambda_{29} \\ 0 & \mu_{32} & -\gamma_3 & \lambda_{34} & 0 & 0 & 0 & \lambda_{38} & \lambda_{39} \\ 0 & 0 & \mu_{43} & -\gamma_4 & \lambda_{45} & 0 & 0 & \lambda_{48} & \lambda_{49} \\ 0 & 0 & 0 & 0 & -\gamma_5 & \lambda_{56} & 0 & \lambda_{58} & \lambda_{59} \\ 0 & 0 & 0 & 0 & 0 & -\gamma_6 & \lambda_{67} & 0 & \lambda_{69} \\ 0 & 0 & 0 & 0 & 0 & 0 & -\lambda_{79} & 0 & \lambda_{79} \\ 0 & 0 & 0 & 0 & 0 & 0 & 0 & -\lambda_{89} & \lambda_{89} \\ 0 & 0 & 0 & 0 & 0 & 0 & 0 & 0 & 0 \end{bmatrix}.$$

$\begin{bmatrix}\pi_1 & \pi_2 & \pi_3 & \pi_4 & \pi_5 & \pi_6 & \pi_7 & \pi_8 & \pi_9\end{bmatrix}$ at a specific time point is obtained by solving this system of differential equations. Solving these differential equations for this complex chain is cumbersome.

If the limit of $\pi_z = \lim_{t\to\infty}\pi_z\,(t)$ exists, then there is a stationary or steady state distribution, and as $t \to \infty$, $\frac{d}{dt}\pi_j\,(t) = 0$, since $\pi_z\,(t)$ does not depend on time. Therefore, $\frac{d}{dt}\pi\ (t) = \pi\ (t)\, Q$ will reduce to $\pi\ (t)\, Q = 0$. The stationary state probability distribution is obtained by solving $\pi(t)Q = 0$ subject to $\sum_{all\ z}\pi_z = 1$.

For this NAFLD process (refer to **Supplementary Material Section 4**).

4.1. Asymptotic Covariance of the State Probability Distribution

The multivariate delta method is applied to the following function $Q'\pi = F\,(\theta_h, \pi_i) = 0$ to obtain the asymptotic covariance matrix of the state probability distribution, as π is not a simple function of theta.

Differentiating $F\,(\theta_h, \pi_i)$ implicitly with respect to θ_h is used in the following manner (9):

$$\frac{\partial}{\partial\theta_h}F\,(\theta_h, \pi_i) = \frac{\partial}{\partial\theta_h}Q'\pi_i = 0. \tag{9}$$

$$\frac{\partial}{\partial\theta_h}Q'\pi_i = \left[Q'\right]\left[\frac{\partial}{\partial\theta_h}\pi_i\right] + \pi_i\left[\frac{\partial}{\partial\theta_h}Q'\right]^T = 0$$

$$let's\ call\quad \pi_i\left[\frac{\partial}{\partial\theta_h}Q'\right]^T = C\,(\theta)\,.$$

$$\left[Q'\right]\left[\frac{\partial}{\partial\theta_h}\pi_i\right] + C\,(\theta) = 0.$$

$$solving\ for\ \left[\frac{\partial}{\partial\theta_h}\pi_i\right],$$

$$\left[\frac{\partial}{\partial\theta_h}\pi_i\right] = -\left[Q'\right]^{-1} C\,(\theta)\,.$$

$$Let\ \left[\frac{\partial}{\partial\theta_h}\pi_i\right] = A\,(\theta)\,.$$

By multivariate delta method

$$var\,(\pi) = A\,(\theta)\, var\,(\theta)\, A\,(\theta)',\ \ where\ \ var\,(\theta) = [M\,(\theta)]^{-1}\,.$$

For this NAFLD process: (refer to **Supplementary Material Section 4.1**).

5. LIFE EXPECTANCY OF THE PATIENT IN THE NAFLD PROCESS

The disease process is composed of eight transient states and one absorbing state (death state). So, the Q matrix is partitioned into four sets:

$$Q = \begin{bmatrix} B & A \\ 0 & 0 \end{bmatrix},$$

where

$$B = \begin{bmatrix} -\gamma_1 & \lambda_{12} & 0 & 0 & 0 & 0 & 0 & \lambda_{18} \\ \mu_{21} & -\gamma_2 & \lambda_{23} & 0 & 0 & 0 & 0 & \lambda_{28} \\ 0 & \mu_{32} & -\gamma_3 & \lambda_{34} & 0 & 0 & 0 & \lambda_{38} \\ 0 & 0 & \mu_{43} & -\gamma_4 & \lambda_{45} & 0 & 0 & \lambda_{48} \\ 0 & 0 & 0 & 0 & -\gamma_5 & \lambda_{56} & 0 & \lambda_{58} \\ 0 & 0 & 0 & 0 & 0 & -\gamma_6 & \lambda_{67} & 0 \\ 0 & 0 & 0 & 0 & 0 & 0 & -\lambda_{79} & 0 \\ 0 & 0 & 0 & 0 & 0 & 0 & 0 & -\lambda_{89} \end{bmatrix}.$$

Additionally, the differential equations can be partitioned into the following (10):

$$\left[\acute{P}(t)\ \ \acute{P}_k\,(t)\right] = \left[P\,(t)\ \ P_k\,(t)\right]\begin{bmatrix} B & A \\ 0 & 0 \end{bmatrix} \tag{10}$$

B is the transition rate matrix among the transient states and column vector A is the transition rate from each transient state to the absorbing (death) state.

$$A = -B1^T\ such\ that 1^T is\ a\ column\ vector\ of\ (k-1)\times 1$$

$$with\ all\ its\ elements\ equal\ to\ one$$

$$\left[\acute{P}(t)\ \ \acute{P}_k\,(t)\right] = \left[P\,(t)\ \ P_k\,(t)\right]\begin{bmatrix} B & A \\ 0 & 0 \end{bmatrix} can\ be\ written\ as:$$

$$P'\,(t) = P\,(t)\, B\ and\ \acute{P}_k\,(t) = P\,(t)\, A.$$

$$The\ solution\ to\ \acute{P}\ (t) = P\,(t)\, B \quad is \quad P\,(t) = P\,(0)\, e^{Bt}$$

$$\text{then} \quad \acute{P}_k(t) = P(0)\, e^{Bt} A.$$

$$\text{and} \quad e^{Bt} = 1 + Bt + \frac{(Bt)^2}{2!} + \frac{(Bt)^3}{3!} + \frac{(Bt)^4}{4!} + \cdots = \sum_{j=0}^{\infty} \frac{(Bt)^j}{j!}.$$

If τ_k is the time taken from state i to reach the absorbing death state from the initil time

$$F_k(t) = pr[\,\tau_k \le t] = pr\left[X(t) = k\right] = P_k(t) = 1^T - P(t)\,1^T$$
$$= 1^T - P(0)\, e^{Bt} 1^T.$$

The moment theory for the Laplace transform can be used to obtain the mean of the time that has the above cumulative distribution function. CTMC can be written in a Laplace transform (11) such that:

$$\left[sP^*(s) - P(0)\;\; sP^*{}_k(s)\right] = \left[P^*(s)\;\; P^*{}_k(s)\right] \begin{bmatrix} B & A \\ 0 & 0 \end{bmatrix} \quad (11)$$
$$\therefore\; sP^*(s) - P(0) = P^*(s)\, B \; and \; sP^*{}_k(s) = P^*(s)\, A.$$

Rearrange:

$$\therefore\; sP^*(s) - P^*(s)\, B = P(0).$$
$$P^*(s)\,[sI - B] = P(0) \rightarrow \quad P^*(s) = P(0)\,[sI - B]^{-1}.$$
$$\therefore\; sP^*{}_k(s) = P^*(s)\, A \;\; \rightarrow P^*{}_k(s)$$
$$= \frac{1}{s}\; P^*(s)\; A = \frac{1}{s}\; P(0)\,[sI - B]^{-1} A.$$
$$F^*{}_k(s) = \frac{1}{s}\; P(0)\,[sI - B]^{-1} A.$$
$$f^*{}_k(s) = s\, F^*{}_k(s) = P(0)\,[sI - B]^{-1} A;$$
$$where\; A = -B1^T.$$

Mean time to absorption:

$$E(\tau_k) = (-1)\; \frac{df^*{}_k(s)}{ds}\bigg|_{s=0} = (-1)\; P(0)\,[sI - B]^{-2} A\big|_{s=0}$$
$$= P(0)\,[-B]^{-1}\, 1^T.$$

For this NAFLD process: (refer to **Supplementary Material Section 5**).

6. EXPECTED NUMBER OF PATIENTS IN EACH STATE

Let $u(0)$ be the size of patients in a specific state at a specific time $t = 0$. The initial size of patients $U(0) = u_j(0)$, as there are eight transient states and one absorbing state, where $u_j(0)$ is the initial size or number of patients in state j at time $t = 0$ given that $u_9(0) = 0$, i.e., the initial size of patients in state 9 (absorbing death state) is zero at initial time point $t = 0$. As the transition or the movement of the patients among states is independent, at the end of the whole time interval $(0, t)$ and according to Chiang [16], there will be $u_j(t)$ patients in the transient states at time t, and there will also be $u_9(t)$patients in state 9 (death state) at time t.

$$E\left[u_j(t)\,|u_j(0)\right] = \sum_{j=1, i=1}^{9} u_j(0)\, P_{ij}(t),$$
$$i \;\&\; j = 1, \ldots, 9$$

For this NAFLD process: (refer to **Supplementary Material Section 6**).

7. HYPOTHETICAL NUMERICAL EXAMPLE

To illustrate the above concepts and discussion, a hypothetical numerical example is introduced. It does not represent real data but it is for demonstrative purposes (refer to **Supplementary Material Section 7**).

A study was conducted over 15 years on 1,050 patients with risk factors for developing NAFLD such as type 2 diabetes mellitus, obesity, and hypertension acting alone or together as a metabolic syndrome. The patients were scheduled to be followed up every year by a liver biopsy to identify the NAFLD cases, but the actual observations were recorded as shown in the (**Supplementary Material**). **Table 1** shows the observed transition counts.

The observed transition rate matrix Q over the whole period of the study (15 years) is:

$$Q = \begin{bmatrix} -0.3931 & 0.3864 & 0 & 0 & 0 & 0 & 0 & 0 & 0.0067 \\ 0.018 & -0.2808 & 0.25 & 0 & 0 & 0 & 0 & 0 & 0.0128 \\ 0 & 0.05 & -0.3717 & 0.2248 & 0 & 0 & 0 & 0.05 & 0.0469 \\ 0 & 0 & 0.0458 & -0.5502 & 0.2844 & 0 & 0 & 0.11 & 0.11 \\ 0 & 0 & 0 & 0 & -0.346 & 0.188 & 0 & 0.059 & 0\;0.099 \\ 0 & 0 & 0 & 0 & 0 & -0.9375 & 0.75 & 0 & 0.1875 \\ 0 & 0 & 0 & 0 & 0 & 0 & -0.423 & 0 & 0.423 \\ 0 & 0 & 0 & 0 & 0 & 0 & 0 & -0.7419 & 0.7419 \\ 0 & 0 & 0 & 0 & 0 & 0 & 0 & 0 & 0 \end{bmatrix}$$

TABLE 1 | The observed transition counts in the whole period of the study (15 years) regardless of the time interval between observations.

	State 1	State 2	State 3	State 4	State 5	State 6	State 7	State 8	State 9	Total
State 1	1,175	859	112	32	30	0	0	0	15	2,223
State 2	14	498	195	31	28	0	0	0	10	776
State 3	6	15	152	67	29	0	0	15	14	298
State 4	0	0	5	49	31	0	0	12	12	109
State 5	0	0	0	0	51	19	15	6	10	101
State 6	0	0	0	0	0	1	12	0	3	16
State 7	0	0	0	0	0	0	15	0	11	26
State 8	0	0	0	0	0	0	0	8	23	31
State 9	0	0	0	0	0	0	0	0	0	0

The estimated transition rate matrix $\hat{Q}$ is:

$$\hat{Q} = \begin{bmatrix} -0.397 & 0.39 & 0 & 0 & 0 & 0 & 0 & 0 & 0.007 \\ 0.02 & -0.281 & 0.25 & 0 & 0 & 0 & 0 & 0 & 0.011 \\ 0 & 0.05 & -0.365 & 0.225 & 0 & 0 & 0 & 0.047 & 0.043 \\ 0 & 0 & 0.041 & -0.538 & 0.281 & 0 & 0 & 0.109 & 0.107 \\ 0 & 0 & 0 & 0 & -0.348 & 0.19 & 0 & 0.059 & 0.099 \\ 0 & 0 & 0 & 0 & 0 & -0.934 & 0.767 & 0 & 0.167 \\ 0 & 0 & 0 & 0 & 0 & 0 & -0.421 & 0 & 0.421 \\ 0 & 0 & 0 & 0 & 0 & 0 & 0 & -0.745 & 0.745 \\ 0 & 0 & 0 & 0 & 0 & 0 & 0 & 0 & 0 \end{bmatrix}.$$

Using the above approach as illustrated in the main text and **Supplementary Materials**, the estimated $\hat{Q}$ transition rate matrix is nearly approaching equality to the observed transition rate matrix.

$$var\left(\hat{\theta}\right) = 1 \times 10^{-13} \begin{bmatrix} v_1 & v_2 \\ v_3 & v_4 \end{bmatrix}$$

where

$$v_1 = \begin{bmatrix} 0.3292 & 0.0327 & 0.4414 & 0.0827 & 0.4004 & 0.0268 & 0.2540 & 0.1517 \\ 0.0327 & 0.0064 & 0.0428 & 0.0108 & 0.0385 & 0.0053 & 0.0268 & 0.0159 \\ 0.4414 & 0.0428 & 0.5922 & 0.1100 & 0.5373 & 0.0350 & 0.3400 & 0.2032 \\ 0.0827 & 0.0108 & 0.1100 & 0.0228 & 0.0995 & 0.0088 & 0.0650 & 0.0387 \\ 0.4004 & 0.0385 & 0.5373 & 0.0995 & 0.4876 & 0.0315 & 0.3082 & 0.1843 \\ 0.0268 & 0.0053 & 0.0350 & 0.0088 & 0.0315 & 0.0044 & 0.0219 & 0.0130 \\ 0.2540 & 0.0268 & 0.3400 & 0.0650 & 0.3082 & 0.0219 & 0.1967 & 0.1174 \\ 0.1517 & 0.0159 & 0.2032 & 0.0387 & 0.1843 & 0.0130 & 0.1174 & 0.0702 \end{bmatrix}.$$

v_2 , v_3, and v_4 are all zero matrices of size (8 by 14), (14 by 8), and (14 by 14), respectively.

Transition probability matrix at 1 year:

$$P(1) = \begin{bmatrix} 0.6751 & 0.279 & 0.0345 & 0.0025 & 0.0002 & 0 & 0 & 0.0006 & 0.0082 \\ 0.0143 & 0.7625 & 0.1819 & 0.0190 & 0.0018 & 00.0001 & 0 & 0.0044 & 0.016 \\ 0.0004 & 0.0364 & 0.7017 & 0.144 & 0.0209 & 0.0012 & 0.0002 & 0.0347 & 0.0606 \\ 0 & 0.0007 & 0.0262 & 0.5868 & 0.1810 & 0.0147 & 0.0039 & 0.0630 & 0.1237 \\ 0 & 0 & 0 & 0 & 0.7061 & 0.1015 & 0.0416 & 0.0344 & 0.1163 \\ 0 & 0 & 0 & 0 & 0 & 0.3930 & 0.3938 & 0 & 0.2132 \\ 0 & 0 & 0 & 0 & 0 & 0 & 0.6564 & 0 & 0.3436 \\ 0 & 0 & 0 & 0 & 0 & 0 & 0 & 0.4747 & 0.5253 \\ 0 & 0 & 0 & 0 & 0 & 0 & 0 & 0 & 1 \end{bmatrix}.$$

Mean time spent by the patient in state 1 is ∼2 years and 6 months; in state 2, the mean sojourn time is ∼3 years and 6 months; in state 3, it is ∼2 years and 9 months; in state 4, it is ∼1 year and 10 months; in state 5, it is ∼2 years and 10 months; in state 6, it is ∼1 year and 1 month; in state 7, it is ∼2 years and 5 months and last; in state 8, the mean sojourn time is ∼1 year and 4 months.

If a cohort of 5,000 patients with NAFLD has an initial distribution of $\begin{bmatrix}0.62 & 0.22 & 0.081 & 00.03 & 0.028 & 0.005 & 00.007 & 0.009 & 0\end{bmatrix}$ and the initial counts of patients in each state are $\begin{bmatrix}3100 & 1100 & 405 & 150 & 140 & 25 & 35 & 45 & 0\end{bmatrix}$, then at 1 year, the state probability distribution is $\begin{bmatrix}00.4217 & 0.3437 & 0.1191 & 00.035 & 0.0274 & 0.0054 & 00.0079 & 0.0112 & 0.0287\end{bmatrix}$ and the expected counts of patients are $\begin{bmatrix}2109 & 1718 & 595 & 175 & 137 & 27 & 39 & 56 & 144\end{bmatrix}$.

To calculate the goodness of fit for the multistate model used in this example, it is similar to the procedure used in the contingency table, and it is calculated in each interval and then summed:

Step 1: $H_0 =$ *future state does not depend on the current state.* $H_1 =$ *future state depends on the current state .*

Step 2: Calculate the $P_{ij}\,(\Delta t = 1)$

$$P_{ij}\,(\Delta t = 1) = \begin{bmatrix} 0.6751 & 0.279 & 0.0345 & 0.0025 & 0.0002 & 0 & 0 & 0.0006 & 0.0082 \\ 0.0143 & 0.7625 & 0.1819 & 0.0190 & 0.0018 & 0.0001 & 0 & 0.0044 & 0.016 \\ 0.0004 & 0.0364 & 0.7017 & 0.144 & 0.0209 & 0.0012 & 0.0002 & 0.0347 & 0.0606 \\ 0 & 0.0007 & 0.0262 & 0.5868 & 0.1810 & 0.0147 & 0.0039 & 0.0630 & 0.1237 \\ 0 & 0 & 0 & 0 & 0.7061 & 0.1015 & 0.0416 & 0.0344 & 0.1163 \\ 0 & 0 & 0 & 0 & 0 & 0.3930 & 0.3938 & 0 & 0.2132 \\ 0 & 0 & 0 & 0 & 0 & 0 & 0.6564 & 0 & 0.3436 \\ 0 & 0 & 0 & 0 & 0 & 0 & 0 & 0.4747 & 0.5253 \\ 0 & 0 & 0 & 0 & 0 & 0 & 0 & 0 & 1 \end{bmatrix}.$$

Step 3: Calculate the expected counts in this interval by multiplying each row in the probability matrix with the corresponding total marginal counts in the observed transition counts matrix in the same interval to obtain the expected counts.

	State 1	State 2	State 3	State 4	State 5	State 6	State 7	State 8	State 9	Total
State 1	1000.5	413.5	51.13	3.705	0.3	0	0	0.8892	12.15	1482
State 2	7.4074	394.97	94.22	9.842	0.9324	0.0518	0	2.2792	8.288	518
State 3	0.08	7.28	140.34	28.8	4.18	0.24	0.04	6.94	12.12	200.02
State 4	0	0.0511	1.9126	42.8364	13.213	1.0731	0.2847	4.599	9.0301	73
State 5	0	0	0	0	47.3087	6.8005	2.7872	2.3048	7.7921	66.9933
State 6	0	0	0	0	0	3.93	3.938	0	2.132	10
State 7	0	0	0	0	0	0	11.1588	0	5.8412	17
State 8	0	0	0	0	0	0	0	9.494	10.506	20
State 9	0	0	0	0	0	0	0	0	0	0

Step 4: Apply $\sum_{i=1}^{9}\sum_{j=1}^{9}\frac{(O_{ij}-E_{ij})^2}{E_{ij}} = 2219.118 \sim \chi^2_{(9-1)(9-1)(0.05)}$.

The same steps are used for the observed transition counts in $\Delta t = 2$ and $\Delta t = 3$ with the following results:

$$P_{ij}\,(\Delta t = 2) = \begin{bmatrix} 0.4597 & 0.4023 & 0.0984 & 0.0134 & 0.0019 & 0.0001 & 0.0000 & 0.0032 & 0.0210 \\ 0.0206 & 0.5920 & 0.2674 & 0.0519 & 0.0099 & 0.0008 & 0.0002 & 0.013 & 0.0442 \\ 0.001 & 0.0535 & 0.5028 & 0.1862 & 0.0555 & 0.0055 & 0.0022 & 0.0508 & 0.1425 \\ 0 & 0.0019 & 0.0339 & 0.3481 & 0.2345 & 0.0328 & 0.0182 & 0.074 & 0.2566 \\ 0 & 0 & 0 & 0 & 0.4986 & 0.1116 & 0.0967 & 0.0406 & 0.2525 \\ 0 & 0 & 0 & 0 & 0 & 0.1544 & 0.4133 & 0 & 0.4323 \\ 0 & 0 & 0 & 0 & 0 & 0 & 0.4308 & 0 & 0.5692 \\ 0 & 0 & 0 & 0 & 0 & 0 & 0 & 0.2254 & 0.7746 \\ 0 & 0 & 0 & 0 & 0 & 0 & 0 & 0 & 1 \end{bmatrix}.$$

The expected counts are:

	State 1	State 2	State 3	State 4	State 5	State 6	State 7	State 8	State 9	Total
State 1	272.6	238.56	58.351	7.946	1.1267	0.0593	0	1.8976	12.453	593
State 2	4.2642	122.54	55.35	10.743	2.0493	0.1656	0.0414	2.691	9.1494	207
State 3	0.08	4.28	40.224	14.896	4.44	0.44	0.176	4.064	11.4	80
State 4	0	0.0551	0.9831	10.0949	6.8005	0.9512	0.5278	2.146	7.4414	29
State 5	0	0	0	0	13.4622	3.0132	2.6109	1.0962	6.818	27
State 6	0	0	0	0	0	0.6176	1.6532	0	1.729	4
State 7	0	0	0	0	0	0	3.0156	0	3.984	7
State 8	0	0	0	0	0	0	0	1.8032	6.197	8
State 9	0	0	0	0	0	0	0	0	0	0

$applying: \sum_{i=1}^{9}\sum_{j=1}^{9}\frac{(O_{ij}-E_{ij})^2}{E_{ij}} = 158.571 \sim \chi^2_{(9-1)(9-1)(0.05)}$.

The same steps are used for the observed transition counts $\Delta t = 3$ in with the following results:

$$P_{ij}\,(\Delta t = 3) = \begin{bmatrix} 0.3161 & 0.4386 & 0.1584 & 0.0308 & 0.0066 & 0.0006 & 0.0002 & 0.0079 & 0.0408 \\ 0.0225 & 0.4669 & 0.2974 & 0.0803 & 0.023 & 0.0024 & 0.0011 & 0.0217 & 0.0847 \\ 0.0016 & 0.0595 & 0.3675 & 0.1827 & 0.0835 & 0.0111 & 0.0068 & 0.0555 & 0.2319 \\ 0.0001 & 0.0029 & 0.0333 & 0.2092 & 0.2293 & 0.0418 & 0.036 & 0.0663 & 0.3811 \\ 0 & 0 & 0 & 0 & 0.352 & 0.0945 & 0\ .1282 & 0.0364 & 0.3889 \\ 0 & 0 & 0 & 0 & 0 & 0.0607 & 0.3321 & 0 & 0.6072 \\ 0 & 0 & 0 & 0 & 0 & 0 & 0.2828 & 0 & 0.7172 \\ 0 & 0 & 0 & 0 & 0 & 0 & 0 & 0.107 & 0.893 \\ 0 & 0 & 0 & 0 & 0 & 0 & 0 & 0 & 1 \end{bmatrix}.$$

The expected counts are:

	State 1	State 2	State 3	State 4	State 5	State 6	State 7	State 8	State 9	Total
State 1	46.783	64.913	23.443	4.5584	0.9768	0.0888	0.0296	1.1692	6.0384	148
State 2	1.148	23.812	15.1674	4.0953	1.173	0.1224	0.0561	1.1067	4.3197	51
State 3	0.0288	1.071	6.615	3.2886	1.503	0.1998	0.1224	0.999	4.1742	18
State 4	0.0007	0.0203	0.2331	1.4644	1.6051	0.2926	0.252	0.4641	2.6677	7
State 5	0	0	0	0	2.464	0.6615	0.8974	0.2548	2.7223	7
State 6	0	0	0	0	0	0.1214	0.6642	0	1.2144	2
State 7	0	0	0	0	0	0	0.5656	0	1.4344	2
State 8	0	0	0	0	0	0	0	0.321	2.679	3
State 9	0	0	0	0	0	0	0	0	0	0

$applying: \sum_{i=1}^{9}\sum_{j=1}^{9}\frac{(O_{ij}-E_{ij})^2}{E_{ij}} = 65.37 \sim \chi^2_{(9-1)(9-1)(0.05)}$.

Step 5: Sum up the above results to get:

$$\sum_{i=1}^{9}\sum_{j=1}^{9}\sum_{l=1}^{t=3}\frac{\left(O_{ijl}-E_{ijl}\right)^2}{E_{ijl}} = 2443.06 \sim \chi^2_{(df=192)(0.05)}.$$

Therefore, from the above results, the null hypothesis is rejected, whereas the alternative hypothesis is accepted, and the model fits the data to mean that the future state depends on the current state with the estimated transition rate and probability matrices as obtained.

8. CONCLUSION AND SUMMARY

Continuous time Markov chains are suitable mathematical and statistical tools to be used for the analysis of disease evolution over time. CTMCs are the type of multistate model utilized to study this evolution in patients with NAFLD, with the main phenotypes being NAFL and NASH, as well as to study the associated presence of fibrosis and its stages. The prevalence of NAFLD is rapidly increasing worldwide and parallels the epidemics of obesity and type 2 diabetes. Metabolic syndrome is a well-known risk factor.

In this study, NAFLD is modeled in a more elaborative expanded form, which includes nine states: the first eight states are the states of disease progression as time elapses, while the ninth state is the death state. The importance of such analysis is that health policy makers can predict the number of affected patients at each stage, the needed investigations and medications for each of them, and the costs and budgets that medical insurance should assign to this disease burden. This analysis is of great value and benefit to physicians, as they can conduct longitudinal studies to explore further investigations that better define each stage specifically and efficiently and to explore further treatment needed for each stage. An example of a non-invasive diagnostic tool is the circulating level of cytokeratin-18 fragments; although promising, it is not available in a clinical care setting, and there is no established cutoff value for identifying NASH [17]. Genetic polymorphism of patatin-like phospholipase domain-containing protein 3 gene variants (PNPLA-3) is associated with NASH and advanced fibrosis; however, testing for these variants in routine clinical care is not supported and needs further study.

A hypothetical example of factitious non-real data is used to emphasize the attributes that need to be estimated:

- Transition rate matrix among the various states.
- Transition probability matrix among states.
- Mean sojourn time in each state.
- Life expectancy in each state; in other words, mean time to absorption (death state).
- Expected number of patients in each state.
- State probability distribution at specific time points in the future.

Such analysis may give better insights to physicians, especially when new drug classes will soon be released on the market. What drug classes are to be used first? How can the disease be monitored throughout the journey of treatment? What investigations are to be used in such monitoring? How to modify the drug treatment? What is the target that needs to be achieved, and how can this target be maintained? Moreover, in the late stage of the disease, when patients suffer from decompensated liver cirrhosis, liver transplantation is the treatment of choice to such patients, which increases the economic burden of NAFLD, as was the disease course during treatment in the early stages. Additionally, a load of what are the best economic non-invasive tests to be used in primary health care units for stratification and identification of high-risk patients, whether to perform genetic tests in health insurance settings, and when to refer for liver biopsy in secondary or special clinics should be considered. All these questions can be answered from longitudinal studies conducted on susceptible individuals. Over and above, some of the recently investigated non-invasive scoring systems of fibrosis need further external validation to be generalized in ethnicities other than the one tested upon. There are some controversies regarding the cutoff points of these scoring systems among countries and ethnicities within the same country. Although liver biopsy is considered the standard method for the diagnosis of NAFLD and staging it, its limitations encourage the development of various non-invasive tests, which necessitate better correlation between the findings obtained from the biopsy and the results of these tests to minimize misclassification errors, which hamper good diagnosis and prognosis of the patient. These tests should be easy, feasible, convenient, and have a high safety profile to be used repeatedly in patients for follow-up in such longitudinal studies.

A multistate model represented by CTMC is a valuable statistical methodology for longitudinal studies in medical research to better comprehend and understand the pathophysiology or the mechanism of the NAFLD process, and the interactions between the different modifiers, either external or internal modifiers. The external modifiers reside in bad dietary habits with excessive fat and carbohydrate ingestion, and sedentary life, whereas the internal modifiers are represented in genetic factors affecting the metabolism of the food stuff (fat and carbohydrates) and other cellular functions, such as risk factors for fibrogenesis (formation of fibrous tissue); fibrosis is a detrimental predictor factor for disease progression to liver cirrhosis and its complications. The importance of such understanding has a great impact on revealing the genes that must be tested if ever needed, for whom to do such a test, and should it be in the utilities or services offered by medical insurance. Moreover, should the degradation byproducts resulting from extracellular matrix destruction be used in routine clinical practice to mirror the fibrosis stages?

In Egypt, there are scarce data or maybe no available data about the prevalence of NAFLD and its phenotypes. Guidelines for risk stratification and identification are also lacking. Thus, more longitudinal studies are needed to address these issues.

Multistate models can also be used for the analysis of competing risks of death in such patients, as the first and second most common causes of death in patients with NAFLD are cardiovascular diseases (CVDs) and kidney diseases, whereas liver-related mortality is the third most common cause of death.

Other statistical methodologies, such as semi-Markov and hidden Markov chains, can be used to model NAFLD, especially hidden Markov CTMC can be used to model misclassification errors encountered in studies analyzed by time-homogenous CTMC.

Hint: A MATLAB code is edited to calculate the statistical indices in the hypothetical example. The code can be found published in the code ocean site with the following URL: https://codeocean.com/capsule/7628018/tree/v3; doi: 10.24433/CO.7719785.v3.

AUTHOR CONTRIBUTIONS

IA carried the conceptualization by formulating the goals, aims of the research article, formal analysis by applying the statistical, mathematical and computational techniques to synthesize and analyze the hypothetical data, carried the methodology by creating the model, software programming and implementation, supervision, writing, drafting, editing, preparation, and creation of the presenting work.

SUPPLEMENTARY MATERIAL

The Supplementary Material for this article can be found online at: https://www.frontiersin.org/articles/10.3389/fams.2021.766085/full#supplementary-material

Supplementary Data-sheet 1 | Excel sheet for the timeline of the participants.

Supplementary Data-sheet 2 | Supplementary material for the simple data model.

Supplementary Data-sheet 3 | Supplementary material for the expanded model.

Supplementary Data-sheet 4 | MATLAB code, Appendix A (rate) and Appendix B (probability).

REFERENCES

1. Estes C, Razavi H, Loomba R, Younossi Z, Sanyal AJ. Modeling the epidemic of nonalcoholic fatty liver disease demonstrates an exponential increase in burden of disease. *Hepatology.* (2018) 67:123–33. doi: 10.1002/hep.29466
2. Younossi ZM, Blissett D, Blissett R, Henry L, Stepanova M, Younossi Y, et al. The economic and clinical burden of nonalcoholic fatty liver disease in the United States and Europe. *Hepatology.* (2016) 64:1577–86. doi: 10.1002/hep.28785
3. Chalasani N, Younossi Z, Lavine JE, Charlton M, Cusi K, Rinella M, et al. The diagnosis and management of nonalcoholic fatty liver disease: practice guidance from the American Association for the Study of Liver Diseases. *Hepatology.* (2018) 67:328–57. doi: 10.1002/hep.29367
4. Association E, Association E, Easd D, Association E, Easo O. Clinical practice guidelines EASL – EASD – EASO clinical practice guidelines for the management of non-alcoholic fatty liver disease q. *J Hepatol.* (2016) 64:1388–402. doi: 10.1016/j.jhep.2015.11.004
5. Attia IM. Continuous time markov chains for analysis of non-alcoholic fatty liver disease evolution. *Int J Res Eng Sci.* (2021) 9:1–23.
6. Chalasani N, Wilson L, Kleiner DE, Cummings OW, Brunt EM, Ünalp A, et al. Relationship of steatosis grade and zonal location to histological features of steatohepatitis in adult patients with non-alcoholic fatty liver disease. *J Hepatol.* (2008) 48:829–34. doi: 10.1016/j.jhep.2008.01.016
7. Reeder SB, Cruite I, Hamilton G, Sirlin CB. Quantitative assessment of liver fat with magnetic resonance imaging and spectroscopy. *J Magn Reson Imag.* (2011) 34:729–49. doi: 10.1002/jmri.22580
8. Idilman IS, Keskin O, Celik A, Savas B, Halil Elhan A, Idilman R, et al. A comparison of liver fat content as determined by magnetic resonance imaging-proton density fat fraction and MRS versus liver histology in non-alcoholic fatty liver disease. *Acta radiol.* (2016) 57:271–8. doi: 10.1177/0284185115580488
9. Noureddin M, Lam J, Peterson MR, Middleton M, Hamilton G, Le T, et al. Utility of magnetic resonance imaging versus histology for quantifying changes in liver fat in nonalcoholic fatty liver disease trials. *Hepatology.* (2013) 58:1930–40. doi: 10.1002/hep.26455
10. Lédinghen Vde, Wong GL, Vergniol J, Chan HL, Hiriart J, Chan AW, et al. Controlled attenuation parameter for the diagnosis of steatosis in non-alcoholic fatty liver disease. *J Gastroenterol Hepatol.* (2016) 31:848–55. doi: 10.1111/jgh.13219
11. Paul J. Recent advances in non-invasive diagnosis and medical management of non-alcoholic fatty liver disease in adult. *Egypt Liv J.* (2020) 10:43. doi: 10.1186/s43066-020-00043-x
12. Dongiovanni PM, Anstee Q, Valenti L. Genetic predisposition in NAFLD and NASH: impact on severity of liver disease and response to treatment. *Curr Pharmaceut Design.* (2013) 19:5219–38. doi: 10.2174/1381612811319990381
13. Kalbfleisch JD, Lawless JF. The analysis of panel data under a Markov assumption. *J Am Stat Assoc.* (1985) 80:863–71. doi: 10.1080/01621459.1985.10478195
14. Klotz JH, Sharples LD. Estimation for a Markov heart transplant model. *J Royal Statist Soc Ser D.* (1994) 43:431–8. doi: 10.2307/2348579
15. Cassandras CG, Lafortune S. *Introduction to Discrete Event Systems*. Berlin: Springer Science & Business Media (2009). doi: 10.1007/978-0-387-68612-7
16. Chiang CL. *Introduction to Stochastic Processes in Biostatistics*. Hoboken, NJ: Wiley, & Sons, Inc. (1968).
17. Musso G, Gambino R, Cassader M, Pagano G. Meta-analysis: natural history of non-alcoholic fatty liver disease (NAFLD) and diagnostic accuracy of non-invasive tests for liver disease severity. *Ann Med.* (2011) 43:617–49. doi: 10.3109/07853890.2010.518623

Conflict of Interest: The author declares that the research was conducted in the absence of any commercial or financial relationships that could be construed as a potential conflict of interest.

Publisher's Note: All claims expressed in this article are solely those of the authors and do not necessarily represent those of their affiliated organizations, or those of the publisher, the editors and the reviewers. Any product that may be evaluated in this article, or claim that may be made by its manufacturer, is not guaranteed or endorsed by the publisher.

frontiers in Applied Mathematics and Statistics

ORIGINAL RESEARCH
published: 30 March 2022
doi: 10.3389/fams.2022.847896

On the Global Positivity Solutions of Non-homogeneous Stochastic Differential Equations

Farai Julius Mhlanga and Lazarus Rundora*

Department of Mathematics and Applied Mathematics, University of Limpopo, Turfloop Campus, Sovenga, South Africa

In this article, we treat the existence and uniqueness of strong solutions to the Cauchy problem of stochastic equations of the form $dX_t = \alpha X_t\,dt + \sigma X_t^{\gamma}\,dB_t, X_0 = x > 0$. The construction does not require the drift and the diffusion coefficients to be Lipschitz continuous. Sufficient and necessary conditions for the existence of a global positive solution of non-homogeneous stochastic differential equations with a non-Lipschitzian diffusion coefficient are sought using probabilistic arguments. The special case $\gamma = 2$ and the general case, that is, $\gamma > 1$ are considered. A complete description of every possible behavior of the process X_t at the boundary points of the state interval is provided. For applications, the Cox-Ingersoll-Ross model is considered.

Keywords: geometric Brownian motion, Itô diffusion, Lipschitz continuous, scale function, speed measure

OPEN ACCESS

Edited by:
Ramoshweu Solomon Lebelo, Vaal University of Technology, South Africa

Reviewed by:
Yubin Yan, University of Chester, United Kingdom
Eduardo S. Zeron, Instituto Politécnico Nacional de México (CINVESTAV), Mexico

****Correspondence:***
Farai Julius Mhlanga
farai.mhlanga@ul.ac.za

Specialty section:
This article was submitted to Dynamical Systems, a section of the journal Frontiers in Applied Mathematics and Statistics

Received: *03 January 2022*
Accepted: *21 February 2022*
Published: *30 March 2022*

Citation:
Mhlanga FJ and Rundora L (2022) On the Global Positivity Solutions of Non-homogeneous Stochastic Differential Equations. Front. Appl. Math. Stat. 8:847896. doi: 10.3389/fams.2022.847896

1. INTRODUCTION

The theory of stochastic differential equations was developed by [1]. Stochastic differential equations are valuable tools for modeling systems and processes with stochastic disturbances in many fields of science and engineering. For the general theory of stochastic differential equations, one can refer to [2–5]. Several authors have discussed results concerning the existence and uniqueness of solutions of stochastic differential equations [2, 6, 7]. Mishura and Posashkova [8] provided a sufficient condition on coefficients which ensures almost surely positivity of the trajectories of the solution of the stochastic differential equation with non-homogeneous coefficients and non-Lipschitz diffusion. Appleby et al. [9] investigated highly non-linear stochastic differential equations with delays and showed that properties on the coefficients of stochastic differential equations that guarantee stability also guarantee positivity of solutions as long as the initial value is non-zero. Xu et al. [10] investigated the global positive solution of a stochastic differential equation, where they generalized the mean-reverting constant elasticity of variance process by replacing the constant parameters with the parameters modulated by a continuous-time, finite-state, Markov chain. Zhang [11] treated the properties of solutions to stochastic differential equations with Sobolev diffusion coefficients and singular drifts. Bae et al. [12] proved the existence of and uniqueness of solution to stochastic differential equations under weakened and Hölder conditions and a weakened linear growth condition. Conditions for positivity of solutions of fractional stochastic differential equations with coefficients that do not satisfy the linear growth Lipschitz continuous conditions were obtained by [13].

The aim of this article is to prove the existence of a global positive solution of stochastic differential equations of the form

$$\mathrm{d}X_t = \alpha X_t\,\mathrm{d}t + \sigma X_t^{\gamma}\,\mathrm{d}B_t, X_0 = x > 0, \tag{1}$$

where B_t is a standard Brownian motion, for different values of γ where α denotes the drift, σ denotes the volatility. $X = (X_t)_{t\geq 0}$ describes the underlying asset price. Such stochastic differential equations arise in modeling asset prices and interest rates on financial markets and it is crucial that X_t never becomes negative. Mao and Yuan [2] discussed the analytical properties when $\frac{1}{2} \leq \gamma \leq 1$ and showed that for a given initial value $X_0 = x > 0$, the solution of (1) remains positive with probability 1, namely, $X_t > 0$ for all $t \geq 0$ almost surely. The cases $\gamma = 0$ and $\gamma = 1$ give rise to the Ornstein-Uhlenbeck process and the Geometric Brownian motion, respectively, and this has been dealt with in the literature, see [4, 5, 14, 15]. When $\gamma > 1$, the diffusion coefficient of Equation (1) does not satisfy the linear growth condition, even though it is locally Lipschitz continuous. In view of this, it is not straightforward from the general theory of stochastic differential equations to obtain a unique global positive solution to Equation (1) that is defined for all $t \geq 0$. Nevertheless, there is a way to overcome such difficulties which we present in this article and we also provide detailed proofs that there is unique solutions to equations of the form (1). This article is an extension of the work done in [16] and [17] to non-homogeneous stochastic differential equations.

This article is structured as follows. In Section 2, we consider the existence of a positive global solution for non-homogeneous stochastic differential equations with non-Lipschitz coefficients. In particular, we treat the case $\gamma = 2$ and prove that if $\alpha \geq 0$ and $x \geq 0$ is arbitrary, then a unique strong solution of Equation (1) exists. Section 3 deals with the existence and uniqueness of a positive global solution to non-homogeneous stochastic differential equation (1). In particular, we consider the general case, that is, $\gamma > 1$. We provide a detailed proof of the existence of a unique solution to Equation (1). In Section 4, we investigate the behavior of the underlying process X_t at the boundaries of the state space $(0, \infty)$. The main tool used are simple probabilistic arguments. We only require the coefficients of our model to be continuous in the usual sense. In Section 5, we provide a brief conclusion.

2. EXISTENCE OF POSITIVE GLOBAL SOLUTIONS: $\gamma = 2$

We want to prove that a unique global positive solution to Equation (1) exists and investigate its properties. We notice that if $X_0 = x = 0$, then by strong uniqueness we have $X_t = 0$ for all $t \geq 0$. In addition, if a solution X_t exists for all $t < \tau(\omega) \leq \infty$ for some $x > 0$ and $X_T = 0$ for some $T = T(\omega) < \tau(\omega)$, then by the Strong Markov property we have$X_t = 0$ for all $t \in [T(\omega), \tau(\omega)]$. In particular, $x \geq 0$ implies that $X_t \geq 0$.

We call $(\Omega, \mathcal{F}, (\mathcal{F}_t), \mathbb{P})$ a stochastic basis if $(\Omega, \mathcal{F}, \mathbb{P})$ is a complete probability space and $(\mathcal{F}_t)$ is a right continuous filtration on Ω augmented by the $\mathbb{P}$-null sets. Let $B = (B_t)_{t\geq 0}$ be a standard Brownian motion defined on a stochastic basis $(\Omega, \mathcal{F}, (\mathcal{F}_t), \mathbb{P})$.

We consider a stochastic differential equation of the form

$$\mathrm{d}X_t = \alpha(X_t)\,\mathrm{d}t + \sigma(X_t)\,\mathrm{d}B_t, \tag{2}$$

where the coefficients $\alpha : \mathbf{R} \to \mathbf{R}$ and $\sigma : \mathbf{R} \to \mathbf{R}$ are both Borel measurable functions. By the definition of stochastic differential, Equation (2) is equivalent to the stochastic integral equation:

$$X_t = x + \int_0^t \alpha(X_s)\,\mathrm{d}s + \int_0^t \sigma(X_s)\,\mathrm{d}B_s. \tag{3}$$

Definition 2.1. *[2, p. 48] An **R**-valued stochastic process $\{X_t\}_{t\in[0,T]}$ is called a solution of Equation (2) if it has the following properties:*

1. *$\{X_t\}$ is continuous and $\mathcal{F}_t$-adapted.*
2. *$\int_0^t \mid \alpha(X_s) \mid \mathrm{d}s < \infty$ and $\int_0^t \sigma^2(X_s)\mathrm{d}s < \infty$.*
3. *Equation (3) holds for every $t \in [0, T]$ with probability* 1.

Definition 2.2. *[18, p. 167] A solution (X, B) of Equation (2) defined on $(\Omega, \mathcal{F}, (\mathcal{F}_t), \mathbb{P})$ is said to be a strong solution if X is adapted to the filtration $\{\mathcal{F}_t^B\}$, that is, the filtration of $B = (B_t)_{t\geq 0}$ completed with respect to $\mathbb{P}$.*

Definition 2.3. *[7, p. 300] A weak solution is a triple $((\Omega, \mathcal{F}, \mathbb{P}), (B, X), (\mathcal{F}_t))$ where $(\Omega, \mathcal{F}, \mathbb{P})$ is a probability space, $\{\mathcal{F}_t\}$ is a filtration of sub-σ-fields of $\mathcal{F}$ satisfying the usual conditions, X is a continuous, adapted **R**-valued process, B is the standard Brownian motion such that Equation (3) is satisfied.*

Remark 2.1.

1. Definition 2.2 says that if the probability space $(\Omega, \mathcal{F}, \mathbb{P})$, the filtration $\{\mathcal{F}_t\}_{t\geq 0}$, the Brownian motion B_t and the coefficients $\alpha(x)$ and $\sigma(x)$ are all given in advance, and then the solution X_t is constructed, such a solution is called a strong solution.
2. Definition 2.3 says that if we are only given the coefficients $\alpha(x)$ and $\sigma(x)$, and we are allowed to construct a suitable probability space, a filtration and find a solution to the Equation (2), then such a solution is called a weak solution.

A solution $\{X_t\}_{t\in[0,T]}$ is said to be unique if any other solution $\{\overline{X}_t\}$ is indistinguishable from $\{X_t\}$, that is

$$\mathbb{P}(X_t = \overline{X}_t \ \ \forall\ 0 \leq t \leq T) = 1.$$

Following [19], we impose the following hypothesis:

(H) The drift coefficient is globally Lipschitz, that is, for all $x, y \in \mathbf{R}$,

$$\mid \alpha(x) - \alpha(y) \mid \leq K \mid x - y \mid \tag{4}$$

where K is a fixed constant, while the diffusion coefficient is globally Hölder continuous, that is, for all $x, y \in \mathbf{R}$,

$$\mid \sigma(x) - \sigma(y) \mid \leq h(\mid x - y \mid) \tag{5}$$

where $h:[0,\infty) \rightarrow [0,\infty)$ is a strictly increasing function with $h(0) = 0$ and the integral

$$\int_0^{\varepsilon} \frac{du}{h^2(u)} = \infty, \quad \forall \varepsilon > 0.$$

It is known [see [19]] that under the hypothesis (H), the strong uniqueness solution holds for the stochastic differential equation (2).

For the case $\gamma = 2$, Equation (1) takes the form

$$\mathrm{d}X_t = \alpha X_t \,\mathrm{d}t + \sigma X_t^2 \,\mathrm{d}B_t. \tag{6}$$

If we let $Y_t = \ln \mid X_t \mid$ then an application of Itô's formula yields

$$\mathrm{d}Y_t = (\alpha - \frac{1}{2}\sigma^2 X_t^2)\,\mathrm{d}t + \sigma X_t \,\mathrm{d}B_t \tag{7}$$

which is equivalent to

$$\ln \mid X_t \mid = \ln \mid x \mid + \alpha t - \frac{1}{2}\sigma^2 \int_0^t X_s^2 \,\mathrm{d}s + \sigma \int_0^t X_s \,\mathrm{d}B_s. \tag{8}$$

This solution presents a challenge as the coefficients in Equation (8) do not satisfy the linear growth and Lipschitz conditions. However, there is a way to go around this. In the next result we prove the existence of a global solution to Equation (6) following arguments presented in [20].

Theorem 2.1. *Suppose $\alpha \geq 0$ and $x \geq 0$ is arbitrary, then the stochastic differential equation of the form (6) has a unique, strong solution X_t defined for all $t \geq 0$.*

Proof: The result is proved by a truncation procedure. For each $n \geq 1$, we set $\alpha = \alpha_n(x)$ and the truncation function

$$\sigma_n(x) = \begin{cases} \sigma x^2 & \text{if} \mid x \mid \leq n, \\ \sigma n^2 & \text{if} \mid x \mid > n \end{cases}.$$

Then, $\alpha_n(x)$ and $\sigma_n(x)$ satisfy the hypothesis (H). Hence, there is a unique solution $X_t = X_t^{(n)}$ defined for all t to the equation

$$X_t^{(n)} = x + \int_0^t \alpha_n(X_s^{(n)})\,\mathrm{d}s + \int_0^t \sigma_n(X_s^{(n)})\,\mathrm{d}B_s. \tag{9}$$

Define the stopping time

$$\tau_n = \inf\{t > 0; \mid X_t^{(n)} \mid \geq n\}, \quad n = 1, 2, \ldots. \tag{10}$$

Then, by strong uniqueness we have

$$X_t^{(n)}(\omega) = X_t^{(n+1)}(\omega) \text{ for all } \ t \leq \tau_n \ \ a.s. \tag{11}$$

Therefore,

$$\tau_n = \inf\{t > 0; \mid X_t^{(n)} \mid \geq n\} < \inf\{t > 0; \mid X_t^{(n+1)} \mid \geq n+1\} = \tau_{n+1}. \tag{12}$$

Hence, $\{\tau_n\}$ is an increasing sequence of stopping times. Put

$$\tau(\omega) = \lim_{n\to\infty} \tau_n(\omega) \leq \infty.$$

Then, for $t < \tau(\omega)$, a process X_t can be defined by setting

$$X_t(\omega) = X_t^{(n)}(\omega), \quad \text{if} \quad t < \tau_n(\omega). \tag{13}$$

It is clear that if $t < \tau(\omega)$ then one can easily show that $t < \tau_n(\omega)$ for some n. Therefore, by (11), this defines $X_t(\omega)$ uniquely. Hence, we have

$$X_t = x + \int_0^t \alpha X_s \,\mathrm{d}s + \int_0^t \sigma X_s^2 \,\mathrm{d}B_s \quad \text{for} \quad t < \tau(\omega). \tag{14}$$

3. EXISTENCE AND UNIQUENESS OF POSITIVE GLOBAL SOLUTION

In this section, we provide a detailed proof that there is a unique positive global solution to Equation (1). In particular, we focus on the case $\gamma > 1$. To establish the existence of a unique positive global solution, we need the following result.

Lemma 3.1. *[3, p. 57] The coefficients of Equation (1) satisfy the local Lipschitz condition for given initial condition $X_0 = x > 0$, that is, for every integer $k > 1$, there exists a positive constant L_k and $x, y \in [0, k]$ such that*

$$\mid \alpha x - \alpha y \mid^2 + \mid \sigma x^{\gamma} - \sigma y^{\gamma} \mid^2 \leq L_k \mid x - y \mid^2 . \tag{15}$$

Therefore, there exists a unique local solution to Equation (1).

We now state our result in the following theorem.

Theorem 3.1. *For any given initial value $X_0 = x > 0$, α and $\sigma > 0$ there exists a unique positive global solution X_t to Equation (1) on $t \geq 0$ for $\gamma > 1$.*

Proof: It is clear that the coefficients of Equation (1) are locally Lipschitz continuous. Therefore, for any given initial value $X_0 = x > 0$, there is a unique local solution X_t, $t \in [0, \tau(\omega)]$ of Equation (1) where $\tau(\omega)$ is the explosion time. To prove that the solution is global, it suffices to show that $\tau(\omega) = \infty$ almost surely. We prove this by contradiction. If $\tau(\omega) \neq \infty$, then we can find a pair of positive constants ϵ and T such that

$$\mathbb{P}(\tau(\omega) \leq T) > \epsilon. \tag{16}$$

For each integer $n > 1$, we define a stopping time

$$\tau_n = \inf\{t \geq 0 : \mid X_t \mid \geq n\}. \tag{17}$$

Since $\tau_n \rightarrow \tau(\omega)$ almost surely, we can find a sufficiently large n_0 for which

$$\mathbb{P}(\tau_n \leq T) > \frac{\epsilon}{2}, \quad \text{for all } \ n \geq n_0. \tag{18}$$

For $\theta, \beta > 0$, we define a function $V \in C^2$ as

$$V(X) := \theta\sqrt{X} + \beta X^{-2}, \tag{19}$$

which is continuously twice differentiable in X. We observe that $V(X) \to +\infty$ as $X \to +\infty$ or $X \to 0$. For any $0 < t < T$, an application of Itô formula gives

$$\mathrm{d}V(X_t) = \mathcal{L}V(X_t)\,\mathrm{d}t + \sigma X^{\gamma}\left(\frac{1}{2}\theta X_t^{-\frac{1}{2}} - 2\beta X_t^{-3}\right)\mathrm{d}B_t, \tag{20}$$

where

$$\begin{aligned}\mathcal{L}V(X_t) \;=\; & \alpha X_t\left(\frac{1}{2}\theta X_t^{-\frac{1}{2}} - 2\beta X_t^{-3}\right)\\ & + \frac{1}{2}\sigma^2 X_t^{2\gamma}\left(-\frac{1}{4}\theta X_t^{-\frac{2}{3}} + 6\beta X_t^{-4}\right).\end{aligned} \tag{21}$$

By boundedness of polynomials, there exists a constant K such that

$$\alpha X_t\left(\frac{1}{2}\theta X_t^{-\frac{1}{2}} - 2\beta X_t^{-3}\right) + \frac{1}{2}\sigma^2 X_t^{2\gamma}\left(-\frac{1}{4}\theta X_t^{-\frac{2}{3}} + 6\beta X_t^{-4}\right) \leq K. \tag{22}$$

Therefore, for any $t \in [0, T]$

$$\begin{aligned}\mathbf{E}[V(X_{t\wedge\tau_n})] \;=\; & V(x) + \mathbf{E}\left[\int_0^{t\wedge\tau_n} \mathcal{L}V(X_s)\,\mathrm{d}s\right] \leq V(x) + KT\\ & + K\mathbf{E}\left[\int_0^t \mathbf{E}[V(X_{s\wedge\tau_n})]\,\mathrm{d}s\right].\end{aligned} \tag{23}$$

The application of the Grownwall inequality yields

$$\mathbf{E}[V(X_{T\wedge\tau_n})] \leq [V(x) + KT]e^{KT} \tag{24}$$

which is equivalent to

$$\mathbf{E}[V(X_{\tau_n})\mathbf{1}_{\{\tau_n \leq T\}}] \leq [V(x) + KT]e^{KT}. \tag{25}$$

On the other hand, we define

$$M_n = \inf\{V(X_t) \mid X_t > n,\ t \in [0, T]\}. \tag{26}$$

As $n \to +\infty$, $M_n \to +\infty$. It now follows from (18) and (26) that

$$[V(x) + KT]e^{KT} \geq M_n\mathbb{P}(\{\tau_n \leq T\}) \geq \frac{1}{2}\epsilon M_n. \tag{27}$$

Letting $n \to +\infty$ yields a contradiction, so we must have $\tau(\omega) = \infty$ almost surely. Therefore, there exists a unique positive global solution X_t to Equation (1) for all $t \geq 0$.

4. ANALYSIS OF THE SOLUTION AT THE BOUNDARIES OF THE STATE SPACE

We now investigate the behavior of the underlying process X_t at the boundaries of the state space $(0, \infty)$ using probability arguments. X_t is the solution of the stochastic differential equation (1), where X_t is defined on the state space $(0, \infty)$, that is, the whole positive real line.

We first consider the Itô diffusion of the form

$$\mathrm{d}X_t = \alpha(X_t)\,\mathrm{d}t + \sigma(X_t)\,\mathrm{d}B_t,\ \ X_0 = x, \tag{28}$$

where $\alpha : \mathbf{R} \to \mathbf{R}$ and $\sigma : \mathbf{R} \to \mathbf{R}$ are functions satisfying the hypothesis (H). Note that here we do not have the time argument. We assume that the state space of X_t is a finite or infinite interval. Such a process is a continuous Markov process and under weak regularity conditions the drift coefficient $\alpha(x)$ and the diffusion coefficient $\sigma(x)$ are characterized, respectively, by

$$\alpha(x) = \lim_{h\downarrow 0} h^{-1}\mathbf{E}[X_h - x] \tag{29}$$

and

$$\sigma^2(x) = \lim_{h\downarrow 0} h^{-1}\mathbf{E}[(X_h - x)^2] = \lim_{h\downarrow 0} h^{-1}\mathrm{Var}(X_h). \tag{30}$$

For details about these conditions as well as the foregoing, see [21]. The above conditions can conveniently be weakened to give the following three conditions.

$$h^{-1}\mathbf{E}[(X_h - x)\mathbf{1}_{\{|X_h - x| \leq 1\}}] \to \alpha(x), \tag{31}$$

$$h^{-1}\mathbf{E}[(X_h - x)^2\mathbf{1}_{\{|X_h - x| \leq 1\}}] \to \sigma^2(x), \tag{32}$$

and

$$h^{-1}\mathbb{P}(|X_h - x| > \varepsilon) \to 0\ \ \forall\ \ \varepsilon > 0, \tag{33}$$

where $\mathbf{1}_{\{\cdot\}}$ is the indicator function. These conditions enable us to perform the analysis of (28) without assuming the Lipschitz conditions to the coefficients. We will, however, assume that $\alpha(x)$ and $\sigma(x)$ are continuous.

Fix $q \in \mathbf{R}$ and define the scale function u by

$$u(x) = \int_q^x \exp\left(-\int_q^t \frac{2\alpha(z)}{\sigma^2(z)}\,\mathrm{d}z\right)\mathrm{d}t,\quad u(q) = 0. \tag{34}$$

The function u has a continuous, strictly positive derivative and u'' exists almost everywhere and satisfies

$$u''(x) = -\frac{2\alpha(x)}{\sigma^2(x)}u'(x). \tag{35}$$

We also introduce the speed measure

$$m(dx) = \frac{2}{u'(x)\sigma^2(x)}\,\mathrm{d}x. \tag{36}$$

Now, let $p(t, x, y)$ be the transition density of X_t. Then, the Kolmogorov backward equation is given by

$$\frac{\partial p}{\partial t} = \frac{1}{2}\sigma^2(x)\frac{\partial^2 p}{\partial x^2} + \alpha(x)\frac{\partial p}{\partial x}. \tag{37}$$

At $t = 0$, $p(0, x, y) = \delta(x - y)$, where $\delta(\cdot)$ is Dirac's delta function.

Let $[a, b]$ be a fixed interval and start the process at $X_0 = x \in (a, b)$. We want to find the probability $p_+(x)$ that the process X_t hits b before it hits a. By the Markov property, we have

$$p_+(x) = \mathbf{E}[p_+(X_s)] + O\left(\mathbb{P}(|X_s - x| > \varepsilon)\right).$$

It follows from Equation (33) that

$$s^{-1}\left(\mathbb{P}(|X_s - x| > \varepsilon)\right) \to 0,$$

when $s \downarrow 0$ if $a + \varepsilon < x < b - \varepsilon$. Using the Itô's formula and Equation (37), we can show that $p_+(x)$ satisfies the Kolmogorov's backward equation

$$\frac{1}{2}\sigma^2(x)p''_+(x) + \alpha(x)p'_+(x) = 0, \tag{38}$$

for $x \in (a, b)$ with the boundary conditions $p_+(a) = 0$ and $p_+(b) = 1$. The explicit solution to Equation (38) is

$$p_+(x) = A\int_q^x \exp\left(-\int_q^t \frac{2\alpha(z)}{\sigma^2(z)}\,\mathrm{d}z\right)\mathrm{d}t + B. \tag{39}$$

We can write Equation (39) in the form

$$p_+(x) = Au(x) + B, \tag{40}$$

where $u(x)$ is of the form Equation (34) for a fixed $q \in (a, b)$, with A and B constants. Now, an application of boundary conditions $p_+(a) = 0$ and $p_+(b) = 1$ gives:

$$A = \frac{1}{u(b) - u(a)} \quad \text{and} \quad B = \frac{-u(a)}{u(b) - u(a)},$$

so that

$$p_+(x) = \frac{u(x) - u(a)}{u(b) - u(a)}. \tag{41}$$

Equations (34) and (41) will be important when applied to our specific problem.

Following similar arguments, we define

$$e(x) = \mathbf{E}[T_{ab}], \tag{42}$$

where $T_{ab} = \inf\{t > 0 : X_t \notin (a, b)\}$. An application of the Markov property gives

$$e(x) = s + \mathbf{E}[e(X_s)] + O(\mathbb{P}(|X_s - x| > \varepsilon)).$$

Dividing by s and letting s tend to 0 and an application of the Itô formula gives

$$\frac{1}{2}\sigma^2(x)e''(x) + \alpha(x)e'(x) = -1. \tag{43}$$

This equation can be solved by the standard Green function techniques as follows. The corresponding homogeneous equation is

$$e''(x) + \frac{2\alpha(x)}{\sigma^2(x)}e'(x) = 0$$

and its solution is

$$e(x) = \frac{u(x) - u(a)}{u(b) - u(a)}, \tag{44}$$

with boundary conditions $e(a) = 0$ and $e(b) = 1$ where $u(x)$ is defined in Equation (34). The Green function, $G_{(a,b)}(x, y)$, is calculated as

$$G_{(a,b)}(x, y) = \begin{cases} \frac{1}{W} \cdot e_1(x)e_2(y) & \text{if } x \le y, \\ \frac{1}{W} \cdot e_1(y)e_2(x) & \text{if } x \ge y, \end{cases} \tag{45}$$

where e_1 and e_2 take the form of Equation (44) and W is the Wronskian given by

$$W = \frac{u'(x)}{u(b) - u(a)}.$$

Therefore, the solution to Equation (43) is given by

$$e(x) = \int_a^b G_{(a,b)}(x, y)m(\mathrm{d}y),$$

where $G_{(a,b)}(x, y)$ is given by

$$G_{(a,b)}(x, y) = \begin{cases} \frac{2(u(x)-u(a))(u(b)-u(y))}{u(b)-u(a)} & \text{if} \quad x \le y, \\ \frac{2(u(y)-u(a))(u(b)-u(x))}{u(b)-u(a)} & \text{if} \quad x > y, \end{cases} \tag{46}$$

and $m(dy)$ is given by Equation (36).

We now consider Equation (1). We note that the diffusion coefficient $\sigma(x) = \sigma x^\gamma$ in Equation (1) is defined only on $(0, \infty)$, that is, the state space of the process is made up of the positive reals. The process X_t in Equation (1) is a diffusion process, and the coefficients σ and α are continuous on $(0, \infty)$. Following the arguments in [17], we investigate the behavior of Equation (1) at the boundaries of the state space. It is of interest whether or not the boundary points 0 and/or ∞ can be reached by the process X_t in a finite time.

A boundary point is said to be accessible if it can be reached in finite time with positive probability. Otherwise it is inaccessible [17]. The accessible boundary points are of two different types, namely, the exit and regular boundary points. For the exit boundary, the process is absorbed after the boundary is reached while the regular boundary point is imposed on a standard Brownian motion and could either be absorbed or reflected once the boundary is reached. The inaccessible boundaries are also of two types, namely, the entrance and natural boundary points. The boundary is said to be of entrance type if it is possible to start the process at infinity and then reach the interior of the state interval, otherwise it is called natural.

Let $[a, b]$ be a fixed interval and the process X_t starts in $X_0 = x \in (a, b)$. Let α and σ be continuous on a state interval whose interior is (c, d). We note that we may have $c = -\infty$ and/or $d = +\infty$. It is assumed that $\sigma^2(x) > 0$ on (c, d). Further, let $(\widetilde{c}, \widetilde{d}) = (u(c), u(d))$, where u is the scale function given by Equation (34).

Definition 4.1. *A natural upper boundary point d is said to be attracting if there is a positive probability that X_t shall converge to d as $t \to \infty$.*

The following classification theorem, taken from [17], will be the framework of the analysis of Equation (1).

Theorem 4.1. *Let u be the scale function given by Equation (34) and $m(\mathrm{d}y)$ be the speed measure given by Equation (36). Let b be a point in the interior of the state space (c, d). Then, the following statements hold.*

1. *A necessary and sufficient condition for d to be accessible is that $u(d) < \infty$ and $\int_b^d (u(d) - u(y))m(\mathrm{d}y) < \infty$.*
2. *An accessible boundary point d is regular if and only if $\int_b^d m(\mathrm{d}y) < \infty$. Otherwise it is exit boundary.*
3. *An inaccessible boundary point d is natural if and only if $\int_b^d u(y)m(\mathrm{d}y) = \infty$.*
4. *A natural boundary point d is attracting if and only if $u(d) < \infty$ and at the same time $\int_b^d m(\mathrm{d}y) = \infty$.*

We are now in a position of analyzing the non-homogeneous stochastic differential equation (1), repeated here for convenience,

$$\mathrm{d}X_t = \alpha X_t \,\mathrm{d}t + \sigma X_t^{\gamma} \,\mathrm{d}B_t, \;\; \gamma > 1, \;\; X_0 = x > 0. \tag{47}$$

This is a diffusion process with $\alpha(x) = \alpha x$, $\sigma(x) = \sigma x^{\gamma}$ and natural state interval $c = 0$ to $d = \infty$. Let b be a point in the interior of this state interval. From Equation (34) and (36), we calculate the scale function and speed measure, respectively, corresponding to Equation (47) to be

$$u(x) = \frac{\sigma^2}{2\alpha}\left(b^{2\gamma-1} - x^{2\gamma-1}\exp\left(\frac{\alpha}{\sigma^2(1-\gamma)}(b^{2-2\gamma} - x^{2-2\gamma})\right)\right),$$

and

$$m(dy) = \frac{1}{\sigma^2 y^{2\gamma}}\exp\left(-\frac{\alpha}{\sigma^2(1-\gamma)}(b^{2-2\gamma} - y^{2-2\gamma})\right)\mathrm{d}y. \tag{48}$$

It remains only to classify our boundary points on the basis of these results. We note that

$$u(d) = \frac{\sigma^2}{2\alpha}\left(b^{2\gamma-1} - d^{2\gamma-1}\exp\left(\frac{\alpha}{\sigma^2(1-\gamma)}(b^{2-2\gamma} - d^{2-2\gamma})\right)\right).$$

Since $d = \infty$ in our state space $(0, \infty)$, we use a limiting argument:

$$\lim_{d\to\infty} u(d) = \frac{\sigma^2 b^{2\gamma-1}}{2\alpha},$$

provided $0 < \gamma < \frac{1}{2}$. Now, since b is a finite fixed point in $(0, \infty)$, the limit is finite. We also need to investigate the integral

$$\int_b^d (u(d) - u(y))m(\mathrm{d}y) = \int_b^d \frac{1}{2\alpha y}\,\mathrm{d}y - \frac{1}{2\alpha}\exp\left(\frac{-\alpha}{\sigma^2(1-\gamma)}d^{2-2\gamma}\right)d^{2\gamma-1} \times \int_b^d \frac{1}{y^{2\gamma}}\exp\left(\frac{\alpha}{\sigma^2(1-\gamma)}y^{2-2\gamma}\right)\mathrm{d}y. \tag{49}$$

We observe that as $d \to \infty$ the term $\exp\left(-\frac{\alpha}{\sigma^2(1-\gamma)}d^{2-2\gamma}\right)$ approaches 0 provided $0 < \gamma < 1$. So in this case we remain with

$$\int_b^d (u(d) - u(y))m(\mathrm{d}y) \approx \int_b^d \frac{1}{2\alpha y}\,\mathrm{d}y \longrightarrow \infty \;\; as \;\; d \to \infty.$$

We therefore, according to Theorem 4.1, conclude that the upper boundary point $d = \infty$ is inaccessible if $0 < \gamma < 1$. Now for the lower boundary point 0 we have

$$u(0) = \frac{\sigma^2 b^{2\gamma-1}}{2\alpha} < \infty,$$

since b is a finite fixed point in the state space $(0, \infty)$. We also have

$$\int_0^b (u(0) - u(y))m(\mathrm{d}y) = \int_0^b \frac{1}{2\alpha y}\,\mathrm{d}y \to \infty, \;\; \text{as} \;\; y \to 0.$$

This shows that the boundary point 0 is inaccessible for all $\gamma \neq 1$. It remains to establish whether our boundary points are natural or not. Theorem 4.1 says the boundary point d is natural if and only if

$$\int_b^d u(y)m(\mathrm{d}y) = \infty.$$

Now,

$$\int_b^d u(y)m(\mathrm{d}y) = \int_b^d \left(\frac{b^{2\gamma-1}}{2\alpha y^{2\gamma}}\exp\left(-\frac{\alpha}{\sigma^2(1-\gamma)}(b^{2-2\gamma} - y^{2-2\gamma})\right) - \frac{1}{2\alpha y}\right)\mathrm{d}y = \frac{b^{2\gamma-1}\exp\left(\frac{-\alpha}{\sigma^2(1-\gamma)}b^{2-2\gamma}\right)}{2\alpha}\int_b^d \frac{1}{y^{2\gamma}}\exp\left(\frac{\alpha}{\sigma^2(1-\gamma)}y^{2-2\gamma}\right)\mathrm{d}y - \int_b^d \frac{1}{2\alpha y}\,\mathrm{d}y.$$

We observe that for $0 < \gamma < 1$ the integral

$$\int_b^d \frac{1}{y^{2\gamma}}\exp\left(\frac{\alpha}{\sigma^2(1-\gamma)}y^{2-2\gamma}\right)\mathrm{d}y$$

explodes to infinity very fast as $d \to \infty$. Although the second integral,

$$\int_b^d \frac{1}{2\alpha y}\,\mathrm{d}y,$$

also tends to infinity as $d \to \infty$, the whole integral $\int_b^d u(y)m(\mathrm{d}y)$ tends to infinity as $d \to \infty$ because the second integral goes to infinity very slowly as compared to the first one. Hence,

$$\int_b^d u(y)m(\mathrm{d}y) = \infty,$$

provided $0 < \gamma < 1$. This tells us that the boundary point $d = \infty$ is natural if $0 < \gamma < 1$.
Using similar arguments, we can show that

$$\int_0^b u(y)m(\mathrm{d}y) = \infty.$$

Therefore, for $0 < \gamma < 1$, the boundary point 0 is natural. Next, we investigate if our natural boundary points are attracting. According to Theorem 4.1 the boundary point d is attracting if and only if $u(d) < \infty$ and at the same time $\int_b^d m(\mathrm{d}y) = \infty$. Now we have already seen that $u(d) < \infty$ if $d = 0$ and/or $d = \infty$ provided $0 < \gamma < 1$. Further

$$\int_b^d m(\mathrm{d}y) = \frac{1}{\sigma^2}\exp\left(-\frac{\alpha}{\sigma^2(1-\gamma)}b^{2-2\gamma}\right) \times \int_b^d \frac{1}{y^{2\gamma}}\exp\left(\frac{\alpha}{\sigma^2(1-\gamma)}y^{2-2\gamma}\right)\mathrm{d}y,$$

which, for the reason given before, explodes to infinity as $d \to \infty$ for all $0 < \gamma < 1$. Therefore,

$$\int_b^\infty m(\mathrm{d}y) = \infty,$$

for $0 < \gamma < 1$. Hence, the upper boundary point $d = \infty$ is attracting for $0 < \gamma < 1$. Similarly the lower boundary point 0 is shown to be attracting.

Now, we have established that both boundary points are attracting when $0 < \gamma < 1$. In this case we will show that, by Equation (41), our process will converge to ∞ with probability $p_+(x)$, where $x = X_0 \in (0, \infty)$. It turns out that

$$p_+(x) = \frac{\int_0^x \exp\left(-\frac{\alpha}{\sigma^2(1-\gamma)}y^{2-2\gamma}\right)\mathrm{d}y}{\int_0^\infty \exp\left(-\frac{\alpha}{\sigma^2(1-\gamma)}y^{2-2\gamma}\right)\mathrm{d}y}, \quad 0 < \gamma < 1. \quad (50)$$

Evaluating the integrals yields

$$p_+(x) = \lim_{y\to\infty}\left(\frac{x}{y}\right)^{2\gamma-1}\exp\left(\frac{\alpha}{\sigma^2(1-\gamma)}(y^{2-2\gamma} - x^{2-2\gamma})\right) = 0,$$

for $\frac{1}{2} < \gamma < 1$. This shows that although the upper boundary $d = \infty$ is attracting for $0 < \gamma < 1$, the process X_t will not converge to ∞ if $\frac{1}{2} < \gamma < 1$. Furthermore, the process X_t converges to 0 with probability $1 - p_+(x)$ which turns out to be 1 in this case. Thus it is certain that X_t will converge to 0 when $\frac{1}{2} < \gamma < 1$. We observe that if $0 < \gamma < \frac{1}{2}$ we have a problem since, in this case, it is not possible to proceed using a probabilistic argument. Our analysis is not complete if we do not consider the case $\gamma > 1$. We now proceed to make this analysis. As seen earlier

$$u(d) = \frac{\sigma^2}{2\alpha}\left(b^{2\gamma-1} - d^{2\gamma-1}\exp\left(\frac{\alpha}{\sigma^2(1-\gamma)}(b^{2-2\gamma} - d^{2-2\gamma})\right)\right).$$

If $\gamma > 1$, for example, if $\gamma = 2$, we have

$$u(d) \longrightarrow -\infty \quad as \quad d \to \infty,$$

since α, σ and b are fixed positive numbers. Therefore, we have

$$\lim_{d\to\infty} u(d) < \infty \quad \forall \quad \gamma > 1.$$

Observe also that for such γ we have that

$$u(0) = \frac{\sigma^2 b^{2\gamma-1}}{2\alpha} < \infty,$$

effectively. Now, we consider again Equation (49). If $\gamma > 1$, for instance, $\gamma = 2$, we have

$$\int_b^d (u(d) - u(y))m(\mathrm{d}y) = \int_b^d \frac{1}{2\alpha y}\,\mathrm{d}y - \frac{d^3}{2\alpha}e^{\frac{\alpha}{\sigma^2 d^2}}\int_b^d \frac{1}{y^4}e^{-\frac{\alpha}{\sigma^2 y^2}}\,\mathrm{d}y.$$

We immediately observe that as $d \to \infty$,
$\int_b^d (u(d) - u(y))m(\mathrm{d}y) \to -\infty$ since the integral $\int_b^d \frac{1}{2\alpha y}\,\mathrm{d}y$ goes to ∞ very slowly. Therefore, effectively we have

$$\int_b^d (u(d) - u(y))m(\mathrm{d}y) < \infty,$$

for the boundary point $d = \infty$ and whenever $\gamma > 1$. This, together with $u(d) < \infty$ for $d = \infty$ and $\gamma > 1$, shows that the upper boundary point $d = \infty$ is always accessible whenever $\gamma > 1$. However, it is clear that if $d = 0$,

$$\int_0^b (u(0) - u(y))m(\mathrm{d}y) = \int_0^b \frac{1}{2\alpha y}\,\mathrm{d}y = \infty,$$

which shows that the lower boundary point 0 is always not accessible for $\gamma > 1$. In fact, the boundary point 0 is always inaccessible for all $\gamma \neq 1$ as also shown earlier. So from definition we have seen that the upper boundary point ∞ can be reached in finite time with positive probability provided $\gamma > 1$.

Finally we want to classify the accessible boundary point ∞, that is. is it regular or exit? From Theorem 4.1 it is regular if and only if $\int_b^d m(\mathrm{d}y) < \infty$. Now, as obtained earlier on

$$\int_b^d m(\mathrm{d}y) = \frac{1}{\sigma^2}\exp\left(-\frac{\alpha}{\sigma^2(1-\gamma)}b^{2-2\gamma}\right) \times \int_b^d \frac{1}{y^{2\gamma}}\exp\left(\frac{\alpha}{\sigma^2(1-\gamma)}y^{2-2\gamma}\right)\mathrm{d}y.$$

If $\gamma > 1$, the integral is always less than ∞ because of the negative exponent since α, σ are fixed positive numbers. So we have

$$\int_b^d m(\mathrm{d}y) < \infty \quad \forall \gamma > 1$$

since in this case the exponent is always negative. Hence for $\gamma > 1$, the accessible upper boundary point ∞ is always regular, i.e., apart from absorption and reflection there are also other possibilities after the boundary point is reached.
We, therefore, have the following result.

Theorem 4.2. *Let $x \in (0,\infty)$ with $\alpha \in \boldsymbol{R}$ arbitrary. Then, the stochastic differential equation (1) has a unique strong global solution $X_t : t \geq 0$. The solution has the following properties:*

1. *$x = 0$ implies that $X_t = 0$ for all $t > 0$ and $x \geq 0$ implies $X_t > 0$ for all $t \geq 0$.*
2. *If $\frac{1}{2} < \gamma < 1$, then $\lim_{t\to\infty} X_t = 0$ with probability $1 - p_+(x)$ where $p_+(x)$ is given by Equation (50).*
3. *If $\gamma > 1$, then $\lim_{t\to\infty} X_t = \infty$ with positive probability.*
4. *If $\gamma = 1$, we have the usual Geometric Brownian motion whereas if $\gamma = 0$, we have the Ornstein-Uhlenbeck process.*

In mathematical finance, our result is of particular interest for the Cox-Ingersoll-Roll (CIR) model which describes the stochastic evolution of interest rates $(r_t)_{t\geq 0}$ by the stochastic differential equation

$$\mathrm{d}r_t = \alpha(\mu - r)\,\mathrm{d}t + \sigma\sqrt{r_t}\,\mathrm{d}B_t, \quad t \geq 0,$$

with $r_0 \geq 0$ and $\alpha\mu \geq \frac{1}{2}\sigma^2$ where α, μ and σ denote real constants.

5. CONCLUDING REMARKS

In this article, we proved the existence of global positive solutions to non-homogeneous stochastic differential equations whose diffusion coefficient is non-Lispchitz. We relied on both the classical sense and probabilistic arguments. We provided detailed proofs in both cases. The probability arguments save as an alternative method of dealing with non-homogeneous stochastic differential equations where classical methods cannot be applied. Using the scale function and the speed of measure, we provided a complete classification of boundary types and boundary behavior of Equation (1). The results of this article can be applied to Cox-Ingersoll-Ross model. In addition, the positivity of solutions is important to other non-linear models that arise in sciences and engineering.

DATA AVAILABILITY STATEMENT

The original contributions presented in the study are included in the article/supplementary materials, further inquiries can be directed to the corresponding author.

AUTHOR CONTRIBUTIONS

FM contributed to the conceptualization of the idea for research, development of the methodology, analysis of the model and writing up of the final article. LR conducted the primary research, identified the problem, and discussed the results. Both authors proof read the manuscript and approved the submitted version.

FUNDING

This work was supported by a Newton Fund's Operational Development Assistance grant, ID 32, under the SA-UK partnership. The grant is funded by the UK Department for Business, Energy and Industrial Strategy and Department of Higher Education and Training (DHET) and delivered by the British Council. For further information, please visit www.newtonfund.ac.uk.

ACKNOWLEDGMENTS

The authors are grateful to the referees for constructive comments and suggestions that have improved this article.

REFERENCES

1. Itô K. *On Stochastic Differential Equations*. New York, NY: American Mathematical Society (1951).
2. Mao X, Yuan C. *Stochastic Differential Equations with Markovian Switching*. London: Imperial College Press (2006). doi: 10.1142/p473
3. Mao X. *Stochastic Differential Equations and Applications*. London: Elsevier (2007). doi: 10.1533/9780857099402
4. Øksendal B. *Stochastic Differential Equations: An Introduction With Applications*. New York, NY: Springer Science & Business Media (2013).
5. Ikeda N, Watanabe S. *Stochastic Differential Equations and Diffusion Processes*. North-Holland: Elsevier (2014).
6. Protter PE. Stochastic differential equations. In: Rozavskii B, Yor M, editors. *Stochastic Integration and Differential Equations*. New York, NY: Springer (2005). p. 249–361. doi: 10.1007/978-3-662-10061-5_6
7. Karatzas I, Shreve S. *Brownian Motion and Stochastic Calculus*. vol. 113. New York, NY: Springer Science & Business Media (2012).
8. Mishura Y, Posashkova S. Positivity of solution of nonhomogeneous stochastic differential equation with non-lipschitz diffusion. *Theory Stochast Process*. (2008) 14:77–88. Available online at: http://tsp.imath.kiev.ua/files/172/1434_7.pdf
9. Appleby JA, Kelly C, Mao X, Rodkina A. Positivity and stabilisation for nonlinear stochastic delay differential equations. *Stochastics Int J Probabil Stochast Process*. (2009) 81:29–54. doi: 10.1080/17442500802214097

10. Xu R, Wu D, Yi R. Existence theorem for mean-reverting CEV process with regime switching. In: *2015 International Conference on Mechatronics, Electronic, Industrial and Control Engineering (MEIC-15)*. Atlantis Press (2015). p. 1560–3. doi: 10.2991/meic-15.2015.357
11. Zhang X. Stochastic differential equations with Sobolev diffusion and singular drift and applications. *Ann Appl Probabil*. (2016) 26:2697–732. doi: 10.1214/15-AAP1159
12. Bae MJ, Park CH, Kim YH. An existence and uniqueness theorem of stochastic differential equations and the properties of their solution. *J Appl Math Inform*. (2019) 37:491–506. doi: 10.14317/jami.2019.491
13. Kubilius K, Medziunas A. Positive solutions of the fractional SDEs with non-Lipschitz diffusion coefficient. *Mathematics*. MDPI (2021) 9:1–14. doi: 10.3390/math9010018
14. Duffie D. *Dynamic Asset Pricing Theory*. Princeton, NJ: Princeton University Press (2010).
15. Glasserman P. Monte carlo methods in financial engineering. In: *Stochastic Modelling and Applied Probability*. New York, NY: Springer-Verlag (2003). doi: 10.1007/978-0-387-21617-1
16. Rundora L. *Extension(s) of the Geometric Brownian Motion Model for Pricing of Assets*. Masters Dissertation, Harare: University of Zimbabwe (1997).
17. Helland I. *One-Dimensional Diffusion Processes and Their Boundaries*. (1996).
18. Revuz D, Yor M. *Continuous Martingales and Brownian Motion*. vol. 293. New York, NY: Springer Science & Business Media (2013).
19. Yamada T, Watanabe S. On the uniqueness of solutions of stochastic differential equations. *J Math Kyoto Univ*. (1971) 11:155–67. doi: 10.1215/kjm/1250523691
20. Lungu E, Øksendal B. Optimal harvesting from a population in a stochastic crowded environment. *Math Biosci*. (1997) 145:47–75. doi: 10.1016/S0025-5564(97)00029-1
21. Gualtierotti A. Statistics for stochastic processes: applications to engineering and finance. In: Dodge Y, editor. *Statistical Data Analysis and Inference*. North-Holland: Elsevier (1989). p. 543–55. doi: 10.1016/B978-0-444-88029-1.50054-X

Conflict of Interest: The authors declare that the research was conducted in the absence of any commercial or financial relationships that could be construed as a potential conflict of interest.

Publisher's Note: All claims expressed in this article are solely those of the authors and do not necessarily represent those of their affiliated organizations, or those of the publisher, the editors and the reviewers. Any product that may be evaluated in this article, or claim that may be made by its manufacturer, is not guaranteed or endorsed by the publisher.

frontiers | Frontiers in Applied Mathematics and Statistics

ORIGINAL RESEARCH
published: 21 April 2022
doi: 10.3389/fams.2022.861276

A NSFD Discretization of Two-Dimensional Singularly Perturbed Semilinear Convection-Diffusion Problems

Olawale O. Kehinde[1†], *Justin B. Munyakazi*[1*] *and Appanah R. Appadu*[2]

[1] *Department of Mathematics and Applied Mathematics, University of the Western Cape, Bellville, South Africa,* [2] *Department of Mathematics and Applied Mathematics, Nelson Mandela University, Port Elizabeth, South Africa*

Despite the availability of an abundant literature on singularly perturbed problems, interest toward non-linear problems has been limited. In particular, parameter-uniform methods for singularly perturbed semilinear problems are quasi-non-existent. In this article, we study a two-dimensional semilinear singularly perturbed convection-diffusion problems. Our approach requires linearization of the continuous semilinear problem using the quasilinearization technique. We then discretize the resulting linear problems in the framework of non-standard finite difference methods. A rigorous convergence analysis is conducted showing that the proposed method is first-order parameter-uniform convergent. Finally, two test examples are used to validate the theoretical findings.

Keywords: semilinear singularly perturbed problems, two-dimensional partial differential equations, fitted operator finite difference method, quasilinearization, error analysis, uniform convergence

OPEN ACCESS

Edited by:
Dumitru Trucu,
University of Dundee, United Kingdom

Reviewed by:
Yang Liu,
Inner Mongolia University, China
Omar Abu Arqub,
Al-Balqa Applied University, Jordan

***Correspondence:**
Justin B. Munyakazi
jmunyakazi@uwc.ac.za

[†]*Deceased*

Specialty section:
This article was submitted to Mathematical Biology, a section of the journal Frontiers in Applied Mathematics and Statistics

Received: *24 January 2022*
Accepted: *29 March 2022*
Published: *21 April 2022*

Citation:
Kehinde OO, Munyakazi JB and Appadu AR (2022) A NSFD Discretization of Two-Dimensional Singularly Perturbed Semilinear Convection-Diffusion Problems. Front. Appl. Math. Stat. 8:861276. doi: 10.3389/fams.2022.861276

1. INTRODUCTION

The study of singularly perturbed problems has flourished since the publication of Prandtl's seminal work in 1904 on "boundary layers" [1]. Many researchers have paid attention to the theoretical and computational aspects of those problems. The usual task has been to provide means of dealing with the challenges that come with the perturbation parameter and its impact on the solution behavior. While countless successes have been recorded in the case of linear singularly perturbed problems [see for example [2–7]], little attention has been paid to the non-linear case.

In this article, we study the two-dimensional singularly perturbed semilinear convection-diffusion problems

$$-\varepsilon(u_{xx}+u_{yy})+a_1(x,y)u_x+a_2(x,y)u_y=-f(x,y,u(x,y)),\ (x,y)\in\Omega:=(0,1)\times(0,1), \quad (1.1)$$

subject to boundary conditions

$$u(x,y)=u_0(x,y), \qquad (x,y)\in\partial\Omega, \quad (1.2)$$

where ε is the perturbation parameter with $0<\varepsilon\ll 1$. The semilinear source term $f(x,y,u(x,y))$ and the coefficient functions $a_1(x,y), a_2(x,y)$ are assumed to be sufficiently smooth and satisfy

$$a_1(x,y) \geqslant \alpha_1 > 0, \quad a_2(x,y) \geqslant \alpha_2 > 0, \qquad \forall\ (x,y) \in \bar{\Omega}, \tag{1.3}$$

$$f_u(x,y,u) \geqslant \beta > 0, \qquad \forall\ (x,y) \in \bar{\Omega}, \tag{1.4}$$

where α_1, α_2 and β are constants and $\partial\Omega$ is the boundary of Ω. Under these conditions (1.1)-(1.2) has a unique solution which displays boundary layers at $x = 1$ and $y = 1$ when ε approaches zero.

Problems such as (1.1)-(1.2) are encountered in diverse areas of applied mathematics and engineering such as aerodynamics, liquid crystal modeling, chemical reactor theory, magnetohydrodynamics, oceanography, fluid mechanics, heat conduction, quantum mechanics [see [8–13]]. The difficulty with such problems is that researchers have to deal with both the perturbation parameter and the complexity due to the semilinearity, besides the higher-dimensional aspect. Perhaps, that is the reason why only few people have shown some interest in them.

Sirotkin and Tarvainen [14] proposed the parallel two-level Schwarz methods and studied their convergence properties. Boglaev proposed a number of methods. In [15], he constructed a blocked domain decomposition algorithm. He achieved a first-order rate of convergence on both meshes. In [16], he proposed a uniform monotone iterative method on layer adapted meshes. In [17], he developed a monotone Schwarz algorithm. Boglaev and Duoba [18] designed a multi-domain decomposition algorithm to solve a singularly perturbed advection-diffusion problem with a parabolic layer. The authors achieved a first-order convergence result. Kopteva [19] and Stynes [20] propose finite element methods. Also, Newton and Picard methods were described as the numerical solver for the concerned problems by Vulkov and Zadorin in [21].

All the methods above are based on the use of non-uniform meshes and are essentially first order accurate. Due to the design of the mesh-grid and hence, that of the methods, the order of convergence is usually affected adversely by a logarithmic factor. In this article, we propose a method based on the non-standard finite difference rules of Mickens [22]. It is worth mentioning that these methods are designed on uniform grids. To the best of our awareness, this is the first time that such methods are used on elliptic singularly perturbed semilinear problems in two dimensions. These methods were used in [23, 24] for linear elliptic reaction-diffusion and reaction-convection-diffusion problems in two dimensions, respectively.

We adopt the quasilinearization approach to convert the semilinear problem into a sequence of linear problems. Then, we design a fitted operator numerical method on the converted problems. We show that the method is first order uniformly convergent in both x and y variables with respect to the perturbation parameter. Numerical experiments corroborate the theoretical results.

The rest of the article is structured as follows: In Section 2, we use the quasilinearization technique to linearize the concerned problem and present some qualitative properties of the solution and its derivatives. In Section 3, we present the proposed fitted operator finite difference method while in Section 4, we perform the convergence analysis. In Section 5, we provide some test models to show the efficiency of the presented scheme as well as to validate the theoretical result. The article ends with a brief conclusion in Section 6.

2. QUASILINEARIZATION

We transform the semilinear equation (1.1) using the quasilinearization approach. We choose a reliable initial guess $u^{(0)}(x,y) = u_0(x,y) \equiv u^{(0)}$. Then, we consider a truncated Taylor series expansion of $f(x,y,u)$ about the initial approximation as follows.

$$f(x,y,u^{(1)}) = f(x,y,u^{(0)}) + (u^{(1)} - u^{(0)}) \left(\frac{\partial f}{\partial u}\right)_{(x,y,u^{(0)})} + \cdots. \tag{2.1}$$

We then derive the following iterates through the process by deriving the steps that involve $u^{(2)}(x,y)$, $u^{(3)}(x,y)$, and so on. Assuming that this process converges, we obtain the recurrence relations

$$f(x,y,u^{(r+1)}) = f(x,y,u^{(r)}) + (u^{(r+1)} - u^{(r)}) \left(\frac{\partial f}{\partial u}\right)_{(x,y,u^{(r)})} + \cdots, \tag{2.2}$$

where r is the iteration number (or iteration index) with $r = 0, 1, \cdots$.

Substituting (2.2) into (1.1) results in a 2D linear singularly perturbed convection diffusion problem of the form

$$\begin{aligned} \mathcal{L}u(x,y) \equiv -\varepsilon\left(u_{xx} + u_{yy}\right) + a_1(x,y)u_x + a_2(x,y)u_y \\ +b(x,y)u = z(x,y), \quad (x,y) \in \bar{\Omega}, \end{aligned} \tag{2.3}$$

$$u(x,y) = u_0(x,y), \tag{2.4}$$

where

$$b(x,y) = \frac{\partial f}{\partial u}, \quad \text{and} \quad z(x,y) = f(x,y,u^{(r)}) - u^{(r)}\frac{\partial f}{\partial u}. \tag{2.5}$$

We solve the linear problem (2.3)–(2.4) using fitted operator finite difference scheme. The successive iteration of the 2D linear equations(2.3)–(2.4), with iteration function (2.5) converges to the solution of the semilinear problem (1.1)–(1.2). We take the convergence stopping criteria as

$$\|u^{r+1} - u^r\| < Tol,$$

where *Tol* is the tolerance.

The solution of (2.3)-(2.4) enjoys the properties below [25].

Lemma 2.1. *(Continuous maximum principle) Assume that $v(x,y)$ is sufficiently smooth function which satisfy $v(x,y) \geqslant 0, \quad \forall\ (x,y) \in \partial\Omega$. Then $\mathcal{L}v(x,y) \geqslant 0, \ \forall\ x \in \Omega$, implies that $v(x,y) \geqslant 0, \forall\ (x,y) \in \bar{\Omega}$.*

Lemma 2.2. *(Uniform stability estimate) Let u(x,y) be the solution of (2.3)-(2.4) then we have*

$$\|u(x,y)\| \leqslant \alpha^{-1}\|z\|, \quad \forall x \in \Omega, \tag{2.6}$$

where $\alpha = \min\{\alpha_1, \alpha_2\}$ *is independent of* ε.

Lemma 2.3. *Let u(x,y) be the solution of (2.3)-(2.4) and a(x), b(x), z(x) be smooth functions. Then*

$$|u^{(i,j)}(x,y)| \leqslant C\left(1+\varepsilon^{-(i+j)}\exp\left(-\frac{\alpha_1(1-x)}{\varepsilon}\right)\exp\left(-\frac{\alpha_2(1-y)}{\varepsilon}\right)\right), \ (x,y)\in\bar{\Omega}, \tag{2.7}$$

where α_1, α_2 *and C positive constant independent of* ε.

3. SCHEME FOR THE PROBLEM

Let n and m be two positive integers, we partition the domain $\Omega := [0,1]\times[0,1]$ into n and m equal intervals so the step sizes are $h = 1/n$ and $k = 1/m$, we obtain the nodes as $x_i = x_0 + ih,\ i = 1,\ldots,n-1$ and $y_j = y_0 + jk,\ j = 1,\ldots,m-1$ where $x_0 = y_0 = 0$ and $x_n = y_n = 1$. We denote the approximation of $u(x_i, y_j)$ at the grid points of x_i and y_j by the unknown U_{ij}.

We write the discrete version of (2.3)–(2.4) as

$$\mathcal{L}^{h,k}(U_{i,j}) \equiv -\varepsilon\left[\frac{U_{i+1,j}-2U_{ij}+U_{i-1,j}}{(\phi_{ij})_h^2}\right]-\varepsilon\left[\frac{U_{i,j+1}-2U_{ij}+U_{i,j-1}}{(\phi_{ij})_k^2}\right]+a_{1ij}\frac{U_{ij}-U_{i-1,j}}{h} + a_{2ij}\frac{U_{ij}-U_{i,j-1}}{k}+b_{ij}U_{ij}=z_{ij}, \quad i=1,\ldots,n-1,\ j=1,\ldots,m-1, \tag{3.1}$$

with boundary conditions of the four sides as

$$U_{i,0} = U_{0,j} = U_{i,m} = U_{n,j} = u_{0ij}, \quad i = 0,1,\ldots,n, \quad j = 0,1,\ldots,m. \tag{3.2}$$

The denominator functions ϕ_{ij}^2 are given by

$$(\phi_{ij})_h^2 = \frac{\varepsilon h}{a_{1ij}}\left(\exp\left(\frac{a_{1ij}h}{\varepsilon}\right)-1\right) = h^2 + \mathcal{O}\left(\frac{h^3}{\varepsilon}\right), \tag{3.3}$$

and

$$(\phi_{ij})_k^2 = \frac{\varepsilon k}{a_{2ij}}\left(\exp\left(\frac{a_{2ij}k}{\varepsilon}\right)-1\right) = k^2 + \mathcal{O}\left(\frac{k^3}{\varepsilon}\right). \tag{3.4}$$

We rewrite (3.1) in five term recurrence relation as

$$-r_l^{h+}U_{i+1,j} - r_l^{h-}U_{i-1,j} + r_l^c U_{ij} - r_l^{k+}U_{i,j+1} - r_l^{k-}U_{i,j-1} = z_{ij}, \quad i = 1(1)n-1, \quad j = 1(1)m-1, \tag{3.5}$$

where

$$r_l^{h+} = \frac{\varepsilon}{(\phi_{ij})_h^2}, \quad r_l^{h-} = \left(\frac{\varepsilon}{(\phi_{ij})_h^2}+\frac{a_{1ij}}{h}\right), \quad r_l^{k+} = \frac{\varepsilon}{(\phi_{ij})_k^2}, \quad r_l^{k-} = \left(\frac{\varepsilon}{(\phi_{ij})_k^2}+\frac{a_{2ij}}{k}\right),$$
$$r_l^c = \frac{2\varepsilon}{(\phi_{ij})_h^2}+\frac{2\varepsilon}{(\phi_{ij})_k^2}+\frac{a_{1ij}}{h}+\frac{a_{2ij}}{k}+b_{ij}, \quad \text{and} \quad l = (i-1)(m-1)+j.$$

We form a linear system

$$AU = G,$$

where $\mathbf{U} = [U_{i0},\ldots U_{n-1,0}; U_{1,1}\ldots U_{n-1,1};\ldots; U_{1,j}\ldots U_{n-1,m-1}]^T$.

A is pentadiagonal matrix of size $(n-1)(m-1)\times(n-1)(m-1)$ and G is a column vector of size $(n-1)(m-1)$ with their entries respectively described as follows.

$$\begin{aligned}
&A_{l,l+1} = -r_l^{k+}, && i = 1(1)n-1,\ \ j = 1(1)m-2,\\
&A_{l,l-1} = -r_l^{k-}, && i = 1(1)n-1,\ \ j = 2(1)m-1,\\
&A_{l,l} = r_l^c, && i = 1(1)n-1,\ \ j = 1(1)m-1,\\
&A_{l,l+(n-1)} = -r_l^{h+}, && i = 1(1)n-2,\ \ j = 1(1)m-1,\\
&A_{l,l-(n-1)} = -r_l^{h-}, && i = 2(1)n-1,\ \ j = 1(1)m-1,
\end{aligned} \tag{3.6}$$

and

$$\begin{aligned}
&G_l = z_l + r_l^{h-}\times U(0,y_1) + r_l^{k-}\times U(x_1,0), && i=1,\ j=1,\\
&G_l = z_l + r_l^{h-}\times U(0,y_j), && i=1,\ j=2(1)m-2,\\
&G_l = z_l + r_l^{h-}\times U(0,y_{m-1}) + r_l^{k+}\times U(x_1,1), && i=1,\ j=m-1,\\
&G_l = z_l + r_l^{k-}\times U(x_i,0), && i=2(1)n-2,\ j=1,\\
&G_l = z_l, && i=2(1)n-2,\ j=2(1)m-2,\\
&G_l = z_l + r_l^{k+}\times U(x_i,1), && i=2(1)n-2,\ j=m-1,\\
&G_l = z_l + r_l^{h+}\times U(1,y_1) + r_l^{k-}\times U(x_{n-1},0), && i=n-1,\ j=1,\\
&G_l = z_l + r_l^{h+}\times U(1,y_j), && i=n-1,\ j=2(1)m-2,\\
&G_l = z_l + r_l^{h+}\times U(1,y_{m-1}) + r_l^{k+}\times U(x_{n-1},1), && i=n-1,\ j=m-1.
\end{aligned} \tag{3.7}$$

We provide some results that we will use to prove the convergence of the proposed method. These results are similar to those presented in [24] and can be proven in a similar manner.

Lemma 3.1. *(Discrete maximum principle). Let* $\vartheta_{i,j}$ *be a discrete function define on* Ω *satisfying* $\vartheta_{0,j}\geqslant 0,\ \vartheta_{n,j}\geqslant 0,\ j = 1(1)m-1,\ \vartheta_{i,0}\geqslant 0,\ \vartheta_{i,m}\geqslant 0,\ i = 1(1)n-1$ *and* $\mathcal{L}^{h,k}\vartheta_{i,j}\leqslant 0,\ \forall\ i = 1(1)n-1,\ j = 1(1)m-1$ *then* $\vartheta_{i,j}\geqslant 0\ \forall\ i = 0(1)n,\ j = 0(1)m$.

Lemma 3.2. *(Uniform stability estimate) if* $\mu_{i,j}$ *is any mesh function such that* $\mu_{i,j} = 0$ *on* $\partial\Omega^{(N,M)}$. *Then*

$$|\mu_{l,s}| \leqslant \frac{1}{\alpha}\max_{1\leq j\leq n-1,\ 1\leq j\leq m-1}|\mathcal{L}^{h,k}\mu_{i,j}| \quad \forall l = 0(1)n, \quad s = 0(1)m, \tag{3.8}$$

where $\alpha = \min\{\alpha_1,\ \alpha_2\}$.

4. CONVERGENCE ANALYSIS

The truncation error of the scheme presented in Section 3 is

TABLE 1 | Maximum pointwise errors and rate of convergence for Example 5.1 when $n = m = \{4, 8, 16, 32, 64, 128, 512, 1, 024\}$.

$\downarrow \varepsilon$	8	16	32	64	128	512	1,024
1	4.89E-04	1.18E-04	2.95E-05	7.38E-06	1.84E-06	4.61E-07	1.16E-07
	2.05	2.00	2.00	2.00	2.00	1.99	
10^{-1}	3.90E-03	1.39E-03	5.71E-04	2.54E-04	1.17E-04	5.48E-05	2.61E-05
	1.49	1.28	1.17	1.12	1.09	1.07	
10^{-2}	4.70E-02	1.16E-02	6.14E-03	3.30E-03	1.80E-03	9.71E-04	5.35E-04
	2.01	0.92	0.91	0.91	0.89	0.86	
10^{-3}	3.69E-02	1.89E-02	5.17E-03	1.40E-03	5.05E-04	1.93E-04	7.78E-05
	0.97	1.87	1.84	1.47	1.39	1.31	
10^{-4}	3.69E-02	1.90E-02	9.63E-03	4.81E-03	2.41E-03	1.20E-03	6.00E-04
	0.96	0.98	0.99	1.00	1.00	1.00	
⋮	⋮	⋮	⋮	⋮	⋮	⋮	⋮
10^{-15}	3.69E-02	1.90E-02	9.63E-03	4.81E-03	2.41E-03	1.20E-03	6.00E-04
	0.96	0.98	0.99	1.00	1.00	1.00	
E^n	3.69E-02	1.90E-02	9.63E-03	4.81E-03	2.41E-03	1.20E-03	6.00E-04
P^n	0.96	0.98	0.99	1.00	1.00	1.00	

TABLE 2 | Maximum pointwise errors and rate of convergence for Example 5.2 when $n = m = \{4, 8, 16, 32, 64, 128, 512, 1, 024\}$.

$\downarrow \varepsilon$	8	16	32	64	128	512	1,024
1	2.38E-03	6.44E-04	1.65E-04	4.15E-05	1.04E-05	2.56E-06	6.44E-07
	1.88	1.97	1.99	2.00	2.00	2.01	
10^{-1}	1.89E-02	6.30E-03	1.73E-03	4.42E-04	1.12E-04	2.80E-05	6.98E-06
	1.59	1.87	1.96	1.98	2.00	2.01	
10^{-2}	3.41E-02	2.31E-02	1.42E-02	6.37E-03	2.80E-03	1.11E-03	3.89E-04
	0.56	0.71	1.16	1.20	1.33	1.50	
10^{-3}	3.41E-02	2.32E-02	1.56E-02	1.02E-02	5.80E-03	3.10E-03	1.60E-03
	0.56	0.57	0.61	0.81	0.90	0.95	
10^{-4}	3.41E-02	2.32E-02	1.56E-02	1.02E-02	5.80E-03	3.10E-03	1.61E-03
	0.56	0.57	0.61	0.81	0.90	0.95	
⋮	⋮	⋮	⋮	⋮	⋮	⋮	⋮
10^{-15}	3.41E-02	2.32E-02	1.56E-02	1.02E-02	5.80E-03	3.10E-03	1.61E-03
	0.56	0.57	0.61	0.81	0.90	0.95	
E^n	3.41E-02	2.32E-02	1.56E-02	1.02E-02	5.80E-03	3.10E-03	1.61E-03
P^n	0.56	0.57	0.61	0.81	0.90	0.95	

$$
\begin{aligned}
\mathcal{L}^{h,k}(u-U)_{ij} &= (\mathcal{L}-\mathcal{L}^{h,k})u_{ij} \\
&= -\varepsilon(u_{xx})_{ij} - \varepsilon(u_{yy})_{ij} + a_{1ij}(u_x)_{ij} + a_{2ij}(u_y)_{ij} \\
&+ \frac{\varepsilon}{(\phi_{ij})_h^2}(u_{i+1,j} - 2u_ij + u_{i-1,j}) + \frac{\varepsilon}{(\phi_{ij})_k^2}(u_{i,j+1} - 2u_ij + u_{i,j-1}) \\
&- \frac{a_{1ij}}{h}(u_{ij} - u_{i-1,j}) - \frac{a_{2ij}}{k}(u_{ij} - u_{i,j-1}) \\
&= -\varepsilon(u_{xx})_{ij} - \varepsilon(u_{yy})_{ij} + \left(\frac{\varepsilon}{h^2} - \frac{a_{1ij}}{h} + \frac{a_{1ij}^2}{\varepsilon} - \frac{a_{1ij}^3}{\varepsilon^2}\right) \\
&\times \left(h^2(u_{xx})_{ij} + \frac{h^4}{12}(u_{xxxx})_{ij}\eta_{1ij}\right) + \left(\frac{\varepsilon}{k^2} - \frac{a_{2ij}}{k} + \frac{a_{2ij}^2}{\varepsilon} - \frac{a_{2ij}^3}{\varepsilon^2}\right) \\
&\times \left(k^2(u_{yy})_{ij} + \frac{h^4}{12}(u_{yyyy})_{ij}\eta_{2ij}\right) + \left(\frac{a_{1ij}h}{2}(u_{xx})_{ij} + \frac{a_{1ij}h^2}{6}(u_{xxx})_{ij}\right) \\
&+ \left(\frac{a_{2ij}k}{2}(u_{yy})_{ij} + \frac{a_{2ij}k^2}{6}(u_{yyy})_{ij}\right) \\
&\quad \text{where } \eta_{1ij} \in (u_{i+1,j}, u_{i-1,j}), \quad \eta_{2ij} \in (u_{i,j+1}, u_{i,j-1}) \\
&= -\frac{a_{1ij}h}{2}(u_{xx})_{ij} + \left(\frac{a_{1ij}^2}{\varepsilon}(u_{xx})_{ij} - \frac{a_{1ij}^2}{6}(u_{xxx})_{ij} + \frac{\varepsilon}{12}(u_{xxxx})_{ij}\eta_{1ij}\right)h^2 \\
&+ \left(\frac{a_{1ij}}{12}(u_{xxxx})_{ij}\eta_{1ij} - \frac{a_{1ij}^3}{\varepsilon^3}(u_{xx})_{ij}\eta_{1ij}\right)h^3 + \left(\frac{a_{1ij}^2}{12\varepsilon}(u_{xxx})_{ij}\right)h^4 \\
&- \left(\frac{a_{1ij}^3}{12\varepsilon^2}(u_{xxxx})_{ij}\eta_{1ij}\right)h^5 - \frac{a_{2ij}k}{2}(u_{yy})_{ij} \\
&+ \left(\frac{a_{2ij}^2}{\varepsilon}(u_{yy})_{ij} - \frac{a_{2ij}^2}{6}(u_{yyy})_{ij} + \frac{\varepsilon}{12}(u_{yyyy})_{ij}\eta_{2ij}\right)k^2 \\
&+ \left(\frac{a_{2ij}}{12}(u_{yyyy})_{ij}\eta_{2ij} - \frac{a_{2ij}^3}{\varepsilon^3}(u_{yy})_{ij}\eta_{2ij}\right)k^3 + \left(\frac{a_{2ij}^2}{12\varepsilon}(u_{yyy})_{ij}\right)k^4 \\
&- \left(\frac{a_{2ij}^3}{12\varepsilon^2}(u_{yyyy})_{ij}\eta_{2ij}\right)k^5
\end{aligned}
$$

Applying the bound on the solution and its derivatives in Lemma 2.3 and by Lemma 5.2 of [26], we obtain

$$|\mathcal{L}^{h,k}(u-U)_{ij}| \leqslant C(h+k).$$

Now, using Lemma (3.2) we have

$$\max_{0\leq i\leq n,\ 0\leq j\leq m} |(u-U)_{ij}| \leqslant C(h+k). \tag{4.1}$$

The analysis above is the proof of the following theorem:

Theorem 4.1. *Let $u(x, y)$ be the solution of (2.3)-(2.4) and $U(x, y)$ be the numerical approximation of $u(x, y)$ using the scheme (3.1)-(3.2). If $a_1(x, y)$, $a_2(x, y)$, $b(x, y)$ and $z(x, y)$ are sufficiently smooth functions, then there exists a constant C independent of ε , h and k such that*

$$\max_{0\leq i\leq n,\ 0\leq j\leq m} |(u-U)_{ij}| \leqslant C(h+k). \tag{4.2}$$

5. NUMERICAL RESULTS

In order to validate and confirm our theoretical results, we present two test examples. Since the exact solutions of our models are not available; we oblige to use the double mesh principle [27] to evaluate the maximum pointwise error and the ε-uniform error as follows

$$E_\varepsilon^{n,m} = \max_{(x_i,y_j)\in\bar{\Omega}^{n,m}} \left|U_{i,j}^{n,m} - U_{i,j}^{2n,2m}\right|, \quad E^{n,m} = \max_\varepsilon E_\varepsilon^{n,m}, \tag{5.1}$$

where $U_{i,j}^{n,m}$ is the discrete solution on the mesh $\Omega^{n,m}$ and $U_{i,j}^{2n,2m}$ is the discrete solution on the mesh $\Omega^{2n,2m}$. The corresponding rate of convergence and the ε-uniform rate of convergence are formulated as

$$P_\varepsilon^{n,m} = \log_2\left(\frac{E_\varepsilon^{n,m}}{E_\varepsilon^{2n,2m}}\right), \quad P^{n,m} = \max_\varepsilon P_\varepsilon^{n,m}. \tag{5.2}$$

We define the iteration stopping criterion as

$$\|U^{(r+1)} - U^{(r)}\| \leqslant 10^{-8}, \quad r = 1, 2, \ldots. \tag{5.3}$$

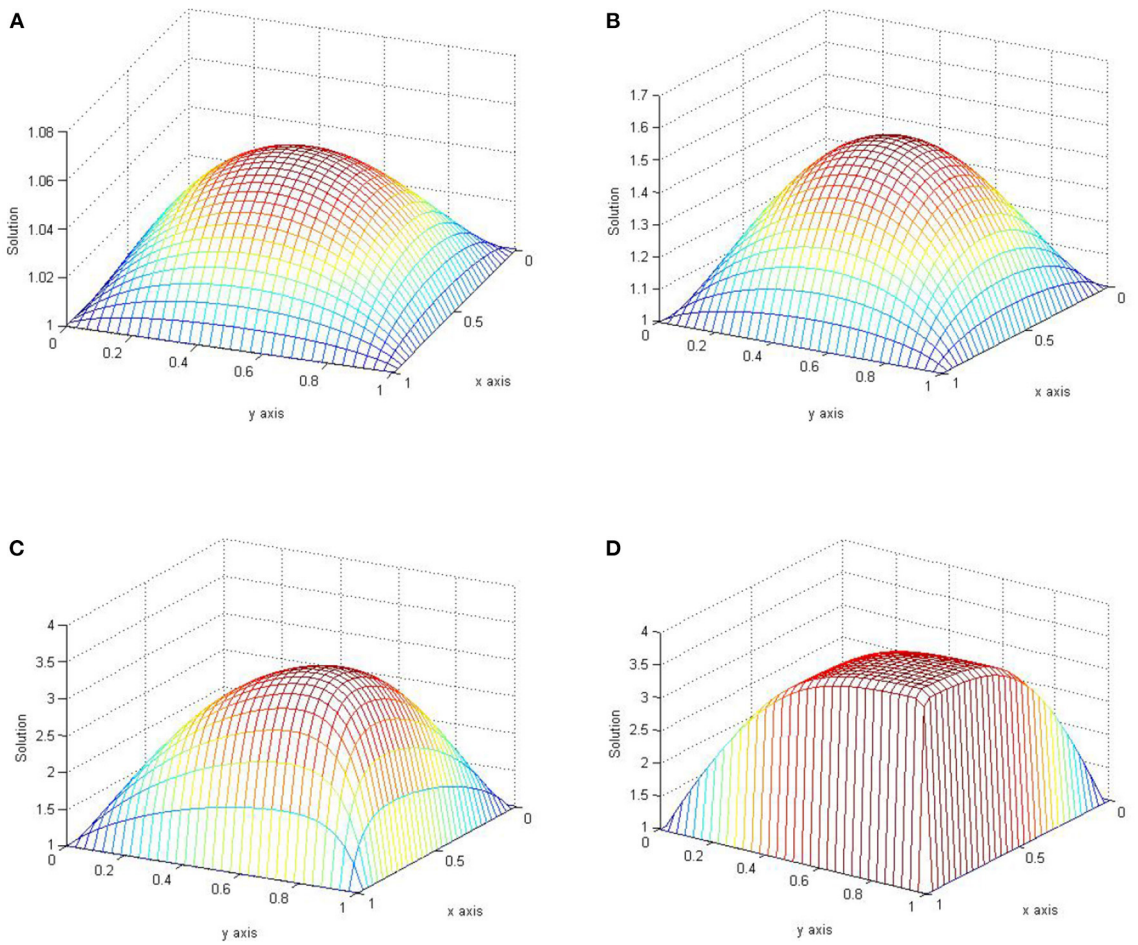

FIGURE 1 | Plots of the approximate solution of Example 5.1 with $n = m = 32$. **(A)** $\varepsilon = 1$. **(B)** $\varepsilon = 10^{-1}$. **(C)** $\varepsilon = 10^{-2}$. **(D)** $\varepsilon = 10^{-4}$.

Example 5.1. Boglaev [16], Consider the following singularly perturbed semilinear problem

$$-\varepsilon(u_{xx} + u_{yy}) + a_1(x,y)u_x + a_2(x,y)u_y + f(x,y,u) = 0,$$

$$(x,y) \in \Omega := (0,1)^2,$$

$$u = 1 \text{ on } \partial\Omega,$$

where $a_1(x,y) = a_2(x,y) = 0.1$, $f(x,y,u) = \dfrac{u-4}{5-u}$.

Example 5.2. Boglaev [15], Consider the following singularly perturbed semilinear problem

$$-\varepsilon(u_{xx} + u_{yy}) + a_1(x,y)u_x + a_2(x,y)u_y + f(x,y,u) = 0,$$

$$(x,y) \in \Omega := (0,1)^2,$$

$$u = 1 \text{ on } \partial\Omega,$$

where $a_1(x,y) = a_2(x,y) = 1$, $f(x,y,u) = 1 - \exp(-u)$.

To demonstrate the efficiency of the proposed scheme, we tabulate the maximum pointwise errors and the corresponding order of convergence. For the sake of simplicity, we considered same values of m and n as shown in **Tables 1**, **2**. These tables indicate a first-order uniform rate of convergence that conforms to the theoretical findings in Section 4. In producing our tables, we were limited by the software used as it could not handle large matrices. Had we been able to produce the tables for larger values of n and m (say, 64, 128, 512, etc.), we would have seen that the rate of convergence is one for Example 5.2 as well.

Figures 1, **2** are plots of the numerical solution of examples 5.1 and 5.2, respectively, for $n = m = 32$ and different values of ε. These plots exhibit the layer behavior of the numerical solution as ε approaches zero.

We wished to compare our results with those existing in the literature however we noticed that authors that published work on this problem focused more on the number of iterations

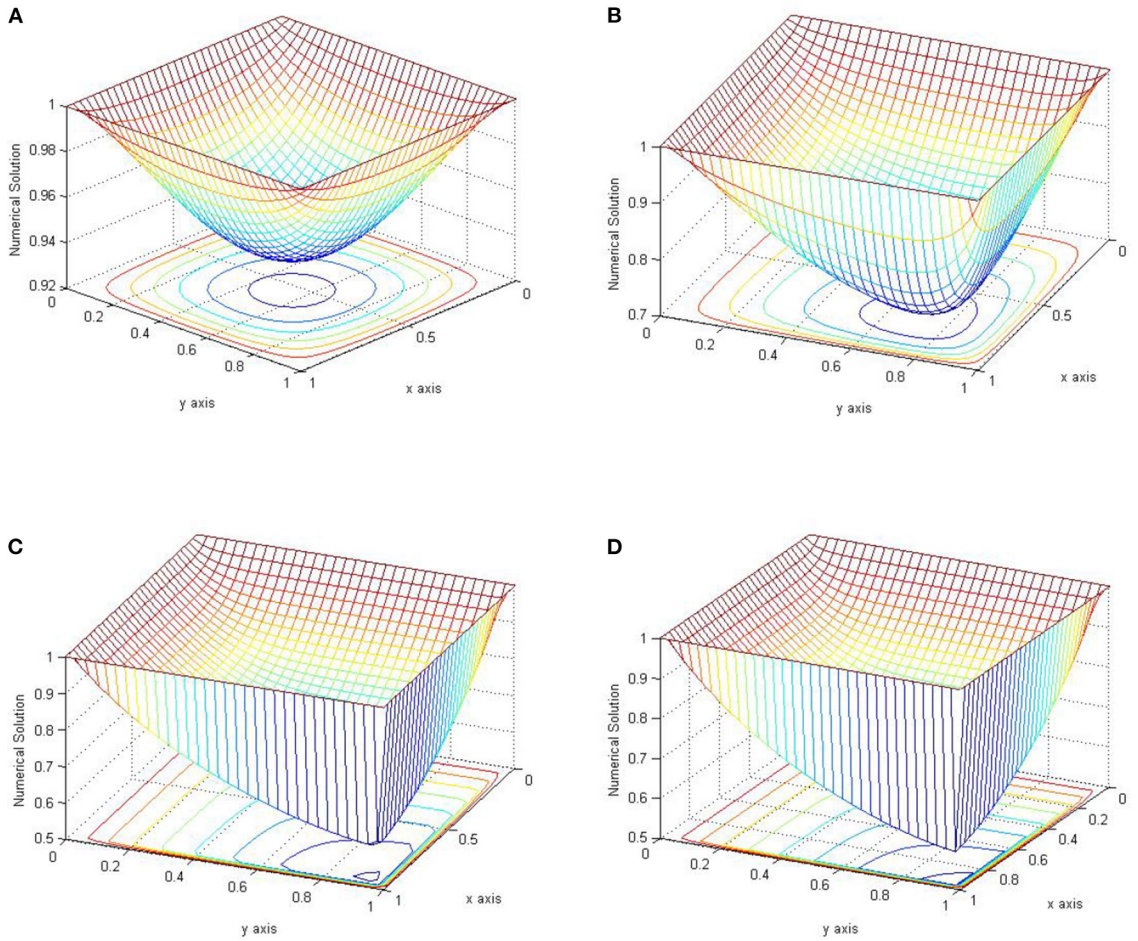

FIGURE 2 | Plots of the approximate solution of Example 5.2 with $n = m = 32$. **(A)** $\varepsilon = 1$. **(B)** $\varepsilon = 10^{-1}$. **(C)** $\varepsilon = 10^{-2}$. **(D)** $\varepsilon = 10^{-4}$.

while our focus is on maximum nodal errors and rates of convergence.

6. CONCLUSION

In this article, we constructed a fitted operator finite difference method to solve two-dimensional semilinear singularly perturbed convection-diffusion problems. First, we converted the semilinear problems into a sequence of linear two-dimensional singularly perturbed convection-diffusion problems *via* the quasilinearization technique. Next, we discretized the problem using the presented non-standard numerical scheme. Then, we performed the error analysis of the method and found that it is first order uniformly convergent in both x and y variables with respect to the perturbation parameter ε. We used two test examples to illustrate the robustness of the method and to validate the theoretical findings.

DATA AVAILABILITY STATEMENT

The original contributions presented in the study are included in the article/supplementary material, further inquiries can be directed to the corresponding author/s.

AUTHOR CONTRIBUTIONS

Plan was prepared by JM and AA. Computations and analysis were done by OK under JM's supervision. Write up was done by all authors. All authors agree to be accountable for the content of this article. All authors contributed to the article and approved submitted version.

ACKNOWLEDGMENTS

The research of JM and AA was supported by the National Research Foundation of South Africa. The authors wish to thank the reviewers for their valuable comments and suggestions that helped improve the quality of this paper.

REFERENCES

1. Prandtl L. Über Flussigkeitsbewegung bei sehr kleiner Reibung. In: *Proc. III Intern. Congr Math*. Heildeberg (1904).
2. He X, Wang K. New finite difference methods for singularly perturbed convection-diffusion equations. *Taiwanese J Math*. (2018) 22:949–78. doi: 10.11650/tjm/171002
3. Kadalbajoo MK, Patidar KC. Spline approximation method for solving self-adjoint singular perturbation problems on nonuniform grids. *J Comput Anal Appl*. (2003) 5:425–51. doi: 10.1155/S0161171203112094
4. Nhan TA, Vulanovic R. The Bakhvalov mesh: a complete finite-difference analysis of two-dimensional singularly perturbed convection-diffusion problems. *Num Algorith*. (2021) 87:203–21. doi: 10.1007/s11075-020-00964-z
5. Rao SCS, Chaturvedi AK. Parameter-uniform numerical method for a two-dimensional singularly perturbed convection-reaction-diffusion problem with interior and boundary layers. *Math Comput Simul*. (2021) 187:656–86. doi: 10.1016/j.matcom.2021.03.016
6. Roos HG, Line T. Gradient recovery for singularly perturbed boundary value problems II: Two-dimensional convection-diffusion. *Math Models Methods Appl Sci*. (2001) 11:1169–79. doi: 10.1142/S0218202501001288
7. Stynes M, Tobiska L. Necessary L2-uniform convergence conditions for difference schemes for two-dimensional convection-diffusion problems. *Comput Math Appl*. (1995) 29:45–53. doi: 10.1016/0898-1221(94)00237-F
8. Alexandrov VM, Pozharskii DA, Tielking JT. Three-dimensional contact problems. *Solid Mech Appl*. (2002) 55:B73–4. doi: 10.1115/1.1483357
9. Beebe NH. *A Complete Bibliography of Lecture Notes in Computational Science and Engineering*. (2017).
10. Gryanik V, Hartmann J. *Towards a Solution of the Closure Problem for Convective Atmospheric Boundary-Layer Turbulence*. Trieste: The Abdus Salam International Centre for Theoretical Physics (2017).
11. Gutkowski W, Kowalewski TA. Mechanics of the 21st century. In: *Proceedings of the 21st International Congress of Theoretical and Applied Mechanics*. Warsaw (2006). doi: 10.1007/1-4020-3559-4
12. Sivertsen OI, Andrianov I. Virtual testing of mechanical systems: theories and techniques. *Adv Eng*. (2002) 55:B66–7. doi: 10.1115/1.1483349
13. Ventsel E, Krauthammer T, Carrera E. Thin plates and shells: theory, analysis, applications. *Appl Mech Rev*. (2002) 55:B72–3. doi: 10.1115/1.1483356
14. Sirotkin V, Tarvainen P. Parallel Schwarz methods for convection-dominated semilinear diffusion problems. *J Comput Appl Math*. (2002) 145:189–211. doi: 10.1016/S0377-0427(01)00575-1
15. Boglaev I. A block monotone domain decomposition algorithm for semilinear convection-diffusion problem. *J Comput Appl Math*. (2005) 173:259–77. doi: 10.1016/j.cam.2004.03.011
16. Boglaev I. Uniform convergence of monotone iterative methods for semilinear singularly perturbed problems of elliptic and parabolic types. *Electron Trans Num Anal*. (2005) 20:86–103.
17. Boglaev I. A monotone Schwarz algorithm for a semilinear convection-diffusion problem. *J Num Math*. (2004) 12:169–91. doi: 10.1515/1569395041931455
18. Boglaev I, Duoba V. Domain decomposition for an advection-diffusion problem with parabolic layers. *Appl Math Comput*. (2003) 146:27–53. doi: 10.1016/S0096-3003(02)00514-3
19. Kopteva N. How accurate is the streamline-diffusion FEM inside characteristic (boundary and interior) layers. *Comput Methods Appl Mech Eng*. (2004) 193:4875–89. doi: 10.1016/j.cma.2004.05.008
20. Stynes M. Convection-diffusion-reaction problems, SDFEM/SUPG and a priori meshes. *Int J Comput Sci Math*. (2007) 1:412–31. doi: 10.1504/IJCSM.2007.016543
21. Vulkov L, Zadorin AI. Two-grid algorithms for the solution of 2D semilinear singularly-perturbed convection-diffusion equations using an exponential finite difference scheme. In: *AIP Conference Proceedings*. American Institute of Physics (2009). p. 371–379. doi: 10.1063/1.3265351
22. Mickens RE. *Nonstandard Finite Difference Models of Differential Equations*. World Scientific (1994). doi: 10.1142/2081
23. Munyakazi JB, Patidar KC. Higher order numerical methods for singularly perturbed elliptic problems. *Neural Parallel Sci Comput*. (2010) 18:75–88.
24. Munyakazi JB, Patidar KC. Novel fitted operator finite difference methods for singularly perturbed elliptic convection-diffusion problems in two dimensions. *J Diff Equat Appl*. (2012) 18:799–813. doi: 10.1080/10236198.2010.513330
25. Miller JJ, O'riordan E, Shishkin GI. *Fitted Numerical Methods for Singular Perturbation Problems: Error Estimates in the Maximum Norm for Linear Problems in One and Two Dimensions*. World Scientific (1996). doi: 10.1142/2933
26. Kadalbajoo MK, Patidar KC. ε-uniformly convergent fitted mesh finite difference methods for general singular perturbation problems. *Appl Math Comput*. (2006) 179:248–66. doi: 10.1016/j.amc.2005.11.096
27. Doolan EP, Miller JJ, Schilders WH. *Uniform Numerical Methods for Problems With Initial and Boundary Layers*. Eindhoven: Boole Press (1980).

Conflict of Interest: The authors declare that the research was conducted in the absence of any commercial or financial relationships that could be construed as a potential conflict of interest.

frontiers | Frontiers in Applied Mathematics and Statistics

ORIGINAL RESEARCH
published: 27 April 2022
doi: 10.3389/fams.2022.872284

To Use Face Masks or Not After COVID-19 Vaccination? An Impact Analysis Using Mathematical Modeling

Musyoka Kinyili, Justin B. Munyakazi and Abdulaziz Y. A. Mukhtar*

Department of Mathematics and Applied Mathematics, Faculty of Natural Sciences, University of the Western Cape, Bellville, South Africa

The question of whether to drop or to continue wearing face masks especially after being vaccinated among the public is controversial. This is sourced from the efficacy levels of COVID-19 vaccines developed, approved, and in use. We develop a deterministic mathematical model that factors in a combination of the COVID-19 vaccination program and the wearing of face masks as intervention strategies to curb the spread of the COVID-19 epidemic. We use the model specifically to assess the potential impact of wearing face masks, especially by the vaccinated individuals in combating further contraction of COVID-19 infections. Validation of the model is achieved by performing its goodness of fit to the Republic of South Africa's reported COVID-19 positive cases data using the Maximum Likelihood Estimation algorithm implemented in the fitR package. We first consider a scenario where the uptake of the vaccines and wearing of the face masks, especially by the vaccinated individuals is extremely low. Second, we consider a scenario where the uptake of the vaccines and wearing of the face masks by people who are vaccinated is relatively high. Third, we consider a scenario where the uptake of the vaccines and wearing of the face masks by the vaccinated individuals is on an upward trajectory. Findings from scenario one and scenario two, respectively, indicate a highly surging number of infections and a low recorded number of infections. For scenario three, it shows that the increased extent of wearing of the face masks by the vaccinated individuals at increasing levels of vaccine and face mask average protection results in a highly accelerated decrease in COVID-19 infections. However, wearing face masks alone also results in the reduction of the peak number of infections at increasing levels of face mask efficacy though the infections delay clearing.

Keywords: mathematical modeling, COVID-19 epidemic, deterministic models, pharmacological and non-pharmacological measures, computer-aided simulations

OPEN ACCESS

Edited by:
Hagos Hailu Gidey, Botswana International University of Science and Technology, Botswana

Reviewed by:
Salisu Garba, University of Pretoria, South Africa
Sourav Das, National Institute of Technology, Jamshedpur, India

****Correspondence:***
Musyoka Kinyili
4100150@myuwc.ac.za

Specialty section:
This article was submitted to Mathematical Biology, a section of the journal Frontiers in Applied Mathematics and Statistics

Received: *09 February 2022*
Accepted: *21 March 2022*
Published: *27 April 2022*

Citation:
Kinyili M, Munyakazi JB and Mukhtar AYA (2022) To Use Face Masks or Not After COVID-19 Vaccination? An Impact Analysis Using Mathematical Modeling. Front. Appl. Math. Stat. 8:872284. doi: 10.3389/fams.2022.872284

1. INTRODUCTION

COVID-19 is the most recent to be experienced in humans among the known coronaviruses such as Severe Acute Respiratory Syndrome (SARS) and Middle East Respiratory Syndrome (MERS) [1, 2]. However, COVID-19 caused by Severe Acute Respiratory Syndrome-Corona-Virus-2 (SARS-CoV-2) [2–6] has taken the longest time to clear from the human host. It seems to be the most devastating

coronavirus with its severity and rapidly spreading trend. Following its first report in December 2019 at Wuhan, Hubei province in China [5, 7–9], it has been among the greatly challenging global health emergencies in recent history [10, 11], especially with many countries world-wide engaged in battling the epidemic. Most countries have experienced at least three waves of the disease triggered by divergent SARS-CoV-2 variants probably resulting from the mutational characteristic of the virus. Each outbreak of the waves has been witnessed to re-surge the plateau number of infections to the extent of even surpassing the peak number of infections for the previous wave. As of January 27, 2022 (06:26 GMT), the world had recorded 363,305,191 COVID-19 positive cases with 5,646,069 deaths. The Republic of South Africa alone had confirmed 3,594,499 COVID-19 positive cases with 67,019 active cases and 94,651 fatalities [12].

Several non-pharmaceutical measure protocols implemented in most countries globally in the prolific effort to contain the spread of the epidemic have been relatively successful [13]. Among these non-pharmaceutical measures is the use of face masks by the general public. Although there was a lot of controversy on the use of face masks during the early outbreak of the disease, it was very well implemented and has played a key role in protection against contraction of the COVID-19 infections. Face masks have been proved to offer wide protection against both coarser droplets and finer aerosol transmission [2]. Now that COVID-19 has been reported to spread from human to human *via* fine respiratory droplets, it clearly implies that face masks have played a key role in breaking the chain of transmission for the epidemic.

On the side of the pharmaceutical pathway, over 50 companies commenced thorough scientific investigations in early 2020 to develop vaccines against COVID-19 [11, 14]. The fruits of these rigorous efforts were the discovery of vaccines such as Pfizer-BioNTech, Moderna, Oxford-AstraZeneca, and Johnson and Johnson's Janssen (J&J) vaccine [14, 15] among others. Furthermore, some regulatory bodies such as Europe Medicine Agency (EMA), US Food and Drug Administration (FDA), and UK Medicine and Health Products Regulatory Agency (MHRA) approved these vaccines for emergency use [11, 16]. The Pfizer-BioNTech vaccine was first approved for use in the UK on December 2, 2020, while the Oxford-AstraZeneca and Moderna vaccines were, respectively, approved on December 20, 2020, and January 8, 2021 [14]. J&J vaccine was approved for use by the US Food and Drug Administration and first rolled out on February 18, 2021, in the Republic of South Africa [12].

Pfizer-BioNTech, Oxford-AstraZeneca, and Moderna vaccines are prescribed to be administered in two doses whereas J&J vaccine is a single-dose prescribed administration [11]. Establishment on monitoring of mass vaccination campaigns and clinical trials have shown that Pfizer-BioNTech, Oxford-AstraZeneca, and Moderna vaccines can offer high levels of moderate to severe COVID-19 symptomatic protection when the two shots are administered 2–4 weeks apart [17–20]. However, most countries globally have a great challenge in the delivery of vaccines mainly due to the supply inadequacy and restricted capacity of distribution [11, 15]. The COVID-19 vaccines are being procured by most low- and middle-income countries *via* the COVAX Advance Market Commitment (AMC) Facility which is a world-wide risk-sharing mechanism for the collaborative procurement of the COVID-19 vaccines [11, 21].

Based on the clinical history regarding the pharmacological action of a wide range of existing vaccines against various diseases, these vaccines have full protection capacity while administered against the targeted disease. The administration of these vaccines demands no further protection action by the patient once administered. However, the COVID-19 vaccines are controversial since, among the so far approved vaccines being used, no single vaccine offers 100% protection against the contraction of the disease. It is clearly evidenced that even when one is vaccinated against COVID-19, there is a possibility of being infected following exposure. Furthermore, most vaccines have a prescription of two-dose administration after some prescribed duration apart. This again gives room for chances of contracting the virus while waiting to receive the second dose and even when there is a delay in availing the second dose. In view of these shortcomings, one natural question arises: Which friendly non-pharmaceutical protocol can be adopted after vaccination? This study attempts to address this question using mathematical modeling.

Mathematical modeling has been widely used by scientists in assessing the impacts of both pharmacological and non-pharmacological strategies in an effort to combat the transmission of the SARS-CoV-2 [1, 22–30]. Particularly, in Sun and Wang [23], mathematical modeling is used to investigate the transmission dynamics of the COVID-19 epidemic. Similarly, more studies are also done in Lukman et al. [31], Wong et al. [22], Sameni [32], Bedi et al. [33], Boukanjime et al. [24], Garba et al. [1], Zhao et al. [34], Gilbert et al. [35], Peirlinck et al. [36], Ishtiaq [6], Salgotra et al. [37], and Amaro et al. [38] on the spread dynamics of COVID-19 using different devised mathematical models. In Eikenberry et al. [2], mathematical modeling is adopted to assess the potential impact of the use of face masks by the general public as a control measure strategy against the COVID-19 epidemic spread. Similar modeling studies addressing the effectiveness of the use of face masks to control the spread of COVID-19 are also done in Yang et al. [39], Li et al. [40], Howard et al. [41], Shen et al. [42], and Stutt et al. [43]. In Garba et al. [1], a compartmental model is employed to study the impacts of social distancing among the public as an intervention strategy to curb the transmission of the COVID-19 pandemic. Modeling studies on the impacts of social distancing besides other containment measure protocols against transmission of SARS-CoV-2 is similarly done in Nyabadza et al. [44], Bastos and Cajueiro [5], Kennedy et al. [25], Lyra et al. [29], and Mason et al. [45]. In Olivares and Staffetti [16], the impact of vaccination, testing against COVID-19 and social distancing is studied using mathematical modeling. In Moore et al. [14], Moghadas et al. [15], Foy et al. [21], Sadarangani et al. [26], Iboi et al. [46], and Gumel et al. [47], similar studies on assessing the potential impacts of vaccination strategy and/or in presence of other containment measures are also done. We note that, among the studies mentioned above, none has considered the aspect of wearing face masks especially after vaccination, hence, it is worthy to bridge this gap.

Therefore, this study seeks to develop a deterministic mathematical model that combines vaccination programs against COVID-19 and the use of face masks as intervention strategies in curbing the spread of the epidemic. The model principally aims to assess the potential impact of wearing face masks, especially on vaccinated individuals.

We organize the rest of the article as follows: In Section 2, we formulate the model. Section 3 presents analytical results of the model covering positivity of solution, biological feasible region, and stability analysis of the infection free equilibrium. In Section 4, we present numerical results and discussion including model calibration, sensitivity analysis, and simulations. Finally, Section 5 gives the conclusion.

2. MODEL FORMULATION

On the grounds of the challenges and drawbacks associated with the entire COVID-19 vaccination program (refer to Section 1), we modify the standard SEIR deterministic model to incorporate a combination of vaccination and wearing of face masks as intervention strategies to combat the spread of the COVID-19 epidemic. For this reason, we add a compartment for vaccinated individuals wearing face masks and a compartment for individuals wearing face masks but not vaccinated. Assuming human-to-human transmission, we subdivide the total human population $N(t)$ into seven mutually exclusive classes namely the susceptible class ($S(t)$), the class of individuals who are vaccinated and wearing face masks ($S_{mv}(t)$), the class of individuals wearing face masks but not vaccinated ($S_m(t)$), the latent class ($E(t)$), the infectious class of individuals who are symptomatic ($I_s(t)$), the infectious class of individuals who are asymptomatic ($I_a(t)$), and the class of individuals who have recovered from the COVID-19 infections ($R(t)$). Therefore, the total human population over time t for the proposed model is

$$N(t) = S(t) + S_{mv}(t) + S_m(t) + E(t) + I_s(t) + I_a(t) + R(t). \quad (1)$$

We stress that the model factors in the use of face masks, especially by the vaccinated individuals since it is evidenced that the so far developed and approved COVID-19 vaccines being used do not offer 100% protection against the disease. Moreover, most of them are even 2-shots vaccines administered after some duration apart thus allowing chances for contracting the disease while waiting for the second dose. Thus, the main aim of this study is to assess the potential impact of the use of face masks by vaccinated individuals in reducing COVID-19 infections.

The model basically indicates that the susceptible individuals ($S(t)$) can either progress to the class of individuals who are vaccinated and wearing face masks ($S_{mv}(t)$), or join the class of individuals who are using (wearing) face masks but not vaccinated ($S_m(t)$), or progress to the class of individuals who are initially neither vaccinated nor wearing face masks ($E(t)$). The model assumes that individuals who are neither vaccinated nor wearing face masks are highly prone to the infections and, thus, proceed directly to latency. The latent class $E(t)$ though mainly contains individuals who are initially neither vaccinated nor wearing face masks, individuals who get vaccinated and/or wear face masks over time may join the class following exposure to the disease. The susceptible population either gets vaccinated and wear face masks at the rate of ω, or wear face masks only at the rate of $(1-\omega)\delta$, or progress to latency at the rate of $(1-\omega)(1-\delta)$ following effective contact rate of β with either symptomatic or asymptomatic infectious individuals. Based on the aforementioned challenges associated with the whole vaccination program, the vaccinated individuals wearing face masks can progress to the latent class $E(t)$ at the rate of $(1-\alpha)$, following exposure to the infection by either symptomatic or asymptomatic infectious individuals. Here, we note that the vaccinated individuals wearing faces masks are less prone to the contraction of the infections due to their boosted immunity and masks' protection effected by the vaccine and mask average protection denoted by α on the model. Similarly, the individuals wearing face masks only ($S_m(t)$) progress to the latent class at the rate of $(1-\sigma)$ following their close contact with either symptomatic or asymptomatic infectious individuals. Notably, these individuals are still protected to some extent against infections due to the masks efficacy of σ. We note that wearing face masks and using face masks means the same in this study.

All the exposed individuals collected in the class of latency $E(t)$, can either progress to the symptomatic class of infectious individuals at the rate of $\eta\rho$ or the asymptomatic class of infectious individuals at the rate of $(1-\rho)\eta$. These are individuals who have completed the incubation period and shed the virus, thus, causing COVID-19 infections. Since the epidemic has been endemic, we consider a recruitment rate of Γ. Despite the fact that individuals from all the seven classes of the model can die naturally at the rate of μ, the symptomatic and the asymptomatic infectious individuals can die due to COVID-19, respectively, at the rates of ε_s and ε_a. Thus, the COVID-19 epidemic induced deaths for the model are given by $\frac{dD(t)}{dt} = \varepsilon_s I_s + \varepsilon_a I_a$. The symptomatic and the asymptomatic individuals recover from the disease at the rates of ϕ and ψ, respectively. The recovered individuals are collected in class $R(t)$. **Figure 1** illustrates the proposed model. The resultant system of nonlinear ordinary differential equations for the model is

$$\frac{dS}{dt} = \Gamma - (\omega + (1-\omega)\delta + \mu)S - (1-\omega)(1-\delta)\gamma_0 S \quad (2)$$

$$\frac{dS_{mv}}{dt} = \omega S - ((1-\alpha)\gamma_1 + \mu)S_{mv} \quad (3)$$

$$\frac{dS_m}{dt} = (1-\omega)\delta S - (1-\sigma)\gamma_2 S_m - \mu S_m \quad (4)$$

$$\frac{dE}{dt} = (1-\omega)(1-\delta)\gamma_0 S + (1-\alpha)\gamma_1 S_{mv} + (1-\sigma)\gamma_2 S_m - (\eta + \mu)E \quad (5)$$

$$\frac{dI_s}{dt} = \rho\eta E - (\phi + \varepsilon_s + \mu)I_s \quad (6)$$

$$\frac{dI_a}{dt} = (1-\rho)\eta E - (\psi + \varepsilon_a + \mu)I_a \quad (7)$$

$$\frac{dR}{dt} = \phi I_s + \psi I_a - \mu R \quad (8)$$

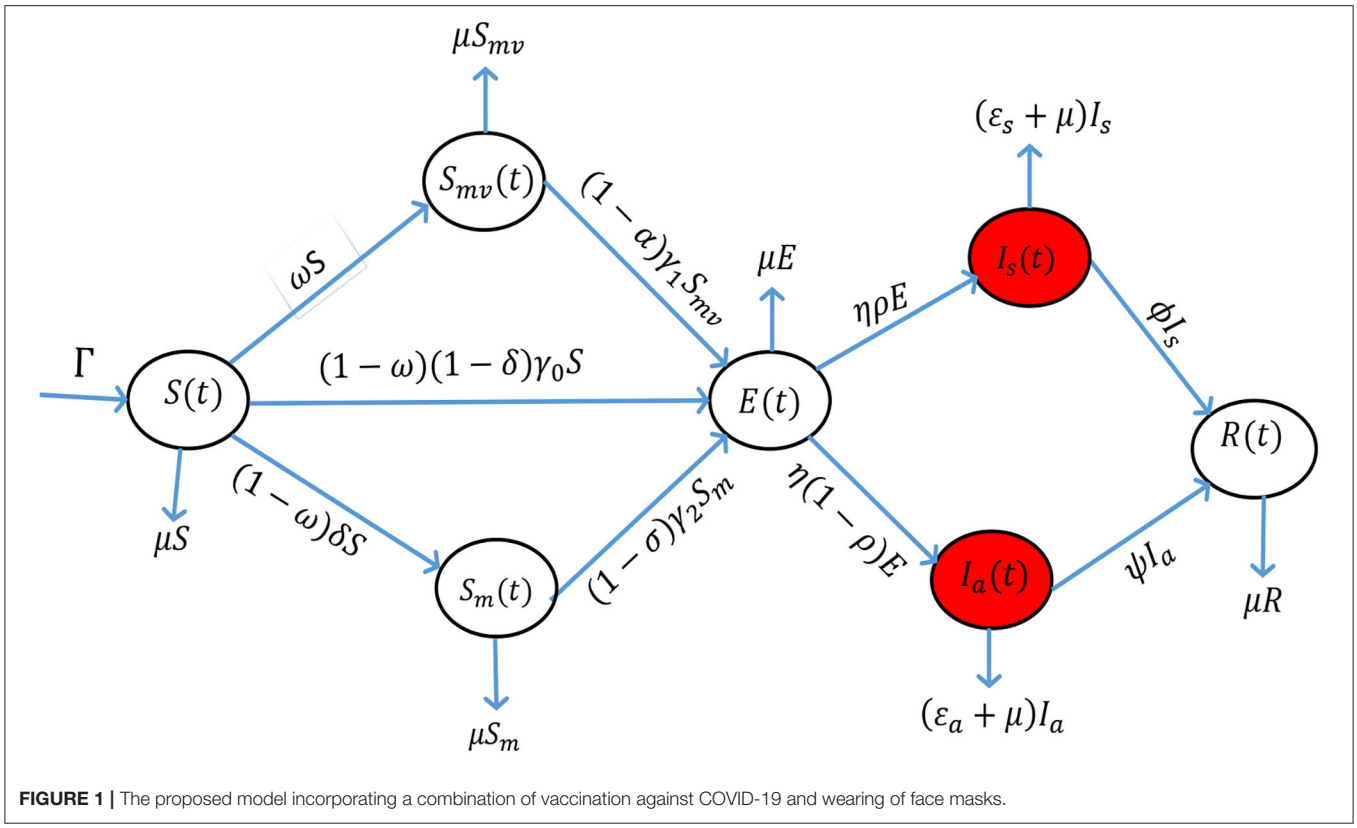

FIGURE 1 | The proposed model incorporating a combination of vaccination against COVID-19 and wearing of face masks.

where

$$\gamma_i = \beta_i(\xi I_s + I_a), i = 0, 1, 2 \tag{9}$$

defines the force of infections for the model with $\xi < 1$ denoting the modification parameter since the asymptomatic individuals are assumed to be more infectious than the symptomatic individuals. We describe the other parameters of the model in **Table 1**.

3. ANALYTICAL RESULTS

We present some results regarding the epidemiological properties of the proposed model (Equations 2–8).

3.1. Positivity of the Solution

Lemma 3.1:

Let $S(0) > 0$, $S_{mv}(0) > 0$, $S_m(0) > 0$, $E(0) > 0$, $I_s(0) > 0$, $I_a(0) > 0$ and $R(0) > 0$. Then $S(t) > 0$, $S_{mv}(t) > 0$, $S_m(t) > 0$, $E(t) > 0$, $I_s(t) > 0$, $I_a(t) > 0$ and $R(t) > 0, \forall\, t \geq 0$.

Proof

Suppose that the solution of the model (Equations 2–8) is not positive for all $t \geq 0$. Then there exist a first time $t^* > 0$ such that

$$t^* = \inf\{t \mid S(t) = 0 \text{ or } S_{mv}(t) = 0 \text{ or } S_m(t) = 0 \text{ or } E(t) = 0 \text{ or } I_s(t) = 0 \text{ or } I_a(t) = 0 \text{ or } R(t) = 0\}.$$

If $S(t^*) = 0$, then $\forall\, t \in (0, t^*)$, $S(t) > 0$, $S_{mv}(t) > 0$, $S_m(t) > 0$, $E(t) > 0$, $I_s(t) > 0$, $I_a(t) > 0$ and $R(t) > 0$, $\frac{dS(t^*)}{dt} < 0$. In contradiction from Equation (2) we have $\frac{dS(t^*)}{dt} = \Gamma > 0$ which implies that $S(t) > 0$ for all $t \geq 0$. Arguing similarly, it can be verified that $S_{mv}(t) > 0$, $S_m(t) > 0$, $E(t) > 0$, $I_s(t) > 0$, $I_a(t) > 0$ and $R(t) > 0$ for all $t \geq 0$.

TABLE 1 | Parameter description for the model (Equations 2–8) and their estimated values.

Symbol	Parameter description	Value per day	Source
Γ	Recruitment rate	11,244	[44]
β_i	Effective contact rate	1.0598	[44]
ω	Extent of vaccination and face masks use	(0,1)	Variable
δ	Measure of face masks use by unvaccinated	0.66	Assumed
α	Measure of vaccine and mask average protection	(0,1)	Variable
ρ	Measure of symptomatic development	0.38	Fitted
η	Incubation period	0.1961	[16, 21]
ξ	Infectious rate by the symptomatic individuals	0.3214	[46]
σ	Measure of face mask efficacy	(0,1)	Variable
ϕ	Rate of recovery by the symptomatic individuals	0.1429	[46, 48]
ψ	Rate of recovery by the asymptomatic individuals	0.3217	Fitted
ε_s	Rate of death by the symptomatic individuals	0.035	[1]
ε_a	Rate of death by the asymptomatic individuals	0.018	[1]
μ	Rate of natural death	0.0001	[48]

3.2. Biological Feasible Region

Lemma 3.2:

$$\text{Let } \Omega_{\mathcal{R}} = \left\{ (S, S_{mv}, S_m, E, I_s, I_a, R) \in \mathbb{R}_+^7 : S + S_{mv} + S_m + E + I_s + I_a + R \leq \frac{\Gamma}{\mu} \right\}$$

be a biological feasible region defined for all $t \geq 0$. Then, $\Omega_{\mathcal{R}}$ is positively invariant and absorbing with respect to the model (Equations 2–8).

Proof

We compute the time derivative of the total population $N(t)$ in line with Equation (1) along the solution to obtain

$$\begin{aligned} \frac{dN}{dt} &= \Gamma - \mu N - \varepsilon_s I_s - \varepsilon_a I_a \\ &\leq \Gamma - \mu N. \end{aligned} \tag{10}$$

Solving Equation (10) by integration and the Gronwall Inequality with $N(0) = N_0$ we get

$$N(t) \leq \frac{\Gamma}{\mu}\left(1 - e^{-\mu t}\right) + N_0 e^{-\mu t}. \tag{11}$$

Employing comparison theorems on ODEs [49], Equation (11) gives

$$\lim_{t \to \infty} N(t) \leq \frac{\Gamma}{\mu}. \tag{12}$$

From Equation (12), we see that $N \leq \frac{\Gamma}{\mu}, \forall t \geq 0$. This shows that N is bounded and, therefore, infers that the biological feasible region $\Omega_{\mathcal{R}}$ is positively invariant and absorbing for all $t \geq 0$. Hence, the dynamics of the model (Equations 2–8) can be considered in $\Omega_{\mathcal{R}}$ for all $t \geq 0$ [50].

3.3. Infection Free Equilibrium and Stability Analysis

At the instant when no individual is infected in the population of concern, then this situation is referred to as infection-free equilibrium [48, 51]. We find that the proposed model has a unique infection-free equilibrium denoted and defined as

$$\mathcal{E}^* = \left(S^*, S_{mv}^*, S_m^*, 0, 0, 0, 0\right) \tag{13}$$

where,

$$\begin{aligned} S^* &= \frac{\Gamma}{\omega + (1-\omega)\delta + \mu}, \\ S_{mv}^* &= \frac{\Gamma\omega}{(\omega + (1-\omega)\delta + \mu)\mu}, \\ S_m^* &= \frac{\Gamma(1-\omega)\delta}{(\omega + (1-\omega)\delta + \mu)\mu}. \end{aligned} \tag{14}$$

3.3.1. Reproduction Number and Local Stability

We analyze the model's infection-free equilibrium local asymptotic stability by first computing the reproduction number. Since the model incorporates vaccination and the use of face masks as control measure strategies against COVID-19, some proportion of the susceptible population has adopted the measures, and thus, we define the vaccination-mask reproduction number which we denote by $\mathcal{R}_{vm}$. The $\mathcal{R}_{vm}$ here is defined as the mean secondary number of infections sourced by one infectious individual when introduced into a susceptible population where a proportion is vaccinated and/or wear face masks. We adopt the next generation operator technique for the computation of the $\mathcal{R}_{vm}$ [51]. The Jacobian for secondary infections $\mathcal{F}$ and transfer of infections $\mathcal{V}$ for the model (Equation 2–8) are respectively given by

$$\mathcal{F} = \begin{pmatrix} 0 & \frac{\beta\xi\Gamma}{\omega+(1-\omega)\delta+\mu}\ell & \frac{\beta\Gamma}{\omega+(1-\omega)\delta+\mu}\ell \\ 0 & 0 & 0 \\ 0 & 0 & 0 \end{pmatrix}, \tag{15}$$

where

$$\ell = (1-\omega)(1-\delta) + \frac{(1-\alpha)\omega}{\mu} + \frac{(1-\sigma)(1-\omega)\delta}{\mu}$$

and

$$\mathcal{V} = \begin{pmatrix} \eta + \mu & 0 & 0 \\ -\rho\eta & \phi + \mu & 0 \\ -(1-\rho)\eta & 0 & \psi + \mu \end{pmatrix}, \tag{16}$$

thus

$$\mathcal{F}\mathcal{V}^{-1} = \begin{pmatrix} \frac{\beta\Gamma}{(\omega+(1-\omega)\delta+\mu)(\eta+\mu)}\ell\left\{\frac{\rho\eta\xi}{\phi+\mu} + \frac{(1-\rho)\eta}{\psi+\mu}\right\} & \frac{\beta\Gamma\xi}{(\omega+(1-\omega)\delta+\mu)(\phi+\mu)}\ell & \frac{\beta\Gamma}{(\omega+(1-\omega)\delta+\mu)(\psi+\mu)}\ell \\ 0 & 0 & 0 \\ 0 & 0 & 0 \end{pmatrix}. \tag{17}$$

Hence, the model's reproduction number is

$$\mathcal{R}_{vm} = \frac{\beta\Gamma}{(\omega + (1-\omega)\delta + \mu)(\eta + \mu)}\ell\left\{\frac{\xi\rho\eta}{\phi + \mu} + \frac{(1-\rho)\eta}{\psi + \mu}\right\}. \tag{18}$$

Therefore, the infection-free equilibrium of the proposed model is locally asymptotically stable if

$$\mathcal{R}_{vm} = \frac{\beta\Gamma}{(\omega + (1-\omega)\delta + \mu)(\eta + \mu)}\ell\left\{\frac{\xi\rho\eta}{\phi + \mu} + \frac{(1-\rho)\eta}{\psi + \mu}\right\} < 1. \tag{19}$$

We note that the symptomatic and the asymptomatic individuals account for the new COVID-19 infections, and therefore, we can re-write (Equation 18) as

$$\mathcal{R}_{vm} = \mathcal{R}_{vm-s} + \mathcal{R}_{vm-a} \tag{20}$$

where

$$\mathcal{R}_{vm-s} = \frac{\beta\Gamma}{(\omega+(1-\omega)\delta+\mu)(\eta+\mu)}\ell\left\{\frac{\xi\rho\eta}{\phi+\mu}\right\} \quad (21)$$

and

$$\mathcal{R}_{vm-a} = \frac{\beta\Gamma}{(\omega+(1-\omega)\delta+\mu)(\eta+\mu)}\ell\left\{\frac{(1-\rho)\eta}{\psi+\mu}\right\}. \quad (22)$$

3.3.2. Global Stability

We adopt the approach used by Castillo-Chavez et al. [51] to prove the global stability of the model's infection-free equilibrium.

Theorem 3.3.2

Let the model be expressible in the form, $\frac{d\mathbf{P}}{dt} = Y(\mathbf{P},\mathbf{Q})$, $\frac{d\mathbf{Q}}{dt} = M(\mathbf{P},\mathbf{Q})$, $M(\mathbf{P},0) = 0$, where $\mathbf{P}$ denotes the collection of non-disease classes and $\mathbf{Q}$ represents the collection of disease classes of the model. The equilibrium point $\mathcal{E}^* = (\mathbf{P}^*, 0)$ of the model is globally asymptotically stable (g. a. s) if and only if $\mathcal{R}_{vm} < 1$ and satisfies the following conditions

C_1 : $\frac{d\mathbf{P}}{dt} = Y(\mathbf{P},0)$, $\mathbf{P}^*$ is globally asymptotically stable.

C_2 : $M(\mathbf{P},\mathbf{Q}) = N\mathbf{Q} - \widetilde{M}(\mathbf{P},\mathbf{Q})$, $\widetilde{M}(\mathbf{P},\mathbf{Q}) \geq 0$ for $(\mathbf{P},\mathbf{Q}) \in \mathbb{R}^7_+$ where $N = \frac{\partial M}{\partial \mathbf{Q}}\mathcal{E}^*$ and $\mathbb{R}^7_+$ is the region where the model makes biological sense.

Proof

We deduce that $\mathbf{P} = (S, S_{mv}, S_m, R)^T$ and $\mathbf{Q} = (E, I_s, I_a)^T$ from the model (Equations 2–8). The infection-free equilibrium of the model is $\mathcal{E}^* = (\mathbf{P}^*, 0) = \left(S^*, S^*_{mv}, S^*_m, 0, 0, 0, 0\right)$ as established by Equation (13). The point $\mathcal{E}^* = (\mathbf{P}^*, 0)$ is g. a. s if $\mathcal{R}_{vm} < 1$, hence

$$\frac{d\mathbf{P}}{dt} = Y(\mathbf{P},0) = \begin{bmatrix} \Gamma - (\omega+(1-\omega)\delta+\mu)S \\ \omega S - \mu S_{mv} \\ (1-\omega)\delta S - \mu S_m \\ 0 \\ 0 \end{bmatrix},$$

and, therefore, C_1 is satisfied. We next check the satisfaction of C_2 as

$$N\mathbf{Q} = \begin{pmatrix} -(\eta+\mu) & 0 & 0 \\ \rho\eta & -(\phi+\mu) & 0 \\ (1-\rho)\eta & 0 & -(\psi+\mu) \end{pmatrix}\begin{pmatrix} E \\ I_s \\ I_a \end{pmatrix}$$

and

$$M(\mathbf{P},\mathbf{Q}) = \begin{pmatrix} \beta(\xi I_s + I_a)(1-\omega)(1-\delta)S + (1-\alpha)\beta(\xi I_s + I_a)S_{mv} + (1-\sigma)\varepsilon\beta(\xi I_s + I_a)S_m \\ \rho\eta E - (\phi+\mu)I_s \\ (1-\rho)\eta E - (\psi+\mu)I_a \end{pmatrix}.$$

Using $M(\mathbf{P},\mathbf{Q}) = N\mathbf{Q} - \widetilde{M}(\mathbf{P},\mathbf{Q})$ then,

$$\widetilde{M}(\mathbf{P},\mathbf{Q}) = \begin{pmatrix} \beta(\xi I_s + I_a)\left\{(1-\omega)(1-\delta)\left(1-\frac{S}{N}\right) + (1-\alpha)\left(1-\frac{S_{mv}}{N}\right) + (1-\sigma)\varepsilon\left(1-\frac{S_m}{N}\right)\right\} \\ 0 \\ 0 \end{pmatrix}.$$

therefore $\widetilde{M}(\mathbf{P},\mathbf{Q}) \geq 0$ hence C_2 is satisfied. Thus, we conclude that the model's infection-free equilibrium is globally asymptotically stable whenever $\mathcal{R}_{vm} < 1$.

4. NUMERICAL RESULTS AND DISCUSSION

4.1. Calibration of the Model

We use the Maximum Likelihood Estimation algorithm implemented in the fitR package for calibrating the model (Equations 2–8). The public data used are the daily COVID-19 positive cases as reported by the government of the Republic of South Africa from June 01, 2020, to September 08, 2020 [12]. The goodness of fit is established in **Figure 2**.

4.2. Sensitivity Analysis

We perform the sensitivity analysis for the model graphically using Equation (18) to assess the impacts of the parameters of interest on the vaccination-mask reproduction number $\mathcal{R}_{vm}$. The cardinal parameters of scrutiny for this research are ω for the measure of the extent of vaccination and face mask use, α for the measure of vaccine and face mask average protection, and σ for the measure of face mask efficacy. The vaccine and face mask average protection here refers to the mean value protection against the contraction of the infections brought about by the combination of the vaccine efficacy and face mask efficacy. This aspect only occurs to those people who are vaccinated and still wear face masks. They enjoy double protection in which one is facilitated by the vaccine and the second is facilitated by the face mask. Those people who wear face masks only enjoy the benefit of face masks protection brought about by the face mask efficacy. We define to have a poor extent of vaccination and face mask use, a poor extent of vaccine and face mask average protection, and poor face mask efficacy if each of the parameters approach zero whereas the perfect extent of vaccination and face mask use, the perfect extent of vaccine and face mask average protection, and perfect face mask efficacy are attained when each of the parameters tends to unity, hence, $0 < \omega < 1$, $0 < \alpha < 1$, and $0 < \sigma < 1$. We consider four levels of the extent of vaccine and face mask average protection (α) such that $\alpha = 20\%$, $\alpha = 50\%$, $\alpha = 70\%$, and $\alpha = 95\%$. For the face mask efficacy (σ), we also consider four levels, i.e., $\sigma = 20\%$, $\sigma = 40\%$, $\sigma = 60\%$, and $\sigma = 80\%$. The impacts assessment is depicted in **Figure 3**.

The figure demonstrates the variation of the reproduction number with ω when α and σ are simultaneously endorsed in at increasing levels as aforementioned. We clearly observe that $\mathcal{R}_{vm}$ decreases gently with an increase in ω at each level of α and σ. Distinctively, the figure reveals an incredible shift of $\mathcal{R}_{vm}$ values tending to less than unity when the α and σ levels are simultaneously increased. We see that increasing levels of α and σ accelerates the reduction in the value of the reproduction

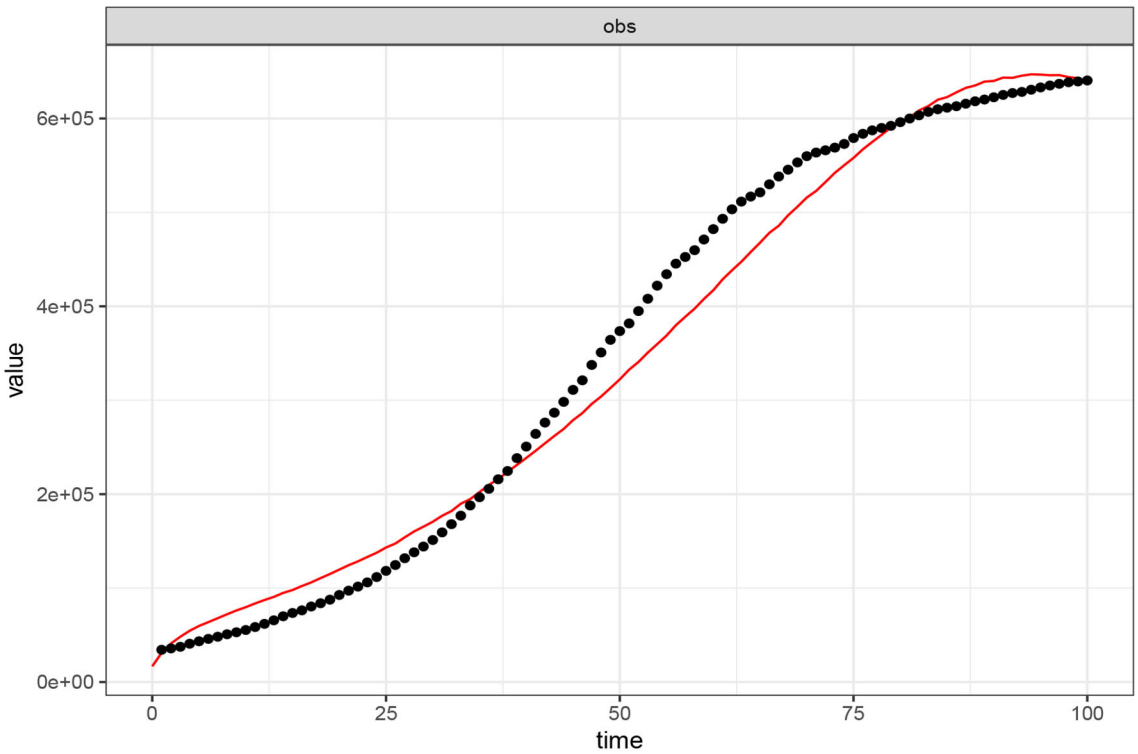

FIGURE 2 | Calibration of the model (Equations 2–8) to COVID-19 positive reported cases (01 June–08 September, 2020) in the Republic of South Africa. The black dotted line shows the reported data while the red-continuous line depicts the model's goodness of fit. Parameter values used are as listed in **Table 1** where $\omega = 0.00001$, $\alpha = 0.00001$, and $\sigma = 0.00001$.

number. This distinct observed trend stipulates that increasing the extent of vaccination against COVID-19 simultaneously with the wearing of face masks, highly reduces the value of basic reproduction. This consequentially leads to the speeding up of the stabilization of the infection-free equilibrium, hence, leading to the eradication of the epidemic over a relatively shorter time.

4.3. Simulations

We test for different scenarios with respect to the parameters of interest *via* numerical simulations using the calibrated model. We concentrate the simulations on the disease classes of the model which include the latent class, the symptomatic, and the asymptomatic infectious classes. The principal purpose of the model (Equations 2–8) was actually to assess the impact of wearing face masks on those individuals who are vaccinated against the COVID-19 epidemic. This is based on the grounds that with the already developed and approved vaccines in use, it is evidenced that no vaccine offers 100% efficacy, and therefore, individuals who are vaccinated have a chance of contracting the infections. Furthermore, some vaccines are prescribed to be administered in 2 doses after some duration apart, and thus, a vaccinated individual can also contract the infections while waiting to receive the second dose. Hence, we carry out simulations varying the aforementioned parameters of interest for this study. The other parameter values used are listed in **Table 1**.

We first consider a scenario where the uptake of the vaccines and wearing of the face masks especially by the vaccinated individuals is extremely low. Second, we consider a scenario where the uptake of the vaccines and wearing of the face masks by people who are vaccinated is relatively high. Third, we consider a scenario where the uptake of the vaccines and wearing of the face masks by the vaccinated individuals is on an upward trajectory. Under this third scenario, we consider four levels of the extent of vaccine and face mask average protection (α) such that $\alpha = 20\%$, $\alpha = 50\%$, $\alpha = 70\%$, and $\alpha = 95\%$ as considered during the sensitivity analysis. For the face mask efficacy (σ), we also consider four level that is, $\sigma = 20\%$, $\sigma = 40\%$, $\sigma = 60\%$, and $\sigma = 80\%$.

Figures 4A–C, respectively, show the trajectory of the symptomatic, the asymptomatic, and the latent classes of the model (Equations 2–8) when the uptake of the COVID-19 vaccines and wearing of face masks by the vaccinated individuals is extremely low. In this situation, we clearly observe a highly surging number of recorded symptomatic infections, asymptomatic infections, and latent cases as a result. This observation suggests that the absence or low implementation of these control measure strategies would lead to a resurgence in the peak number of COVID-19 infections as well as rising exposure cases. Furthermore, it is observed that the infections take a relatively long time to clear from the human host.

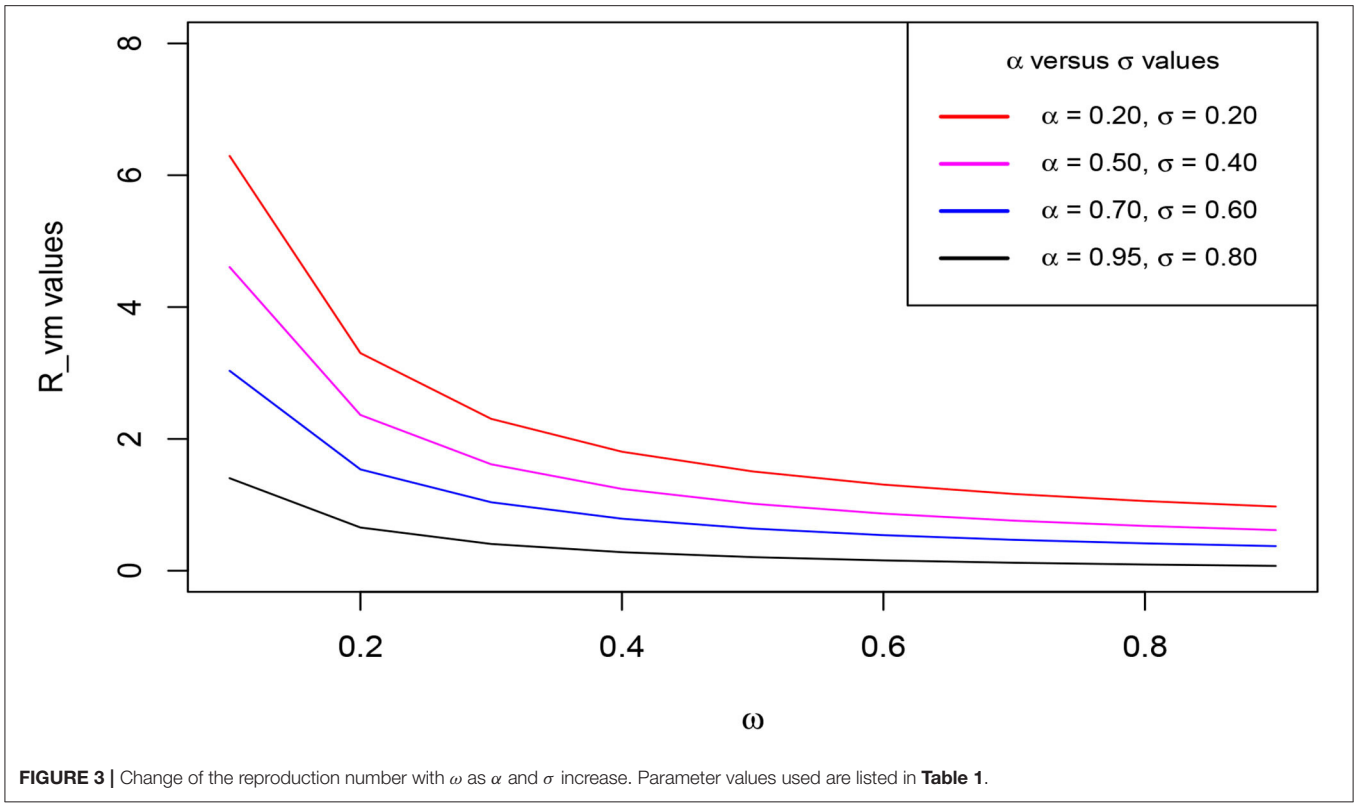

FIGURE 3 | Change of the reproduction number with ω as α and σ increase. Parameter values used are listed in **Table 1**.

Figures 5A–C, respectively, illustrate the trajectory of the symptomatic, the asymptomatic, and the latent classes of the model (Equations 2–8) when the uptake of the COVID-19 vaccines and wearing of face masks by the vaccinated individuals is relatively high. The Figures show low numbers of recorded symptomatic infections, asymptomatic infections, and latent cases consequentially. These observations stipulate that serious uptake or implementation of these control measure strategies would result in an accelerated reduction in the peak number of COVID-19 infections and reduction in the latent cases. Moreover, we observe that the infections clear within a relatively shorter time span.

Figures 6A–D (left-hand-side sub-figures) and **Figures 1–4** (right-hand-side sub-figures), respectively, show the trajectory of the symptomatic cases and the asymptomatic cases of the model (Equations 2–8) as ω varies when $\alpha = 20\%$, $\alpha = 50\%$, $\alpha = 70\%$, and $\alpha = 95\%$. We observe that the number of symptomatic infections and the asymptomatic infections reduces as ω increases at each level of α. Remarkably, we see that a concurrent increase in ω and α accelerates the reduction in the number of both symptomatic and asymptomatic infections. In other words, continuous increase in ω at relatively higher levels of α, speed up reduction in the recorded symptomatic and asymptomatic infections. This situation results in a decrease in the cumulative peak number of infections. These observations are explained by the fact that, when more people are vaccinated and continue to wear face masks, their chances of being infected are highly reduced following the combined protection brought about by the vaccine efficacy and the face mask efficacy. Therefore, we infer that serious uptake of the COVID-19 vaccines with the simultaneous wearing of face masks even after vaccination can eradicate the epidemic within a relatively shorter period of time.

We note that wearing the face masks by the general public is one of the non-pharmaceutical control measure protocols which was immediately introduced right from the early outbreak of the COVID-19 pandemic. As it is captured in Section 1, it was highly and well implemented hence playing a key role in containing the spread of the pandemic. In reality, wearing face masks has been greatly adhered to by a greater proportion of the population in various countries where the COVID-19 epidemic has been seriously observed. Although this model assumes that about 66% of the Republic of South Africa's population at higher risk of contracting the disease wear face masks, especially in public areas, we consider varying the parameter δ for the measure of wearing of the face masks by unvaccinated individuals. This is done considering four levels of the face masks efficacy denoted by σ such that $\sigma = 20\%$, $\sigma = 40\%$, $\sigma = 60\%$, and $\sigma = 80\%$. The trajectories of the symptomatic infections and the asymptomatic infections of the model (Equations 2–8) are, respectively, established by the **Figures 7A–D** (left-hand-side sub-figures) and **Figures 1–4** (right-hand-side sub-figures) of **Figure 7**. The figure shows that as δ increases at each level of σ, the peak number for both the symptomatic and the asymptomatic infections decreases. However, we observe that as δ increases at each level of σ, the infections delay clearing, hence, taking a relatively long time span. This observation implies that the use of

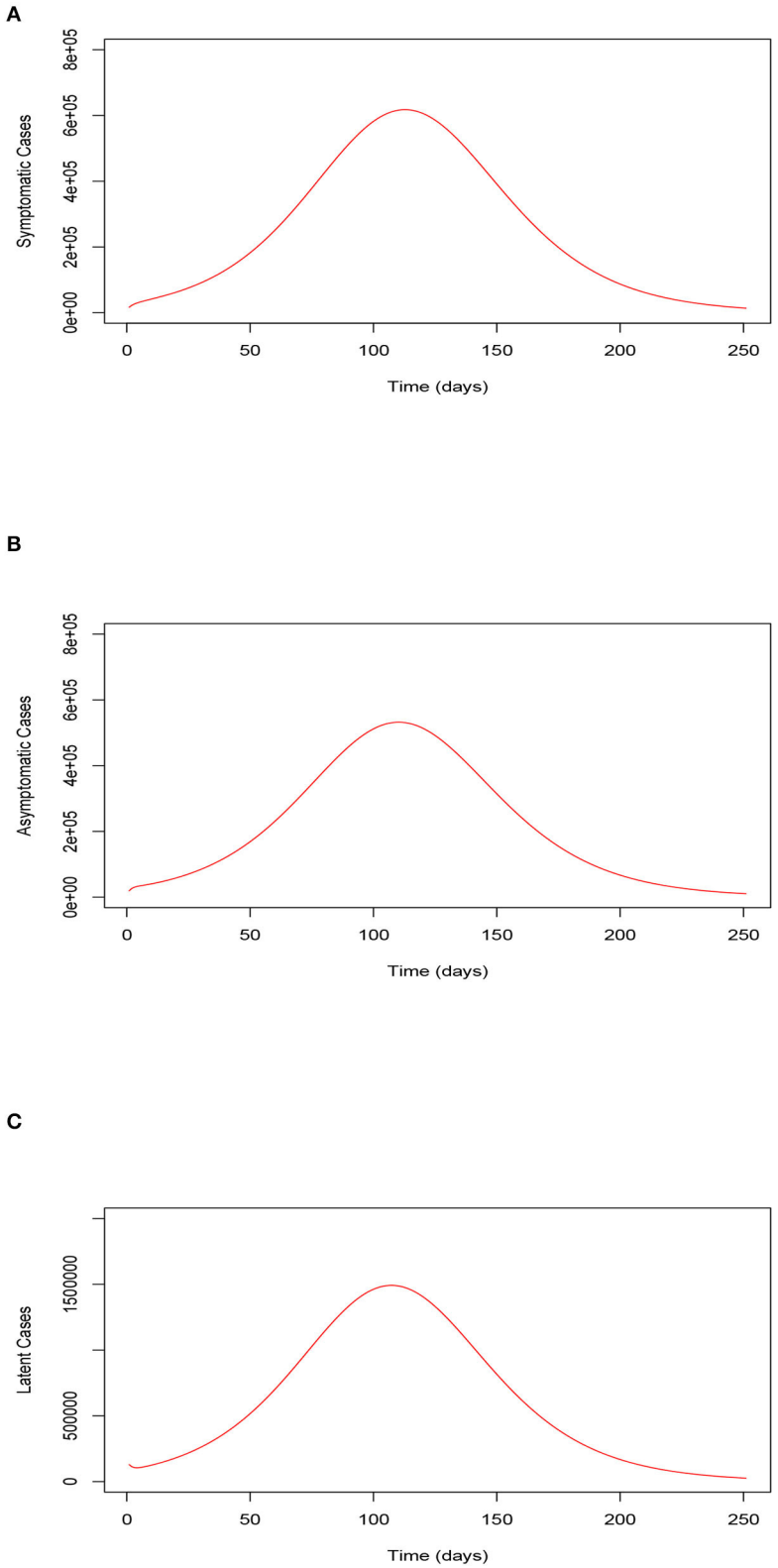

FIGURE 4 | (A) Trajectory of the symptomatic infections for the model (Equations 2–8) when the uptake of the COVID-19 vaccines and the use of face masks by the vaccinated is extremely low. **(B)** Trajectory of the asymptomatic infections for the model (Equations 2–8) when the uptake of the COVID-19 vaccines and the use of face masks by the vaccinated is extremely low. **(C)** Trajectory of the latent cases for the model (Equations 2–8) when the uptake of the COVID-19 vaccines and the use of face masks by the vaccinated is extremely low. Trajectory of the symptomatic, asymptomatic, and latent classes of the model (Equations 2–8) when the uptake of the COVID-19 vaccines and the wearing of face masks by the vaccinated is extremely low.

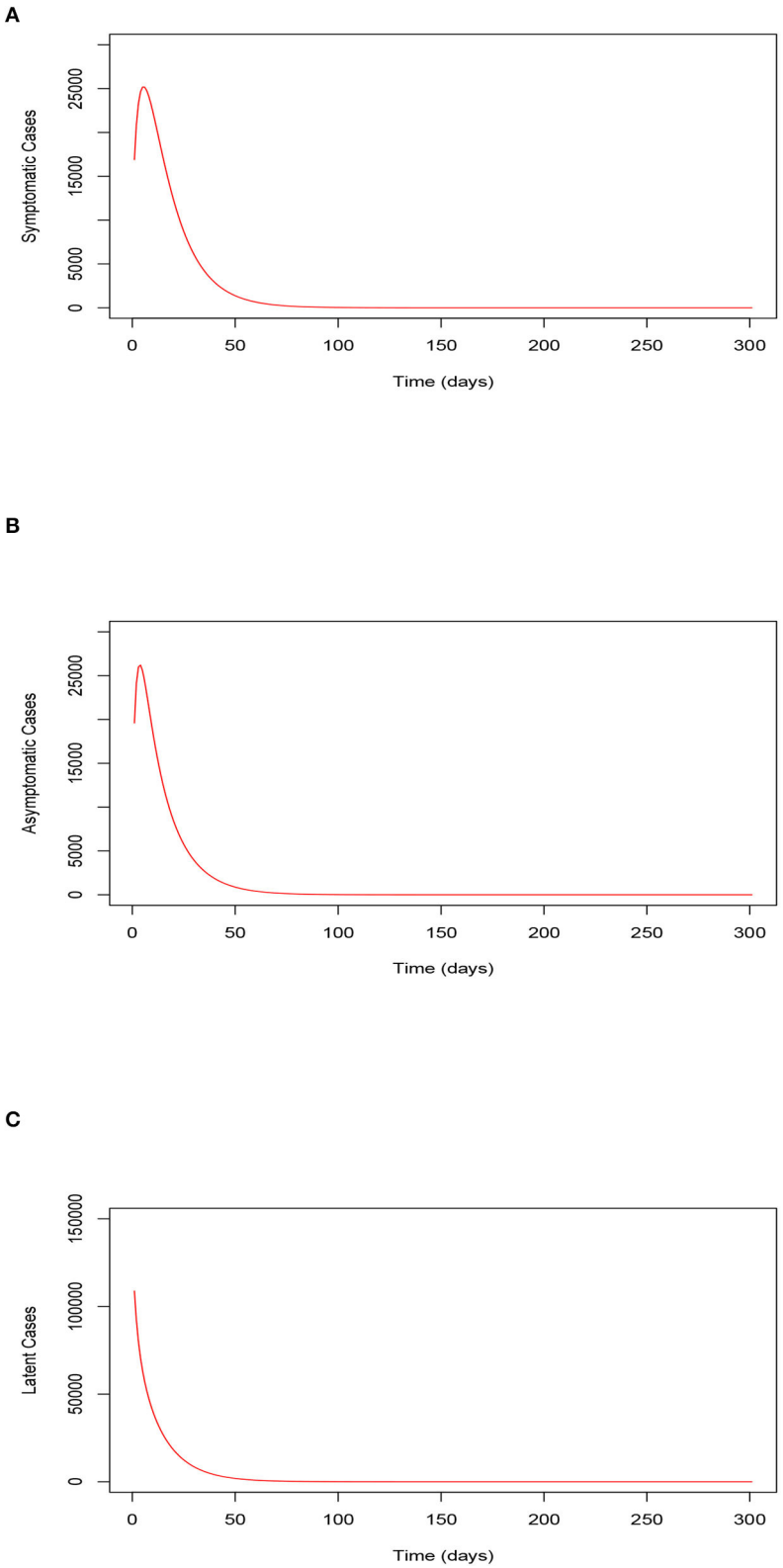

FIGURE 5 | (A) Trajectory of the symptomatic infections for the model (Equations 2–8) when the uptake of the COVID-19 vaccines and the use of face masks by the vaccinated is relatively high (80%). **(B)** Trajectory of the asymptomatic infections for the model (Equations 2–8) when the uptake of the COVID-19 vaccines and the use of face masks by the vaccinated is relatively high (80%). **(C)** Trajectory of the latent cases for the model (Equations 2–8) when the uptake of the COVID-19 vaccines and the use of face masks by the vaccinated is relatively high (80%). Trajectory of the symptomatic, asymptomatic, and latent classes of the model (Equations 2–8) when the uptake of the COVID-19 vaccines and the use of face masks by the vaccinated is relatively high (80%).

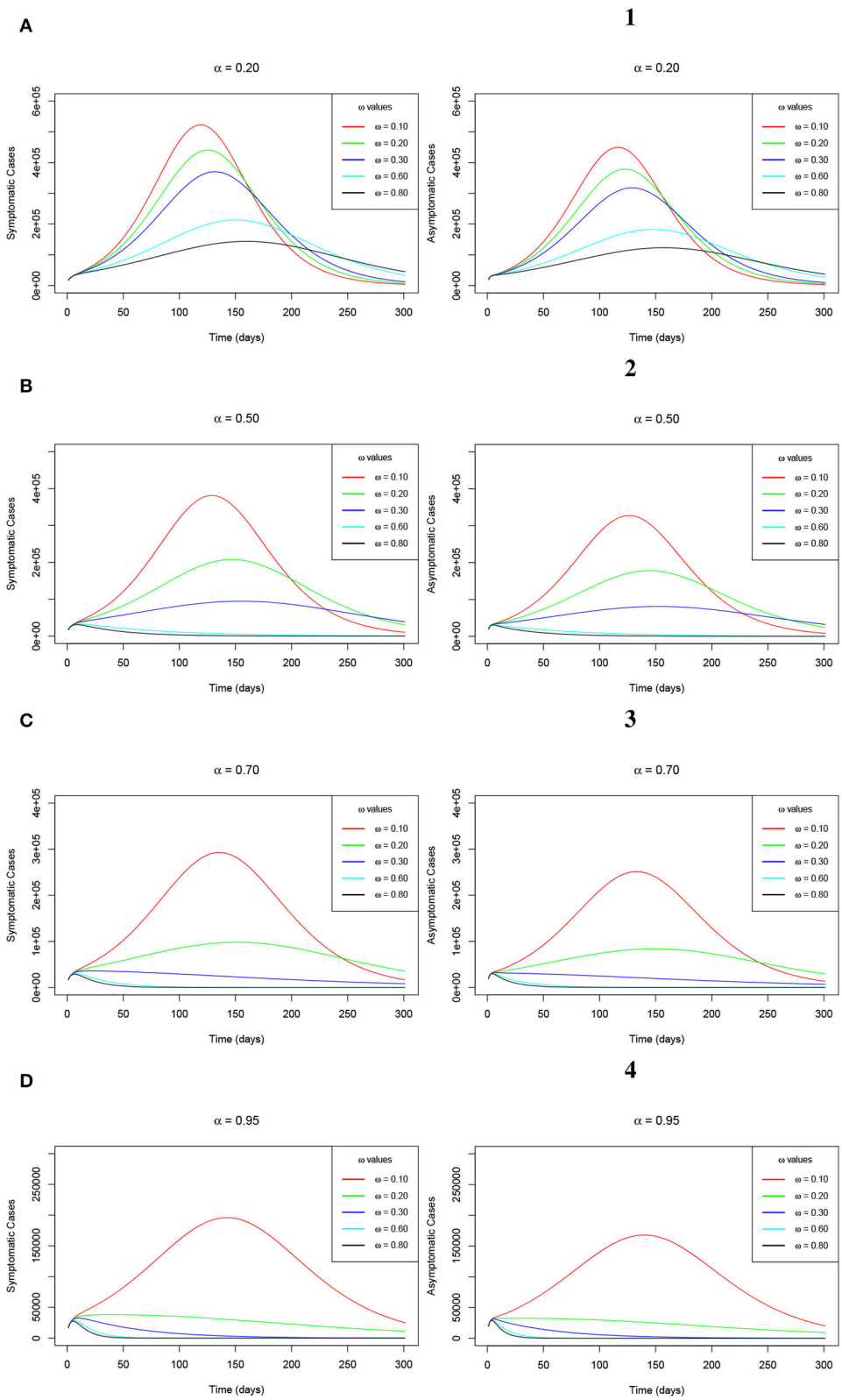

FIGURE 6 | (A–D) Simulations of the model (Equations 2–8) showing the trajectory of the number of symptomatic infections (left-hand-side sub-figures) and the number of asymptomatic infections (right-hand-side sub-figures) as ω varies at changing levels of α.

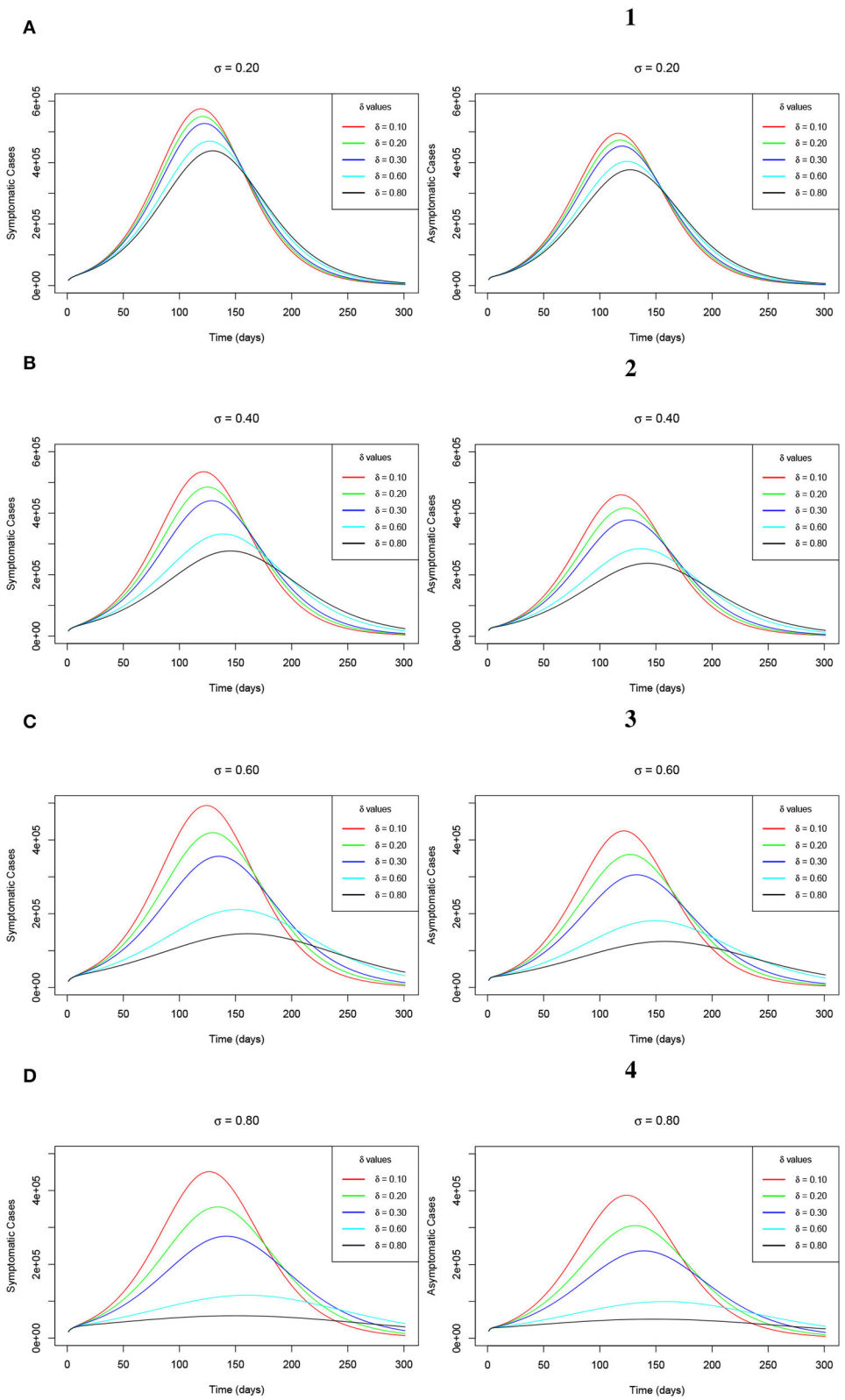

FIGURE 7 | (A–D) Simulations of the model (Equations 2–8) showing the trajectory of the number of symptomatic infections (left-hand-side sub-figures) and the number of asymptomatic infections (right-hand-side sub-figures) as δ varies at changing levels of σ.

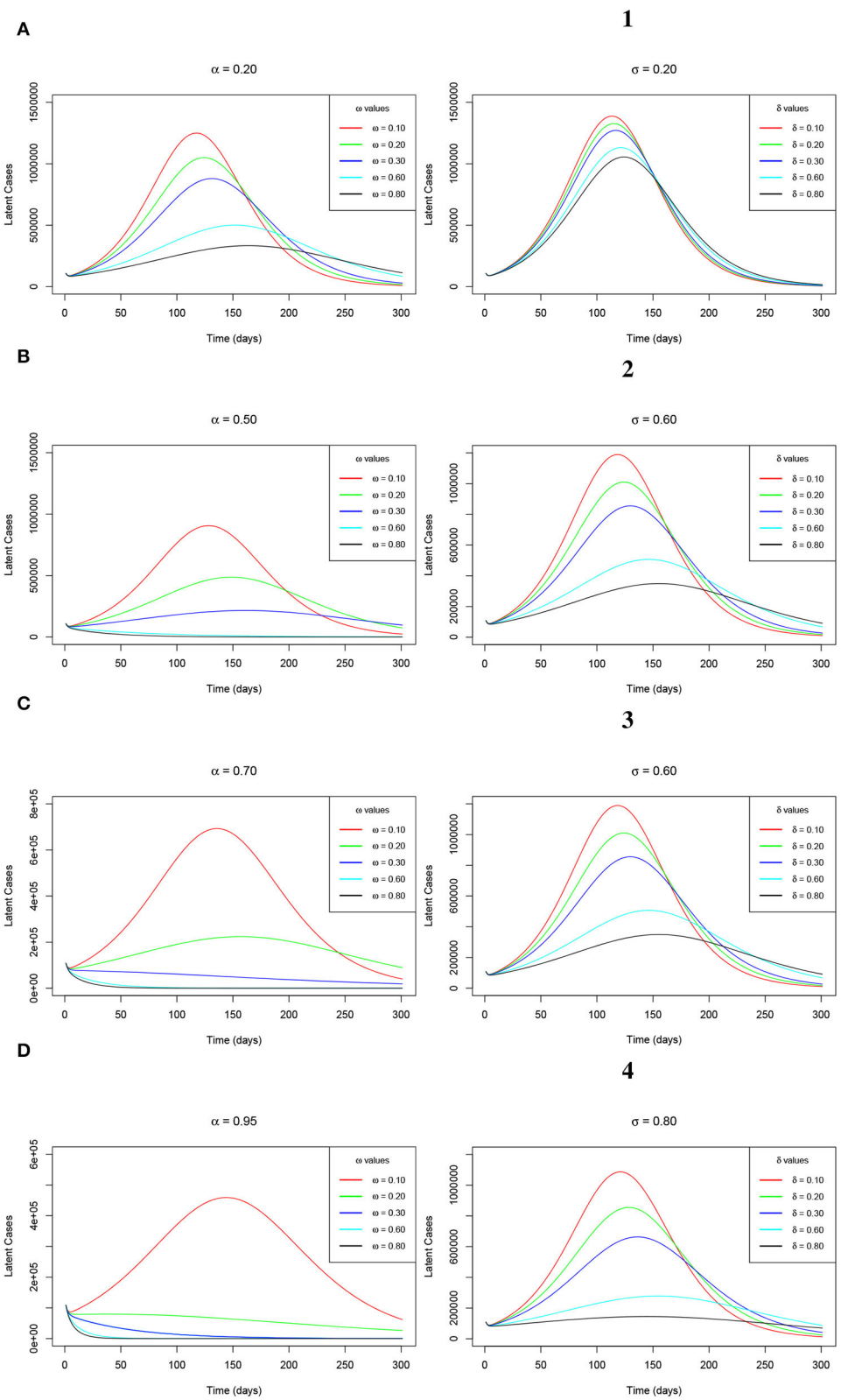

FIGURE 8 | (A–D) Simulations of the model (Equations 2–8) showing the trajectory of the latent cases as ω varies at changing levels of α (left-hand-side sub-figures) and the latent cases as δ varies at changing levels of σ (right-hand-side sub-figures).

the face masks alone may facilitate the clearance of the infections from the human host though within a relatively long time as compared to when vaccination is combined with the wearing of the face masks. The advantage for both cases is that the plateau number of infections keeps on reducing.

Additionally, as a result of a greatly accelerated reduction in the recorded numbers of both the symptomatic and the asymptomatic COVID-19 infections across all the observed levels of α and σ, the plateau number of the latent cases keep on decreasing, respectively as ω and δ increase. This observation is clearly evidenced by **Figures 8A–D** (left-hand-side sub-figures) and **Figures 1–4** (right-hand-side sub-figures), respectively, for varying values of ω at the aforementioned levels of α and for changing values of δ at the earlier stated levels of σ. This trend is completely in order since as much as the peak infections reduce, then the risk of exposure decreases hence triggering low latent cases consequentially.

5. CONCLUSION

In this study, we developed a modified SEIR deterministic model which factored in the combination of the COVID-19 vaccination program and the wearing of face masks as intervention strategies to curb the spread of COVID-19 infections. The developed model principally aimed at assessing the potential impact of wearing the face masks, especially by the vaccinated individuals in combating further contraction and spread of COVID-19. This special consideration was made since it was learned that people who are already vaccinated still had a probability of further being infected following their exposure to infectious individuals. This was based on the reasons aforementioned in Section 1.

Analytical results on epidemiological properties of the model ascertained that the model's solution remained positive and bounded within a defined biological feasible region for all non-negative time. We further adopted the Maximum Likelihood Estimation algorithm which was implemented in the fitR package to calibrate the developed model. We used the Republic of South Africa's COVID-19 positive cases reported data from June 01, 2020, to September 08, 2020, in calibrating the model. This important exercise was performed majorly to authenticate the model for use in testing different scenarios. For the sensitivity analysis, we used the expression for the reproduction number $\mathcal{R}_{vm}$ to plot the $\mathcal{R}_{vm}$ against the ω for the measure of the extent of vaccination and face mask use, while endorsing α for the measure of vaccine and face mask average protection and σ for the measure of face mask efficacy at simultaneously increasing levels. It was found that $\mathcal{R}_{vm}$ decreased gently with an increase in ω at each level of α and σ. Uniquely, it was discovered that there was an incredible shift of $\mathcal{R}_{vm}$ values tending to less than unity when the α and σ levels were simultaneously increased. Furthermore, increasing the levels of α and σ accelerated the reduction in the value of the reproduction number.

For the numerical simulations, we first considered a scenario where the uptake of the vaccines and wearing of the face masks especially by the vaccinated individuals was extremely low. Second, we considered a scenario where the uptake of the vaccines and wearing of the face masks by people who are vaccinated was relatively high. Third, we considered a scenario where the uptake of the vaccines and wearing of the face masks by the vaccinated individuals was on an upward trajectory. Under the third scenario, we considered four levels of the extent of vaccine and face mask average protection (α) such that $\alpha = 20\%$, $\alpha = 50\%$, $\alpha = 70\%$, and $\alpha = 95\%$. We also considered four levels of the face mask efficacy (σ), such that $\sigma = 20\%$, $\sigma = 40\%$, $\sigma = 60\%$, and $\sigma = 80\%$.

Results indicated a highly surging number of infections and a low recorded number of infections for scenario one and scenario two, respectively. For the third scenario, it was observed that the increased extent of wearing face masks by the vaccinated individuals at increasing levels of vaccines and face mask average protection resulted in a highly accelerated decrease in COVID-19 infections. This situation triggered the clearance of the COVID-19 infections from the human host within a relatively shorter period of time. Wearing face masks alone also resulted in a reduction in the peak number of infections at increasing levels of face mask efficacy though the infections were delayed to clear. This aspect would make the clearance of the COVID-19 infections take a relatively long span of time. Thus, this study advocates for the continued wearing of face masks even after full vaccination.

DATA AVAILABILITY STATEMENT

The datasets presented in this study can be found in online repositories. The names of the repository/repositories and accession number(s) can be found below: https://www.sacoronavirus.co.za.

AUTHOR CONTRIBUTIONS

MK, JM, and AM conceptualized the research and developed the model. MK carried out analysis, simulations, and wrote the original draft. JM and AM supervised and proofread the manuscript. All authors contributed to the article and approved the submitted version.

ACKNOWLEDGMENTS

MK acknowledges the German Academic Exchange Service - DAAD. JM thanks the National Research Foundation of the Republic of South Africa. All authors thank the reviewers for their help to improve the quality of the article *via* review comments.

REFERENCES

1. Garba SM, Lubuma JM, Tsanou B. Modeling the transmission dynamics of the COVID-19 Pandemic in South Africa. *Math Biosci*. (2020) 328:108441. doi: 10.1016/j.mbs.2020.108441
2. Eikenberry SE, Mancuso M, Iboi E, Phan T, Eikenberry K, Kuang Y, et al. To mask or not to mask: modeling the potential for face mask use by the general public to curtail the COVID-19 pandemic. *Infect Dis Model*. (2020) 5:293–308. doi: 10.1016/j.idm.2020.04.001
3. Mukandavire Z, Nyabadza F, Malunguza NJ, Cuadros DF, Shiri T, Musuka G. Quantifying early COVID-19 outbreak transmission in South Africa and exploring vaccine efficacy scenarios. *PLoS ONE*. (2020) 15:e0236003. doi: 10.1371/journal.pone.0236003
4. Arashi M, Bekker A, Salehi M, Millard S, Erasmus B, Cronje T, et al. Spatial analysis and prediction of COVID-19 spread in South Africa after lockdown. *arXiv preprint arXiv*. (2020) 2005:09596.
5. Bastos SB, Cajueiro DO. Modeling and forecasting the early evolution of the Covid-19 pandemic in Brazil. *Sci Rep*. (2020) 10:1-10. doi: 10.1038/s41598-020-76257-1
6. Ishtiaq A. Dynamics of COVID-19 transmission: compartmental-based mathematical modeling. *Life Sci*. (2020) 1:5. doi: 10.37185/LnS.1.1.134
7. Mollalo Vahedi B, Rivera KM. GIS-based spatial modeling of COVID-19 incidence rate in the continental United States. *Sci Total Environ*. (2020) 1:138884. doi: 10.1016/j.scitotenv.2020.138884
8. Atangana I, Araz S. Mathematical model of COVID-19 spread in Turkey and South Africa: theory, methods, and applications. *Adv Diff Equat*. (2020) 1:1–89. doi: 10.1186/s13662-020-03095-w
9. Góis N, Laureano EE, Santos DD, Sánchez DE, Souza LF, Vieira RD, et al. Lockdown as an intervention measure to mitigate the Spread of COVID-19: a modeling study. *Rev Soc Bras Med Trop*. (2020) 53:e20200417. doi: 10.1590/0037-8682-0417-2020
10. Makhoul M, Chemaitelly H, Ayoub H, Seedat SL, Abu-Raddad J. Epidemiological differences in the impact of COVID-19 vaccination in the United States and China. *Vaccines*. (2021) 9:223. doi: 10.3390/vaccines9030223
11. Kinyili M, Munyakazi JB, Mukhtar AYA. Assessing the impact of vaccination on COVID-19 in South Africa using mathematical modeling. *Appl Math Inf Sci*. (2021) 15:1–16. doi: 10.18576/amis/150604
12. The Republic of South Africa's department of Health online resource and news portal on COVID-19. Available online at: https://www.SAcoronavirus.co.za.
13. Jentsch PC, Anand M, Bauch CT. Prioritising COVID-19 vaccination in changing social and epidemiological landscapes: a mathematical modelling study. *Lancet Infect Dis*. (2021) 21:1097–106. doi: 10.1101/2020.09.25.20201889
14. Moore S, Hill EM, Tildesley MJ, Dyson L, Keeling MJ. Vaccination and non-pharmaceutical interventions for COVID-19: a mathematical modelling study. *Lancet Infect Dis*. (2021) 21:793–802. doi: 10.1016/S1473-3099(21)00143-2
15. Moghadas SM, Vilches TN, Zhang K, Nourbakhsh S, Sah P, Fitzpatrick MC, et al. Evaluation of COVID-19 vaccination strategies with a delayed second dose. *PLoS Biol*. (2021) 19:e3001211. doi: 10.1371/journal.pbio.3001211
16. Olivares A, Staffetti E. Uncertainty quantification of a mathematical model of COVID-19 transmission dynamics with mass vaccination strategy. *Chaos Solitons Fractals*. (2021) 146:110895. doi: 10.1016/j.chaos.2021.110895
17. Polack FP, Thomas SJ, Kitchin N, Absalon J, Gurtman A, Lockhart S, et al. Bailey Safety and efficacy of the BNT162b2 mRNA Covid-19 vaccine. *N Engl J Med*. (2020) 383:2603–15. doi: 10.1056/NEJMoa2034577
18. Baden LR, El Sahly HM, Essink B, Kotloff K, Frey S, Novak R, et al. Efficacy and safety of the mRNA-1273 SARS-CoV-2 vaccine. *N Engl J Med*. (2021) 384:403–16. doi: 10.1056/NEJMoa2035389
19. Voysey M, Clemens SAC, Madhi SA, Weckx LY, Folegatti PM, Aley PK, et al. Safety and efficacy of the ChAdOx1 nCoV-19 vaccine (AZD1222) against SARS-CoV-2: an interim analysis of four randomised controlled trials in Brazil, South Africa, and the UK. *Lancet*. (2021) 397:99–111. doi: 10.1016/S0140-6736(20)32661-1
20. Dagan N, Barda N, Kepten E, Miron O, Perchik S, Katz MA, et al. BNT162b2 mRNA Covid-19 vaccine in a nationwide mass vaccination setting. *N Engl J Med*. (2021) 384:1412–23. doi: 10.1056/NEJMoa2101765
21. Foy BH, Wahl B, Mehta K, Shet A, Menon GI, Britto C. Comparing COVID-19 vaccine allocation strategies in India: a mathematical modelling study. *Int J Infect Dis*. (2021) 103:431–8. doi: 10.1016/j.ijid.2020.12.075
22. Wong GN, Weiner ZJ, Tkachenko AV, Elbanna A, Maslov S, Goldenfeld N. Modeling COVID-19 dynamics in Illinois under nonpharmaceutical interventions. *Phys Rev X*. (2020) 10:041033. doi: 10.1103/PhysRevX.10.041033
23. Sun T, Wang Y. Modeling COVID-19 epidemic in Heilongjiang province, China. *Chaos Solitons Fractals*. (2020) 138:109949. doi: 10.1016/j.chaos.2020.109949
24. Boukanjime B, Caraballo T, El Fatini M. El Khalifi M. Dynamics of a stochastic coronavirus (COVID-19) epidemic model with Markovian switching. *Chaos Solitons Fractals*. (2020) 141:110361. doi: 10.1016/j.chaos.2020.110361
25. Kennedy M, Zambrano GJ, Wang Y, Neto OP. Modeling the effects of intervention strategies on COVID-19 transmission dynamics. *J Clin Virol*. (2020) 128:104440. doi: 10.1016/j.jcv.2020.104440
26. Sadarangani M, Raya A, Conway B, Iyaniwura JM, Falcao SA, Colijn RC, et al. Importance of COVID-19 vaccine efficacy in older age groups. *Vaccine*. (2021) 39:2020–3. doi: 10.1016/j.vaccine.2021.03.020
27. Bubar KM, Reinholt K, Kissle SM, Lipsitch M, Cobey S, Grad YH, et al. Model-informed COVID-19 vaccine prioritization strategies by age and serostatus. *Science*. (2021) 371:916–21. doi: 10.1126/science.abe6959
28. Thompson RN, Hollingsworth TD, Isham V, Arribas-Bel D, Ashby B, Britton T, et al. Key questions for modelling COVID-19 exit strategies. *Proc R Soc*. (2020) 287:20201405. doi: 10.1098/rspb.2020.1405
29. Lyra W, do Nascimento Jr JD, Belkhiria J, de Almeida L, Chrispim PP, de Andrade I. COVID-19 pandemics modeling with modified determinist SEIR, social distancing, age *stratification. The effect of vertical confinement and release in Brazil. PLoS ONE*. (2020) 15:e0237627. doi: 10.1371/journal.pone.0237627
30. Libotte GB, Lobato FS, Platt GM, Neto AJ. Determination of an optimal control strategy for vaccine administration in COVID-19 pandemic treatment. *Comput Methods Programs Biomed*. (2020) 196:105664. doi: 10.1016/j.cmpb.2020.105664
31. Lukman F, Rauf RI, Abiodun O, Oludoun O, Ayinde K, Ogundokun RO. COVID-19 prevalence estimation: four most affected African countries. *Infect Dis Model*. (2020) 1:827–38. doi: 10.1016/j.idm.2020.10.002
32. Sameni R. Mathematical modeling of epidemic diseases; a case study of the COVID-19 coronavirus. *arXiv preprint arXiv*. (2020) 11371.
33. Bedi P, Gole P, Gupta N, Jindal V. Projections for COVID-19 spread in India and its worst affected five states using the modified SEIRD and LSTM models. *arXiv preprint arXiv*. (2020) 06457. doi: 10.1007/s42979-021-00598-5
34. Zhao Z, Li X, Liu F, Zhu G, Ma C, Wang L. Prediction of the COVID-19 spread in African countries and implications for prevention and control: a case study in South Africa, Egypt, Algeria, Nigeria, Senegal and Kenya. *Sci Total Environ*. (2020) 729:138959. doi: 10.1016/j.scitotenv.2020.138959
35. Gilbert M, Pullano G, Pinotti F, Valdano E, Poletto C, Boëlle FY, et al. Gutierrez Preparedness and vulnerability of African countries against importations of COVID-19: a modelling study. *Lancet*. (2020) 395:871–7. doi: 10.1016/S0140-6736(20)30411-6
36. Peirlinck M, Linka K, Costabal FS, Kuhl E. Outbreak dynamics of COVID-19 in China and the United States. *Biomech Model Mechanobiol*. (2020) 19:2179–93. doi: 10.1007/s10237-020-01332-5
37. Salgotra R, Gandomi M, Gandomi AH. Evolutionary modelling of the COVID-19 pandemic in fifteen most affected countries. *Chaos Solitons Fractals*. (2020) 140:110118. doi: 10.1016/j.chaos.2020.110118
38. Amaro JE, Dudouet J, Orce JN. Global analysis of the COVID-19 pandemic using simple epidemiological models. *Appl Math Model*. (2020) 90:995–1008. doi: 10.1016/j.apm.2020.10.019
39. Yang Q, Yi C, Vajdi A, Cohnstaedt LW, Wu H, Guo X, et al. Short-term forecasts and long-term mitigation evaluations for the COVID-19 epidemic in Hubei Province, China. *Infect Dis Model*. (2020) 5:563–74. doi: 10.1016/j.idm.2020.08.001

40. Li T, Liu Y, Li M, Qian X, Dai SY. Mask or no mask for COVID-19: a public health and market study. *PLoS ONE*. (2020) 15:e0237691. doi: 10.1371/journal.pone.0237691
41. Howard J, Huang A, Li Z, Tufekci Z, Zdimal V, van der Westhuizen HM, et al. An evidence review of face masks against COVID-19. *Proc Natl Acad Sci USA*. (2021) 118:e2014564118. doi: 10.1073/pnas.2014564118
42. Shen M, Zu J, Fairley CK, Pagán JA, Ferket B, Liu B, et al. Effects of New York's executive order on face mask use on COVID-19 infections and mortality: a modeling study. *J Urban Health*. (2021) 98:197–204. doi: 10.1101/2020.10.26.20219527
43. Stutt RO, Retkute R, Bradley M, Gilligan CA, Colvin JA. Modelling framework to assess the likely effectiveness of facemasks in combination with 'lock-down' in managing the COVID-19 pandemic. *Proc R Soc*. (2020) 476:20200376. doi: 10.1098/rspa.2020.0376
44. Nyabadza F, Chirove F, Chukwu CW, Visaya MV. Modelling the potential impact of social distancing on the COVID-19 epidemic in South Africa. *Comput Math Methods Med*. (2020) 2020:5379278. doi: 10.1101/2020.04.21.20074492
45. Mason DM, Kapinaj M, Martínez AP, Stella L. Impact of social distancing to mitigate the spread of COVID-19 in a virtual environment. In: *ACM Symposium on Virtual Reality Software and Technology*. (2020). p. 1–3.
46. Iboi Ngonghala CN, Gumel AB. Will an imperfect vaccine curtail the COVID-19 pandemic in the US?. *Infect Dis Model*. (2020) 5:510–24. doi: 10.1016/j.idm.2020.07.006
47. Gumel B, Iboi EA, Ngonghala CN, Ngwa GA. Mathematical assessment of the roles of vaccination and non-pharmaceutical interventions on COVID-19 dynamics: a multigroup modeling approach. *medRxiv*. (2021) 2020–12. doi: 10.1101/2020.12.11.20247916
48. Kinyili M, Justin Munyakazi B, Abdulaziz A. Mukhtar Y. Mathematical Modeling and Impact Analysis of the use of COVID Alert SA app. *AIMS Public Health*. (2022) 9:106–28. doi: 10.3934/publichealth.2022009
49. Smith HL, Waltman P. *The Theory of the Chemostat: Dynamics of Microbial Competition*. Cambridge: Cambridge University Press (1995).
50. Garba SM, Safi MA, Usaini S. Mathematical model for assessing the impact of vaccination and treatment on measles transmission dynamics. *Math Methods Appl Sci*. (2017) 40:6371–88. doi: 10.1002/mma.4462
51. Castillo-Chavez Song B, Huang W. On the computation of R_0 and its role in global stability. *Math Appl*. (2002) 1:229–50. doi: 10.1007/978-1-4757-3667-0_13

Conflict of Interest: The authors declare that the research was conducted in the absence of any commercial or financial relationships that could be construed as a potential conflict of interest.

frontiers | Frontiers in Applied Mathematics and Statistics

ORIGINAL RESEARCH
published: 26 May 2022
doi: 10.3389/fams.2022.860840

On the Dynamics of Sexually Transmitted Diseases Under Awareness and Treatment

Suares Clovis Oukouomi Noutchie, Ntswaki Elizabeth Mafatle, Richard Guiem and Rodrigue Yves M'pika Massoukou*

Pure and Applied Analytics, School of Mathematical and Statistical Sciences, North-West University, Potchefstroom, South Africa

In this paper, we develop and extend the work of Jia and Qin on sexually transmitted disease models with a novel class of non-linear incidence. Awareness plays a central role both in the susceptible and the infectious classes. The Existence, uniqueness, boundedness, and positivity of solutions are systematically established. Concavity arguments and the occurrence of a vertical asymptote are essential in the proof of the existence of a unique endemic equilibrium. Conditions for the stability of all steady states are investigated. In particular, numerical simulations are performed in order to capture the asymptotic behavior of solutions.

AMS Classification: 92D30, 34D23.

Keywords: stability, non-linear response, concavity, vertical asymptote, awareness, disease

Edited by:
Ramoshweu Solomon Lebelo, Vaal University of Technology, South Africa

Reviewed by:
Appanah Rao Appadu, Nelson Mandela University, South Africa
Marin I. Marin, Transilvania University of Braşov, Romania

****Correspondence:***
Suares Clovis Oukouomi Noutchie
23238917@nwu.ac.za

Specialty section:
This article was submitted to Mathematical Biology, a section of the journal Frontiers in Applied Mathematics and Statistics

Received: *23 January 2022*
Accepted: *19 April 2022*
Published: *26 May 2022*

Citation:
Oukouomi Noutchie SC, Mafatle NE, Guiem R and M'pika Massoukou RY (2022) On the Dynamics of Sexually Transmitted Diseases Under Awareness and Treatment. Front. Appl. Math. Stat. 8:860840. doi: 10.3389/fams.2022.860840

1. INTRODUCTION

Disease incidence plays a crucial role in mathematical epidemiology and it is essential in the computation of the basic reproduction number. Non-linear incidences are known to induce complex or chaotic behavior as oppose to standard incidences frequently used in classical infectious disease models [1–6]. A class of non-linear incidences particularly useful in the modeling of sexually transmitted diseases was introduced in [7] by the authors in the modeling of HIV/AIDS epidemic. The model considered however was not properly conceptualized as the density of individuals with full-blown AIDS not receiving ARV treatment did not bear any influence on the infection rate of the disease. In addition a number of inaccuracies are displayed in this paper like the unknown variable T missing in the third equation of system (2.1) and also a mistake occurred in the computation of the sign of a_3 in the proof of the stability of the endemic equilibrium. The purpose of this paper is to develop and extend the work on [7] by deriving a realistic model for sexually transmitted diseases with a proper non-linear incidence rate with a valid biological significance and perform a full analysis of the resulting model. In Section 2, the model is derived and presented. Well-posedness analysis, positivity and boundedness are considered in Section 3 followed by stability analysis of the critical points of the system in Section 4, numerical simulations in Section 5 and the conclusion.

2. THE MODEL

In this paper, a model with five compartments is formulated with non-linear incidence $Sg(t, I)$ incorporated into it. The incidence is presumed to be a time dependent non-linear response to the

size of the infectious population.

The compartments are denoted by $S(t), I(t), T(t), A(t)$ and $R(t)$ which represent the number of susceptible individuals, the number of infected individuals with the potential of transmitting the disease as they are not under treatment and do not take any form of protection while engaging in sexual activities, the number of individuals under treatment, the number of infectious individuals engaging in safe sex, and heathy individuals that engage in safe sex, respectively, at time t. The model represented in **Figure 1** is governed by the system of nonlinear ordinary differential equations

$$\begin{cases} \dfrac{dS}{dt} &= \Gamma - Sg(t,I) - (\omega_1 + d)S, \\ \dfrac{dI}{dt} &= Sg(t,I) + \nu_1 T - (d + \tau_1 + \tau_2)I, \\ \dfrac{dT}{dt} &= \tau_2 I - \nu_2 T - (d + \nu_1)T, \\ \dfrac{dA}{dt} &= \tau_1 I - dA + \nu_2 T, \\ \dfrac{dR}{dt} &= \omega_1 S - dR, \end{cases} \tag{1}$$

endowed with initial conditions

$S(0) \equiv S_0 > 0,\ I(0) \equiv I_0 > 0,\ T(0) \equiv T_0 \geq 0,\ A(0) \equiv A_0 \geq 0,\ R(0) \equiv R_0 \geq 0.$

The parameters in the evolution system (1) are described in **Table 1**:

The total population $N(t)$ is given by $S(t) + I(t) + T(t) + A(t) + R(t)$. By adding all the equations of the system (1), we obtain the rate of change of $N(t)$, which is given by

$$\frac{dN}{dt} = \Gamma - dN \tag{2}$$

and $N(t)$ varies over time and is nearing a stable fixed point $\dfrac{\Gamma}{d}$ as $t \to \infty$. Therefore, the biologically feasible region for the system (1) is given by

$$\Psi = \left\{ (S, I, T, A, R) \in \mathbb{R}^5_+ \mid 0 < S(t) + I(t) + T(t) + A(t) + R(t) \leq \frac{\Gamma}{d} \right\}.$$

It is easy to see that the set Ψ is positively invariant. Next we present a systematic analysis of our evolution equation.

3. MATHEMATICAL ANALYSIS

We start by investigating the well-posedness of the model (1). Given the fact that the variables represent biologically densities, it is important to show that all the variables remain positive at all time.

Lemma 1. *For any non-negative initial conditions $(S_0, I_0, T_0, A_0, R_0)$, system (1) has a local solution which is unique.*

Proof : Let $x = (S,\ I,\ T,\ A,\ R)$, system (1) can be rewritten as $x'(t) = f(t, x(t))$, where $f : \mathbb{R}^6 \to \mathbb{R}^5$ is a C^1 vector field. By the classical differential equation theory, we can confirm that system (1) has a unique local solution defined in a maximum interval $[0, t_m)$. □

Lemma 2. *For any non-negative initial conditions $(S_0, I_0, T_0, A_0, R_0)$, the solution of (1) is non-negative and bounded for all $t \in [0, t_m)$.*

Proof : We start by showing positivity of the local solution for any non-negative initial conditions. It is easy to see that $S(t) \geq 0$ for all $t \in [0, t_m)$. Indeed, assume the contrary and let $t_1 > 0$ be the first time such that $S(t_1) = 0$ and $S'(t_1) < 0$. From the first equation of the system (1), we have $S'(t_1) = \Gamma > 0$, which presents a contradiction. Therefore $S(t) \geq 0$ for all $t \in [0, t_m)$. Using the same argument, positivity $I(t),\ T(t),\ A(t)$ and $R(t)$ in the interval $[0, t_m)$ are established. Furthermore from (2), we have that

$$N(t) = \frac{\Gamma}{d} + N(0)e^{-dt} \leq \frac{\Gamma}{d} + N(0). \tag{3}$$

Therefore the solution $N(t)$ is bounded in the interval $[0, t_m)$. □

Theorem 1 *For any non-negative initial conditions $(S_0, I_0, T_0, A_0, R_0)$, system (1) has a unique global solution. Moreover, this solution is non-negative and bounded for all $t \geq 0$.*

Proof : The solution does not blow up in a finite time as it is bounded, it is therefore defined at all time $t \geq 0$. Other properties of the solution follow from lemma (1) and lemma (2). □

Setting $m = d + \tau_1 + \tau_2$ and $n = d + \nu_1 + \nu_2$, system (1) transforms into a reduced system

$$\begin{cases} \dfrac{dS}{dt} &= \Gamma - Sg(t,I) - (\omega_1 + d)S, \\ \dfrac{dI}{dt} &= Sg(t,I) + \nu_1 T - mI, \\ \dfrac{dT}{dt} &= \tau_2 I - nT, \\ \dfrac{dA}{dt} &= \tau_1 I - dA + \nu_2 T, \\ \dfrac{dR}{dt} &= \omega_1 S - dR. \end{cases} \tag{4}$$

4. MODELS WITH TIME INDEPENDENT NON-LINEAR RESPONSE

In this section, we assume that the non-linear response function is not time dependent, ie $g(t, I) \equiv g(I)$. Following [7], it is further

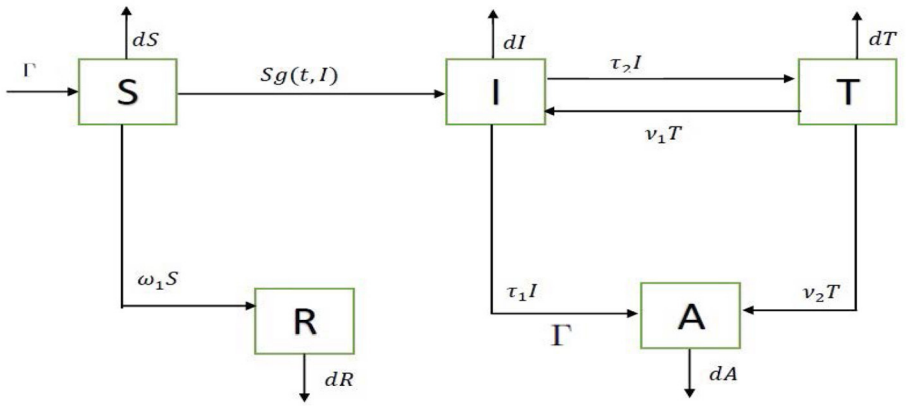

FIGURE 1 | Flow diagram.

TABLE 1 | Biological meaning of parameters.

Parameter	Biological meaning
Γ	Recruitment rate
d	Natural death rate
τ_1	The rate at which infected individuals adhere to safe sex practices
τ_2	The rate at which infected individuals receive antiviral drugs
ω_1	The rate at which susceptible individuals adhere to safe sex practices
ν_1	The rate of defaulting from treatment
ν_2	The rate at which treated individuals adhere to safe sex practices .

assumed that

$$(\mathrm{H}_1): g(0)=0,\ g'(0)>0,\ g''(I)\le 0 \ \text{ for } I\ge 0,$$
$$(\mathrm{H}_2): \lim_{I\to 0^+}\frac{g(I)}{I}=k,\ 0<k<\infty.$$

4.1. The Basic Reproduction Number

In this section, we use the next generation method [8] to obtain the basic reproduction number. Let z be the transpose of (I, A, T, S, R). We rewrite the system (4) in the matrix form

$$\frac{dz}{dt}=\mathcal{F}(z)-\mathcal{V}(z),$$

where

$$\mathcal{F}(z)=\begin{pmatrix} Sg(I)\\ 0\\ 0\\ 0\end{pmatrix}$$

and

$$\mathcal{V}(z)=\begin{pmatrix} mI-\nu_1 T\\ dA-\tau_1 I-\nu_2 T\\ nT-\tau_2 I\\ Sg(I)+(\omega_1+d)S-\Gamma\\ dR-\omega_1 S\end{pmatrix}.$$

The disease free equilibrium of system (4) takes the form

$$E^0=(I^0,A^0,T^0,S^0,R^0)=\left(0,0,0,\frac{\Gamma}{\omega_1+d},\frac{\omega_1\Gamma}{d(\omega_1+d)}\right).$$

Following [8], we compute the basic reproduction number using the formula below

$$\mathcal{R}_0=\rho(FV^{-1}),$$

where

$$F=\left[\begin{array}{ccc}\frac{\partial\mathcal{F}_1}{\partial E} & \frac{\partial\mathcal{F}_1}{\partial I} & \frac{\partial\mathcal{F}_1}{\partial T}\\ 0 & 0 & 0\\ 0 & 0 & 0\end{array}\right]\Bigg|_{(E^0,I^0,T^0,S^0,R^0)}=\left[\begin{array}{ccc}\frac{\alpha\Gamma}{\omega_1+d} & 0 & 0\\ 0 & 0 & 0\\ 0 & 0 & 0\end{array}\right]$$

and

$$V=\left[\begin{array}{ccc}\frac{\partial\mathcal{V}_1}{\partial E} & \frac{\partial\mathcal{V}_1}{\partial I} & \frac{\partial\mathcal{V}_1}{\partial T}\\ \frac{\partial\mathcal{V}_2}{\partial E} & \frac{\partial\mathcal{V}_2}{\partial I} & \frac{\partial\mathcal{V}_2}{\partial T}\\ \frac{\partial\mathcal{V}_3}{\partial E} & \frac{\partial\mathcal{V}_3}{\partial I} & \frac{\partial\mathcal{V}_3}{\partial T}\end{array}\right]\Bigg|_{(E^0,I^0,T^0,S^0,R^0)}=\left[\begin{array}{ccc} m & 0 & -\nu_1\\ -\tau_1 & d & -\nu_2\\ -\tau_2 & 0 & n\end{array}\right]$$

and ρ is the spectral radius of the matrix FV^{-1}. Given the fact that

$$V^{-1} = \frac{1}{d(mn - \nu_1\tau_2)} \begin{bmatrix} nd & 0 & -\nu_1 d \\ \tau_1 n - \nu_2\tau_2 & mn - \nu_1\tau_2 & \nu_2 m - \nu_1\tau_1 \\ \tau_2 d & 0 & md \end{bmatrix},$$

it follows that

$$\mathcal{R}_0 = \frac{\alpha n\Gamma}{(\omega_1 + d)(mn - \nu_1\tau_2)}. \tag{5}$$

4.1.1. Stability of the Disease-Free Equilibrium

The stability of the disease-free equilibrium will be investigated in this subsection.

Theorem 2 *The disease free equilibrium E^0 is globally asymptotically stable if $0 < \mathcal{R}_0 < 1$, and unstable if $\mathcal{R}_0 > 1$.*

Proof : The Jacobian matrix (J_{E^0}), evaluated at E^0, is given by

$$J_{E^0} = \begin{pmatrix} -(\omega_1 + d) & \frac{-\alpha\Gamma}{\omega_1 + d} & 0 & 0 & 0 \\ 0 & \frac{\alpha\Gamma}{\omega_1 + d} - m & \nu_1 & 0 & 0 \\ 0 & \tau_2 & -n & 0 & 0 \\ 0 & \tau_1 & \nu_2 & -d & 0 \\ \omega_1 & 0 & 0 & 0 & -d \end{pmatrix}. \tag{6}$$

The characteristic equation that results from the Jacobian matrix (J_{E^0}) is given by $\det(J_{E^0} - \lambda I) = 0$. Thus, we get

$$(d+\lambda)^2[(\omega_1+d)+\lambda]\left[\left(m - \frac{\alpha\Gamma}{\omega_1 + d} + \lambda\right)(n + \lambda) - \nu_1\tau_2\right] = 0. \tag{7}$$

The characteristic equation (7) has three negative real roots, which are

$$\lambda_1 = -d,$$
$$\lambda_2 = \lambda_3 = -(\omega_1 + d),$$

and the other 2 roots, λ_4 and λ_5, are roots of the equation

$$f(\lambda) = \left[\left(m - \frac{\alpha\Gamma}{\omega_1 + d}\right) + \lambda\right](n+\lambda) - \nu_1\tau_2 \equiv \lambda^2 + a_1\lambda + a_2 = 0, \tag{8}$$

where

$$a_1 = m + n - \frac{\alpha\Gamma}{\omega_1 + d},$$
$$a_2 = mn - \nu_1\tau_2 - \frac{\alpha n\Gamma}{\omega_1 + d}.$$

We now need to consider the signs of λ_4 and λ_5. Note that

$$mn - \nu_1\tau_2 > 0.$$

Assuming

$$\mathcal{R}_0 = \frac{\alpha n\Gamma}{(\omega_1 + d)(mn - \nu_1\tau_2)} < 1,$$

we have that

$$mn - \nu_1\tau_2 - \frac{\alpha n\Gamma}{\omega_1 + d} = a_2 > 0.$$

Moreover

$$\frac{\alpha n\Gamma}{\omega_1 + d} < mn - \nu_1\tau_2 < mn.$$

It implies that

$$m - \frac{\alpha\Gamma}{\omega_1 + d} > 0.$$

It follows that $a_1 > 0$. As a result the roots λ_4 and λ_5 are strictly negative. We can conclude that all roots of (7) have negative real parts, therefore, the disease free equilibrium is locally asymptotically stable [8–10]. Furthermore assuming that

$$\mathcal{R}_0 = \frac{\alpha n\Gamma}{(\omega_1 + d)(mn - \nu_1\tau_2)} > 1,$$

we have that $a_2 < 0$, it follows that the characteristic equation $f(\lambda) = 0$ has a least a strictly positive root. Therefore, the disease free equilibrium E^0 is unstable.

4.2. Existence of an Endemic Equilibrium

In this subsection, we investigate the existence of an endemic equilibrium for the system (4).

Proposition 1. *The system of differential equations (4) admits a unique endemic equilibrium if and only if $\mathcal{R}_0 > 1$.*

Proof : Let $E^* = (S^*, I^*, T^*, A^*, R^*)$ be an equilibrium point. Then the components of E^* satisfy the following set of equations

$$\begin{cases} \Gamma - S^* g(I^*) - (\omega_1 + d)S^* = 0, \\ S^* g(I^*) + \nu_1 T^* - mI^* = 0, \\ \tau_2 I^* - nT^* = 0, \\ \tau_1 I^* - dA^* + \nu_2 T^* = 0, \\ \omega_1 S^* - dR^* = 0. \end{cases} \tag{9}$$

From the last three equations of the system (9), we have that

$$T^* = \frac{\tau_2 I^*}{n},$$
$$A^* = \frac{\tau_1 + \frac{\nu_2\tau_2}{n}}{d} I^*,$$
$$R^* = \frac{\omega_1 S^*}{d}.$$

Substituting T^*, A^* and R^* into the first two equations, we obtain

$$\Gamma - S^* g(I^*) - (\omega_1 + d)S^* = 0,$$
$$S^* g(I^*) - \left(\frac{\nu_1 \tau_2}{n} - m\right) I^* = 0.$$

It follows that

$$S^* = \frac{\left(m - \frac{\nu_1 \tau_2}{n}\right) I^*}{g(I^*)} \tag{10}$$

and

$$\Gamma - \left(m - \frac{\nu_1 \tau_2}{n}\right) I^* - (\omega_1 + d)\frac{\left(m - \frac{\nu_1 \tau_2}{n}\right) I^*}{g(I^*)} = 0. \tag{11}$$

Next we set

$$h(I) := \frac{(\omega_1 + d)\left(m - \frac{\nu_1 \tau_2}{n}\right) I}{\Gamma - \left(m - \frac{\nu_1 \tau_2}{n}\right) I}. \tag{12}$$

It is enough to show that there exists a point $I^* \in \mathbb{R}^+$ such that $h(I^*) = g(I^*)$. In other words, we will show that the curves of the functions h and g intersect at a point I^*.

Note that

$$I = \frac{n\Gamma}{mn - \nu_1 \tau_2}$$

is a vertical asymptote of the function $h(I)$. For all

$$0 < I < \frac{n\Gamma}{mn - \nu_1 \tau_2},$$

we have that

$$h'(I) = \frac{(\omega_1+d)\left(m-\frac{\nu_1\tau_2}{n}\right)\left[\Gamma-\left(m-\frac{\nu_1\tau_2}{n}\right)I\right]+(\omega_1+d)\left(m-\frac{\nu_1\tau_2}{n}\right)^2 I}{\left[\Gamma-\left(m-\frac{\nu_1\tau_2}{n}\right)I\right]^2}$$
$$= \frac{\Gamma(\omega_1+d)\left(m-\frac{\nu_1\tau_2}{n}\right)}{\left[\Gamma-\left(m-\frac{\nu_1\tau_2}{n}\right)I\right]^2} > 0$$

and

$$h''(I) = \frac{2\left[\Gamma - \left(m - \frac{\nu_1 \tau_2}{n}\right) I\right]\left(m - \frac{\nu_1 \tau_2}{n}\right)^2 \Gamma(\omega_1 + d)}{\left[\Gamma - \left(m - \frac{\nu_1 \tau_2}{n}\right) I\right]^4}$$
$$= \frac{2\Gamma(\omega_1 + d)\left(m - \frac{\nu_1 \tau_2}{n}\right)^2}{\left[\Gamma - \left(m - \frac{\nu_1 \tau_2}{n}\right) I\right]^3} > 0.$$

It follows that the function h is increasing and concave upward in the interval

$$\left[0, \frac{n\Gamma}{mn - \nu_1 \tau_2}\right)$$

with a vertical asymptote at the right end of the interval. Note that the function g is increasing and concave downward in the closed interval

$$\left[0, \frac{n\Gamma}{mn - \nu_1 \tau_2}\right].$$

As a result if

$$g'(0) > h'(0) = \frac{(\omega_1 + d)\left(m - \frac{\nu_1 \tau_2}{n}\right)}{\Gamma},$$

which is equivalent to the condition $\mathcal{R}_0 > 1$, then Equation (12) has a unique root I^* in the interval

$$\left(0, \frac{n\Gamma}{mn - \nu_1 \tau_2}\right).$$

Furthermore if

$$I > \frac{n\Gamma}{mn - \nu_1 \tau_2},$$

then $h(I) < 0$. There is no intersection point with $g(I)$ since g is a positive function. Therefore there exists a unique endemic equilibrium point $E^* = (S^*, I^*, T^*, A^*, R^*)$ provided that $\mathcal{R}_0 > 1$. In addition if

$$g'(0) \geq h'(0) = \frac{(\omega_1 + d)\left(m - \frac{\nu_1 \tau_2}{n}\right)}{\Gamma},$$

equivalent to the condition $\mathcal{R}_0 \leq 1$, there is no endemic equilibrium for the system (4).

4.2.1. Stability of the Endemic Equilibrium

Lemma 3. *Let $g(I)$ be a positive smooth function defined on the interval $[0, \infty)$. Suppose that assumptions H_1 and H_2 hold, then the following inequality is satisfied*

$$1 - \frac{Ig'(I)}{g(I)} \geq 0 \text{ for any } I > 0. \tag{13}$$

Proof :
We have that

$$\frac{d[g(I) - Ig'(I)]}{dI} = -Ig''(I) \geq 0$$

as $g''(I) \leq 0$. This implies that the function $g(I) - Ig'(I)$ is increasing on the interval $[0, \infty)$. Given the fact that $g(0) - 0g'(0) = 0$, it follows that $g(I) - Ig'(I) \geq 0$. □

Theorem 3 *If $\mathcal{R}_0 > 1$, then the endemic equilibrium E^* is locally asymptotically stable.*

Proof : The Jacobian matrix of the endemic equilibrium is given by

$$J_{E^*} = \begin{pmatrix} -g(I^*) - (\omega_1 + d) & S^*g'(I^*) & 0 & 0 & 0 \\ g(I^*) & S^*g'(I^*) - m & \nu_1 & 0 & 0 \\ 0 & \tau_2 & -n & 0 & 0 \\ 0 & \tau_1 & \nu_2 & -d & 0 \\ \omega_1 & 0 & 0 & 0 & -d \end{pmatrix}. \quad (14)$$

The characteristic equation that results from the Jacobian matrix (J_{E^*}) is given by $\det(J_{E^*} - \lambda I) = 0$. Thus, we get

$$(d + \lambda)^2(\lambda^3 + b_1\lambda^2 + b_2\lambda + b_3) = 0, \quad (15)$$

where

$$\begin{aligned} b_1 &= g(I^*) + \omega_1 + d + m + n - S^*g'(I^*), \\ b_2 &= (m + n)[g(I^*) + \omega_1 + d] - S^*g'(I^*)(\omega_1 + d + n) + mn - \nu_1\tau_2, \\ b_3 &= (mn - \nu_1\tau_2)[g(I^*) + \omega_1 + d] - n(\omega_1 + d)S^*g'(I^*). \end{aligned}$$

The characteristic Equation (15) has a negative real double root

$$\lambda_1 = \lambda_2 = -d,$$

and three other roots, λ_3, λ_4 and λ_5, which are the roots of the equation

$$\lambda^3 + b_1\lambda^2 + b_2\lambda + b_3 = 0. \quad (16)$$

From Lemma (3), we have that

$$1 - \frac{I^*}{g(I^*)}g'(I^*) \geq 0. \quad (17)$$

It follows that

$$\begin{aligned} m - S^*g'(I^*) &= m - \frac{\left(m - \frac{\nu_1\tau_2}{n}\right)I^*}{g(I^*)}g'(I^*) \\ &> m\left[1 - \frac{I^*}{g(I^*)}g'(I^*)\right] \geq 0. \end{aligned} \quad (18)$$

Hence,

$$\begin{aligned} b_1 &= g(I^*) + \omega_1 + d + m + n - S^*g'(I^*) > 0 \quad \text{using 18}, \\ b_2 &= (m+n)[g(I^*)+\omega_1+d] - S^*g'(I^*)(\omega_1+d+n) + mn - \nu_1\tau_2 \\ &= (m+n)g(I^*) + (\omega_1+d)\left[m+n-S^*g'(I^*)\right] - nS^*g'(I^*) + \\ &\quad mn - \nu_1\tau_2 \\ &= (m+n)g(I^*) + (\omega_1+d)\left[m+n-S^*g'(I^*)\right] + \\ &\quad n\left[m - \frac{\left(m - \frac{\nu_1\tau_2}{n}\right)I^*}{g(I^*)}g'(I^*)\right] - \nu_1\tau_2 \\ &= (m+n)g(I^*) + (\omega_1+d)\left[m+n-S^*g'(I^*)\right] + \\ &\quad (mn - \nu_1\tau_2)\left[1 - \frac{I^*}{g(I^*)}g'(I^*)\right] > 0 \quad \text{using 17}, \end{aligned}$$

and

$$\begin{aligned} b_3 &= (mn - \nu_1\tau_2)[g(I^*) + \omega_1 + d] - n(\omega_1 + d)S^*g'(I^*) \\ &= (mn - \nu_1\tau_2)\left[g(I^*) + \omega_1 + d\right] \\ &\quad - (\omega_1 + d)\left[\frac{(mn - \nu_1\tau_2)I^*}{g(I^*)}g'(I^*)\right] \\ &= (mn - \nu_1\tau_2)\left[g(I^*) + \omega_1 + d - (\omega_1 + d)\frac{I^*}{g(I^*)}g'(I^*)\right] \\ &= (mn - \nu_1\tau_2)\left\{g(I^*) + (\omega_1 + d)\left[1 - \frac{I^*}{g(I^*)}g'(I^*)\right]\right\} > 0 \end{aligned}$$

using 17.

Moreover we have that

$$\begin{aligned} &b_1b_2 - b_3 \\ &= b_1\left\{(m+n)g(I^*) + (\omega_1+d)\left[m+n-S^*g'(I^*)\right]\right\} \\ &\quad - (mn - \nu_1\tau_2)g(I^*) \\ &\quad + b_1\left\{(mn - \nu_1\tau_2)\left(1 - \frac{I^*}{g(I^*)}g'(I^*)\right)\right\} \\ &\quad - \left\{(mn - \nu_1\tau_2)\left[(\omega_1+d)\left(1 - \frac{I^*}{g(I^*)}g'(I^*)\right)\right]\right\}. \end{aligned}$$

It follows that

$$\begin{aligned} &b_1b_2 - b_3 \\ &> n\left\{(m+n)g(I^*) + (\omega_1+d)\left[m+n-S^*g'(I^*)\right]\right\} - mn\,g(I^*) + \\ &\left\{(mn - \nu_1\tau_2)\left[(\omega_1+d)\left(1 - \frac{I^*}{g(I^*)}g'(I^*)\right)\right]\left[g(I^*) + m - S^*g'(I^*)\right]\right\} \\ &> 0. \end{aligned}$$

As a result, by the Routh−Hurwitz stability criterion [11], all the roots of the characteristic polynomial (15) have strictly negative real parts. Therefore the endemic equilibrium is locally asymptotically stable.

5. NUMERICAL SIMULATIONS

In this section, we provide numerical simulations for the evolution system of ordinary differential equations (1) to support the theoretical findings. Without loss of generality we set

$$g(I) = \frac{\alpha(t)I}{1 + \beta(t)I}.$$

Note that conditions of assumptions (H_1) and (H_2) are satisfied. Furthermore we let

$$\begin{aligned} &\Gamma = 150, \omega_1 = 1, d = 2, \nu_1 = 1, \\ &\nu_2 = 1, \tau_1 = 2, \tau_2 = 3. \end{aligned}$$

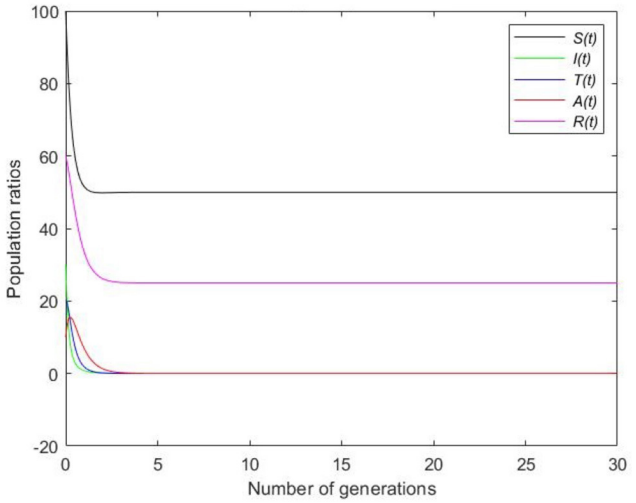

FIGURE 2 | Static simulation for disease-free equilibrium.

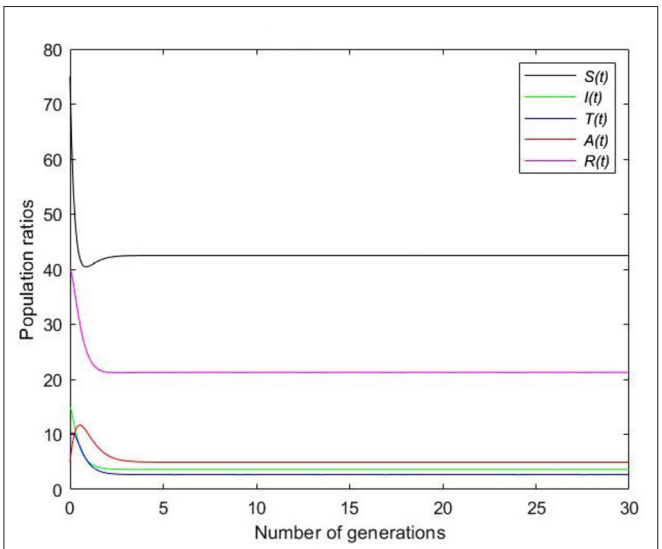

FIGURE 3 | Static simulation for endemic equilibrium.

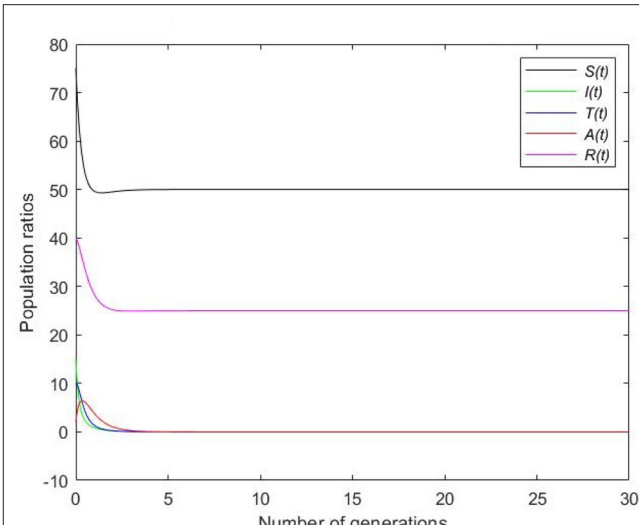

FIGURE 4 | Simulation with time dependence for disease-free equilibrium.

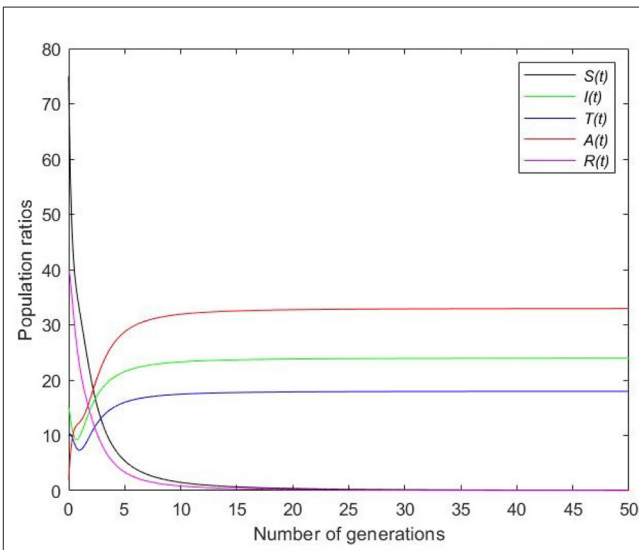

FIGURE 5 | Simulation with time dependence for endemic equilibrium.

Next we explore two scenarios involving static simulations and time-dependent simulations respectively.

5.1. Static Simulations

Picking $\alpha = \frac{1}{12}$ and $\beta = 1$ and substituting in the expression of the basic reproduction number, we get that $\mathcal{R}_0 = \frac{2}{3} < 1$. According to Theorem 2 the disease-free equilibrium, $E^0 = (50, 0, 0, 0, 25)$, is globally asymptotically stable. In **Figure 2**, it clearly shows that the disease eventually dies out.

Picking $\alpha = \frac{1}{5}$ and $\beta = 0.1$ and substituting in the expression of the basic reproduction number, we get that $\mathcal{R}_0 = 1.6 > 1$. According to Theorem 3 the endemic equilibrium, $E^* = (42.5, 3.6, 2.7, 4.9, 21.2)$, is locally asymptotically stable. In **Figure 3**, all the graphs converge to the endemic equilibrium.

5.2. Time-Dependent Simulations

Picking $\alpha(t) = \frac{1}{5+2t}$, it can be observed in **Figure 4** that graphs converge to the disease free equilibrium as time increases. It therefore suggests the global asymptotical stability of the disease free equilibrium and the extension of the disease in time.

Picking $\alpha(t) = t^2 + \frac{5}{4}$, **Figure 5** clearly shows that the susceptible population vanishes in a short span of time and the disease essentially affects all people in the population.

6. CONCLUDING REMARKS

In this paper, we formulated and investigated a mathematical model describing the dynamics on sexually transmitted disease

models with a novel class of non-linear incidence. We showed that the derived non-autonomous system of differential equations governing the evolution of the process was well-posed and the solution happened to be positive and bounded. The role of awareness in the susceptible and infectious classes was explored and investigated. A vertical asymptote and concavity arguments were critical in the proof of existence of an endemic equilibrium for the system and its asymptotical stability. In particular, numerical simulations were performed in order to predict the asymptotic behavior of solutions and support the theoretical findings.

DATA AVAILABILITY STATEMENT

The original contributions presented in the study are included in the article/supplementary material, further inquiries can be directed to the corresponding author/s.

AUTHOR CONTRIBUTIONS

All authors contributed to all critical aspects of the analysis and simulations. All authors contributed to the article and approved the submitted version.

REFERENCES

1. Mbokoma M, Oukouomi Noutchie SC. A stochastic analysis of HIV dynamics driven by fractional Browanian motion. *J Algebra Appl Math.* (2017) 15:1–31.
2. Mbokoma M, Oukouomi Noutchie SC. A theoretical analysis of the dynamics of AIDS with random condom use. *J Anal Appl.* (2017) 15:85–115.
3. Marin M, Othman MIA, Abbas IA. An extension of the domain of influence theorem for generalized thermoelasticity of anisotropic material with voids. *J Comput Theoret Nanosci.* (2015) 12:1594–8. doi: 10.1166/jctn.2015.3934
4. Ogunlaran OM, Oukouomi Noutchie SC. Mathematical model for an effective management of HIV infection. *Biomed Res Int.* (2016) 2016:4217548. doi: 10.1155/2016/4217548
5. Othman MIA, Said S, Marin M. A novel model of plane waves of two-temperature fiber-reinforced thermoelastic medium under the effect of gravity with three-phase-lag model. *Int J Num Methods Heat Fluid Flow*. (2019) 29:4788-806. doi: 10.1108/HFF-04-2019-0359
6. Tewa JJ, Bowong S, Oukouomi Noutchie SC. Mathematical analysis of a two-patch model of tuberculosis disease with staged progression. *Appl Math Modell.* (2012) 36:5792–807. doi: 10.1016/j.apm.2011.09.004
7. Jia J, Qin G. Stability analysis of HIV/AIDS epidemic model with nonlinear incidence and treatment. *Adv Diff Equat.* (2017) 2017:136. doi: 10.1186/s13662-017-1175-5
8. Van den Driessche P, Watmough J. Reproduction numbers and sub-threshold endemic equilibria for compartmental models of disease transmission. *Math. Biosci.* (2002) 180:29–48. doi: 10.1016/S0025-5564(02)00108-6
9. Verhulst F. *Nonlinear Differential Equations and Dynamical Systems*. New York, NY: Springer-Verlag (1990).
10. LaSalle JP. *The Stability of Dynamical Systems*. Philadelphia, PA: SIAM (1976).
11. Murray JD. *Mathematical Biology I. An Introduction.* 3rd ed., New York: Springer-Verlag. (2002).

Conflict of Interest: The authors declare that the research was conducted in the absence of any commercial or financial relationships that could be construed as a potential conflict of interest.

Publisher's Note: All claims expressed in this article are solely those of the authors and do not necessarily represent those of their affiliated organizations, or those of the publisher, the editors and the reviewers. Any product that may be evaluated in this article, or claim that may be made by its manufacturer, is not guaranteed or endorsed by the publisher.

frontiers | Frontiers in Applied Mathematics and Statistics

ORIGINAL RESEARCH
published: 16 June 2022
doi: 10.3389/fams.2022.899247

Log-Linear Model and Multistate Model to Assess the Rate of Fibrosis in Patients With NAFLD

*Iman M. Attia**

Department of Mathematical Statistics, Faculty of Graduate Studies for Statistical Research, Cairo University, Giza, Egypt

In this paper, the deleterious effects of obesity, type II diabetes, and insulin resistance, systolic and diastolic hypertension on the rate of progression of fibrosis in patients with non-alcoholic fatty liver disease (NAFLD) are illustrated using a new approach utilizing the Poisson regression to model the transition rate matrix. The observed counts in the transition count matrix are used as the response variables and the covariates are the risk factors for fatty liver. Then, the estimated counts from running the Poisson regression are used to estimate the transition rates using the continuous-time Markov chains (CTMCs) followed by exponentiation of the estimated rate matrix to obtain the transition probability matrix at specific time points. A depicted, hypothetical, observational, prospective longitudinal study of 150 participants followed up every year for a total of 29 years recording their demographic characteristics and their timeline follow-up is demonstrated. The findings revealed that insulin resistance expressed by HOMA2-IR had the most deleterious effects among other factors on increasing the rate of fibrosis progression from state 1 to state 2, from state 2 to state 3, and from state 3 to state 4. The higher the level of HOMA2-IR is, the more rapid the rate of progression is. This analysis helps the health policymakers and medical insurance managers to allocate the financial and human resources for investigating and treating high-risk patients with NAFLD. In addition, this analysis can be used by pharmaceutical companies to conduct longitudinal studies to assess the effectiveness of the newly emerging anti-fibrotic drugs.

Keywords: log-linear model, multistate model, non-alcoholic fatty liver disease, NAFLD, Poisson regression, continuous-time Markov chains, longitudinal studies, HOMA2-IR

OPEN ACCESS

Edited by:
Appanah Rao Appadu, Nelson Mandela University, South Africa

Reviewed by:
Ashish Awasthi, NITc, India
Farai Julius Mhlanga, University of Limpopo, South Africa

***Correspondence:**
Iman M. Attia
imanattiathesis1972@gmail.com
orcid.org/0000-0002-7333-9713

Specialty section:
This article was submitted to Mathematical Biology, a section of the journal Frontiers in Applied Mathematics and Statistics

Received: *18 March 2022*
Accepted: *12 April 2022*
Published: *16 June 2022*

Citation:
Attia IM (2022) Log-Linear Model and Multistate Model to Assess the Rate of Fibrosis in Patients With NAFLD. Front. Appl. Math. Stat. 8:899247. doi: 10.3389/fams.2022.899247

INTRODUCTION

Continuous-time Markov chains (CTMCs) are valuable mathematical and statistical tools. They are of great potential to evaluate the disease progression over time. NAFLD is an increasingly worldwide epidemic, paralleling the rise in the incidence of obesity and type II diabetes which are approaching a pandemic level. This emerging health problem is mainly due to sedentary life styles and western eating habits of ingesting high-fat and cholesterol diets. The pathological milestone for NAFLD is insulin resistance and hyperinsulinemia. This hyperinsulinemia will eventually result in type II diabetes with adverse complications like vascular diseases and fatty liver disease. On the other hand, NAFLD can cause type II diabetes, as the prevalence of diabetes in NAFLD ranges between 18 and 45%. Moreover, the prevalence of NAFLD in type II diabetic patients ranges between 49 and 75% [1].

Non-alcoholic fatty liver disease can be modeled using the simplest form for health, disease, and death model. It is composed of four states. One state is for susceptible individuals with risk factors like type II diabetes, dyslipidemia, obesity, and hypertension. The second state is the NAFLD phenotypes. The other two competing states for death are: one for liver-related mortality as a complication of NAFLD and the other state is the death causes unrelated to liver disease [2]. This model is shown in **Figure 1**.

In addition, NAFLD can be modeled in more elaborate expanded form which includes nine states [3]. The first eight states are the states of disease progression over time and the ninth state is the death state [2], as illustrated in **Figure 2**.

Moreover, fibrogenesis is a dynamic process that goes back and forth among the early stages of the expanded model. Stages of fibrous tissue formation are early seen in NAFLD process. Fibrosis progresses if the risk factors for its formation are not eliminated. Fibrosis is an ominous sign for loss of liver functions. When the fibrous tissue develops, a subset of the early states is used to relate these risk factors to the rates. Definition of each state is shown in **Figure 3** [4, 5]. F0 indicates that there is no fibrous tissue. F1 means that fibrous tissue is deposited due to non-alcoholic steatohepatitis (NASH) and not due to any other causes of liver disease; all other stages (F2 and F3) are maintained and are progressing over time by the presence of NASH till the liver cirrhosis (F4). If this NASH is well-treated by controlling the risk factors that induce it, the fibrous tissue formation and deposition will regress as shown in the **Figure 3**.

Kalbfleisch and Lawless [6] related the instantaneous rate of transitions from state i to state j to covariates, by regression modeling of the Q transition rate matrix using log-linear model for the Markov rates.

The previous studies, as will be later mentioned in the discussion, mainly included the evaluation of 2 paired biopsies, initial and second biopsies, then grouping the patients according to the findings into stable, regressors, slow progressors, and rapid progressors without precise estimation of specific transition rates among states and without proper estimation of the predictive value of each variable on these specific rates. The rate of fibrosis progression was estimated by dividing the difference in fibrosis stage between biopsies by the time interval (in years), and this was performed to account for the time differences between the biopsies [7]. Additionally, either univariate or multivariate linear regression was used to relate the risk factors with the rate of progression. As will be later mentioned in the discussion, some studies utilized multivariate logistic regression instead of linear regression.

This depicted study differs from the previous studies in many aspects. First, it proposes recording multiple repeated observations over time. Second, it suggests running Poisson regression to relate the transition rates among states with the risk

Abbreviations: CC, compensated cirrhosis (stage 4); CTMC, continuous-time Markov chains; DCC, de-compensated cirrhosis (stage 5); EM, extramortality (stage 9); HCC, hepatocellular carcinoma (stage 8); LT, liver transplant (stage 6); NAFLD, non-alcoholic fatty liver disease; NAFL-NO FB, non-alcoholic fatty liver with no fibrosis (stage 1); NASH, non-alcoholic steatohepatitis; NASH-NO FB, non-alcoholic steatohepatitis with no fibrosis (stage 2); NASH-FB, non-alcoholic steatohepatitis with fibrosis (stage 3); PLT, post-liver transplant (stage 7); T2DM, type 2 diabetes mellitus.

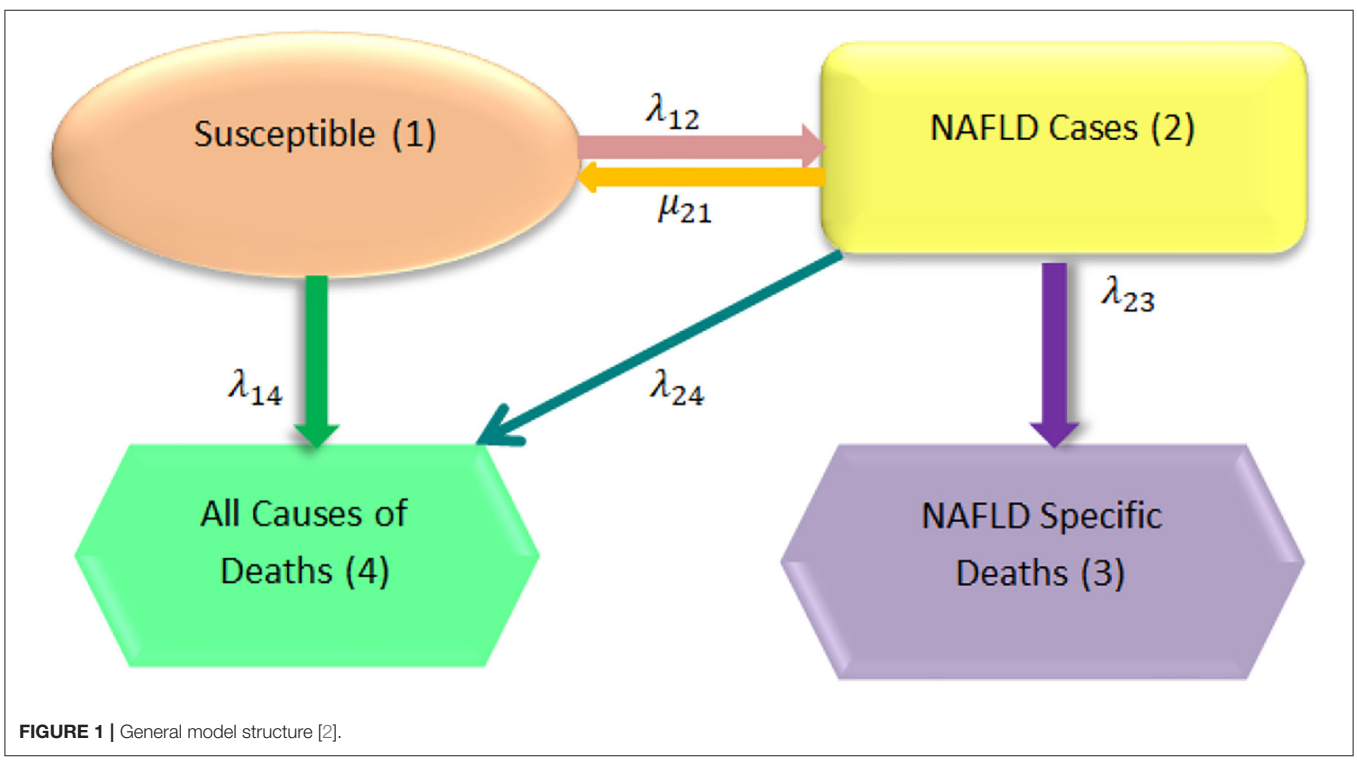

FIGURE 1 | General model structure [2].

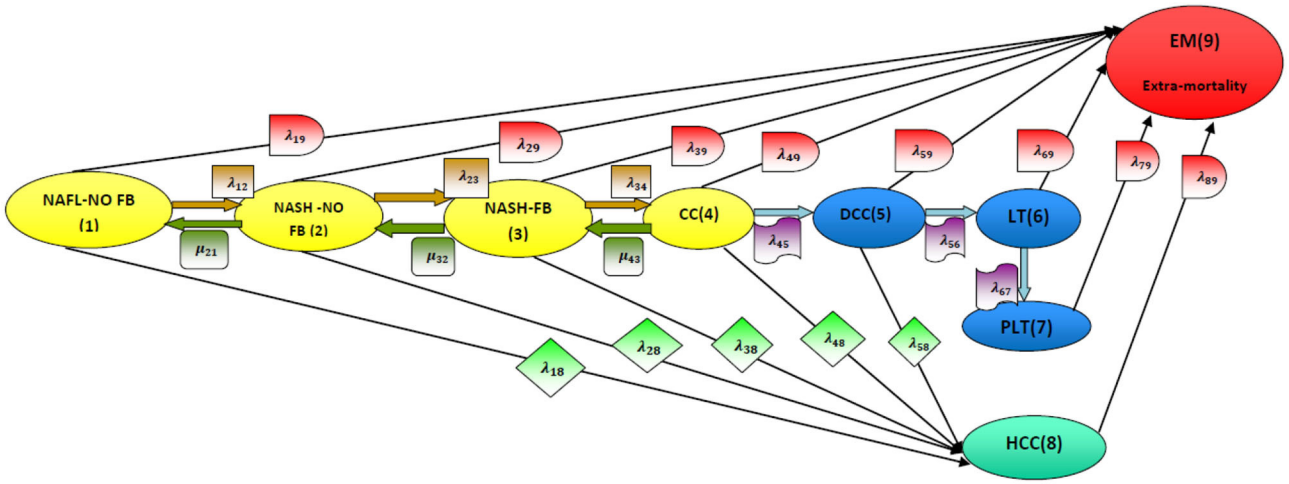

FIGURE 2 | Disease model structure [2]. NAFL-NO FB, non-alcoholic fatty liver with no fibrosis (stage 1); NASH-NO FB, non-alcoholic steatohepatitis with no fibrosis (stage 2); NASH-FB, non-alcoholic steatohepatitis with fibrosis (stage 3); CC, compensated cirrhosis (stage 4); DCC, de-compensated cirrhosis (stage 5); LT, liver transplant (stage 6); PLT, post-liver transplant (stage 7); HCC, hepatocellular carcinoma (stage 8); EM, extramortality (stage 9).

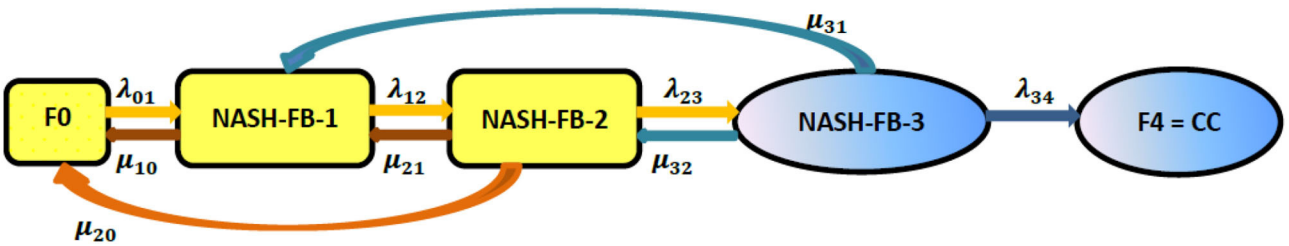

FIGURE 3 | NAFLD with the evolving fibrosis stages [4]. F0, no fibrosis (stage 0); NASH-FB-1, non-alcoholic steatohepatitis with mild fibrosis (stage 1); NASH -FB-2, NASH with moderate fibrosis (stage 2); NASH -FB-3, NASH with advanced or severe fibrosis (stage 3); CC, compensated cirrhosis (stage 4) which is the more severe or advanced form of fibrosis.

factors. Third, it recommends using continuous-time Markov chains to obtain the transition probabilities and predict the expected counts of patients in each state at a specific time point in the future. The counts of each transition can be modeled as a function of some explanatory variables reflecting the characteristics of the patients. The Poisson regression model specifies that each response y_i is drawn from a Poisson population with parameter λ_i, related to the covariates. The primary equation of the model is

$$P\left(Y = y_i|X_i\right) = \frac{\exp\left(-\lambda_i\right) \times \lambda_i^{y_i}}{y_i!}.$$

The most common formulation for the λ_i is the log-linear model:

$$\ln \lambda_i = X_i^{'}\beta = b_0 + b_1 x_{i1} + b_2 x_{i2} + b_3 x_{i3} + \ldots . + b_k x_{im}.$$

where β is the k $\times$ 1 parameter vector, m is the number of predictors, and Xs are the predictors.

The expected number of events per period is given by:

$$E\left[y_i|X_i\right] = var\left[y_i|X_i\right] = \lambda_i = \exp\left(X_i^{'}\beta\right).$$

The observed counts in the transition counts matrix are used as response variables. The covariates are the risk factors for the fatty liver, where the participants are subjected to the same follow-up periods. Then, the estimated counts obtained from running the Poisson regression are used as input to estimate the transition probability matrix using the CTMC. The author clarifies this procedure using a hypothetical example in the form of an observational prospective longitudinal study.

Attia [8] used the same data in previous work. Still, in this article, the author discusses the issue of multicollinearity, the equidispersion Poisson of response variables in the presence of excess zeros, and more comparisons between this work and previous works. Finally, the author highlights the benefit of such analysis to pharmacoeconomic evaluation and healthcare economics.

MATERIALS AND METHODS

Patients

A total of one hundred fifty participants were followed up every year for 29 years, and during each visit, the characteristics

TABLE 1 | Summary of transition counts among the states.

Counts	Transition 0→ 1	Transition 1→ 2	Transition 2→ 3	Transition 3→ 4	Transition 1→ 0	Transition 2→ 1	Transition 3→ 2	Transition 2→ 0	Transition 3→ 1
0	63	96	121	128	121	127	130	138	139
1	58	43	23	22	24	17	17	11	9
2	25	9	4		3	5	3	1	2
3	4	2	2		2	1			

TABLE 2 | Observed transition counts of the patients over the 29 years.

	State 0	State 1	State 2	State 3	State 4	total
State 0	1,909	120	15	6	0	2,050
State 1	36	1,116	67	28	0	1,247
State 2	13	30	703	37	0	783
State 3	11	14	23	50	22	120
State 4	0	0	0	0	0	0
						4,200

of the participants were recorded like sex (0 = female, 1 = male), age, body mass index (BMI), low-density lipoprotein (LDL)-chol, homeostatic model assessment-insulin resistance (HOMA2-IR), and systolic blood and diastolic blood pressure. For each participant, the recorded value is the mean of the follow-up measurements. The age is the median value. The participants were followed up till the end of the study or having liver cirrhosis (F4).

Statistical Analysis

The relationship between the response variable (counts of transitions) and the predictors was non-linear as shown by Lowess smoother. Restricted cubic spline was used to obtain a suitable functional form of the predictors to fit a Poisson model using STATA 14. The CTMCs were used to obtain transition probability matrix and transition rate matrix. p-Value of <0.05 was considered statistically significant; all tests were two-sided tests (refer to **Appendix A**).

RESULTS

Summary of the transition counts among the states is shown in **Table 1**. The observed counts of the participants over the 29 years of follow-up are demonstrated in **Table 2**. The distribution of these counts was Poisson (mean = variance). The dispersion indices for the nine response variables ranged between 0.82 and 1.34. In **Appendix B**, more figures illustrate the dispersion of these response variables. They were also correlated with high statistical significance (p-value = 0.000) as shown in **Table 3**.

Initial observed rates are as follows:

$$\lambda_{01} = \frac{120}{2050} = 0.059,\ \lambda_{12} = \frac{67}{1247} = 0.0537,$$
$$\lambda_{23} = \frac{37}{783} = 0.047\,,\ \lambda_{34} = \frac{22}{120} = 0.183$$

$$\mu_{10} = \frac{36}{1247} = 0.0288,\ \mu_{21} = \frac{30}{783} = 0.0383,$$
$$\mu_{32} = \frac{23}{120} = 0.191,\ \mu_{20} = \frac{13}{783} = 0.016,$$
$$\mu_{31} = \frac{14}{120} = 0.116$$

Although the response counts showed excess zeros, they fitted Poisson distribution and the zero inflated Poisson model. Their mean and variance were approximately equal as evident by their dispersion indices. So, Poisson regression was conducted for each transition count. Most statistical software packages conduct Poisson regression or generalized linear model utilizing log-link function with only one response variable. Thus, using STATA14, Poisson regression was conducted with one response variable. The response variable could not be used as a matrix to conduct the regression as multivariate regression with multiple response variables.

The application of Lowess smoother showed the non-linear relationship between the predictors and the response variables as shown in **Figure 4**. In **Supplementary Materials**, more figures illustrating these relationships between the different predictors and response variables are clearly shown (refer to also **Appendix B**).

The continuous predictors (age, BMI, HOMA2-IR, LDL-chol, and systolic and diastolic blood pressure) were highly correlated with a correlation coefficient of 0.99 and a condition number for data matrix (X'X) of 453.57. The condition number for the data matrix (X'X) constructed from the transformed variables used in the analysis (HOMAsp1, HOMAsp2, LDLsp2, sysPS2, diasPS2) was 54.89. These transformed variables were also highly correlated. However, the condition number did not exceed 100. Thus, this multicollinearity can be considered non-harmful, and it will not affect the analysis [9].

The observed counts were the response variables used to fit the Poisson regression model. For each transition count, the model that represented the most explainable covariates with their estimated beta coefficients and the corresponding incidence rate ratios were illustrated in **Appendix B**. The transitions were subdivided into progressive transitions and regressive transitions. The main important result is that HOMA2-IR is positively correlated with all progressive transitions and is inversely related to the regressive transitions, with control of other variables, as shown in **Tables 4**, **5**.

TABLE 3 | Correlation between the different response variables.

	F0→ F1	F1→ F2	F2→ F3	F3→ F4	F1→ F0	F2→ F1	F3→ F2	F2→ F0	F3→ F1
F0→ F1	1	0.794 (0.000)	0.794 (0.000)	0.70 (0.000)	0.798 (0.000)	0.719 (0.000)	0.693 (0.000)	0.559 (0.000)	0.548 (0.000)
F1→ F2	0.798 (0.000)	1	0.785 (0.000)	0.709 (0.000)	0.76 (0.000)	0.762 (0.000)	0.719 (0.000)	0.728 (0.000)	0.711 (0.000)
F2→ F3	0.794 (0.000)	0.785 (0.000)	1	0.82 (0.000)	0.99 (0.000)	0.928 (0.000)	0.868 (0.000)	0.768 (0.000)	0.791 (0.000)
F3→ F4	0.709 (0.000)	0.709 (0.000)	0.82 (0.000)	1	0.813 (0.000)	0.898 (0.000)	0.897 (0.000)	0.687 (0.000)	0.643 (0.000)
F1→ F0	0.798 (0.000)	0.76 (0.000)	0.99 (0.000)	0.813 (0.000)	1	0.911 (0.000)	0.867 (0.000)	0.753 (0.000)	0.778 (0.000)
F2→ F1	0.719 (0.000)	0.765 (0.000)	0.928 (0.000)	0.898 (0.000)	0.911 (0.000)	1	0.921 (0.000)	0.824 (0.000)	0.81 (0.000)
F3→ F2	0.693 (0.000)	0.719 (0.000)	0.868 (0.000)	0.897 (0.000)	0.867 (0.000)	0.921 (0.000)	1	0.798 (0.000)	0.796 (0.000)
F2→ F0	0.559 (0.000)	0.728 (0.000)	0.768 (0.000)	0.687 (0.000)	0.753 (0.000)	0.824 (0.000)	0.798 (0.000)	1	0.935 (0.000)
F3→ F1	0.548 (0.000)	0.711 (0.000)	0.791 (0.000)	0.643 (0.000)	0.778 (0.000)	0.81 (0.000)	0.796 (0.000)	0.935 (0.000)	1

In each cell, the Pearson correlation coefficient, for transitions among the different states, is shown with the significant p-value below this coefficient between the brackets.

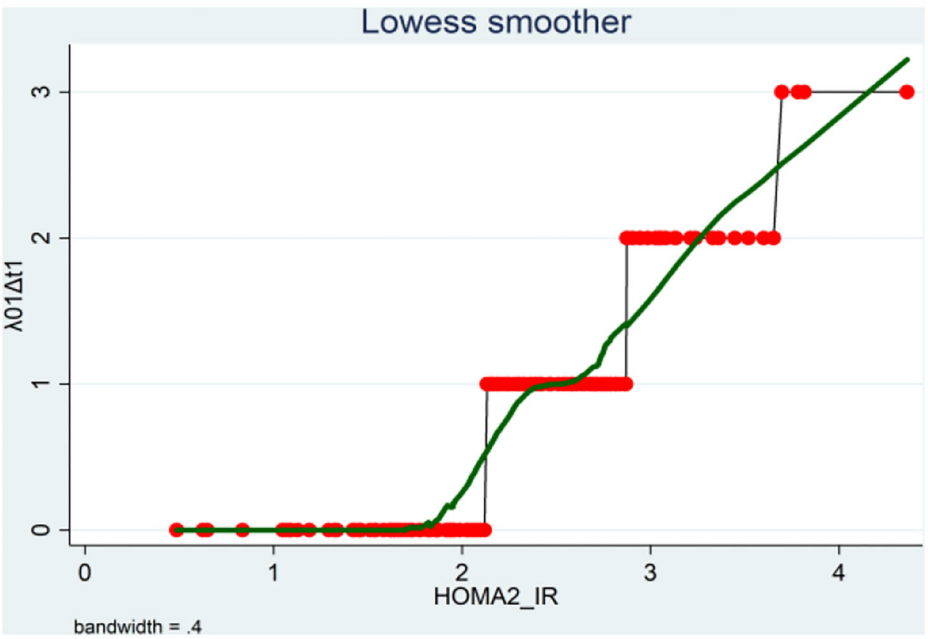

FIGURE 4 | Lowess smoother showing the non-linear relationship between the transition counts from F0 to F1 and the HOMA2-IR levels.

Progressive Transitions With Rates λ_{01}, λ_{12}, λ_{23}, λ_{34}

Persons with high insulin resistance (elevated HOMA2-IR) had 60 times the rate of transition from F0 to F1 compared to persons with normal level of HOMA2-IR (persons with normal insulin sensitivity), also the rate increased to 240 times for the rate of transition from F1 to F2, increased to 480 times for the rate of transition from F2 to F3, and increased to more than 50,000 times for the rate of transition from F3 to F4. Statistically speaking, the expected increase in log count of transition from F0 to F1 for one-unit increase in transformed HOMA is 4.096, which is highly statistically significant ($p = 0.000$). The expected increase in log count of transition from F1 to F2 for one-unit increase in transformed HOMA is 5.486, which is highly statistically significant ($p = 0.000$). The expected increase in log count of transition from F2 to F3 for one-unit increase in transformed

TABLE 4 | Parameters for each transition.

	LDLsp2	HOMAsp1	SysSP2	LDLsp2# HOMAsp1	LDLsp2# SysSP2	HOMAsp1# SysSP2
Transition from F0 to F1						
$\hat{b}$ co.(P)	0.523 (0.032)	4.096 (0.000)	−0.628 (0.070)	−0.179 (0.011)	0.003 (0.000)	0.151 (0.122)
CI for $\hat{b}$ co	(0.046, 1.000)	(3.452, 4.740)	(−1.308, 0.052)	(−0.317, −0.041)	(0.002, 0.003)	(−0.040, 0.342)
IRR	1.687	60.097	0.534	0.836	1.003	1.163
CI for IRR	(1.047, 2.718)	(31.569, 114.4)	(0.270, 1.054)	(0.728, 0.960)	(1.002, 1.003)	(0.960, 1.408)
Transition from F1 to F2						
$\hat{b}$ co.(P)	0.311 (0.432)	5.486 (0.000)	−0.314 (0.564)	−0.105 (0.367)		0.079 (0.616)
CI for $\hat{b}$ co	(−0.465, 1.086)	(4.366, 6.606)	(−1.383, 0.754)	(−0.332, 0.123)		(−0.231, 0.389)
IRR	1.364	241.179	0.730	0.901		1.083
CI for IRR	(0.628, 2.962)	(78.690, 739.192)	(0.251, 2.126)	(0.717, 1.131)		(0.794, 1.476)
Transition from F2 to F3						
$\hat{b}$ co.(P)	−1.480 (0.031)	6.174 (0.046)	2.497 (0.010)	0.390 (0.042)	−0.001 (0.687)	−0.655 (0.017)
CI for $\hat{b}$ co	(−2.823, −0.137)	(0.112, 12.237)	(0.602, 4.391)	(0.014, 0.766)	(−0.005, 0.004)	(−1.191, −0.118)
IRR	0.228	480.318	12.143	1.477	0.999	0.520
CI for IRR	(0.059, 0.872)	(1.118, 2.06e+5)	(1.826, 80.754)	(1.014, 2.151)	(0.995, 1.004)	(0.304, 0.889)
Transition from F3 to F4						
$\hat{b}$ co.(P)	0.452 (0.000)	10.866 (0.000)	0.073 (0.141)	−0.166 (0.000)		
CI for $\hat{b}$ co	(0.345, 0.559)	(8.119, 13.613)	(−0.024, 0.171)	(−0.201, −0.131)		
IRR	1.571	52375.984	1.076	0.847		
CI for IRR	(1.412, 1.748)	(3,357.9, 8.17e+5)	(0.976, 1.187)	(0.818, 0.877)		

B co. (p), the estimated B coefficient with p-value in the brackets; CI for B co., confidence interval for the estimated B coefficient; IRR, incidence rate ratio; CI for IRR stands for confidence interval for IRR; LDLsp2, the transformed LDL variable using restricted cubic spline method; HOMAsp1, the transformed HOMA2-IR variable using restricted cubic spline method; sysSp2, the transformed systolic blood pressure variable using restricted cubic spline method; LDLsp2 # HOMAsp1, interaction between the 2 variables.

HOMA is 6.174, which is not highly statistically significant ($p = 0.046$). The expected increase in log count of transition from F3 to F4 for one-unit increase in transformed HOMA is 10.866, which is highly statistically significant ($p = 0.000$).

Regressive Transitions With Rates

μ_{10}, μ_{21}, μ_{32}, μ_{20}, μ_{31}

Persons with high insulin resistance (elevated HOMA2-IR) had 0.011 times the rate of transition from F1 to F0 compared to persons with normal level of HOMA2-IR (persons with normal insulin sensitivity), also the rate decreased to 0.037 times for the rate of transition from F2 to F1, decreased to 0.005 times for the rate of transition from F3 to F2, decreased to 0.066 times for the rate of transition from F2 to F0, and decreased to 0.084 times for the rate of transition from F3 to F1. Statistically speaking, the expected decrease in log count of transition from F1 to F0 for one-unit increase in transformed HOMA is 4.489, which is not statistically significant ($p = 0.13$). The expected decrease in log count of transition from F2 to F1 for one-unit increase in transformed HOMA is 3.288, which is not statistically significant ($p = 0.242$). The expected decrease in log count of transition from F3 to F2 for one-unit increase in transformed HOMA is 5.214, which is not statistically significant ($p = 0.103$). The expected decrease in log count of transition from F2 to F0 for one-unit increase in transformed HOMA is 2.713, which is highly statistically significant ($p = 0.000$). The expected decrease in log count of transition from F3 to F1 for one-unit increase in transformed HOMA is 2.476, which is highly statistically significant ($p = 0.000$).

Validation and Residual Analysis

Poisson model fitted the data. When comparing the full model to the null model, there was a marked decrease in the deviance goodness of fit. Also, the akaike information criteria (AIC) and bayesian information criteria (BIC) were less than their values in the null model, indicating the full model improvement. In addition, there was an increase in the pseudo-R^2, indicating the ability of the model to predict the outcome better than the null model. The output results of the null model for each of the transition counts are shown in **Tables 6**, **7**.

The observed rates were approximately equal to the estimated rates after running the Poisson model as shown in **Table 8**.

Analysis of residuals especially Pearson residuals, for all transitions, revealed that they were not normally distributed. The Q-Q plot for these residuals did not exhibit normality. The Pearson dispersion statistics for each count was less than one supporting no evidence of overdispersion of the fitted model despite the apparent excess zeros (**Appendix B**, Table 21). Generalized Poisson regression did not fit the data. In **Appendix C**, more figures of these residuals are presented [10, 11].

This observational study aims to obtain preliminary and explanatory ideas about the effects of each risk factor on the different transition counts among the states. This

TABLE 5 | Parameters for each transition.

	LDLsp2	HOMAsp2	SysSP2	LDLsp2# HOMAsp2	LDLsp2# SysSP2	HOMAsp2# SysSP2
Transition from F1 to F0						
B co.(P)	−0.454 (0.063)	−4.489 (0.130)	1.340 (0.000)	0.290 (0.002)	−0.010 (0.005)	−0.286 (0.048)
CI for B co	(−0.932, 0.024)	(−10.294, 1.316)	(0.729, 1.951)	(0.102, 0.478)	(−0.017, – 0.003)	(−0.571, −0.002)
IRR	0.635	0.011	3.820	1.337	0.990	0.751
CI for IRR	(0.394, 1.024)	(0.000, 3.730)	(2.074, 7.034)	(1.108, 1.612)	(0.983, 0.997)	(0.565, 0.998)
Transition from F2 to F1						
B co.(P)	−0.128 (0.499)	−3.288 (0.242)	0.913 (0.000)	0.152 (0.022)	−0.010 (0.003)	−0.114 (0.317)
CI for B co	(−0.499, 0.243)	(−8.800, 2.224)	(0.519, 1.307)	(0.022, 0.282)	(−0.017, −0.003)	(−0.338, 0.109)
IRR	0.880	0.037	2.492	1.164	0.990	0.892
CI for IRR	(0.607, 1.275)	(0.000, 9.244)	(1.681, 3.694)	(1.022, 1.326)	(0.983, 0.997)	(0.713, 1.116)
Transition from F3 to F2						
B co.(P)	0.302 (0.154)	−5.214 (0.103)	0.422 (0.142)	0.002 (0.984)	−0.012 (0.006)	0.132 (0.375)
CI for B co	(−0.113, 0.716)	(−11.478, 1.05)	(−0.142, 0.987)	(−0.198, 0.202)	(−0.02, −0.003)	(−0.16, 0.425)
IRR	1.352	0.005	1.526	1.002	0.998	1.142
CI for IRR	(0.893, 2.047)	(0.000, 2.859)	(0.868, 2.683)	(0.821, 1.223)	(0.98, 0.997)	(0.852, 1.529)

	LDLsp2	HOMAsp2	SysSP2	DiasSP2
Transition from F2 to F0				
B co.(P)	0.076 (0.335)	−2.713 (0.000)	−0.123 (0.010)	0.358 (0.001)
CI for B co	(−0.079, 0.231)	(−4.102, −1.324)	(−0.216, −0.030)	(0.143, 0.573)
IRR	1.079	0.066	0.884	1.430
CI for IRR	(0.924, 1.260)	(0.017, 0.266)	(0.806, 0.970)	(1.154, 1.773)
Transition from F3 to F1				
B co.(P)	0.145 (0.038)	−2.476 (0.000)	−0.129 (0.004)	0.276 (0.003)
CI for B co	(0.008, 0.282)	(−3.769, −1.183)	(−0.216, −0.042)	(0.093, 0.459)
IRR	1.156	0.084	0.879	1.318
CI for IRR	(1.008, 1.326)	(0.023, 0.306)	(0.805, 0.959)	(1.098, 1.582)

B co. (p), the estimated B coefficient with p-value in the brackets; CI for B co., confidence interval for the estimated B coefficient; IRR, incidence rate ratio; CI for IRR stands for confidence interval for IRR; LDLsp2, the transformed LDL variable using restricted cubic spline method; HOMAsp2, the transformed HOMA2-IR variable using restricted cubic spline method; sysSp2, the transformed systolic blood pressure variable using restricted cubic spline method; DiasSp2, the transformed diastolic blood pressure variable using restricted cubic spline method; LDLsp2 # HOMAsp1, the interaction between the 2 variables.

Poisson regression is not aiming for future prediction of counts. Although the residuals are not normally distributed, such analysis can give fair provisional ideas about the effects of the risk factors. The Poisson model gives unbiased estimates for the regression coefficients, but these coefficients' statistical significance should be cautiously taken.

CTMCs Utilize the Estimated Counts From Log-Linear Model to Obtain the Transition Probability Matrix

For each of the transitions from state (i) to state (j), where λ_{ij} denotes the counts of transition from state (i) to state (j), and after running the Poisson model, the linear predictor $\ln \lambda_{ij} = X_n^{'} B$ for each participant (n) is exponentiated, $E\left[y_n \middle| X_n\right] = \lambda_{ij} = \exp\left(X_n^{'} B\right)$, to obtain the expected counts of transition that this participant had accomplished during this 29 years. Then, the result is rounded to the appropriate integer and summed to get all counts for this transition and then compared to the observed counts accomplished by all participants.

The n_{i+} is the total marginal transition counts out of this state, which is assumed to be constant. The estimated counts from running the Poisson model will be substituted in the transition count table. Because the marginal counts are assumed to be the same and when using the initial rates calculated as $\theta_0 = \frac{n_{ij}}{n_{i+}}$ where the n_{ij} is the transition counts from state i to state j, the Q matrix can be estimated. (Hint: the numerators below are the estimated counts obtained from running the Poisson regression).

$$\hat{Q} = \begin{bmatrix} -\lambda_{01} & \lambda_{01} & 0 & 0 & 0 \\ \mu_{10} & -(\lambda_{12}+\mu_{10}) & \lambda_{12} & 0 & 0 \\ \mu_{20} & \mu_{21} & -(\lambda_{23}+\mu_{21}+\mu_{20}) & \lambda_{23} & 0 \\ 0 & \mu_{31} & \mu_{32} & -(\lambda_{34}+\mu_{32}+\mu_{31}) & \lambda_{34} \\ 0 & 0 & 0 & 0 & 0 \end{bmatrix}$$

TABLE 6 | Comparison between null and full model as regards the progressive transitions.

	Cons. Co.	C.I. of CO.	Log pseu. like	Pseudo R^2	Deviance GOF	Pearson GOF	AIC	BIC
Transition F0 to F1								
Null model	−0.223	(−0.385, −0.061)	−171.273	0.000	149.236	122.5	344.55	347.56
	$P = 0.007$				$P = 0.4792$	$P = 0.944$		
Full model	−9.510	(−10.930, −8.089)	−110.43	0.355	27.55	24.458	234.86	255.94
	$P = 0.000$				$P = 1$	$P = 1$		
Transition F1 to F2								
Null model	−0.806	(−1.046, −0.566)	−130.82	0.000	146.133	150.16	263.64	266.65
	$P = 0.00$				$P = 0.551$	$P = 0.458$		
Full model	−14.884	(−17.555,−12.213)	−67.887	0.481	20.27	18.12	147.77	165.84
	$P = 0.000$				$P = 1$	$P = 1$		
Transition F2 to F3								
Null model	−1.4	(−1.767,−1.032)	−95.146	0.000	127.853	194.08	192.29	195.3
	$P = 0.000$				$P = 0.894$	$P = 0.007$		
Full model	−20.866	(−35.160, −6.572)	−37.87	0.6020	13.29	12.42	89.73	110.81
	$P = 0.004$				$P = 1$	$P = 1$		
Transition F3 to F4								
Null model	−1.92	(−2.307,−1.532)	−64.23	0.000	84.46	128	130.46	133.47
	$P = 0.00$				$P = 1$	$P = 0.89$		
Full model	−34.034	(−41.608, −26.459)	−26.97	0.58	9.94	8.96	63.94	78.99
	$P = 0.000$				$P = 1$	$P = 1$		

TABLE 7 | Comparison between null and full model as regards the regressive transitions.

	Cons. Co.	C.I. of CO.	Log pseu. like.	Pseudo R^2	Deviance GOF	Pearson GOF	AIC	BIC
Transition F1 to F0								
Null model	−1.427	(−1.795, −1.059)	−93.039	0.000	124.25	189	188.08	191.08
	$P = 0.000$				$P = 0.931$	$P = 0.015$		
Full model	−5.916	(−6.912, −4.921)	−38.14	0.59	14.46	13.55	90.29	111.36
	$P = 0.000$				$P = 1$	$P = 1$		
Transition F2 to F1								
Null model	−1.609	(−2.024, −1.195)	−83.54	0.000	117.021	200	169.08	172.09
	$P = 0.000$				$P = 0.975$	$P = 0.003$		
Full model	−7.666	(−8.875, −6.457)	−29.96	0.64	9.86	8.97	73.92	94.99
	$P = 0.000$				$P = 1$	$P = 1$		
Transition F3 to F2								
Null model	−1.875	(−2.307, −1.444)	−68.208	0.000	94.574	166.13	138.42	141.43
	$P = 0.000$				$P = 0.999$	$P = 0.16$		
Full model	−7.363	(−8.855, −5.871)	−26.37	0.61	10.89	9.77	66.74	87.81
	$P = 0.000$				$P = 1$	$P = 1$		
Transition F2 to F0								
Null model	−2.446	(−3.009, −1.882)	−45.487	0.000	66.3	160.	92.97	95.98
	$P = 0.000$				$P = 1$	$P = 0.253$		
Full model	−7.034	(−8.015, −6.053)	−15.63	0.656	6.65	7.36	41.26	56.31
	$P = 0.000$				$P = 1$	$P = 1$		
Transition F3 to F1								
Null model	−2.446	(−3.048, −1.843)	−46.18	0.000	69.133	183.15	94.36	97.37
	$P = 0.000$				$P = 1$	$P = 0.029$		
Full model	−7.584	(−8.934, −6.235)	−14.18	0.693	5.14	6.09	38.36	53.42
	$P = 0.000$				$P = 1$	$P = 1$		

Cons.Co, constant coefficient; C.I. of CO., confidence interval of constant; Log pseu.like., Log pseudolikelihood.

TABLE 8 | The comparison between observed and estimated response rate after fitting Poisson model.

		Comparison between observed and estimated progressive counts				Comparison between observed and estimated regressive counts	
		Observed response count	Estimated mean response count			Observed response count	Estimated mean response count
0→ 1	Mean	0.8	0.8	1→ 0	Mean	0.24	0.24
	Variance	0.658	0.619		Variance	0.305	0.314
1→ 2	Mean	0.45	0.45	2→ 1	Mean	0.2	0.2
	Variance	0.45	0.45		Variance	0.268	0.284
2→ 3	Mean	0.25	0.25	3→ 2	Mean	0.15	0.15
	Variance	0.32	0.318		Variance	0.171	0.173
3→ 4	Mean	0.15	0.15	2→ 0	Mean	0.09	0.09
	Variance	0.126	0.126		Variance	0.093	0.101
				3→ 1	Mean	0.09	0.09
					Variance	0.106	0.11

where

$$\lambda_{01} = \frac{120}{2050} = 0.059,\ \lambda_{12} = \frac{64}{1247} = 0.051,$$
$$\lambda_{23} = \frac{35}{783} = 0.045\ ,\ \lambda_{34} = \frac{20}{120} = 0.167$$
$$\mu_{10} = \frac{36}{1247} = 0.029,\ \mu_{21} = \frac{26}{783} = 0.033,$$
$$\mu_{32} = \frac{19}{120} = 0.158,\ \mu_{20} = \frac{12}{783} = 0.015,$$
$$\mu_{31} = \frac{13}{120} = 0.108$$

The probability matrix at any specific time point in the future can be obtained by exponentiation of this matrix because the chain is homogenous continuous-time Markov chains with constant rates over time. This result can also be obtained by solving the forward Kolmogorov differential equations, which will yield the same result as the exponentiation of the estimated Q matrix (refer to **Appendix D**).

The transition probability matrix is obtained by exponentiation of this estimated $\hat{Q}$ matrix after 1 year:

$$P\left(t=1\right) = \exp\left(\hat{Q}t\right) = \begin{bmatrix} P_{00} & P_{01} & P_{02} & P_{03} & P_{04} \\ P_{10} & P_{11} & P_{12} & P_{13} & P_{14} \\ P_{20} & P_{21} & P_{22} & P_{23} & P_{24} \\ P_{30} & P_{31} & P_{32} & P_{33} & P_{34} \\ 0 & 0 & 0 & 0 & P_{44} \end{bmatrix}$$
$$= \begin{bmatrix} 0.944 & 0.055 & 0.001 & 0 & 0 \\ 0.027 & 0.925 & 0.047 & 0.001 & 0.0001 \\ 0.014 & 0.033 & 0.915 & 0.035 & 0.003 \\ 0.002 & 0.086 & 0.125 & 0.651 & 0.136 \\ 0 & 0 & 0 & 0 & 1 \end{bmatrix}$$

Goodness of Fit for the Multistate Markov Model

To calculate goodness of fit for multistate model used in this example, it is like the procedure used in contingency table:

TABLE 9 | The expected transition counts after one year of the follow-up.

	State 0	State 1	State 2	State 3	State 4
State 0	1934.175	112.955	2.87	0	0
State 1	34.168	1153.101	58.484	1.122	0.125
State 2	11.275	25.604	716.367	27.248	2.506
State 3	0.276	10.356	14.94	78.144	16.284
State 4	0	0	0	0	0

Step 1: $H_0 =$ *future state does not depend on the current state*
$H_1 =$ *future state depends on the current state*

Step 2: After obtaining the estimated Q matrix, the probability matrix is calculated in time interval equals one because the participants' follow-up period was done every year.

$$p_{ij}\left(\triangle t=1\right) = \exp\left(\hat{Q}\times\triangle t\right) = \begin{bmatrix} P_{00} & P_{01} & P_{02} & P_{03} & P_{04} \\ P_{10} & P_{11} & P_{12} & P_{13} & P_{14} \\ P_{20} & P_{21} & P_{22} & P_{23} & P_{24} \\ P_{30} & P_{31} & P_{32} & P_{33} & P_{34} \\ 0 & 0 & 0 & 0 & P_{44} \end{bmatrix}$$
$$= \begin{bmatrix} 0.9435 & 0.0551 & 0.0014 & 0 & 0 \\ 0.0274 & 0.9247 & 0.0469 & 0.0009 & 0.0001 \\ 0.0144 & 0.0327 & 0.9149 & 0.0348 & 0.0032 \\ 0.0023 & 0.0863 & 0.1245 & 0.6512 & 0.1357 \\ 0 & 0 & 0 & 0 & 1 \end{bmatrix}$$

Step 3: Calculate the expected counts in this interval.

$$E_{ij} = n_{i+}\,P_{ij}\left(t\right).$$
$$n_{1+} = 2050,\ n_{2+} = 1247,\ n_{3+} = 783,\ n_{4+} = 120$$

Multiplying each row in the probability matrix with the corresponding total marginal counts in the observed transition counts table in the same interval yields the expected counts as shown in **Table 9**.

Step 4: The observed counts, O_{ij}, are shown in **Table 2**. The expected counts, E_{ij}, are obtained from the previous step and are shown in **Table 9**. Then, apply the Pearson statistic formula which yields a value of 1,140.097 with high statistical significance ($p = 0.000$). Apply $\sum_{i=1}^{5}\sum_{j=1}^{5}\frac{(O_{ij}-E_{ij})^2}{E_{ij}} = 1140.097 \sim \chi^2_{(5-1)(5-1)(.05)}$.

So, from the above results, the null hypothesis is rejected while the alternative hypothesis is accepted and the multistate Markov model fits the data, that is to mean, the future state depends on the current state with the estimated transition rates and probability matrices as obtained.

Health Economics

This transition probability matrix can predict the count of patients in each state at specific time point, for example, if a cohort of 6,000 patients with the following number in each state is $\begin{bmatrix}3000 & 1800 & 1020 & 180 & 0\end{bmatrix}$, after 1 year the predicted counts will be $\begin{bmatrix}2895 & 1879 & 1044 & 154 & 28\end{bmatrix}$. This count can be achieved by multiplying the initial count distribution of the patients with the transition probability calculated at the required specific time point, $p_{ij}(t) = \exp\left(\hat{Q}t\right)$

$$E\left[u_j(t)\,|u_j(0)\right] = \sum_{j=1,i=1}^{5} u_j(0)\,P_{ij}(t) \quad i,\ j = 1,..,5$$

Let $u(0)$ be the size of patients in a specific state at specific time $t = 0$. The initial size of patients is $U(0) = u_j(0)$, as there are 4 transient states (F0 to F3) and 1 absorbing state (F4), where $u_j(0)$ is the initial size or the number of patients in state j at time $t = 0$ given that $u_5(0) = 0$, i.e., initial size of patients in state 5 (absorbing state) is zero at initial time point = 0. As the transition or the movement of the patients among states is independent, at the end of the whole time interval $(0, t)$, there will be $u_j(t)$ patients in the transient states at time t, and there will also be $u_5(t)$patients in state 5 (F4 = liver cirrhosis) at time t.

In addition, the state probability distribution $\pi(t)$, which is the probability distribution for each state at a specific time point given the initial probability distribution $\pi(0)$, can be estimated by applying the following formula:

$$\pi(t) = \pi(0)\,P(t).$$

In this example, the cohort of 6,000 patients has initial probability distribution of $\begin{bmatrix}0.5 & 0.3 & 0.17 & 0.03 & 0\end{bmatrix}$, after 1 year, the state probability distribution will be $\begin{bmatrix}0.4825 & 0.3131 & 0.174 & 0.0257 & 0.0046\end{bmatrix}$.

Pharmaco-economic evaluation can be assessed in three categories: the cost-benefit analysis, the cost-effectiveness analysis, and the cost-utility analysis. The evaluation utilizes the predicted number of patients in each state estimated every year, the state probability distribution predicted every year, the costs of investigations and treatments, and the quality adjusted life years for the patients [12, 13].

This approach differs from the one used by Rustgi et al. [14] who depends on calculating the cost-effectiveness analysis by following a cohort of patients, all starting at the same initial state till death. While in the approach proposed in this article, sampling the population and estimating the transition probability matrix to predict the counts in the future, any cohort of patients can be followed up utilizing the information gained from sampling the high-risk population.

DISCUSSION

The following discussion elucidates the agreements and comparisons between the findings in this study with the findings in the previous one high-lightening the effects of various factors on progression rate of fibrosis in NAFLD patients.

Hui et al. [15] conducted a study on 17 patients who had previous liver biopsy showing evidence of steatosis with or without the presence of necroinflammation and fibrosis. Those patients underwent second liver biopsies with a median of 6 years apart (range: 3.8–8 years). More than half of them developed progressive fibrosis compared to the initial biopsy; because that these patients suffered from steatohepatitis, although there was no significant correlation between the degree of steatohepatitis and the degree of fibrosis between the two biopsies. However, the correlation was significant between the initial stage of fibrosis and the fibrosis grade in the second biopsy. Also, the clinical and laboratory parameters were not statistically significant between the recorded values during the first and the second biopsies. The changes in these parameters also showed no significant correlation with changes in the scores of steatosis, necroinflammation, or fibrosis. There was a negative correlation, although non-significant, between the change in the score of fibrosis and each of the changes: in the BMI, plasma total cholesterol levels, plasma triglyceride levels, and glycosylated hemoglobin. During the follow-up, two patients developed type II diabetes and one developed hypertension but without progression of fibrosis, their initial biopsy revealed F0, and the second one was also F0. Another patient developed type II diabetes with evolution of the fibrosis from F0 to F2, and another 2 patients developed hypertension with advancement of fibrosis from F0 to F1.

Fassio et al. [16] conducted a study on 22 patients who had liver biopsy with evidence of NASH and found that 31.8% (7 patients = P group, progressors) had progression of liver fibrosis over a median follow-up of 4.7 years. The other group was 68.2% (15 patients = NP group, non-progressors) and did not progress over a median follow-up of 4.3 years. The rate of progression in the entire population was estimated as 0.059 fibrosis units per year (mean difference in fibrosis score divided by mean interval in years between the first and second biopsies = 0.32/5.34 = 0.059), the rate of progression in the P group was 1.85/6.59 = 0.28. There was no statistical difference as regards the clinical, biochemical, grade of steatosis, and grade of inflammation between the two groups except for the presence of obesity and higher BMI (progressor was more obese with higher BMI than the non-progressor) whether this was performed during the initial liver biopsy or the final liver biopsy. Within each group, the gradients between the final and basal results were not

statistically significant as regards the clinical, biochemical, grade of steatosis, and grade of inflammation between the two groups including the BMI.

Adams et al. [7] conducted a study on 103 patients who had performed two liver biopsies with mean follow-up period of 3.2 ± 3 years (range = 0.7–21) between the first and the second biopsies. A total of 38 patients were progressors, 35 patients were stable, and 30 patients were regressors. No clinical or biochemical variables were statistically different among the progressors, stable, and regressors. The rate of fibrosis change varied from −2.05 to 1.7 stages/year and calculated as stated in the introduction. Using univariate regression model, the presence of diabetes, AST/ALT ratio, steatosis grades, and fibrosis stage were the only significant variables. By multivariate linear regression analysis and adjusting for age and BMI, only the presence of diabetes and earlier fibrosis stage were significantly associated with a higher rate of fibrosis progression. He also found no significant correlation between rate of progression and HOMA.

There are many studies performed by Ekstedt et al. [17], Teli et al. [18], Pais et al. [19], Argo et al. [20], Evans et al. [21], Hamaguchi et al. [22], and Wong et al. [23]. The reader can refer to them (refer to **Appendix E**).

The findings of the present study demonstrate that HOMA2-IR has a positive and a statistically significant effect on progression of fibrosis among the different states. Running multivariate Poisson regression reveals that the main players for progression are the HOMA2-IR, LDL-chol, and systolic blood pressure explaining about 35–60% of variability in the rates of progression. However, HOMA2-IR has a negative effect that is not statistically significant on the rate of remission or regression from F1 to F0, from F2 to F1, and from F3 to F2, but it is statistically significant on the rate of remission from F2 to F0 and from F3 to F1. Poisson regression model explained that the same factors and their interactions were responsible for about 60–70% of variability in the rates of remission among the states. The high HOMA2-IR levels significantly decrease the effects of high LDL levels on the progression rate from F0 to F1 and from F3 to F4. Thus, this interaction can be a protective mechanism to slow down the progression rate of fibrosis. The low HOMA2-IR levels significantly increase the effect of low LDL levels on the remission rate from F1 to F0 and from F2 to F1. Thus, this interaction can be a protective mechanism to accelerate the remission rate of fibrosis. The rate of fibrosis decreases with the help of rigorous control of the blood level of insulin, glucose, cholesterol, and blood pressure. The high levels of systolic blood pressure significantly decrease the effect of low LDL levels on the remission rate of fibrosis from F1 to F0, from F2 to F1, and from F3 to F2. Thus, controlling the most harmful factors like hyperinsulinemia and hypercholestrolemia, even in the absence of strict control of hypertension, can still benefit repressing the fibrogenesis. Lifestyle modification, in the form of physical exercise and a low caloric diet, and controlling the risk factors greatly impact arresting the process of fibrogenensis.

The newly emerging anti-fibrotic drugs will also help physicians treat fibrogenesis. In the FLINT study conducted on 283 non-cirrhotic patients taking obeticholic acid (OCA), 25 mg daily; the improvement in the histology detected by NAFLD activity score (NAS) was two points or more with no deterioration of fibrosis, and 35% of patients taking OCA had a decrement in fibrosis score by at least one stage in comparison with 19%in the placebo arm. REGENERATE study (still in progress, with the estimated primary completion date is on September 2025 as shown on clinicaltrials.gov official site) will evaluate safety and efficacy of obeticholic acid (OCA) in NASH patients with fibrosis who are randomized to a daily dose of 25 mg, 10 mg, and placebo, with endpoints like amelioration of fibrosis by at least one stage and decaying of NASH with no deterioration of fibrosis. At 18 month of randomization, liver biopsy revealed statistically significant histological amelioration of fibrosis and decaying of NASH with no deterioration in fibrosis for both 10 and 25 mg doses. In the GOLDEN study, conducted on 274 NASH patients, 120 mg elafibranor taken daily for 52 weeks induced decaying of moderate to severe NASH in a meaningfully higher percentage of patients than placebo; these patients also showed lowering in fibrosis stage compared to non-resolving NASH patients. The RESOLVE-IT trial (last update was on 30 November 2020, as shown on clinicaltrials.gov official site, but the study is still in progress according to Guirguis et al. [24]) emerged in May 2020 had shown that 19.2% of patients, on 120 mg daily elafibranor, had NASH decay without deterioration of fibrosis compared to 14.7% in the placebo group, which was not statistically significant. Furthermore, 24.5% of patients had shown fibrosis amelioration of more than one stage compared to 22.4% in the placebo group, which was also not statistically significant. In CENTAUR trial, conducted over 289 patients taking cenicriviroc (CVC), 150 mg daily and placebo for 52 weeks, no comparative betterment in NAS between NASH group and placebo was seen; however, there was one stage or more amelioration of fibrosis with no deterioration of NASH in the group taking the CVC compared to placebo group. The AURORA trial (primary completion dates were October 2021 according to clinicaltrials.gov site while the completion date will be October 2028 according to Guirguis et al. [24]) will evaluate long-term safety and efficacy of 150 mg daily CVC for the treatment of fibrosis in NASH adult at 2 phases: the first has endpoint of at least one stage amelioration of fibrosis without deterioration of NASH at month 12, and phase 2 has endpoint that is cirrhosis, liver-related outcome as HCC, and all causes of mortality. In a small, open-label, randomized phase II trial including 72 biopsy-proven NASH patients (NAS ≥ 5 and stage 2–3 liver fibrosis) receiving 18 mg daily selonsertib for 24 weeks, there was a significant improvement in liver disease activity, fibrosis, stiffness, liver fat content, and progression to cirrhosis [25].

FLINT, GOLDEN, and CENTAUR are phase IIb placebo-controlled randomized control trials (RCTs), whereas REGENERATE, RESOLVE-IT, and AURORA are randomized, placebo-controlled, double-blinded, multicenter phase III trials.

The distribution of the counts was Poisson distribution (mean = variance); that is to mean, these counts were equidispersed. However, all the counts showed excess zeros except for the transition from F0 to F1 where the zeros constituted 42% of the total count of this transition. Tlhaloganyang and Sakia

found that the equidispersed counts data with excessive zeros can be modeled with Poisson regression, the best model to represent the data. Also, the AIC scores obtained by them after running Poisson regression, on their tested data whether simulated or real, were less than the AIC scores after running ZIP on the same datasets [26]. In this article, the predictors were normally distributed, and applying the restricted cubic spline transformation was used to better specify the functional form of these predictors. The raw predictors and the transformed predictors were highly correlated. But the condition number obtained from the transformed predictors is below 100, which is not harmful for the analysis as shown in the Results. Vatcheva et al. [27] highlighted the fact that the majority of researchers do not mention the multicollinearity diagnostics when running the regression models, discussed the causes and effects of this lack, and proposed some remedies to treat multicollinearity such as: principal component analysis, partial least squares regression, and ridge regression analysis. Akram et al. [28] used principal component ridge type estimator for the inverse Gaussian regression model. Many investigators such as, Liu [29], Kibria and Lukman [30], and Lukman et al. [31] had proposed different techniques to manage the multicollinearity problem between the predictors when running regression models. Some of them, who developed methods for Poisson regression, are Månsson and Shukur [32], Månsson et al. [33], Lukman et al. [34], Lukman et al. [35], and Qasim et al. [36]. In this paper, none of these methods were used as the Poisson model was mainly used to give preliminary vision about the effects of the high-risk factors on the transition counts. Also, it was not used for prediction, and the condition number was <100. Once the estimated counts were obtained, they were fed to the CTMC to estimate the transition rate matrix and transition probability matrix at any specified time point. Thus, physicians can follow a cohort of any patients in various states and obtain their state probability distribution at different time points.

The strength of this study is the conduction of multiple frequent repeated observations over a long period of follow-up on a large number of high-risk participants for developing NAFLD and performing a liver biopsy during each visit. Although this may be realistically infeasible during each visit, non-invasive techniques [37, 38] can substitute the invasive liver biopsy. The advantage of techniques like MRI and machine learning [39], to assess the liver texture and correlate these findings with the histological findings in liver biopsy, can overcome this weakness. Liver biopsy can also be reserved in situations where non-invasive tests are inconclusive. These non-invasive tests decrease the number of liver biopsies each patient may encounter. The proposed follow-up period is too long to wait for the obtained results, which can be overcome by using adaptive clinical trials. The weakness of the study is the presence of dependency among the response variables which was not treated by the statistical analysis used in this study. A copula modeling discrete random vectors like the counts in this study can be used in future analysis. However, a copula of discrete vectors is not fully identifiable and thus causes serious inconsistencies [40], especially when modeling nine variables like the variables used in this study.

CONCLUSION

In the present study, running Poisson regression model is used to obtain the expected counts of transition among states. These counts are used as input into the homogenous CTMC. Using this CTMC, the transition rate matrix is estimated, and thus, the probability of progression of participants from specific state to another one at specific time point can be estimated by exponentiation of this rate matrix. This probability matrix at any specific time point multiplied by the initial probability distribution of a cohort of patients can be used to predict the number of the participants in each state later on at different time points. This predicted number of participants helps health policymakers and insurance managers allocate the human and financial resources to investigate and treat the high-risk patients for developing NAFLD. The Poisson regression model relates these high-risk covariates to the transition rates among states. Also, this approach can be used in the clinical trials to assess the effectiveness of the newly emerging anti-fibrotic drugs. The epidemiologists can utilize this methodology to estimate the effect of risk factors on the incidence rates of progression and remission among the different states of liver fibrosis due to NAFLD.

This hypothetical study is coded by stata-14 and is published in code ocean site with the following URL: https://codeocean.com/capsule/4752445/tree/v3.

The code to estimate the Q transition rate matrix for the observed transition counts using continuous-time Markov chains is published in the code Ocean site with following URL: https://codeocean.com/capsule/6377472/tree/v2.

The code for solving the forward Kolmogorov equations using the estimated Q rate matrix is published in the code Ocean site with following URL: https://codeocean.com/capsule/7258626/tree/v1.

The dataset is present on IEEE Data Port site with the following URL: https://ieee-dataport.org/documents/fibrosis-nfld#files, with the following doi: 10.21227/dr5j-gs46.

REGENERATE study URL: https://clinicaltrials.gov/ct2/show/NCT02548351.

RESOLVET-IT study URL: https://clinicaltrials.gov/ct2/show/NCT02704403.

A medical appendix briefly clarifies the stages of fibrosis due to NAFLD. See also the presentation (in the **Supplementary Materials**).

DATA AVAILABILITY STATEMENT

The original contributions presented in the study are included in the article/**Supplementary Material**, further inquiries can be directed to the corresponding author/s.

AUTHOR CONTRIBUTIONS

IA carried out the conceptualization by formulating the goals, aims of the research article, formal analysis by applying

the statistical, mathematical and computational techniques to synthesize and analyze the hypothetical data, the methodology by creating the model, software programming and implementation, supervision, writing, drafting, editing, preparation, and creation of the presenting work.

SUPPLEMENTARY MATERIAL

The Supplementary Material for this article can be found online at: https://www.frontiersin.org/articles/10.3389/fams.2022.899247/full#supplementary-material

REFERENCES

1. Younossi ZM, Gramlich T, Matteoni CA, Boparai N, McCullough AJ. Nonalcoholic fatty liver disease in patients with type 2 diabetes. *Clin Gastroenterol Hepatol.* (2004) 2:262–5. doi: 10.1016/S1542-3565(04)00014-X
2. Younossi ZM, Blissett D, Blissett R, Henry L, Stepanova M, Younossi Y, et al. The economic and clinical burden of nonalcoholic fatty liver disease in the United States and Europe. *Hepatology.* (2016) 64:1577–86. doi: 10.1002/hep.28785
3. Attia IM. Novel approach of multistate markov chains to evaluate progression in the expanded model of non-alcoholic fatty liver disease. *Front Appl Math Stat.* (2022) 7:766085. doi: 10.3389/fams.2021.766085
4. Younossi ZM, Tampi RP, Racila A, Qiu Y, Burns L, Younossi I, et al. Economic and clinical burden of nonalcoholic steatohepatitis in patients with type 2 diabetes in the US. *Diabetes Care.* (2020) 43:283–9. doi: 10.2337/dc19-1113
5. Singh S, Allen AM, Wang Z, Prokop LJ, Murad MH, Loomba R. Fibrosis progression in nonalcoholic fatty liver vs nonalcoholic steatohepatitis: a systematic review and meta-analysis of paired-biopsy studies. *Clin Gastroenterol Hepatol.* (2015) 13:643–54. doi: 10.1016/j.cgh.2014.04.014
6. Kalbfleisch JD, Lawless JF. The analysis of panel data under a Markov assumption. *J Am Stat Assoc.* (1985) 80:863–71. doi: 10.1080/01621459.1985.10478195
7. Adams LA, Sanderson S, Lindor KD, Angulo P. The histological course of nonalcoholic fatty liver disease: a longitudinal study of 103 patients with sequential liver biopsies. *J Hepatol.* (2005) 42:132–8. doi: 10.1016/j.jhep.2004.09.012
8. Attia IM. Prognostic factors for evolution of non alcoholic fatty liver disease patients utilizing poisson regression and continuous time markov chains. *Int J Res Eng Sci.* (2021) 9:61–71.
9. Lazaridis A. A note regarding the condition number: the case of spurious and latent multicollinearity. *Qual Quant.* (2007) 41:123–35. doi: 10.1007/s11135-005-6225-5
10. Hilbe JM. Modeling count data. In: Lovric, editor. *International Encyclopedia of Statistical Science.* Springer (2011). 836–9.
11. Cameron AC, Trivedi PK. *Regression Analysis of Count Data.* 2nd ed. Cambridge University Press (2013).
12. O'Hara J, Finnegan A, Dhillon H, Ruiz-Casas L, Pedra G, Franks B, et al. Cost of non-alcoholic steatohepatitis in Europe and the USA: the GAIN study. *JHEP Rep.* (2020) 2:100142. doi: 10.1016/j.jhepr.2020.100142
13. Noureddin M, Jones C, Alkhouri N, Gomez EV, Dieterich DT, Rinella ME, et al. Screening for nonalcoholic fatty liver disease in persons with type 2 diabetes in the United States is cost-effective: A comprehensive cost-utility analysis. *Gastroenterology.* (2020) 159:1985–7. doi: 10.1053/j.gastro.2020.07.050
14. Rustgi VK, Duff SB, Elsaid MI. Cost-effectiveness and potential value of pharmaceutical treatment of nonalcoholic fatty liver disease. *J. Med. Econ.* (2022) 25:347–355. doi: 10.1080/13696998.2022.2026702
15. Hui AY, Wong V, Chan H, Liew C, Chan J, Chan F, et al. Histological progression of non-alcoholic fatty liver disease in Chinese patients. *Aliment Pharmacol Ther.* (2005) 21:407–13. doi: 10.1111/j.1365-2036.2005.02334.x
16. Fassio E, Álvarez E, Domínguez N, Landeira G, Longo C. Natural history of nonalcoholic steathepatitis: a longitudinal study of repeat liver biopsies. *Hepatology.* (2004) 40:820–6. doi: 10.1002/hep.1840400411
17. Ekstedt M, Franzén LE, Mathiesen UL, Thorelius L, Holmqvist M, Bodemar G, et al. Long-term follow-up of patients with NAFLD and elevated liver enzymes. *Hepatology.* (2006) 44:865–73. doi: 10.1002/hep.21327
18. Teli MR, James OFW, Burt AD, Bennett MK, Day CP. The natural history of nonalcoholic fatty liver: a follow-up study. *Hepatology.* (1995) 22:1714–9. doi: 10.1002/hep.1840220616
19. Pais R, Charlotte F, Fedchuk L, Bedossa P, Lebray P, Poynard T, et al. A systematic review of follow-up biopsies reveals disease progression in patients with non-alcoholic fatty liver. *J Hepatol.* (2013) 59:550–6. doi: 10.1016/j.jhep.2013.04.027
20. Argo CK, Northup PG, Al-Osaimi AMS, Caldwell SH. Systematic review of risk factors for fibrosis progression in non-alcoholic steatohepatitis. *J Hepatol.* (2009) 51:371–9. doi: 10.1016/j.jhep.2009.03.019
21. Evans CDJ, Oien KA, MacSween RNM, Mills PR. Non-alcoholic steatohepatitis: A common cause of progressive chronic liver injury? *J Clin Pathol.* (2002) 55:689–92. doi: 10.1136/jcp.55.9.689
22. Hamaguchi E, Takamura T, Sakurai M, Mizukoshi E, Zen Y, Takeshita Y, et al. Histological course of nonalcoholic fatty liver disease in Japanese patients: Tight glycemic control, rather than weight reduction, ameliorates liver fibrosis. *Diabetes Care.* (2010) 33:284–6. doi: 10.2337/dc09-0148
23. Wong VW-S, Wong GL-H, Choi PC-L, Chan AW-H, Li MK-P, Chan H-Y, et al. Disease progression of non-alcoholic fatty liver disease: a prospective study with paired liver biopsies at 3 years. *Gut.* (2010) 59:969–74. doi: 10.1136/gut.2009.205088
24. Guirguis E, Grace Y, Bolson A, DellaVecchia MJ, Ruble M. Emerging therapies for the treatment of nonalcoholic steatohepatitis: a systematic review. *Pharmacotherapy.* (2021) 41:315–28. doi: 10.1002/phar.2489
25. Alkhouri N, Poordad F, Lawitz E. Management of nonalcoholic fatty liver disease: lessons learned from type 2 diabetes. *Hepatol Commun.* (2018) 2:778–85. doi: 10.1002/hep4.1195
26. Tlhaloganyang BP, Sakia RM. Zero inflated Poisson distribution in equidispersed data with excessive zeros. *Res J Math Stat Sci.* (2020) 8:31–4.
27. Vatcheva KP, Lee M, McCormick JB, Rahbar MH. Multicollinearity in regression analyses conducted in epidemiologic studies. *Epidemiology.* (2016) 6:227. doi: 10.4172/2161-1165.1000227
28. Akram M, Amin M, Lukman A, Afzal S. Principal component ridge type estimator for the inverse Gaussian regression model. *J Stat Comput Simul.* (2022) 1–30. doi: 10.1080/00949655.2021.2020274
29. Liu K. Using liu-type estimator to combat collinearity. *Commun Stat Theory Methods.* (2003) 32:1009–20. doi: 10.1081/STA-120019959
30. Kibria BMG, Lukman AF. A new ridge-type estimator for the linear regression model: simulations and applications. *Scientifica.* (2020) 2020:e9758378. doi: 10.1155/2020/9758378
31. Lukman AF, Ayinde K, Binuomote S, Clement OA. Modified ridge-type estimator to combat multicollinearity: application to chemical data. *J Chemom.* (2019) 33:e3125. doi: 10.1002/cem.3125
32. Månsson K, Shukur G. A Poisson ridge regression estimator. *Econ Model.* (2011) 28:1475–81.
33. Månsson K, Kibria BMG, Sjölander P, Shukur G. Improved liu estimators for the poisson regression model. *Int J Stat Prob.* (2012) 1:2–6. doi: 10.5539/ijsp.v1n1p2
34. Lukman AF, Adewuyi E, Månsson K, Kibria BMG. A new estimator for the multicollinear Poisson regression model: simulation and application. *Sci Rep.* (2021) 11:3732. doi: 10.1038/s41598-021-82582-w
35. Lukman AF, Aladeitan B, Ayinde K, Abonazel MR. Modified ridge-type for the Poisson regression model: simulation and application. *J Appl Stat.* (2021) 1–13. doi: 10.1080/02664763.2021.1889998
36. Qasim M, Kibria BMG, Månsson K, Sjölander P. A new Poisson Liu Regression Estimator: method and application. *J Appl Stat.* (2020) 47:2258–71. doi: 10.1080/02664763.2019.1707485
37. Petitclerc L, Sebastiani G, Gilbert G, Cloutier G, Tang A. Liver fibrosis: review of current imaging and MRI quantification techniques. *J Magn Reson Imaging.* (2017) 45:1276–95. doi: 10.1002/jmri.25550
38. Musso G, Gambino R, Cassader M, Pagano G. Meta-analysis: Natural history of non-alcoholic fatty liver disease (NAFLD) and diagnostic accuracy

of non-invasive tests for liver disease severity. *Ann Med.* (2011) 43:617–49. doi: 10.3109/07853890.2010.518623

39. Schawkat K, Ciritsis A, von Ulmenstein S, Honcharova-Biletska H, Jüngst C, Weber A, et al. Diagnostic accuracy of texture analysis and machine learning for quantification of liver fibrosis in MRI: correlation with MR elastography and histopathology. *Eur Radiol.* (2020) 30:4675–85. doi: 10.1007/s00330-020-06831-8
40. Geenens G. Copula modeling for discrete random vectors. *Depend Model.* (2020) 8:417–40. doi: 10.1515/demo-2020-0022

Conflict of Interest: The author declares that the research was conducted in the absence of any commercial or financial relationships that could be construed as a potential conflict of interest.

frontiers | Frontiers in Applied Mathematics and Statistics

ORIGINAL RESEARCH
published: 13 July 2022
doi: 10.3389/fams.2022.921170

Convergence Analysis and Approximate Optimal Temporal Step Sizes for Some Finite Difference Methods Discretising Fisher's Equation

Koffi Messan Agbavon[1], *Appanah Rao Appadu*[2]*, *Bilge Inan*[3] and *Herve Michel Tenkam*[1]

[1] Department of Mathematics and Applied Mathematics, North-West University Potchefstroom Campus, Potchefstroom, South Africa, [2] Department of Mathematics and Applied Mathematics, Nelson Mandela University, Gqeberha, South Africa, [3] Department of Basic Sciences of Engineering, Faculty of Engineering and Natural Sciences, İskenderun Technical University, Hatay, Turkey

OPEN ACCESS

Edited by:
Raluca Eftimie,
University of Franche-Comté, France

Reviewed by:
Soheil Salahshour,
Bahcesehir University, Turkey
Oluwaseun F. Egbelowo,
University of Texas at Austin,
United States

***Correspondence:**
Appanah Rao Appadu
rao.appadu@mandela.ac.za

Specialty section:
This article was submitted to Mathematical Biology, a section of the journal Frontiers in Applied Mathematics and Statistics

Received: 15 April 2022
Accepted: 09 June 2022
Published: 13 July 2022

Citation:
Agbavon KM, Appadu AR, Inan B and Tenkam HM (2022) Convergence Analysis and Approximate Optimal Temporal Step Sizes for Some Finite Difference Methods Discretising Fisher's Equation. Front. Appl. Math. Stat. 8:921170. doi: 10.3389/fams.2022.921170

In this study, we obtain a numerical solution for Fisher's equation using a numerical experiment with three different cases. The three cases correspond to different coefficients for the reaction term. We use three numerical methods namely; Forward-Time Central Space (FTCS) scheme, a Nonstandard Finite Difference (NSFD) scheme, and the Explicit Exponential Finite Difference (EEFD) scheme. We first study the properties of the schemes such as positivity, boundedness, and stability and obtain convergence estimates. We then obtain values of L_1 and L_∞ errors in order to obtain an estimate of the optimal time step size at a given value of spatial step size. We determine if the optimal time step size is influenced by the choice of the numerical methods or the coefficient of reaction term used. Finally, we compute the rate of convergence in time using L_1 and L_∞ errors for all three methods for the three cases.

Keywords: Fisher's equation, FTCS, NSFD, EEFD, optimal, convergence estimate, rate of convergence, coefficient of reaction

1. INTRODUCTION

The most enthralling recent progress of nonlinear science in particular mathematical science of partial differential equations, theoretical physics, chemistry, and engineering sciences has been a growth of strategy or procedure to try to find exact solutions for nonlinear differential equations. This is substantial due to the fact that countless mathematical models are described by nonlinear differential equations. To mention few among others the inverse scattering transform [1], the singular manifold method [2], the transformation method [3], the tanh-function method [4], and the Weierstrass function method [5] are subservient in many applications and known as stunning techniques to look for solutions of exactly solvable nonlinear partial differential equations.

In Kudryashov [6] developed a new numerical method for the solution of nonlinear partial differential equations. Amajor novelty of that technique is the utilization of finite Fourier series for the numerical approximation of the spatial derivative terms of the equations. It was proved that the precision of this method

is that the order of accuracy is greater than that found by approximating the spatial derivative terms by finite-difference methods [6]. The numerical performance of this method, which was called the Accurate Space Derivatives (ASD) approach, can be run accurately by the utilization of the Fast Fourier Transform (FFT) algorithm [7]. In Kudryashov [6], the ASD approach was used to obtain the solution of nonlinear hyperbolic equations depicting convective fluid flows. Furthermore, the ASD approach was used in Gazdag and Canosa [8] to solve Fisher's equation, a nonlinear diffusion equation portraying the rate of advance of a new advantageous gene within a population of constant density inhabiting a one dimensional habitat [9]. An outstanding and compendious debate of Fisher's equation in the framework of the genetic problem can be found in Moran [10] and Kendall [11].
Kolmogorov [12] used the traveling waves with wave speed c to solve the problem. They showed that by assuming that when the initial condition belongs to the interval $[0, 1]$, the speed of propagation c of the waves is superior to two and the solution is in the form $u(x, t) = w(\xi)$ where $\xi = x - ct$. They further demonstrated that there are no solutions for $c \in [0, 1)$.
Fisher's equation has a limitless number of traveling wave solutions and each wave propagates at a characteristic speed, $c > 2$. This result appears to point out that the velocity of gene advance is undefined. Gazdag and Canosa [8] studied the problem of the indeterminacy of the diffusion speed of Fisher's equation which has not been plainly investigated in Kolmogorov [12]. Furthermore, a modification was made by Fisher [9] to his original model, he demonstrated that the rate of gene advance became the minimum one when $c = 2$. Kendall [11] investigated a linear model portraying a population that undergoes a Brownian motion and spreads geometrically at the same time. Canosa [13] demonstrated that all waves are stable against local perturbations but are linearly unstable against general perturbations of limitless magnitude. It is worthy to emphasize that the traveling wave profiles of Fisher's equation are similar to some of the steady-state solutions of the Korteweg-de Vries-Burgers equation which is a third-order nonlinear partial differential equation integrating diffusive and dispersive effects which have been found useful to represent blood flow through an artery, shallow water waves and plasma shocks disseminating perpendicularly to a magnetic field [13, 14].

Kudryashov [6] showed that a simple stability analysis enables us to see the estimation which is unstable against the roundoff errors growing up at the right tail of the waves. This is due to the physical nature of the problem depicted by the equation, not to the numerical method utilized and moreover entailed an exponential growth of the solution when roundoff errors are exponentially small. This simple issue makes it hard to do a strict simulation of the solutions of Fisher's equation. Kudryashov [6] went on with the removal of the forward tail of the wave of advance. This removal is necessary for the numerical stability of the Accurate Space Derivatives (ASD) approach and is physically conclusive because it is approximately equivalent to assuming that the role of long-distance dissipation in the spread of the gene is insignificant and probably effective for some species but not for others. Other numerical computations present how fast the asymptotic minimum speed wave is reached from an initial step function and confirm the local stability analysis of Kudryashov [6] which unveils that local perturbations are flattened very rapidly, even from superspeed waves. Another amazing result of the estimation is obtained for an initial dispensation localized in space which further gives rise to two identical waves of minimum speed evolution cases, one disseminating to the right and the other to the left.

1.1. Some Generalized and Conserved Fisher's Equation

Fisher's equation can be represented as generalized or conserved forms. Fisher's equation is the elementary model of spatial dynamics, in which competitive interactions between individuals happen locally. In Kudryashov and Zakharchenko [15], the generalized form is written as

$$u_t = u_x(u^l\, u_x) + u^a\,(1 - u^b) \tag{1}$$

where t stands for time, x stands for spatial coordinate, u is a population density, and a, b, and l are all positive parameters.
Fisher's equation can also forecast circumstances where population regulation happens globally due to the existence of a secondary agent (the controller agent is itself dispersed over a scale significantly greater than the dispersal distance of the individuals themselves). It is, thus, of notice to envisage a simple model of spatial population dynamics in which the total population size is controlled *via* a nonlocal mechanism. In that case in Newman et al. [16], the conserved equation is written as

$$u_t = D\,\nabla^2\, u + r(t)\, u(t) - K(t)\, u(t)^2 \tag{2}$$

where D stands for the mobility of the individuals, r stands for the reproduction rate in the absence of competition. K is a parameter representing the carrying capacity of the system and regulating the population density through competition. The auxiliary equation related to Equation (2) is

$$r(t) = K(t) \int d^d\, x\, u(x, t) \tag{3}$$

It is worth mentioning that Fisher's equation belongs to the class of partial differential equations called Reaction-Diffusion equations. This class of equations has broad applications in science and engineering for instance transport of air, adsorption of pollutants in soil, food processing, and modeling of biological and ecological systems [17, 18]. Several reaction-diffusion equations involve traveling waves fronts yielding a fundamental role in the understanding of physical, chemical, and biological phenomena [19]. Reaction-diffusion systems clarify how the condensation of one or more substances diffused in space varies by the impact of two operations: first, it is local chemical reactions in which the substances are modified into each other, and second, it is the diffusion that sustains the substances to smear over a surface in space [20]. Reaction-diffusion systems are regularly used in chemistry. Nonetheless, the system can also portray the dynamical processes of non-chemical nature. Reaction-diffusion systems have mathematically the form of semi-linear parabolic

partial differential equations. They are often written in the form of

$$u_t = D\,\nabla^2 u + R(u), \tag{4}$$

where each component of vector $u(x,t)$ stands for the concentration of one substance, x is the space variable, and t is the time. D is the diffusion coefficient and R represents the reaction term. The solution of reaction-diffusion equations shows an ample scale of behaviors, enclosing the formation of traveling waves. These waves are like phenomena and self-organized patterns which are e.g., stripes, hexagons, or more complicated fabrics such as dissipative solutions [20]. Reaction-diffusion equations are also grouped as one component, two components, or more component diffusion equations counting upon the component involved in the reaction. The basic reaction-diffusion equation regarding the concentration u of a mere substance in one spatial dimension is

$$u_t = D\,u_{xx} + R(u). \tag{5}$$

If the reaction $R(u)$ term goes away, then the equation gives a pure diffusion process and if the thermal diffusivity term appears instead of diffusion term D then the equation will turn into a parabolic partial differential equation in one dimensional space [20]. The choice $R(u) = u\,(1-u)$ yields Fisher's equation. Those reaction-diffusion equations arise also in flame propagation, the branching Brownian motion process, and nuclear reactor theory [20]. Many methods such as Adomian Decomposition [21], Variational Iteration [22], Factorization [23], Nonstandard Finite Difference, and Exponential Finite Difference methods [24, 25] are used to solve Fisher's equation.

Anguelov et al. [26] investigated the same Fisher's equation by the means of a periodic initial data with θ-non standard approach and found that the Nonstandard Finite Difference approach is elementary stable in the limit case of space independent variable, stable in regard to the boundedness and positivity property. Finally also stable in regard to the conservation of energy in the stationary case.

Let us consider simple Fisher's equation given by

$$u_t = u_{xx} + R(u), \tag{6}$$

where $R(u) = u(1-u)$ and $x \in \mathbb{R}$, t positive. The boundary and initial conditions are as follows

$$\lim_{x\to+|\epsilon|\infty} u(x,t) = \begin{cases} 1 & \text{if} \quad \epsilon = 1 \\ \\ 0 & \text{if} \quad \epsilon = -1, \end{cases} \tag{7}$$

$$u(x,0) = u_0(x). \tag{8}$$

Hagstrom and Keller [27] revealed that when a positive function is taken as an initial condition satisfying

$$u_0(x) \sim \exp(-\alpha) \quad \text{when} \quad x \to \infty, \tag{9}$$

then the solution u develops a traveling wave speed in function of α which is

$$c(\alpha) = \begin{cases} \alpha + \frac{1}{\alpha}, & \alpha \le 1, \\ 2, & \alpha \ge 1. \end{cases} \tag{10}$$

2. ORGANIZATION OF THE ARTICLE

The organization of this article is as follows. In Section 3, we present the general form of the exact solution of Fisher's equation and in Section 4, we describe the numerical experiment [28]. In Section 5, we make use of Forward in Time Central Space (FTCS) in order to discretize Fisher's equation, study the stability and consistency and we also obtain error estimates. Sections 6, 7 discuss stability, consistency, and error estimates for NSFD and EEFD schemes. In Section 8, we conclude by presenting the important highlights of this article. The computations are performed by making use of MATLAB R2014a software on an intel core2 as CPU.

3. EXACT SOLUTION

In this section, we present the exact solution of generalized Fisher's equations as described in Kudryashov and Zakharchenko [15]. The nonlinear evolutional equation of that generalized Fisher's equation gives one dimensional diffusion models (for insect, animal dispersal, and invasion) as

$$u_t = u_x(u^l\,u_x) + u^a\,(1-u^b), \tag{11}$$

where t stands for time, x stands for spatial coordinate, u is population density, and a, b, and l are positive parameters. The first term, $u_x(u^l\,u_x)$ on the right-hand side of Equation (11) stands for the growth of population. The term u^l represents the diffusion process depending on the population density.

Let us consider $l \neq 0$ and $u(x,t) = v(\xi)$ and $\xi = s\,x - ct$, $s \neq 0$. Equation (11) gives the following nonlinear ordinary differential equation

$$s^2\frac{d}{d\xi}\left(v^l\,\frac{dv}{d\xi}\right) + v^a - v^{a+b} + c\,\frac{dv}{d\xi} = 0. \tag{12}$$

For $l \neq 0$, $v^l = w$. Replacing v by $w^{\frac{1}{l}}$ in Equation (12) gives

$$\frac{s^2}{l}w_\xi^2 + s^2\,w\,w_{\xi\xi} - l\,w^{\frac{a+b+l-1}{l}} + w^{\frac{a+l-1}{l}} + \xi\,w_\xi = 0. \tag{13}$$

Using the Q function method as it is in Kudryashov [29], one has

$$w(\xi) = \sum_{j=0}^{P} P_j\,Q^j(\xi), \quad Q(\xi) = \frac{1}{1+e^{\xi-\xi_0}} \tag{14}$$

where P stands for the pole order and ξ_0 stands as an arbitrary constant. $Q(\xi)$ is the solution of

$$Q_\xi = Q - Q^2. \tag{15}$$

Using Equation (15), we obtain w_ξ and $w_{\xi\xi}$ by using polynomials of Q. Replacing $w \simeq Q^P$ into Equation (15), we have for $b \geq 0$, the following equality

$$\frac{a+b+l-1}{l} = 2 + \frac{2}{P}. \tag{16}$$

To have an integer value $\frac{a+b+l-1}{l}$, P should be 1 or 2. In that case

$$w(\xi) = \begin{cases} P_0 + P_1\, Q(\xi) \\ P_0 + P_1\, Q(\xi) + P_2\, Q^2(\xi) \end{cases} \tag{17}$$

For $P = 1$, $a = 3\,l + 1 - b$, Equation (13) becomes

$$\frac{s^2}{l}\, w_\xi^2 + s^2\, w\, w_{\xi\xi} - l\, w^4 + w^{4-\frac{b}{l}} + \xi\, w_\xi = 0. \tag{18}$$

We have the following solutions

$$w(x,t) = \begin{cases} \text{No exact solutions,} \quad b = l \text{ and } b = 3\,l, \\ \pm 1 \pm 2\, Q(\pm \frac{2\,l}{\sqrt{2l+1}}\, x \pm \frac{2\,l}{2l+1}\, t), \quad b = 2\,l, \\ \pm 1 \pm 2\, Q(\pm \frac{2\,l}{\sqrt{2l+1}}\, x \pm \frac{4l\,(l+1)}{2l+1}\, t), \quad b = 4\,l, \\ \quad \text{or} \\ \pm i \pm 2\, i\, Q(\pm \frac{2\,l}{\sqrt{2l+1}}\, x \pm \frac{4l\,(l+1)}{2l+1} i\ t), \ b = 4\,l. \end{cases} \tag{19}$$

We finally get as exact solution

$$u(x,t) = \begin{cases} \sqrt[l]{\pm 1 \pm 2\, Q\left(\pm \frac{2\,l}{\sqrt{2l+1}}\, x \pm \frac{2\,l}{2l+1}\, t\right)}, \quad V_1 = \pm \frac{1}{\sqrt{2l+1}}, \\ \sqrt[l]{\pm 1 \pm 2\, Q\left(\pm \frac{2\,l}{\sqrt{2l+1}}\, x \pm \frac{4l\,(l+1)}{2l+1}\, t\right)}, \quad V_2 = \pm \frac{2\,(l+1)}{\sqrt{2\,l+1}}, \\ \quad \text{or} \\ \sqrt[l]{\pm i \pm 2\, i\, Q\left(\pm \frac{2\,l}{\sqrt{2l+1}}\, x \pm \frac{4l\,(l+1)}{2l+1} i\ t\right)}, \quad V_2 = \pm \frac{2\,(l+1)}{\sqrt{2l+1}}, \end{cases} \tag{20}$$

where V_1 and V_2 stand for velocity.

For $P = 2$, $a = 2\,l + 1 - b$. With the same reasoning as above, we have

$$u(x,t) = \begin{cases} \text{No exact solutions,} \quad b = 2\,l \text{ and } b = 3\,l, \\ \sqrt[l]{\frac{2(3\,l+2)}{l+1}\left(Q\left(\pm \frac{l}{\sqrt{l+1}} i\, x\right) - Q^2\left(\pm \frac{l}{\sqrt{l+1}} i\, x\right)\right)}, \ b = l. \end{cases} \tag{21}$$

The case of $l = 0$, $a = 1$ and $b = 2$, one obtains the Burgers-Huxley equation and the case of $l = 0$, $a = 1$, $b = 1$, we have Fisher's equation. The exact solution of Equation (11) is described in Li et al. [28] as a scaled Fisher's equation in the form

$$u_t = u_{xx} + \rho u(1-u), \tag{22}$$

with $x \in \mathbb{R}$, t positive, and ρ is a positive constant. The Equations (7) and (8) stand for boundary and initial conditions, respectively. The traveling exact solution to this problem as presented in Polyanim and Zaitsev [30] is

$$u(x,t) = \left[1 + c\, \exp\left(\sqrt{\frac{\rho}{6}} x - \frac{5\rho}{6} t\right)\right]^{-2}, \tag{23}$$

where $c = 5\sqrt{\rho/6}$ stands for the wave speed with the minimum value, $2\sqrt{\rho}$.

4. NUMERICAL EXPERIMENTS

We consider the following problem from Qiu and Sloan [31].

Solve

$$u_t = u_{xx} + \rho\, u(1-u),$$

for $x \in [-0.2, 0.8]$ and $t \in [0,\ T_{max}]$ where $T_{max} = 2.5 \times 10^{-3}$. The initial data is given by

$$u(x,0) = \left[1 + \exp\left(\sqrt{\frac{\rho}{6}} x\right)\right]^{-2}. \tag{24}$$

The exact solution is given by

$$u(x,t) = \left[1 + \exp\left(\sqrt{\frac{\rho}{6}} x - \frac{5\rho}{6} t\right)\right]^{-2}. \tag{25}$$

The boundary conditions are as follows

$$u(-0.2,t) = \left[1 + \exp\left(-0.2\sqrt{\frac{\rho}{6}} - \frac{5\rho}{6} t\right)\right]^{-2} \text{ and}$$
$$u(0.8,t) = \left[1 + \exp\left(0.8\sqrt{\frac{\rho}{6}} - \frac{5\rho}{6} t\right)\right]^{-2}.$$

We consider three cases ρ namely; 1, 10^2, 10^4, and obtain a solution at time, $t = T_{max}$.

DEFINITION 1. *Miyata and Sakai [32]. For a vector* $\overline{x} \in \mathbb{R}^N$, $\| \overline{x} \|_1 = \sum_{i=1}^N |\overline{x}^i|$ *and* $\| \overline{x} \|_\infty = \max\{|\overline{x}^i|,\ i = 1, \cdots, N\}$.

DEFINITION 2. *Sutton [33]. Suppose* $\{t^n\}_0^N$ *forms a partition of* $[0, T]$, *with* $t_n = n\Delta t$ *for* $n = 0, \cdots, N$, *where* $\Delta t = T/N$. *Suppose a vector* $\overline{x} \in \mathbb{R}^N$, *defined by*

$$\| \overline{x} \|_{L^P(0,t^n)} = \begin{cases} \left(\| \overline{x} \|_{L^P(0,t^{n-1})} + \tau(\overline{x}^n)^p\right)^{\frac{1}{p}} \ \text{for } p \in [0,\infty), \\ \max\{\| \overline{x} \|_{L^P(0,t^{n-1})}, \overline{x}^n\} \quad \text{for } p = \infty. \end{cases} \tag{26}$$

The rate of convergence with respect to time is defined by

$$rate_i(t) = \frac{\log(\overline{x}^i(t)) - \log(\overline{x}^{i-1}(t))}{\log(\Delta t^i) - \log(\Delta t^{i-1})}.$$

5. FORWARD IN TIME CENTRAL SPACE

The discretization of Equation (22) using the FTCS method gives [34].

$$\frac{u_m^{n+1}-u_m^n}{k}=\frac{u_{m+1}^n-2u_m^n+u_{m-1}^n}{h^2}+\rho u_m^n(1-u_m^n), \quad (27)$$

which leads to

$$u_m^{n+1}=(1-2R)u_m^n+k\rho u_m^n(1-u_m^n)+R(u_{m+1}^n+u_{m-1}^n), \quad (28)$$

or

$$u_m^{n+1}=(1-2R+k\ \rho)\,u_m^n-k\,\rho\,(u_m^n)^2+R\,u_{m+1}^n+R\,u_{m-1}^n, \quad (29)$$

where $R=\frac{k}{h^2}$.

5.1. Stability

The investigation regarding the stability of the scheme given by Equation (28) was done in Agbavon et al. [35]. Nevertheless, we highlight briefly some points. The stability of finite difference methods discretizing nonlinear partial differential equations is not straightforward. Subsequently, freezing the coefficients is needed before using Von Neumann stability analysis [36].

THEOREM 1. *Agbavon et al. [35]. The FTCS scheme given by Equation (28) is conditionally stable, and the stability region is*

$$k\leq\frac{h^2}{2} \quad (30)$$

for given spatial step size $h>0$ and the time step size $k>0$. FTCS is first order and second order accurate in time and space, respectively.

Proof. The stability region of the Zabusky and Kruskal scheme using the Korteweg de Vries (KdV) equation was found by Taha and Ablowitz [37] by using the freezing coefficients method and Von Neumann Stability Analysis. The derived scheme by Zabusky and Kruskal [38] for the KdV equation, $u_t+6uu_x+u_{xxx}=0$ is

$$\frac{u_m^{n+1}-u_m^{n-1}}{2k}+6\left(\frac{u_{m+1}^n+u_m^n+u_{m-1}^n}{3}\right)\left(\frac{u_{m+1}^n-u_{m-1}^n}{2h}\right)+\frac{1}{2h^3}\left(u_{m+2}^n-2u_{m+1}^n+2u_{m-1}^n-u_{m-2}^n\right)=0. \quad (31)$$

Taha and Ablowitz [37] express $u\,u_x$ as $u_{max}\,u_x$ and utilize the ansatz
$u_m^n=\xi^n e^{Imw}$ where w stands for the phase angle. They obtain

$$\left(\xi-\xi^{-1}\right)(2k)^{-1}+(h)^{-1}(6u_{max})\mathrm{I}\sin(w)+(2h^3)^{-1}(e^{2Iw}-2e^{Iw}+2e^{-Iw}-e^{-2Iw})=0,$$

which can be rewritten as

$$\xi=\xi^{-1}-(h)^{-1}(12ku_{max})\mathrm{I}\sin(w)-(h^3)^{-1}k(e^{2Iw}-2e^{Iw}+2e^{-Iw}-e^{-2Iw}) \quad (32)$$

where $u_{max}=\max|u(x,t)|$. The requirement for the linear stability is

$$(h)^{-1}k\left|2u_{max}-(h^2)^{-1}\right|\leq 2(3\sqrt{3})^{-1}. \quad (33)$$

For obtaining the stability region of the FTCS scheme discretizing Equation (28), we rewrite Equation (28) using the same idea as

$$u_m^{n+1}=\left(1-(h^2)^{-1}2k\right)u_m^n+(h^2)^{-1}(k)(u_{m+1}^n+u_{m-1}^n)+k\,\rho\,u_m^n-k\,\rho\,(u_m^n)^2. \quad (34)$$

Utilization of Fourier series analysis on Equation (34), gives the amplification factor

$$\xi=1-(h^2)^{-1}(2k)(1-\cos(w))+k\rho(1-u_{max}), \quad (35)$$

where u_{max} is frozen coefficient. For the numerical experiment considered, we have $u_{max}=1$, and therefore,

$$\xi=1-(h^2)^{-1}(4k)\sin^2\left(\frac{w}{2}\right). \quad (36)$$

The stability is obtained by solving $|\xi|\leq 1$ for $w\in[-\pi,\pi]$, and we obtain $k\leq\frac{h^2}{2}$.
Using Taylor series expansion about the point (n,m) of Equation (28), we get

$$\begin{aligned}&u+ku_t+\frac{k^2}{2}u_{tt}+\frac{k^3}{6}u_{ttt}+O(k^4)\\&=\left(1-(h^2)^{-1}(2k)+k\rho\right)u-k\rho u^2\\&+(h^2)^{-1}(k)\left(u+hu_x+\frac{h^2}{2}u_{xx}+\frac{h^3}{6}u_{xxx}+\frac{h^4}{24}u_{xxxx}+O(h^5)\right)\\&+(h^2)^{-1}(k)\left(u-hu_x+\frac{h^2}{2}u_{xx}-\frac{h^3}{6}u_{xxx}+\frac{h^4}{24}u_{xxxx}+O(h^5)\right),\end{aligned} \quad (37)$$

which can be written as

$$u_t-u_{xx}-\rho u(1-u)=-\frac{k}{2}u_{tt}-\frac{k^2}{6}u_{ttt}+\frac{h^2}{12}u_{xxxx}+O(k^4)+O(h^5). \quad (38)$$

Hence, FTCS is first order and second order accurate in time and space, respectively.

5.2. Error Estimates

THEOREM 2. *Let $u\in C^{4,2}(Q)$, Q defined by $Q=\{(x,t)/\ a\leq x\leq b,\ 0<t\leq T,\ a,b\in\mathbb{R}\}$. If spatial step size, h and time*

step size, k are such that the stability condition (30) holds, then the error estimate, E_m^n for Equation (28) is given by

$$E_m^n \leq (1+3\,k\,\rho)^n\,E_m^0 + \frac{1}{9}\frac{M\,h^2}{\rho\,k}\left[(1+3\,k\,\rho)^n - 1\right] \tag{39}$$

where $M = \max_{\{(x,t)\}\in Q}\left\{|u_{xxxx}(x,t)|,\ |u_{tt}(x,t)|\right\}$ *and* Θ *such that* $\Theta(k,h)u_{ttt} = O(k,h) \to 0$, *for* $k,\ h \to 0$.

Proof.
Forward in Time Central Space scheme is given by

$$u_m^{n+1} = (1-2R+k\ \rho)\,u_m^n - k\,\rho\,(u_m^n)^2 + R\,u_{m+1}^n + R\,u_{m-1}^n. \tag{40}$$

Taylor series expansion about $(n,\ m)$ gives

$$\begin{aligned}
&7v + kv_t + \frac{k^2}{2}v_{tt} + \frac{k^3}{6}v_{ttt} + O(k^4)\\
&= \left(1-(h^2)^{-1}(2k)+k\rho\right)v - k\rho v^2\\
&+(h^2)^{-1}(k)\left(v + hv_x + \frac{h^2}{2}v_{xx} + \frac{h^3}{6}v_{xxx} + \frac{h^4}{24}v_{xxxx} + O(h^5)\right)\\
&+(h^2)^{-1}(k)\left(v - h\,v_x + \frac{h^2}{2}v_{xx} - \frac{h^3}{6}v_{xxx} + \frac{h^4}{24}v_{xxxx} + O(h^5)\right),
\end{aligned} \tag{41}$$

which can be rewritten as

$$v_t - v_{xx} - \rho\,v\,(1-v) = -\frac{k}{2}v_{tt} - \frac{k^2}{6}v_{ttt} + \frac{h^2}{12}v_{xxxx} + ..., \tag{42}$$

and let $\Theta(k,h)v_{ttt} = O(k,h) = -\frac{k^2}{6}v_{ttt} \to 0$ for $k,\ h \to 0$. The exact discrete equation is

$$\begin{aligned}
&u_m^{n+1} = (1-2R)\,u_m^n + k\rho\,u_m^n(1-u_m^n) + R(u_{m+1}^n + u_{m-1}^n)\\
&+\frac{k}{2}u_{tt}(x,\tau_n) - \frac{h^2}{12}u_{xxxx}(X_m,t)
\end{aligned} \tag{43}$$

where $x_m < X_m < x_{m+1}$ and $t_n < \tau_n < t_{n+1}$. We define

$$e_m^n = u_m^n - v_m^n \implies e_m^{n+1} = u_m^{n+1} - v_m^{n+1}.$$

It follows that

$$\begin{aligned}
&e_m^{n+1} = (1-2R)\,(u_m^n - v_m^n) + k\,\rho\,u_m^n(1-u_m^n)\\
&-k\,\rho\,v_m^n(1-v_m^n) + R\,(u_{m+1}^n + u_{m-1}^n)\\
&-R\,(v_{m+1}^n + v_{m-1}^n) + \frac{k}{2}u_{tt}(x,\tau_n) - \frac{h^2}{12}u_{xxxx}(X_m,t).
\end{aligned} \tag{44}$$

We have

$$\begin{aligned}
&e_m^{n+1} = (1-2R)\,(u_m^n - v_m^n) + k\,\rho\,u_m^n - k\,\rho\,(u_m^n)^2 - k\,\rho\,v_m^n\\
&+k\,\rho\,(v_m^n)^2 + R\,(u_{m+1}^n - v_{m+1}^n)\\
&-R\,(u_{m-1}^n - v_{m-1}^n) + \frac{k}{2}u_{tt}(x,\tau_n) - \frac{h^2}{12}u_{xxxx}(X_m,t),
\end{aligned} \tag{45}$$

which can be rewritten as

$$\begin{aligned}
&e_m^{n+1} = (1-2R)\,(u_m^n - v_m^n) + k\,\rho\,(u_m^n - v_m^n)\\
&-k\,\rho\,(u_m^n - v_m^n)(u_m^n + v_m^n) + R\,(u_{m+1}^n - v_{m+1}^n)\\
&-R\,(u_{m-1}^n - v_{m-1}^n) + \frac{k}{2}u_{tt}(x,\tau_n) - \frac{h^2}{12}u_{xxxx}(X_m,t).
\end{aligned} \tag{46}$$

Using the properties of absolute values $|a+b| \leq |a| + |b|$ for $a,\ b \in \mathbb{R}$, we have

$$\begin{aligned}
&|e_m^{n+1}| \leq |1-2R|\,|e_m^n| + |k\,\rho|\,|e_m^n| + |k\,\rho|\,|e_m^n||u_m^n + v_m^n|\\
&+R\,|e_{m+1}^n|\\
&+R\,|e_{m-1}^n| + M\left(\frac{k}{2} + \frac{h^2}{12}\right),
\end{aligned} \tag{47}$$

where $M = \max_{\{(x,t)\in Q\}}\left\{|u_{xxxx}(x,t)|,\ |u_{tt}(x,t)|\right\}$. Since $0 \leq u_m^n \leq 1$ and $0 \leq v_m^n \leq 1$, based on numerical experiment chosen, we have

$$\begin{aligned}
&|e_m^{n+1}| \leq |1-2R|\,|e_m^n|\\
&+k\,\rho\,|e_m^n| + 2\,k\,\rho\,|e_m^n| + R\,|e_{m+1}^n|\\
&+R\,|e_{m-1}^n| + M\left(\frac{k}{2} + \frac{h^2}{12}\right).
\end{aligned} \tag{48}$$

Let $E_m^n = \max_{0<m<N}\left\{|e_m^n|)|\right\}$. We have

$$\begin{aligned}
&|e_m^{n+1}| \leq (|1-2R| + k\,\rho + 2\,k\,\rho + 2R)\,|E_m^n|\\
&+M\left(\frac{k}{2} + \frac{h^2}{12}\right),
\end{aligned} \tag{49}$$

and for stability $R \leq 1/2$, therefore, $|1-2\,R| = 1-2\,R \geq 0$. We finally obtain

$$\begin{aligned}
|e_m^{n+1}| &\leq (1+3\,k\,\rho)\,E_m^n\\
&+ M\left(\frac{k}{2} + \frac{h^2}{12}\right).
\end{aligned} \tag{50}$$

Let $E_m^{n+1} = (1+3\,k\,\rho)\,E_m^n + \left(\frac{k}{2} + \frac{h^2}{12}\right)M$. We have

For $n=0$, $E_m^1 = (1+3\,k\,\rho)\,E_m^0 + \left(\frac{k}{2} + \frac{h^2}{12}\right)M$.
For $n=1$, we have

$$E_m^2 = (1+3\,k\,\rho)\,E_m^1 + \left(\frac{k}{2} + \frac{h^2}{12}\right)M \tag{51}$$

$$\begin{aligned}
&= (1+3\,k\,\rho)^2\,E_m^0 + (1+3\,k\,\rho)^1\left(\frac{k}{2}\right.\\
&\left.+\ \frac{h^2}{12}\right)M + (1+3\,k\,\rho)^0\left(\frac{k}{2} + \frac{h^2}{12}\right)M
\end{aligned} \tag{52}$$

$$\begin{aligned}
&= (1+3\,k\,\rho)^2\,E_m^0 + \left[(1+3\,k\,\rho)^1\right.\\
&\left.+(1+3\,k\,\rho)^0\ \right]\left(\frac{k}{2} + \frac{h^2}{12}\right)M
\end{aligned} \tag{53}$$

For $n = 2$, we have

$$E_m^3 = (1 + 3\,k\,\rho)^3\,E_m^2 + \left(\frac{k}{2} + \frac{h^2}{12}\right) M \tag{54}$$

$$= (1 + 3\,k\,\rho)^3\,E_m^0 + (1 + 3\,k\,\rho)^2\,(\,\frac{k}{2} + \frac{h^2}{12}\right) M + (1 + 3\,k\,\rho)^1 \left(\frac{k}{2} + \frac{h^2}{12}\right) M + (1 + 3\,k\,\rho)^0 \left(\frac{k}{2} + \frac{h^2}{12}\right) M \tag{55}$$

$$= (1 + 3\,k\,\rho)^3\,E_m^0 + [\,(1 + 3\,k\,\rho)^2 + (1 + 3\,k\,\rho)^1 + (1 + 3\,k\,\rho)^0\,]\left(\frac{k}{2} + \frac{h^2}{12}\right) M \tag{56}$$

For n, we have

$$E_m^n = (1 + 3\,k\,\rho)\,E_m^{n-1} + \left(\frac{k}{2} + \frac{h^2}{12}\right) M$$
$$= (1 + 3\,k\,\rho)^n\,E_m^0 + \left[(1 + 3\,k\,\rho)^{n-1} + (1 + 3\,k\,\rho)^{n-2} + \cdots + (1 + 3\,k\,\rho)^1 + (1 + 3\,k\,\rho)^0\,\right]\left(\frac{k}{2} + \frac{h^2}{12}\right) M$$
$$= (1 + 3\,k\,\rho)^n\,E_m^0 + \left[\sum_{i=0}^{n-1}(1 + 3\,k\,\rho)^i\right]\left(\frac{k}{2} + \frac{h^2}{12}\right) M$$
$$= (1 + 3\,k\,\rho)^n\,E_m^0 + \left[\frac{1 - (1 + 3\,k\,\rho)^n}{1 - (1 + 3\,k\,\rho)}\right]\left(\frac{k}{2} + \frac{h^2}{12}\right) M$$
$$= (1 + 3\,k\,\rho)^n\,E_m^0 - \frac{1}{3\,k\,\rho}\left[1 - (1 + 3\,k\,\rho)^n\right]\left(\frac{k}{2} + \frac{h^2}{12}\right) M \tag{57}$$

Hence, for $k \leq \frac{h^2}{2}$, we can also write

$$E_m^n \leq (1 + 3\,k\,\rho)^n\,E_m^0 + \frac{1}{9}\frac{M\,h^2}{\rho\,k}\left[(1 + 3\,k\,\rho)^n - 1\right] \tag{58}$$

6. NONSTANDARD FINITE DIFFERENCE SCHEME (NSFD)

Over the past decade, the NSFD has been used extensively and often abbreviated as NSFD. The method was introduced by Mickens for the approximation of solutions of partial differential equations and is largely based on the concept of dynamical consistency [39] which plays a significant role in the construction of discrete models whose numerical solution can be complicated to compute. The dynamical consistency is bound to a precise property of a physical system (and varies according to the systems). To mention few among others these properties include the preservation of positivity, boundedness, monotonicity of the solutions, and stability of fixed-points [39]. The main advantage of this method was the dismissal of the primary numerical instabilities [40] caused by the use of standard methods. In order to reduce numerical sensitivities appearing using the classical finite difference methods, these NSFD were developed.

For practical use, the construction of NSFD methods is based on the following basic rules [39]:

(1) The order of discrete derivatives should be equal to the order of corresponding derivatives appearing in the differential equation.
(2) Discrete representation for derivatives, in general, have non trivial denominator functions, e.g.,

$$u_t \approx \frac{u_m^{n+1} - u_m^n}{\phi(\Delta t, \lambda)} \tag{59}$$

where

$$\phi(\Delta t, \lambda) = \Delta t + O(\Delta t^2). \tag{60}$$

6.1. Example of the Definition of the Function ϕ

Consider the following decay equation and logistic growth equation, respectively as in Anguelov et al. [26]

$$\begin{cases} u' = \lambda\,u, & u(0) = u_0,\ \lambda \neq 0, \\ u' = \lambda\,u(1 - u), & u(0) = u_0,\ \lambda > 0, \end{cases} \tag{61}$$

and the respective solutions at the time $t = t_{n+1}$ are

$$\begin{cases} u(t_{n+1}) = u_0\,e^{\lambda\,t_{n+1}}, \\ u(t_{n+1}) = \frac{u_0}{e^{-\lambda\,t_{n+1}} + (1 - e^{-\lambda\,t_{n+1}})\,u_0}. \end{cases} \tag{62}$$

Let $u(t_n) = u^n$. We have

$$\begin{cases} \frac{u^{n+1} - u^n}{(e^{\lambda\,\Delta t} - 1)\lambda^{-1}} = \lambda\,u^n, \\ \frac{u^{n+1} - u^n}{(e^{\lambda\,\Delta t} - 1)\lambda^{-1}} = \lambda\,u^n(1 - u^n). \end{cases} \tag{63}$$

The Equation (63) is called the exact scheme. The function ϕ can be then defined as

$$\phi(\Delta t, \lambda) = \frac{e^{\lambda\,\Delta t} - 1}{\lambda} \text{ or } \phi(\Delta t, \lambda) = \frac{1 - e^{-\lambda\,\Delta t}}{\lambda}$$

(3) Nonlocal discrete representations of nonlinear terms. For instance

$$u_m^2 \approx u_m\,u_{m+1},\ , u_m^2 \approx \left(\frac{u_{m-1} + u_m + u_{m-1}}{3}\right) u_m, \tag{64}$$

and

$$u^3 \approx 2u_m^3 - u_m^2 u_{m+1},\ u_m^3 \approx u_{m-1}u_m u_{m+1}. \tag{65}$$

In Agbavon et al. [35], followed by the rule of Mickens [39] a **NSFD**
for Equation (22) is

$$\frac{u_m^{n+1}-u_m^n}{\phi(\Delta t)} = \frac{u_{m+1}^n - 2u_m^n + u_{m-1}^n}{(\Delta x)^2} + \rho u_m^n - \rho\left(\frac{u_{m+1}^n + u_m^n + u_{m-1}^n}{3}\right) u_m^{n+1}, \quad (66)$$

where

$$\phi(\Delta t) = \phi(k) = \frac{1-e^{-\lambda k}}{\lambda};\ (\Delta x)^2 = h^2. \quad (67)$$

The Equation (66) gives the following single expression

$$u_m^{n+1} = \frac{\left(1 - \frac{2\phi(k)}{h^2} + \rho\,\phi(k)\right) u_m^n + \frac{\phi(k)}{h^2}\left(u_{m+1}^n + u_{m-1}^n\right)}{1 + \frac{\rho\phi(k)}{3}\left(u_{m+1}^n + u_m^n + u_{m-1}^n\right)}. \quad (68)$$

6.2. Positivity and Boundedness

In this section, the dynamical consistency and some useful relationship between time and space step-sizes of NSFD are presented.

THEOREM 3. *The dynamical consistency (positivity and boundedness) of NSFD constructed in Equation (68) holds for Equation (22) and for relevant time step k, spatial step h if the following conditions hold*

(a) $\phi(k) \le \frac{h^2}{2-\rho\,h^2}\,[1-\Gamma]$ *with* $\Gamma = 1 - 2\,(h^2)^{-1}\phi(k) + \rho\,\phi(k)$,

(b) For $u_m^i \in [0,1], \forall\ i.\ \Gamma = (h^2)^{-1}(\phi(k)) = \frac{1}{2}\left[\frac{1}{1-\frac{\rho h^2}{2}}\right]$ *and* $\Gamma' = \sigma\,\Gamma$.

Proof.
We assume $u(x,0) = h(x) \in [0,1]$. We have, therefore, $u(x,t) \in [0,1]$ [24]. We assume also $u_m^n \ge 0$. The quantity u_m^{n+1} from Equation (68) is positive ($u_m^{n+1} \ge 0$) if only

$$\Gamma = 1 - 2(h^2)^{-1}\phi(k) + \rho\,\phi(k) \ge 0, \quad (69)$$

It follows that

$$0 \le 1 - \Gamma = (2(h^2)^{-1} - \rho)\phi(k) \le 1. \quad (70)$$

Hence, in Mickens [24], the condition required for positivity is

$$\phi(k) \le \frac{h^2}{2-\rho\,h^2}\,[1-\Gamma] \ \text{ and } \ 0 \le \Gamma < 1,\ \rho\,h^2 \ne 2. \quad (71)$$

We investigate next the boundedness by assuming $u_m^n \in [0,1]$. Equation (68) is rewritten as follows

$$u_m^{n+1} = \frac{\Gamma u_m^n + R\left(u_{m+1}^n + u_{m-1}^n\right)}{1 + \left(\frac{\rho\phi(k)}{3}\right)\left(u_{m+1}^n + u_m^n + u_{m-1}^n\right)}. \quad (72)$$

where $\Gamma = 1 - 2(h^2)^{-1}\phi(k) + \rho\,\phi(k)$, $R = \frac{\phi(k)}{h^2}$.
Following the idea of Mickens [24], Equation (72) takes the symmetric form if $\Gamma = R$. Therefore, it follows that

$$\Gamma = \frac{\phi(k)}{h^2} = \frac{1}{3} + \frac{\rho\,\phi(k)}{3}. \quad (73)$$

We also have from Equation (71)

$$\phi(k) \le \frac{h^2}{2-\rho\,h^2}\,[1-\Gamma] \implies \frac{\phi(k)}{h^2} \le \frac{1}{2}\left[\frac{1}{1-\frac{\rho h^2}{2}}\right] \quad (74)$$

Based on the symmetric condition, we can take

$$\Gamma = \frac{\phi(k)}{h^2} = \frac{1}{2}\left[\frac{1}{1-\frac{\rho h^2}{2}}\right] \quad (75)$$

With regard to the symmetric condition (Equations 73), Equation (72) can be rewritten as

$$u_m^{n+1} = \frac{\Gamma\left(u_m^n + u_{m+1}^n + u_{m-1}^n\right)}{1 + \left(\frac{\rho\,\phi(k)}{3}\right)\left(u_{m+1}^n + u_m^n + u_{m-1}^n\right)}. \quad (76)$$

We know by the assumption that $u_j^n \in [0,1], \forall\, j$. We have

$$0 \le \frac{u_m^n + u_{m+1}^n + u_{m-1}^n}{3} \le 1. \quad (77)$$

By multiplying Equation (77) by $1 - \frac{\rho h^2}{2}$ and dividing by $1 - \frac{\rho h^2}{2}$ and expanding, we have

$$\frac{u_m^n + u_{m+1}^n + u_{m-1}^n}{3\left[1-\frac{\rho h^2}{2}\right]} - \left[\frac{\rho h^2}{2}\right]\frac{u_m^n + u_{m+1}^n + u_{m-1}^n}{3\left[1-\frac{\rho h^2}{2}\right]} \le 1. \quad (78)$$

From Equation (78), we have

$$\frac{u_m^n + u_{m+1}^n + u_{m-1}^n}{3\left[1-\frac{\rho h^2}{2}\right]} \le 1 + \rho\,\frac{h^2}{2}\frac{1}{3}\left[\frac{1}{1-\frac{\rho h^2}{2}}\right](u_m^n + u_{m+1}^n + u_{m-1}^n). \quad (79)$$

Let $\Gamma' = \sigma\,\Gamma, \sigma \ne 0$. Then

$$\Gamma' = \frac{\sigma}{2}\left[\frac{1}{1-\frac{\rho h^2}{2}}\right] = \sigma\frac{\phi(k)}{h^2} \quad (80)$$

If $\frac{\sigma}{2} = \frac{1}{3}$, then $\sigma = \frac{2}{3}$ and using Equation (79), we have

$$\Gamma'(u_m^n + u_{m+1}^n + u_{m-1}^n) \le 1 + \frac{\rho\,\phi(k)}{3}(u_m^n + u_{m+1}^n + u_{m-1}^n). \quad (81)$$

Hence,

$$0 \leq u_m^{n+1} = \frac{\Gamma^{'}\left(u_m^n + u_{m+1}^n + u_{m-1}^n\right)}{1 + \left(\frac{\rho\,\phi(k)}{3}\right)\left(u_{m+1}^n + u_m^n + u_{m-1}^n\right)} \leq 1. \quad (82)$$

Thus, the boundedness of u_m^{n+1}.

6.3. Error Estimate

THEOREM 4. *Let $u \in C^{4,2}(Q)$ where Q is defined by*

$$Q = \{(x,t)/\ a \leq x \leq b,\ 0 < t \leq T,\ T > 0,\ a,\ b \in \mathbb{R}\}.$$

Assume h and k are such that the Theorem 3 is satisfied and $e_m^n = u_m^n - v_m^n$, is the defined error of the scheme constructed. NSFD is consistent, and the estimate error e_m^n is defined by

$$|e_m^n| \leq E_m^n = (3\,\Gamma)^n\,E_m^0 + \left(\frac{1-(3\,\Gamma)^n}{1-3\,\Gamma}\right)$$
$$\left[\left(\frac{\phi(k)}{2} + \rho\,\frac{\phi(k)^2}{2} + \frac{h^2}{12} + \rho\frac{h^4}{36}\right)M + \rho\,h^4\frac{\phi(k)^2}{72}\,M^2\right] \quad (83)$$

where Γ defined in 3 M is defined by $M = \max_{\{(x,t)\}\in Q}\left\{|u_{xxxx}(x,t)|,\ |u_{tt}(x,t)|\right\}$, and Θ_i, $i = 1,\ 2,\ 3$ such that

$$\Theta_1(\phi(k),h) = \rho\,\frac{h^2}{3}\,u - \rho\,h^2\,\frac{\phi(k)^2}{6}\,u_{tt}$$
$$\Theta_2(\phi(k),h) = -\frac{\phi(k)^2}{6} + \rho\frac{\phi(k)}{3}$$
$$\left[\frac{\phi^2(k)}{2}\,u + h^2\,\frac{\phi^2}{6}\,u_{xx} + h^4\,\frac{\phi(k)^2}{72}u_{xxxx}\right]$$
$$\Theta_3(\phi(k),h) = -\phi(k)\,v - \rho\,h^2\,\frac{\phi(k)}{3} - \rho\,h^4\frac{\phi(k)}{36}\,u_{xxxx} \quad (84)$$

and

$\Theta_1(\phi(k),h)\,u_{xx} + \Theta_2(\phi(k),h)\,u_{ttt} + \Theta_3(\phi(k),h)\,u_t = O\left(\phi(k),h\right) \to 0$ *when* $\phi(k) \to 0$ *and* $h \to 0$.

Proof.

$$v_m^{n+1} = \frac{\Gamma\,v_m^n + R\left(v_{m+1}^n + v_{m-1}^n\right)}{1 + \left(\frac{\rho\phi(k)}{3}\right)\left(v_{m+1}^n + v_m^n + v_{m-1}^n\right)}, \quad (85)$$

where $\Gamma = 1 - 2\frac{\phi(k)}{h^2} + \rho\phi(k)$, $R = \frac{\phi(k)}{h^2}$. Taylor series expansion of Equation (85) about (t_n, x_m) gives

$$\left(v + \phi(k)\,v_t + \frac{(\phi(k))^2}{2}v_{tt} + \frac{(\phi(k))^3}{6}v_{ttt} + O\left((\phi(k))^4\right)\right)$$
$$\left(1 + \rho\frac{\phi(k)}{3}\left\{\begin{array}{l} v + v + h\,v_x + \frac{h^2}{2}\,v_{xx} + \frac{h^3}{6}\,v_{xxx} + \frac{h^4}{24}\,v_{xxxx} \\ +v - h\,v_x + \frac{h^2}{2}\,v_{xx} - \frac{h^3}{6}\,v_{xxx} + \frac{h^4}{24}\,v_{xxxx}\end{array}\right\}\right)$$
$$= \left(1 - \frac{2\phi(k)}{h^2} + \rho\,\phi(k)\right)v$$
$$+\frac{\phi(k)}{h^2}\left\{\begin{array}{l} v + h\,v_x + \frac{h^2}{2}\,v_{xx} + \frac{h^3}{6}\,v_{xxx} + \frac{h^4}{24}\,v_{xxxx} \\ +v - h\,v_x + \frac{h^2}{2}\,v_{xx} - \frac{h^3}{6}\,v_{xxx} + \frac{h^4}{24}\,v_{xxxx}\end{array}\right\}$$

This gives

$$v + \phi(k)\,v_t + \frac{(\phi(k))^2}{2}v_{tt} + \frac{(\phi(k))^3}{6}v_{ttt}$$
$$+\rho\frac{\phi(k)}{3}\left(v + \phi(k)\,v_t + \frac{(\phi(k))^2}{2}v_{tt} + \frac{(\phi(k))^3}{6}v_{ttt}\right)$$
$$\left(3\,v + h^2\,v_{xx} + \frac{h^4}{12}\,v_{xxxx}\right)$$
$$= v + \left(-\frac{2\phi(k)}{h^2} + \rho\,\phi(k)\right)v + \frac{\phi(k)}{h^2}\left(2\,v + h^2\,v_{xx} + +\frac{h^4}{12}\,v_{xxxx}\right). \quad (86)$$

It follows after division by $\phi(k)$ and simplification, we have

$$v_t + \frac{(\phi(k))}{2}v_{tt} + \frac{(\phi(k))^2}{6}v_{ttt}$$
$$+\frac{\rho}{3}\left(\phi(k)\,v_t + \frac{(\phi(k))^2}{2}v_{tt} + \frac{(\phi(k))^3}{6}v_{ttt}\right)$$
$$\left(3\,v + h^2\,v_{xx} + \tfrac{h^4}{12}\,v_{xxxx}\right)$$
$$+\frac{\rho}{3}\,v(3\,v) + \frac{\rho}{3}\,v\left(h^2\,v_{xx} + \tfrac{h^4}{12}\,v_{xxxx}\right)$$
$$= v_{xx} + \rho\,v + \frac{h^2}{12}\,v_{xxxx}. \quad (87)$$

It follows that

$$v_t - v_{xx} + \rho\,v^2 - \rho\,v$$
$$= \left\{\begin{array}{l} \left(\frac{h^2}{12} - \rho\frac{h^4}{36}\,v\right)v_{xxxx} - \left(\frac{\phi(k)}{2} + \rho\,h^4\frac{\phi(k)^2}{72}\,v_{xxxx} + \rho\,\frac{\phi^2(k)}{2}\,v\right)v_{tt} \\ +\left(\rho\,\frac{h^2}{3}\,v - \rho\,h^2\,\frac{\phi(k)^2}{6}v_{tt}\right)v_{xx} \\ +\left(-\frac{\phi(k)^2}{6} + \rho\frac{\phi(k)}{3}\left[\frac{\phi(k)^2}{2}\,v + h^2\,\frac{\phi^2(k)}{6}\,v_{xx} + h^4\,\frac{\phi(k)^2}{72}v_{xxxx}\right]\right)v_{ttt} \\ +\left(-\phi(k)\,v - \rho\,h^2\,\frac{\phi(k)}{3} - \rho\,h^4\frac{\phi(k)}{36}\,v_{xxxx}\right)v_t \end{array}\right\} \quad (88)$$

If $\phi(k) \to 0$ and $h \to 0$, Equation (88) reduces to $v_t - v_{xx} + \rho\,v^2 - \rho\,v \to 0$. Hence, the consistency.

For the simplicity of the proof, we consider the function Θ_i, $i = 1,\ 2,\ 3$ such that

$$\Theta_1(\phi(k),h) = \rho\,\frac{h^2}{3}\,v - \rho\,h^2\,\frac{\phi(k)^2}{6}v_{tt}$$
$$\Theta_2(\phi(k),h) = -\frac{\phi(k)^2}{6} + \rho\frac{\phi(k)}{3}$$
$$\left[\frac{\phi^2(k)}{2}\,v + h^2\,\frac{\phi^2}{6}\,v_{xx} + h^4\,\frac{\phi(k)^2}{72}v_{xxxx}\right]$$
$$\Theta_3(\phi(k),h) = -\phi(k)\,v - \rho\,h^2\,\frac{\phi(k)}{3} - \rho\,h^4\frac{\phi(k)}{36}\,v_{xxxx} \quad (89)$$

and $\Theta_1(\phi(k),h)\,v_{xx} + \Theta_2(\phi(k),h)\,v_{ttt} + \Theta_3(\phi(k),h)\,v_t = O\left(\phi(k),h\right) \to 0$ when $\phi(k) \to 0$ and $h \to 0$.

The exact discrete equation is

$$u_m^{n+1} = \frac{\Gamma u_m^n + R\left(u_{m+1}^n + u_{m-1}^n\right)}{1 + \frac{\rho\phi(k)}{3}(u_{m+1}^n + u_m^n + u_{m-1}^n)} + \left(\frac{\phi(k)}{2} + \rho\, h^4 \frac{\phi(k)^2}{72}\, u_{xxxx}(\varepsilon_m, t) + \rho\, \frac{\phi^2(k)}{2}\, u\right) u_{tt}(x, \tau_n) - \left(\frac{h^2}{12} - \rho \frac{h^4}{36}\, u\right) u_{xxxx}(\varepsilon_m, t) \quad (90)$$

where $\Gamma = 1 - 2\frac{\phi(k)}{h^2} + \rho\phi(k)$, $R = \frac{\phi(k)}{h^2}$, and $x_m < \varepsilon_m < x_{m+1}$ and $t_n < \tau_n < t_{n+1}$.

We define $e_m^n = u_m^n - v_m^n \equiv e_m^{n+1} = u_m^{n+1} - v_m^{n+1}$. It follows by considering symmetry condition $\Gamma = R$

$$u_m^{n+1} - v_m^{n+1} = \left\{ \begin{array}{l} \frac{\Gamma\left(u_{m+1}^n + u_m^n + u_{m-1}^n\right)}{1+\frac{\rho\phi(k)}{3}(u_{m+1}^n + u_m^n + u_{m-1}^n)} - \frac{\Gamma\left(v_{m+1}^n + v_m^n + v_{m-1}^n\right)}{1+\frac{\rho\phi(k)}{3}(v_{m+1}^n + v_m^n + v_{m-1}^n)} \\ + \left(\frac{\phi(k)}{2} + \rho\, h^4 \frac{\phi(k)^2}{72}\, u_{xxxx}(\varepsilon_m, t) + \rho\, \frac{\phi^2(k)}{2}\, u\right) u_{tt}(x, \tau_n) \\ - \left(\frac{h^2}{12} - \rho\, \frac{h^4}{36}\, u\right) u_{xxxx}(\varepsilon_m, t) \end{array} \right\}. \quad (91)$$

It follows

$$e_m^{n+1} = \frac{\Gamma\left(e_{m+1}^n + e_m^n + e_{m-1}^n\right)}{\left(1 + \frac{\rho\phi(k)}{3}(u_{m+1}^n + u_m^n + u_{m-1}^n)\right)\left(1 + \frac{\rho\phi(k)}{3}(v_{m+1}^n + v_m^n + v_{m-1}^n)\right)} + \left(\frac{\phi(k)}{2} + \rho\, h^4 \frac{\phi(k)^2}{72}\, u_{xxxx}(\varepsilon_m, t) + \rho\, \frac{\phi(k)^2}{2}\, u\right) u_{tt}(x, \tau_n) - \left(\frac{h^2}{12} - \rho \frac{h^4}{36}\, u\right) u_{xxxx}(\varepsilon_m, t) \quad (92)$$

Let $M = \max_{\{(x,t)\} \in Q} \left\{|u_{xxxx}(x,t)|,\ |u_{tt}(x,t)|\right\}$ and $E_m^n = \max_{0<m<N}\{|e_m^n|\}$. We have

$$\left(1 + \frac{\rho\phi(k)}{3}(u_{m+1}^n + u_m^n + u_{m-1}^n)\right) \left(1 + \frac{\rho\phi(k)}{3}(v_{m+1}^n + v_m^n + v_{m-1}^n)\right) > 1,$$

$\forall\, u_i^n,\ v_i^n \in [0,1],\ i = m-1,\ m,\ m+1$
and by using Theorem 3, we have

$$\begin{aligned} |e_m^{n+1}| &\le |\Gamma|(|e_{m+1}^n| + |e_m^n| + |e_{m-1}^n|) \\ &+ \left|\left(\frac{\phi(k)}{2} + \rho\, h^4 \frac{\phi(k)^2}{72}\, u_{xxxx}(\varepsilon_m, t) + \rho\, \frac{\phi(k)^2}{2}\, u\right)\right| \\ &|u_{tt}(x, \tau_n)| + \left|-\left(\frac{h^2}{12} - \rho \frac{h^4}{36}\, u\right)\right| |u_{xxxx}(\varepsilon_m, t)| \\ &\le 3\,\Gamma\, E_m^n + \left(\frac{\phi(k)}{2} + \rho\, \frac{\phi(k)^2}{2} + \frac{h^2}{12} + \rho \frac{h^4}{36}\right) M \\ &+ \rho\, h^4 \frac{\phi(k)^2}{72}\, M^2 \end{aligned} \quad (93)$$

Let

$$E_m^{n+1} = 3\,\Gamma\, E_m^n + \left(\frac{\phi(k)}{2} + \rho\, \frac{\phi(k)^2}{2} + \frac{h^2}{12} + \rho \frac{h^4}{36}\right) M + \rho\, h^4 \frac{\phi(k)^2}{72}\, M^2.$$

We have

$$|e_m^{n+1}| \le E_m^{n+1} = 3\,\Gamma\, E_m^n + \left(\frac{\phi(k)}{2} + \rho\, \frac{\phi(k)^2}{2} + \frac{h^2}{12} + \rho \frac{h^4}{36}\right) M + \rho\, h^4 \frac{\phi(k)^2}{72}\, M^2 \quad (94)$$

For $n = 0$, $E_m^1 = 3\,\Gamma\, E_m^0 + \left(\frac{\phi(k)}{2} + \rho\, \frac{\phi(k)^2}{2} + \frac{h^2}{12} + \rho \frac{h^4}{36}\right) M + \rho\, h^4 \frac{\phi(k)^2}{72}\, M^2$
For $n = 1$, we have

$$\begin{aligned} E_m^2 &= 3\,\Gamma\, E_m^1 + \left(\frac{\phi(k)}{2} + \rho\, \frac{\phi(k)^2}{2} + \frac{h^2}{12} + \rho \frac{h^4}{36}\right) M \\ &+ \rho\, h^4 \frac{\phi(k)^2}{72}\, M^2 \\ &= 3\Gamma\,(\,3\,\Gamma\, E_m^0 + \left(\frac{\phi(k)}{2} + \rho\, \frac{\phi(k)^2}{2} + \frac{h^2}{12} + \rho \frac{h^4}{36}\right) M \\ &+ \rho\, h^4 \frac{\phi(k)^2}{72}\, M^2\,) \\ &+ \left(\frac{\phi(k)}{2} + \rho\, \frac{\phi(k)^2}{2} + \frac{h^2}{12} + \rho \frac{h^4}{36}\right) M + \rho\, h^4 \frac{\phi(k)^2}{72}\, M^2 \\ &= (3\,\Gamma)^2\, E_m^0 + (1 + 3\,\Gamma) \\ &\left[\left(\frac{\phi(k)}{2} + \rho\, \frac{\phi(k)^2}{2} + \frac{h^2}{12} + \rho \frac{h^4}{36}\right) M + \rho\, h^4 \frac{\phi(k)^2}{72}\, M^2\right] \end{aligned} \quad (95)$$

For $n = 2$, we have

$$\begin{aligned} E_m^3 &= 3\,\Gamma\, E_m^2 + \left(\frac{\phi(k)}{2} + \rho\, \frac{\phi(k)^2}{2} + \frac{h^2}{12} + \rho \frac{h^4}{36}\right) M + \rho\, h^4 \frac{\phi(k)^2}{72}\, M^2 \\ &= 3\Gamma\left(3^2\,\Gamma^2 + (1 + 3\,\Gamma)\left[\left(\frac{\phi(k)}{2} + \rho\, \frac{\phi(k)^2}{2} + \frac{h^2}{12} + \rho \frac{h^4}{36}\right)\ M\right.\right. \\ &\left.\left. + \rho\, h^4 \frac{\phi(k)^2}{72}\, M^2\,\right]\right) \\ &+ \left(\frac{\phi(k)}{2} + \rho\, \frac{\phi(k)^2}{2} + \frac{h^2}{12} + \rho \frac{h^4}{36}\right) M + \rho\, h^4 \frac{\phi(k)^2}{72}\, M^2 \\ &= (3\,\Gamma)^3\, E_m^0 + (1 + 3\,\Gamma + (3\,\Gamma)^2)\left[\left(\frac{\phi(k)}{2} + \rho\, \frac{\phi(k)^2}{2} + \frac{h^2}{12} + \rho \frac{h^4}{36}\right) M\right. \\ &\left. + \rho\, h^4 \frac{\phi(k)^2}{72}\, M^2\right] \end{aligned} \quad (96)$$

By recurrence for n, we have

$$E_m^{n+1} = (3\,\Gamma)^n\,E_m^0 + \left(\sum_{i=0}^{i-1}(3\,\Gamma)^i\right)\left[\left(\frac{\phi(k)}{2} + \rho\,\frac{\phi(k)^2}{2} + \frac{h^2}{12} + \rho\frac{h^4}{36}\right)M + \rho\,h^4\frac{\phi(k)^2}{72}\,M^2\right] = (3\,\Gamma)^n\,E_m^0 + \left(\frac{1-(3\,\Gamma)^n}{1-3\,\Gamma}\right)\left[\left(\frac{\phi(k)}{2} + \rho\,\frac{\phi(k)^2}{2} + \frac{h^2}{12} + \rho\frac{h^4}{36}\right)M + \rho\,h^4\frac{\phi(k)^2}{72}\,M^2\right] \tag{97}$$

7. EXPLICIT EXPONENTIAL FINITE DIFFERENCE SCHEME

The EFFD method was developed by Bhattacharya [41] (primarily called the Bhattacharya method) for the numerical solution of the heat equation. The Exponential Finite Difference method was utilized to solve Burgers' equation and generalized Huxley and Burgers-Huxley equations [42–44]. Later, Macías-Díaz and Ĭnan [45] used modified exponential methods to obtain the solution of the Burgers' equation. Furthermore, Inan et al. [46] utilized the EEFD method for numerical solutions for the Newell-Whitehead-Segel type equations which are very useful in biomathematics. They showed convergence, consistency, and stability of the method.

In this section, we obtain numerical solutions of the equation by **EEFD** method. The solution domain are discretized into cells as (x_m, t_n) in which $x_m = mh$, $(m = 0, 1, 2, ..., N)$ and $t_n = nk$, $(n = 0, 1, 2, ...)$, $h = \Delta x = \frac{b-a}{N}$ is the spatial mesh size and $k = \Delta t$ is the time step, u_m^n denotes the **EEFD** approximation and $u(x, t)$ denotes the exact solution.

Dividing Equation (6) by u gives

$$\frac{\partial \ln u}{\partial t} = \frac{1}{u}\left(u\,(1-u) + \frac{\partial^2 u}{\partial x^2}\right). \tag{98}$$

Using the finite difference approximations for derivatives, Equation (98) gives

$$u_m^{n+1} = u_m^n \exp\left\{k\left(1-u_m^n\right) + R\left(\frac{u_{m+1}^n - 2u_m^n + u_{m-1}^n}{u_m^n}\right)\right\} \tag{99}$$

where $R = \frac{k}{h^2}$. Equation (99) gives the expression for the **EEFD** method for Fisher's equation.

7.1. Convergence and Estimate Error

For stability analysis, we require non-iterative exponential time-linearization and iterative exponential quasilinearization techniques for Equation (6) which are found in the discretization of the time derivative, the freezing of the coefficients of the resulting linear ordinary differential equations, and the piecewise analytical solution of these ordinary differential equations. These techniques give three-point finite difference expressions that depend in an exponential manner on either the diffusion, reaction, and transient terms or the diffusion and reaction terms. Following the idea of Ramos [25], we transform (Equations 6, 99) into a linear ordinary differential equation by discretizing the time derivative by means of θ-method [25] and linearizing the nonlinear source term, $u(1-u)$, with respect to either the previous time level or the previous iteration with Jacobian, $J = \frac{d(u(1-u))}{du} = 1 - 2\,u$:

a) If the linearization is performed with respect to the previous time level, one obtains

$$\frac{u_m^{n+1} - u_m^n}{k} = \theta\,\frac{u_{m-1}^{n+1} - 2\,u_m^{n+1} + u_{m+1}^{n+1}}{h^2} + (1-\theta)\,\frac{u_{m-1}^n - 2\,u_m^n + u_{m+1}^n}{h^2} + u_m^n(1-u_m^n) + \theta\,J_m^n\,(u_m^{n+1} - u_m^n) \tag{100}$$

which yields a non-iterative time linearization method.

b) If the linearization is performed with respect to the previous iteration, one obtains

$$\frac{u_m^{i+1} - u_m^n}{k} = \theta\,\frac{u_{m-1}^{i+1} - 2\,u_m^{i+1} + u_{m+1}^{i+1}}{h^2} + (1-\theta)\,\frac{u_{m-1}^n - 2\,u_m^n + u_{m+1}^n}{h^2} + (1-\theta)\,u_m^n(1-u_m^n) + \theta\,u_m^{n+1}(1-u_m^{i+1}) + \theta\,J_m^{i+1}\,(u_m^{i+1} - u_m^n) \tag{101}$$

which corresponds to an iterative quasilinear technique and $i = 1,\ 2, \cdots, n$.

Equations (100) and (101) can be solved in closed form in $(x_{m-1},\ x_{m+1})$ subject to the following conditions:

$$u(x_{m-1}) = u_{m-1},\ \ u(x_m) = u_m,\ \ u(x_{m+1}) = u_{m+1} \tag{102}$$

and yield exponential solutions in $(x_{m-1},\ x_{m+1})$ which are analytical in that interval and continuous everywhere. Since Equations (100) and (101) are very similar, we will only present in detail exponential methods for Equation (100) in the following subsections.

7.1.1. Time-Linearized Full Exponential Techniques

The piecewise analytical solution of Equation (100) can be rewritten as

$$\left(\theta\,J_m^n - \frac{1}{k}\right)u_m^{n+1} + \theta\,\frac{u_{m-1}^{n+1} - 2\,u_m^{n+1} + u_{m+1}^{n+1}}{h^2} = \left(\theta\,J_m^n - \frac{1}{k}\right)u_m^n - (1-\theta)\,\frac{u_{m-1}^n - 2\,u_m^n + u_{m+1}^n}{h^2} - u_m^n(1-u_m^n). \tag{103}$$

TABLE 1 | L_1 and L_∞ errors at some different values of time-step size, k with $\rho = 1$ at time, $T_{max} = 2.5 \times 10^{-3}$ with spatial mesh size, $h = 0.01$ using three methods.

Values of k	FTCS		NSFD		EEFD	
	L_1 error	L_∞ error	L_1 error	L_∞ error	L_1 error	L_∞ error
$T_{max}/52$	5.4192×10^{-9}	6.3334×10^{-9}	3.2264×10^{-8}	3.7216×10^{-8}	4.1091×10^{-9}	5.1492×10^{-9}
$T_{max}/100$	2.8854×10^{-9}	3.3694×10^{-9}	1.7026×10^{-8}	1.9624×10^{-8}	2.0683×10^{-9}	2.6091×10^{-9}
$T_{max}/200$	1.5135×10^{-9}	1.7645×10^{-9}	8.7757×10^{-9}	1.0098×10^{-8}	9.6251×10^{-10}	1.2354×10^{-9}
$T_{max}/300$	1.0563×10^{-9}	1.7645×10^{-9}	6.0260×10^{-9}	6.0260×10^{-9}	5.9431×10^{-10}	7.7761×10^{-10}
$T_{max}/400$	8.2780×10^{-10}	9.6234×10^{-10}	4.6512×10^{-9}	5.3361×10^{-9}	4.1024×10^{-10}	5.4763×10^{-10}
$T_{max}/500$	6.9066×10^{-10}	8.0194×10^{-10}	3.8264×10^{-9}	4.3837×10^{-9}	2.9973×10^{-10}	4.1032×10^{-10}
$T_{max}/600$	5.9924×10^{-10}	6.9502×10^{-10}	3.2766×10^{-9}	3.7488×10^{-9}	2.2612×10^{-10}	3.1904×10^{-10}
$T_{max}/700$	5.3392×10^{-10}	6.1863×10^{-10}	2.8838×10^{-9}	3.2954×10^{-9}	1.7352×10^{-10}	2.5366×10^{-10}
$T_{max}/800$	4.8495×10^{-10}	5.6136×10^{-10}	2.5894×10^{-9}	2.9554×10^{-9}	1.3402×10^{-10}	2.0476×10^{-10}
$T_{max}/900$	4.4686×10^{-10}	5.1681×10^{-10}	2.3602×10^{-9}	2.6910×10^{-9}	1.0334×10^{-10}	1.6694×10^{-10}
$T_{max}/1{,}000$	4.1639×10^{-10}	4.8117×10^{-10}	2.1769×10^{-9}	2.4795×10^{-9}	7.8784×10^{-11}	1.3668×10^{-10}
$T_{max}/1{,}100$	3.9144×10^{-10}	4.5199×10^{-10}	2.0269×10^{-9}	2.3064×10^{-9}	5.8705×10^{-11}	1.1192×10^{-10}
$T_{max}/1{,}200$	3.7066×10^{-10}	4.2769×10^{-10}	1.9019×10^{-9}	2.1622×10^{-9}	4.1956×10^{-11}	9.1419×10^{-11}
$T_{max}/1{,}300$	3.5308×10^{-10}	4.0714×10^{-10}	1.7962×10^{-9}	2.0402×10^{-9}	3.0241×10^{-11}	7.4118×10^{-11}
$T_{max}/1{,}400$	3.3801×10^{-10}	3.8953×10^{-10}	$\mathbf{1.7056 \times 10^{-9}}$	$\mathbf{1.9356 \times 10^{-9}}$	2.3908×10^{-11}	5.9401×10^{-11}
$T_{max}/1{,}500$	3.2496×10^{-10}	3.7427×10^{-10}	1.6270×10^{-9}	1.8449×10^{-9}	2.1174×10^{-11}	4.6738×10^{-11}
$T_{max}/1{,}600$	3.1353×10^{-10}	3.6091×10^{-10}	1.5583×10^{-9}	1.7656×10^{-9}	$\mathbf{2.0904 \times 10^{-11}}$	$\mathbf{3.5802 \times 10^{-11}}$
$T_{max}/1{,}700$	3.0345×10^{-10}	3.4913×10^{-10}	1.4976×10^{-9}	1.6956×10^{-9}	2.2344×10^{-11}	4.2194×10^{-11}
$T_{max}/1{,}800$	2.9449×10^{-10}	3.3866×10^{-10}	1.4438×10^{-9}	1.6335×10^{-10}	2.4984×10^{-11}	4.8536×10^{-11}
$T_{max}/2{,}000$	$\mathbf{2.9449 \times 10^{-10}}$	$\mathbf{3.3866 \times 10^{-10}}$	$\mathbf{1.3521 \times 10^{-9}}$	$\mathbf{1.5279 \times 10^{-10}}$	3.2504×10^{-11}	5.9412×10^{-11}

Bold values indicate the lowest errors.

TABLE 2 | L_1 and L_∞ errors at some different values of time-step size, k with $\rho = 10^2$ at time, $T_{max} = 2.5 \times 10^{-3}$ with spatial mesh size, $h = 0.01$ using three methods.

Values of k	FTCS		NSFD		EEFD	
	L_1 error	L_∞ error	L_1 error	L_∞ error	L_1 error	L_∞ error
$T_{max}/52$	3.2613×10^{-5}	6.9142×10^{-5}	6.3178×10^{-5}	1.3471×10^{-4}	2.2654×10^{-5}	7.2263×10^{-5}
$T_{max}/100$	1.7120×10^{-5}	3.6652×10^{-5}	3.3705×10^{-5}	7.2133×10^{-5}	1.1628×10^{-5}	3.7401×10^{-5}
$T_{max}/200$	8.7183×10^{-6}	1.9060×10^{-5}	1.7709×10^{-5}	3.8414×10^{-5}	5.6602×10^{-6}	1.8584×10^{-5}
$T_{max}/300$	5.9159×10^{-6}	1.3196×10^{-5}	1.2371×10^{-5}	2.7303×10^{-5}	3.6732×10^{-6}	1.2324×10^{-5}
$T_{max}/400$	4.5154×10^{-6}	1.0268×10^{-5}	9.7020×10^{-6}	2.1809×10^{-5}	2.6794×10^{-6}	9.1874×10^{-6}
$T_{max}/500$	3.6749×10^{-6}	8.5169×10^{-6}	8.1001×10^{-6}	1.8545×10^{-5}	2.0833×10^{-6}	7.3251×10^{-6}
$T_{max}/600$	3.1146×10^{-6}	7.3489×10^{-6}	7.0319×10^{-6}	1.6379×10^{-5}	1.6864×10^{-6}	6.0864×10^{-6}
$T_{max}/700$	2.7143×10^{-6}	6.5146×10^{-6}	6.2689×10^{-6}	1.4842×10^{-5}	1.4024×10^{-6}	5.2014×10^{-6}
$T_{max}/800$	2.4141×10^{-6}	5.8925×10^{-6}	5.6966×10^{-6}	1.3689×10^{-5}	1.1903×10^{-6}	4.5376×10^{-6}
$T_{max}/900$	2.1806×10^{-6}	5.4093×10^{-6}	5.2515×10^{-6}	1.2802×10^{-5}	1.0244×10^{-6}	4.0219×10^{-6}
$T_{max}/1{,}000$	1.9941×10^{-6}	5.0227×10^{-6}	4.8954×10^{-6}	1.2093×10^{-5}	8.9174×10^{-7}	3.6143×10^{-6}
$T_{max}/1{,}100$	1.8416×10^{-6}	4.7064×10^{-6}	4.6040×10^{-6}	1.1513×10^{-5}	7.8356×10^{-7}	3.2846×10^{-6}
$T_{max}/1{,}200$	1.7144×10^{-6}	4.4428×10^{-6}	4.3612×10^{-6}	1.1030×10^{-5}	7.0876×10^{-7}	3.0099×10^{-6}
$T_{max}/1{,}300$	1.6068×10^{-6}	4.2197×10^{-6}	4.1557×10^{-6}	1.0621×10^{-5}	6.5558×10^{-7}	2.7774×10^{-6}
$T_{max}/1{,}400$	1.5153×10^{-6}	4.0298×10^{-6}	3.9797×10^{-6}	1.0274×10^{-5}	6.1557×10^{-7}	2.5767×10^{-6}
$T_{max}/1{,}500$	1.4371×10^{-6}	3.8658×10^{-6}	3.8279×10^{-6}	9.9737×10^{-6}	5.8466×10^{-7}	2.4043×10^{-6}
$T_{max}/1{,}600$	1.3698×10^{-6}	3.7222×10^{-6}	3.6960×10^{-6}	9.7113×10^{-6}	5.6048×10^{-7}	2.2528×10^{-6}
$T_{max}/1{,}700$	1.3113×10^{-6}	3.5956×10^{-6}	3.5803×10^{-6}	9.4798×10^{-6}	5.4168×10^{-7}	2.1186×10^{-6}
$T_{max}/1{,}800$	1.2601×10^{-6}	3.4830×10^{-6}	3.4781×10^{-6}	9.2740×10^{-6}	5.2654×10^{-7}	2.0034×10^{-6}
$T_{max}/2{,}000$	$\mathbf{1.1748 \times 10^{-6}}$	$\mathbf{3.2916 \times 10^{-6}}$	$\mathbf{3.3055 \times 10^{-6}}$	$\mathbf{8.9242 \times 10^{-6}}$	$\mathbf{5.0458 \times 10^{-7}}$	$\mathbf{1.807 \times 10^{-6}}$

Bold values indicate the lowest errors.

TABLE 3 | L_1 and L_∞ errors at some different values of time-step size, k with $\rho = 10^4$ at time, $T_{max} = 2.5 \times 10^{-3}$ with spatial mesh size, $h = 0.01$ using three methods.

Values of k	FTCS		NSFD		EEFD	
	L_1 error	L_∞ error	L_1 error	L_∞ error	L_1 error	L_∞ error
$T_{max}/52$	3.6440×10^{-1}	1.6012	1.1960×10^{-1}	9.1526×10^{-1}	over flow	over flow
$T_{max}/100$	6.5143×10^{-2}	6.9877×10^{-1}	7.0119×10^{-2}	7.1253×10^{-1}	1.3594×10^{-2}	1.5978×10^{-1}
$T_{max}/200$	3.2980×10^{-2}	3.9927×10^{-1}	3.6170×10^{-2}	4.1776×10^{-1}	1.0084×10^{-2}	1.1786×10^{-1}
$T_{max}/300$	2.0726×10^{-2}	2.5613×10^{-1}	2.3034×10^{-2}	2.7854×10^{-1}	8.9264×10^{-3}	1.0476×10^{-1}
$T_{max}/400$	1.4262×10^{-2}	1.7830×10^{-1}	1.6098×10^{-2}	1.9602×10^{-1}	8.3519×10^{-3}	9.8394×10^{-2}
$T_{max}/500$	1.0268×10^{-2}	1.2943×10^{-1}	1.1810×10^{-2}	1.4691×10^{-1}	8.0087×10^{-3}	9.4591×10^{-2}
$T_{max}/600$	7.5556×10^{-3}	9.5604×10^{-2}	8.8965×10^{-3}	1.1270×10^{-1}	7.7810×10^{-3}	9.2071×10^{-2}
$T_{max}/700$	5.5928×10^{-3}	7.1037×10^{-2}	6.7882×10^{-3}	8.7558×10^{-2}	7.6182×10^{-3}	9.0294×10^{-2}
$T_{max}/800$	4.1067×10^{-3}	5.2473×10^{-2}	5.1924×10^{-3}	6.8387×10^{-2}	7.4974×10^{-3}	8.8949×10^{-2}
$T_{max}/900$	2.9425×10^{-3}	3.7988×10^{-2}	3.9442×10^{-3}	5.3326×10^{-2}	7.4020×10^{-3}	8.7921×10^{-2}
$T_{max}/1,000$	2.0059×10^{-3}	2.6389×10^{-2}	2.9442×10^{-3}	4.1202×10^{-2}	7.3264×10^{-3}	8.7094×10^{-2}
$T_{max}/1,100$	1.2403×10^{-3}	1.6901×10^{-2}	2.1334×10^{-3}	3.1242×10^{-2}	7.2643×10^{-3}	8.6421×10^{-2}
$T_{max}/1,200$	6.2582×10^{-4}	9.0012×10^{-3}	1.4824×10^{-3}	2.2920×10^{-2}	7.2120×10^{-3}	8.5864×10^{-2}
$T_{max}/1,300$	**1.9347×10^{-4}**	**2.3239×10^{-3}**	9.7801×10^{-4}	1.5866×10^{-2}	7.1694×10^{-3}	8.5384×10^{-2}
$T_{max}/1,400$	4.2509×10^{-4}	4.3457×10^{-3}	6.3252×10^{-4}	9.8126×10^{-3}	7.1310×10^{-3}	8.4982×10^{-2}
$T_{max}/1,500$	8.3336×10^{-4}	8.7691×10^{-3}	**4.5235×10^{-4}**	**4.5623×10^{-3}**	7.0992×10^{-3}	8.4631×10^{-2}
$T_{max}/1,600$	1.1913×10^{-3}	1.3138×10^{-2}	5.0611×10^{-4}	5.3708×10^{-3}	7.0703×10^{-3}	8.4321×10^{-2}
$T_{max}/1,700$	1.5077×10^{-3}	1.7003×10^{-2}	8.4385×10^{-4}	7.6874×10^{-3}	7.0451×10^{-3}	8.4052×10^{-2}
$T_{max}/1,800$	1.7895×10^{-3}	2.0446×10^{-2}	1.1467×10^{-3}	1.0154×10^{-2}	7.0231×10^{-3}	8.3812×10^{-2}
$T_{max}/2,000$	1.5538×10^{-2}	1.8402×10^{-1}	1.6628×10^{-3}	1.5383×10^{-2}	**6.9852×10^{-3}**	**8.3399×10^{-2}**

Bold values indicate the lowest errors.

Let $\left(\theta\, J_m^n - \frac{1}{k}\right) u_m^{n+1} + \theta\, \frac{u_{m-1}^{n+1} - 2\,u_m^{n+1} + u_{m+1}^{n+1}}{h^2} = z_m^{n+1}$. Equation (103) becomes

$$z_m^{n+1} = \left(\theta\, J_m^n - \frac{1}{k}\right) u_m^n - (1-\theta)\, \frac{u_{m-1}^n - 2\,u_m^n + u_{m+1}^n}{h^2} - u_m^n(1-u_m^n) \tag{104}$$

which accounts for diffusion, reaction, and transient effects in the differential operator [25]. The solution of Equation (104) depends on the sign of $D_m^n \equiv \theta\, J_m^n - \frac{1}{k}$. We have the following three cases:

a) If $D_m^n = 0$, the solution of Equation (104) subject to the condition (102) gives the finite difference expression

$$z_m^{n+1} = \frac{u_{m-1}^n - 2\,u_m^n + u_{m+1}^n}{h^2}. \tag{105}$$

b) If $D_m^n = -\theta\,(\lambda_m)^2 < 0$,the solution of Equation (104) subject to the condition (102) gives the three-point finite difference expression

$$z_m^{n+1} = \frac{D_m^n}{2}\left(\frac{u_{m-1}^n - 2\,\cosh(\lambda_m h)\,u_m^n + u_{m+1}^n}{1 - \cosh(\lambda_m h)}\right). \tag{106}$$

c) If $D_m^n = \theta\,(\lambda_m)^2 > 0$, the solution of Equation (104) subject to the condition (102) gives the three-point finite difference expression

$$z_m^{n+1} = \frac{D_m^n}{2}\left(\frac{u_{m-1}^n - 2\,\cos(\lambda_m h)\,u_m^n + u_{m+1}^n}{1 - \cos(\lambda_m h)}\right). \tag{107}$$

REMARK 1. *We can make the following remarks*

a) The values $\theta = \frac{1}{2}$, 1, corresponding to the time linearization methods.

b) The quasilinear full exponential corresponds to the iterative solution of

$$z_m^{i+1} = -(1-\theta)\,\frac{u_{m-1}^n - 2\,u_m^n + u_{m+1}^n}{h^2} - (1-\theta)\,u_m^n(1-u_m^n) - \theta\; u_m^i(1-u_m^i) + \theta\, J_m^i\, u_m^i - \frac{u_m^n}{k} \tag{108}$$

for $i = 1, 2, \cdots, n-1$, have analogous solutions to those reported in time-linearized full exponential techniques section and the cases $\theta = \frac{1}{2}$ and 1, corresponding to the quasilinear methods.

7.1.2. Time-Linearized Exponential Techniques

The time-linearized exponential techniques presented in this section consider the following differential operator.

$$\theta\, J_m^n\, u_m^{n+1} + \theta\, \frac{u_{m-1}^{n+1} - 2\,u_m^{n+1} + u_{m+1}^{n+1}}{h^2} = \theta\, J_m^n\, u_m^n - (1-\theta)\,\frac{u_{m-1}^n - 2\,u_m^n + u_{m+1}^n}{h^2} + \frac{u_m - u_m^n}{k} - u_m^n(1-u_m^n) \tag{109}$$

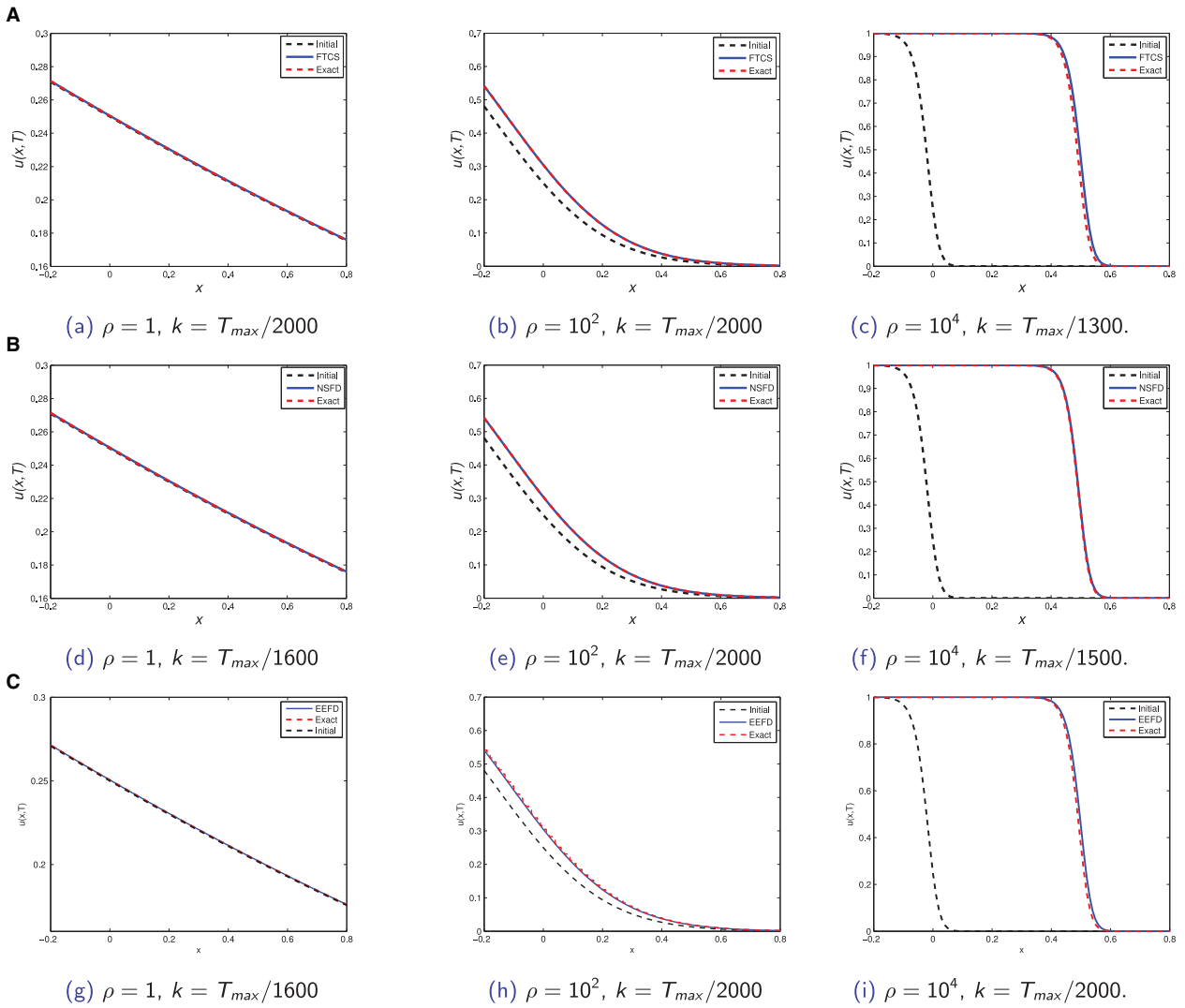

FIGURE 1 | Plot of initial solution, numerical solution of (FTCS), NSFD, and EEFD respectively in **(A–C)** and exact solution against x at time, $T_{max} = 2.5 \times 10^{-3}$ using $h = 0.01$ and optimal value of time step size of k for three different values of ρ namely 1, 10^2, and 10^4.

Let $\theta\, J_m^n\, u_m^{n+1} + \theta\, \frac{u_{m-1}^{n+1} - 2\,u_m^{n+1} + u_{m+1}^{n+1}}{h^2} = z_m^{n+1}$. The Equation (109) becomes

$$z_m^{n+1} = \theta\, J_m^n\, u_m^n - (1-\theta)\, \frac{u_{m-1}^n - 2\,u_m^n + u_{m+1}^n}{h^2} + \frac{u_m - u_m^n}{k} - u_m^n(1-u_m^n) \tag{110}$$

which only accounts for reaction and diffusion processes and whose solutions depend on the sign of J_m^n. We have therefore the solution of Equation (110) subject to the condition (Equation 102) gives the solution in form of:

a) If $J_m^n = 0$

$$u_{m-1} - \left(2 + \frac{h^2}{k}\right) u_m + u_{m+1} = -\frac{h^2}{k}(u_m^n + k\, u_m^n\,(1-u_m^n)),\quad t^n < t < t^{n+1}. \tag{111}$$

b) If $J_m^n = -(\lambda_m)^2 < 0$

$$u_{m-1} - \frac{2 + (k\,J_m^n - 1)(e^{-\lambda_m h} + e^{\lambda_m h})}{k\,J_m^n}\, u_m + u_{m+1} = \frac{2 - (e^{-\lambda_m h} + e^{\lambda_m h})}{k\,J_m^n} [-u_m + k\,(J_m^n\, u_m - u_m^n\,(1-u_m^n))],\quad t^n < t < t^{n+1}. \tag{112}$$

c) If $J_m^n = (\lambda_m)^2 > 0$

$$u_{m-1} - 2\frac{1 + (k\,J_m^n - 1)cos(\lambda_m\,h)}{k\,J_m^n}\,u_m + u_{m+1} = 2\frac{1 - (cos(\lambda_m\,h)}{k\,J_m^n}\,[-u_m + k\,(J_m^n\,u_m - u_m^n\,(1 - u_m^n))],$$
$$t^n < t < t^{n+1}. \tag{113}$$

REMARK 2. *The quasilinear full exponential corresponds to the iterative solution of*

$$\theta\,J_m^i\,u_m^{n+1} + \theta\,\frac{u_{m-1}^{n+1} - 2\,u_m^{n+1} + u_{m+1}^{n+1}}{h^2} = \theta\,J_m^n\,u_m^n$$
$$-(1-\theta)\,\frac{u_{m-1}^n - 2\,u_m^n + u_{m+1}^n}{h^2} + \frac{u_m - u_m^n}{k}$$
$$-(1-\theta)\,u_m^n(1-u_m^n) - \theta\,u_m^i\,(1-u_m^i) \tag{114}$$

for $i = 1,\ 2\ \cdots\ n-1$, have analogous solutions to those reported in time-linearized exponential techniques Section 7.1.2.

REMARK 3. *The principal primacy of the full exponential techniques is that they reckon for the reaction, diffusion, and transient terms in finding the homogeneous solution of Equation (103). Notwithstanding, this technique also has the disadvantage that the time step cannot be chosen carelessly because, if $k \ll \frac{1}{\theta\,J_i^n}$ then the reaction terms do not influence the values of λ_m despite the fact that they do influence the particular solution of Equation (103) through z_m^{n+1}. On top of that, the portion of the transient term influences the ordinary differential operator and, therefore, the homogeneous solution, though the other part influences the particular solution. These obstacles are fully suppressed with the exponential techniques displayed in the time-linearized exponential techniques and the quasilinear full exponential in Section 7.1.2.*

THEOREM 5. *Ramos [25]. The schemes displayed in Equations (100) and (101) are convergent and convergence is reached when*

$$(e_m^n)^2 = \frac{1}{N}\sum_{j=1}^{N}(u_j^{i+1} - u_j^i)^2 \le 10^{-|\alpha|} \tag{115}$$

where $i = 1,\ 2\ \cdots n$ and $|\alpha|$ is an integer obtained from numerical computation, N denotes the number of grid points, and e_m^n is the error which is defined by $e_m^n = u_m^n - v_m^n$.

Proof. The full proof of this theorem is detailed in Ramos [25].

8. NUMERICAL RESULTS

The stability region of FTCS is $k \le \frac{h^2}{2}$. For $h = 0.01$, we obtain $k \le 5 \times 10^{-5}$. In the case of NSFD, the condition for positivity gives $\phi(k) \le \frac{h^2}{2}$ where $\phi(k) = \frac{1-e^{\lambda\,k}}{\lambda}$. We tabulate L_1 and L_∞ errors at certain values of k using $\rho = 1$, $h = 0.01$, at time, $T_{max} = 2.5 \times 10^{-3}$ using FTCS, NSFD, and EEFD schemes at certain various values of time-step size as chosen from $T_{max}/52$, $T_{max}/100$, $T_{max}/200$, $\cdots$, $T_{max}/1{,}800$, $T_{max}/1{,}900$ and $T_{max}/2{,}000$. The errors are shown in **Table 1**.

TABLE 4 | Rate of convergence in time for FTCS using different values of ρ at time, $T_{max} = 2.5 \times 10^{-3}$ with $h = 0.01$.

Values of ρ	Values of k	Rate of convergence in time using L_1	Rate of convergence in time using L_∞ error
1	$T_{max}/100$		
	$T_{max}/200$	0.9309	0.9332
	$T_{max}/400$	0.8705	0.8746
	$T_{max}/800$	0.7714	0.7776
10^2	$T_{max}/100$		
	$T_{max}/200$	0.9736	0.9433
	$T_{max}/400$	0.9492	0.8924
	$T_{max}/800$	0.9034	0.8012
10^4	$T_{max}/100$		
	$T_{max}/200$	0.9820	0.8075
	$T_{max}/400$	1.2094	1.1631

TABLE 5 | Rate of convergence in time for NSFD using different values of ρ at time, $T_{max} = 2.5 \times 10^{-3}$ with $h = 0.01$.

Values of ρ	Values of k	Rate of convergence in time using L_1	Rate of convergence in time using L_∞ error
1	$T_{max}/100$		
	$T_{max}/200$	0.9561	0.9585
	$T_{max}/400$	0.9159	0.9202
10^2	$T_{max}/100$		
	$T_{max}/200$	0.9284	0.9090
	$T_{max}/400$	0.8681	0.8167
10^4	$T_{max}/100$		
	$T_{max}/200$	0.9769	0.7702

TABLE 6 | Rate of convergence in time for EEFD using different values of ρ at time, $T_{max} = 2.5 \times 10^{-3}$ with $h = 0.01$.

Values of ρ	Values of k	Rate of convergence in time using L_1	Rate of convergence in time using L_∞ error
1	$T_{max}/100$		
	$T_{max}/200$	1.1030	1.0795
	$T_{max}/400$	1.2306	1.1727
10^2	$T_{max}/100$		
	$T_{max}/200$	1.0384	1.0091
	$T_{max}/400$	1.0789	1.0162
	$T_{max}/800$	1.1714	1.0176
10^4	$T_{max}/100$		
	$T_{max}/200$	0.4317	0.4388

In the case of FTCS, NSFD, minimum L_1, and L_∞ errors occur at $k = T_{max}/2{,}000$ while in the case of EEFD, the errors are least $k = T_{max}/1{,}600$. The least error is of order 10^{-9} and 10^{-10} in the case of NSFD and FTCS respectively while the least error is of order 10^{-11} in the case of EEFD. EEFD is a better scheme than FTCS at all values of k used.

We obtain values for L_1 and L_∞ errors at certain values of k using $\rho = 10^2$, $h = 0.01$, at time, $T_{max} = 2.5 \times 10^{-3}$ using the three methods in **Table 2**. The schemes behave differently. In all the three methods FTCS, NSFD, and EEFD, the L_1 and L_∞ errors keep on decreasing as the values of k are decreased gradually from $k = T_{max}/52$ to $k = T_{max}/2{,}000$.

L_1 and L_∞ errors for the third case using $\rho = 10^4$, $h = 0.01$ are displayed in **Table 3**. Again, the schemes behave differently from each other. Optimal k using FTCS occurs when $k \approxeq T_{max}/1{,}300$. The optimal k using NSFD and EEFD are $k \approxeq T_{max}/1{,}500$ and $k \approxeq T_{max}/2{,}000$, respectively. Once that optimal is reached the error starts increasing again. The least L_1 and L_∞ errors using NSFD are 4.5235×10^{-4} and 4.5623×10^{-3}. The corresponding errors are 1.9347×10^{-4} and 2.3239×10^{-3} when FTCS is used. In the case of EEFD, least L_1 is 6.9852×10^{-3} and least L_∞ is 8.3399×10^{-2}.

We obtain plots of numerical solution vs. x at time, $T_{max} = 2.5 \times 10^{-3}$ using three methods FTCS, NSFD, and EEFD in **Figure 1**.

9. CONCLUSION

We have investigated in this paper the spectral analysis and optimal step sizes for some finite difference methods discretising Fisher's equation. We used three methods namely; FTCS, NSFD, and EEFD in order to solve Fisher's equation with a coefficient of reaction being 10, 10^2, and 10^4. We studied the properties of the methods such stability, positivity, and boundedness. This is the one of rare article which includes the estimate errors for the methods studied. Numerical results are displayed at optimal time step size with $h = 0.01$ for the three cases for the three methods used. We also obtained numerically the rate of convergence as shown in **Tables 4–6**. We have shown from **Tables 1–3** that all the three methods (FTCS, NSFD, and EEFD) perform well for the small coefficient of reaction. It is worthy mentioning that freezing coefficient technique with Von Neumann Stability Analysis only present an approximate stability region for standard methods discretising non linear partial differential equations which might give reason to the standard method in **Table 1** to perform better than the NSFD. Furthermore the NSFD in regard to the discrete representation derivative in Mickens [39] rule has nontrivial denominator function and make use of positivity and boundedness conditions. Finally the results are dependent on initial conditions used. For $\rho = 1$, the difference in L_1 and L_∞ errors from the three methods is very small which lead to conclude that the best methods are FTCS and NSFD. Also for $\rho = 10^2$ and $\rho = 10^4$, the best method are EEFD and NSFD, respectively. Our results matched with the one found in Lubuma and Roux [47] for numerical experiment for small reaction term. Moreover, Lubuma and Roux [47] proved that NSFD is elementary stable. As NSFD methods, the EEFD displayed in this article do not require any knowledge of the exact solution of the differential equation. Contrast to that, the best finite difference scheme is stable for large grid sizes but costly in inaccuracies at the propagation front.

DATA AVAILABILITY STATEMENT

The original contributions presented in the study are included in the article/supplementary material, further inquiries can be directed to the corresponding author/s.

AUTHOR CONTRIBUTIONS

The plan of the paper was prepared by AA. The coding was done by KA and BI. All authors helped in writing the manuscript, contributed to the article, and approved the submitted version.

FUNDING

KA is supported by Postdoctoral Research Fellowship (PDRF) from North-West University (Source of funding: NWU PDRF Fund NW.1G01487). AA is supported by Nelson Mandela University for this research.

ACKNOWLEDGMENTS

KA is grateful to the North-West University for the Postdoctoral Research Fellowship (PDRF). AA thank Nelson Mandela University for the financial support. Finally, all the authors are grateful to the two reviewers who provided feedback which enabled to improve the paper considerably.

REFERENCES

1. Gardner CS, Greene JM, Kruskal MD, Miura RM. Method for solving the Korteweg-de Vries equation. *Front Neurosci Phys Rev Lett*. (1967) 19:1095. doi: 10.1103/PhysRevLett.19.1095
2. Weiss J, Tabor M, Carnevale G. The Painlevé property for partial differential equations. *J Math Phys*. (1983) 155:522–6. doi: 10.1063/1.525721
3. Kudryashov NA. On types of nonlinear nonintegrable equations with exact solutions. *Phys Lett A*. (1991) 24:269–75. doi: 10.1016/0375-9601(91)90481-M
4. Lou SY, Huang GX, Ruan HY. Exact solitary waves in a convecting fluid. *J Phys A Math Gen*. (1991) 24:L587. doi: 10.1088/0305-4470/24/11/003
5. Kudryashov NA. Exact solutions of a family of Fisher equations. *Theor Math Phys*. (1993) 94:211–218. doi: 10.1007/BF01019332
6. Kudryashov NA. Numerical convective schemes based on accurate computation of space derivatives. *J Comput Phys*. (1973) 13:100–13. doi: 10.1016/0021-9991(73)90128-9
7. Cooley JW, Lewis P, Welch P. The finite Fourier transform. *IEEE Trans Audio Electroacoust*. (1969) 17:77–85. doi: 10.1109/TAU.1969.1162036

8. Gazdag J, Canosa J. Numerical solution of Fisher's equation. *J Appl Probab*. (1974) 11:445–57. doi: 10.2307/3212689
9. Fisher RA. The wave of advance of advantageous genes. *Ann Hum Genet*. (1937) 17:355–69. doi: 10.1111/j.1469-1809.1937.tb02153.x
10. Moran PAP. *The Statistical Processes of Evolutionary Theory*. Oxford: Clarendon Press; Oxford University Press (1962).
11. Kendall DG. *A Form of Wave Propagation Associated With the Equation of Heat Conduction*. Cambridge: Cambridge University Press (1948).
12. Kolmogorov AN. Étude de l'équation de la diffusion avec croissance de laquantité de matière et son application à un problème biologique. *Bull Univ Moskow Ser Internat A*. (1937) 1:1–25.
13. Canosa J. On a nonlinear diffusion equation describing population growth. *IBM J Res Dev*. (1937) 17:307–13. doi: 10.1147/rd.174.0307
14. Jeffrey A, Kakutani T. Weak nonlinear dispersive waves: a discussion centered around the Korteweg-de Vries equation. *Siam Rev SIAM*. (1972) 14:582–643. doi: 10.1137/1014101
15. Kudryashov NA, Zakharchenko AS. A note on solutions of the generalized Fisher equation. *Appl Math Lett*. (2014) 32:53–6. doi: 10.1016/j.aml.2014.02.009
16. Newman TJ, Kolomeisky EB, Antonovics J. Population dynamics with global regulation: the conserved Fisher equation. *Phys Rev Lett*. (2004) 92:228103. doi: 10.1103/PhysRevLett.92.228103
17. Chen BM, Kojouharov HV. Non-standard numerical methods applied to subsurface biobarrier formation models in porous media. *Bull Math Biol*. (1999) 61:779–98. doi: 10.1006/bulm.1999.0113
18. Yatat V, Couteron P, Dumont Y. Spatially explicit modelling of tree-grass interactions in fire-prone savannas: a partial differential equations framework. *Ecol Complex*. (2018) 36:290–313. doi: 10.1016/j.ecocom.2017.06.004
19. Wang XY. Exact and explicit solitary wave solutions for the generalised Fisher equation. *Phys Lett A*. (1988) 131:277–9. doi: 10.1016/0375-9601(88)90027-8
20. Chandraker V, Awasthi A, Jayaraj S. A numerical treatment of Fisher equation. *Procedia Eng*. (2015) 131:1256–62. doi: 10.1016/j.proeng.2015.11.481
21. Ismail HN, Raslan K, Rabboh AAA. Adomian decomposition method for Burger's-Huxley and Burger's-Fisher equations. *Appl Math Comput*. (2004) 159:291–301. doi: 10.1016/j.amc.2003.10.050
22. Moghimi M, Hejazi FSA. Variational iteration method for solving generalized Burger-Fisher and Burger equations. *Chaos Solitons Fractals*. (2007) 33:1756–61. doi: 10.1016/j.chaos.2006.03.031
23. Fahmy ES. Travelling wave solutions for some time-delayed equations through factorizations. *Chaos Solitons Fractals*. (2008) 38:1209–16. doi: 10.1016/j.chaos.2007.02.007
24. Mickens RE. Relation between the time and space step-sizes in nonstandard finite-difference schemes for the Fisher equation. *Numer Methods Partial Differ Equ*. (1997) 13:51–5. doi: 10.1002/(SICI)1098-2426(199701)13:1<51::AID-NUM4>3.0.CO;2-L
25. Ramos JI. Exponential methods for one-dimensional reaction-diffusion equations. *Math Methods Appl Sci*. (2005) 170:380–98. doi: 10.1016/j.amc.2004.12.003
26. Anguelov R, Kama P, Lubuma JMS. On non-standard finite difference models of reaction-diffusion equations. *J Comput Appl Math*. (2005) 175:11–29. doi: 10.1016/j.cam.2004.06.002
27. Hagstrom T, Keller HB. The numerical calculation of traveling wave solutions of nonlinear parabolic equations. *SIAM J Scientific Stat Comput*. (1986) 7:978–88. doi: 10.1137/0907065
28. Li S, Petzold L, Ren Y. Stability of moving mesh systems of partial differential equations. *SIAM J Scientific Comput*. (1998) 20:719–38. doi: 10.1137/S1064827596302011
29. Kudryashov NA. One method for finding exact solutions of nonlinear differential equations. *Commun Nonlinear Sci Numer Simulat*. (2012) 17:2248–53. doi: 10.1016/j.cnsns.2011.10.016
30. Polyanim AD, Zaitsev ZF. *Handbook of Nonlinear Partial Differential Equations. 2nd ed*. Chapman and Hall/CRC Press. (2011). p. 1912.
31. Qiu Y, Sloan DM. Numerical solution of Fisher's equation using a moving mesh method. *J Comput Phys*. (1998) 146:726–746. doi: 10.1006/jcph.1998.6081
32. Miyata T, Sakai Y. Vectorized total variation defined by weighted L infinity norm for utilizing inter channel dependency. In: *2012 19th IEEE International Conference on Image Processing*. Orlando, FL: IEEE (2012).
33. Sutton OJ. Long time $L^{\infty}(L^2)$ a posteriori error estimates for fully discrete parabolic problems. *arXiv[Preprint].arXiv:180303207*. (2018). doi: 10.1093/imanum/dry078
34. Chen-Charpentier BM, Kojouharov HV. An unconditionally positivity preserving scheme for advection-diffusion reaction equations. *Math Comput Model*. (2013) 57:2177–85. doi: 10.1016/j.mcm.2011.05.005
35. Agbavon K, Appadu A, Khumalo M. On the numerical solution of Fisher's equation with coefficient of diffusion term much smaller than coefficient of reaction term. *Adv Diff Equat*. (2019) 2019:1–33. doi: 10.1186/s13662-019-2080-x
36. Durran DR. *Numerical Methods for Fluid Dynamics (With Applications to Geophysics)*. Springer Science & Business Media (2010).
37. Taha TR, Ablowitz MI. Analytical and numerical aspects of certain nonlinear evolution equations, III. Numerical, Korteweg-de Vries equation. *J Comput Phys*. (1984) 55:231–53. doi: 10.1016/0021-9991(84)90004-4
38. Zabusky NJ, Kruskal MD. Interaction of solitons in a collisionless plasma and the recurrence of initial states. *Phys Rev Lett*. (1965) 15:240. doi: 10.1103/PhysRevLett.15.240
39. Mickens RE. Dynamic consistency: a fundamental principle for constructing nonstandard finite difference schemes for differential equations. *J Diff Equat Appl*. (2005) 11:645–53. doi: 10.1080/102361904123313 34527
40. Kumar Verma A, Kayenat S. On the stability of Micken's type NSFD schemes for generalized Burgers Fisher equation. *Chaos Solitons Fractals*. (2019) 25:1706–37. doi: 10.1080/10236198.2019.1689236
41. Bhattacharya MC. An explicit conditionally stable finite difference equation for heat conduction problems. *Int J Numer Methods Eng*. (1985) 21:239–65. doi: 10.1002/nme.1620210205
42. Handschuh RF, Keith TG. Applications of an exponential finite-difference technique. *Numer Heat Transfer A Appl*. (1992) 22:363–78. doi: 10.1080/10407789208944773
43. Ĭnan B, Bahadı r AR. An explicit exponential finite difference method for the Burger's equation. *Eur Int J Sci Technol*. (2013) 2:61–72.
44. Ĭnan B, Bahadı r AR. Finite difference methods for the generalized Huxley and Burgers-Huxley equations. *Kuwait J Sci*. (2017) 44:20–7.
45. Macías-Díaz JE, Ĭnan B. Numerical efficiency of some exponential methods for an advection-diffusion equation. *Int J Comput Math*. (2019) 96:1005–29. doi: 10.1080/00207160.2018.1478416
46. Inan B, Osman M, Ak T, Baleanu D. Analytical and numerical solutions of mathematical biology models: the newell-whitehead-segel and allen-cahn equations. *Math Methods Appl Sci*. (2020) 43:2588–600. doi: 10.1002/mma.6067
47. Lubuma J, Roux A. An improved theta-method for systems of ordinary differential equations. *J Diff Equat Appl*. (2003) 9:1023–35. doi: 10.1080/1023619031000146904

Conflict of Interest: The authors declare that the research was conducted in the absence of any commercial or financial relationships that could be construed as a potential conflict of interest.

frontiers | Frontiers in Applied Mathematics and Statistics

TYPE Original Research
PUBLISHED 04 November 2022
DOI 10.3389/fams.2022.1001392

OPEN ACCESS

EDITED BY
Ramoshweu Solomon Lebelo,
Vaal University of Technology,
South Africa

REVIEWED BY
Hira Soomro,
Universiti Teknologi Petronas, Malaysia
Xinyou Meng,
Lanzhou University of
Technology, China

*CORRESPONDENCE
Nabeela Anwar
19036109-002@uog.edu.pk

SPECIALTY SECTION
This article was submitted to Mathematical Biology, a section of the journal Frontiers in Applied Mathematics and Statistics

RECEIVED 23 July 2022
ACCEPTED 28 September 2022
PUBLISHED 04 November 2022

CITATION
Anwar N, Naz S and Shoaib M (2022) Reliable numerical treatment with Adams and BDF methods for plant virus propagation model by vector with impact of time lag and density. *Front. Appl. Math. Stat.* 8:1001392. doi: 10.3389/fams.2022.1001392

Reliable numerical treatment with Adams and BDF methods for plant virus propagation model by vector with impact of time lag and density

Nabeela Anwar[1]*, Shafaq Naz[1] and Muhammad Shoaib[2]

[1]Department of Mathematics, University of Gujrat, Gujrat, Pakistan, [2]Department of Mathematics, Commission on Science and Technology for Sustainable Development in the South University Islamabad, Attock, Pakistan

Plant disease incidence rate and impacts can be influenced by viral interactions amongst plant hosts. However, very few mathematical models aim to understand the viral dynamics within plants. In this study, we will analyze the dynamics of two models of virus transmission in plants to incorporate either a time lag or an exposed plant density into the system governed by ODEs. Plant virus propagation model by vector (PVPMV) divided the population into four classes: susceptible plants [$S(t)$], infectious plants [$I(t)$], susceptible vectors [$X(t)$], and infectious vectors [$Y(t)$]. The approximate solutions for classes $S(t)$, $I(t)$, $X(t)$, and $Y(t)$ are determined by the implementation of exhaustive scenarios with variation in the infection ratio of a susceptible plant by an infected vector, infection ratio of vectors by infected plants, plants' natural fatality rate, plants' increased fatality rate owing to illness, vectors' natural fatality rate, vector replenishment rate, and plants' proliferation rate, numerically by exploiting the knacks of the Adams method (ADM) and backward differentiation formula (BDF). Numerical results and graphical interpretations are portrayed for the analysis of the dynamical behavior of disease by means of variation in physical parameters utilized in the plant virus models.

KEYWORDS

plant virus propagation model by vector (PVPMV), Adams method (ADM), backward differentiation formula (BDF), ordinary differential equations (ODEs), virus transmission, time lag

Introduction

Plants provide food for humans and many other animals. They also provide medicines, clothing fibers, and are necessary for a healthy atmosphere. Plants, on the other hand, are susceptible to diseases, which are mostly triggered by viruses. The plant is frequently killed by these viruses. As a result, virus-related crop losses cost billions of dollars annually. Virus propagation is primarily carried out by a vector; insects which bite infectious plants become infected and subsequently infect susceptible plants. Seasonal behavior is common among insect vectors. They are most active throughout the summer and almost nearly dormant during the winter. Chemical pesticides are

often employed as a control to battle vectors. Regrettably, these chemicals are not only overpriced, but they are also harmful to humans, animal life, as well as environment. Another option is to introduce a predator species, or just boost the population of one that already exists, to predate upon the insects as well as limit the virus's transmission. The vector population can be controlled with a combination of pesticides and predators. An effective mathematical model can be exploited to study the dynamics of pathogenic plant diseases. Indeed, mathematical analysis and numerical simulations are quite valuable in comprehending the dynamics of plant disease propagation and evaluating the impact of various disease control techniques.

Several mathematical models have been established to provide a detailed exposition of how to analyze, interpret, and forecast plant pathogenic farming epidemics as a mechanism for formulating and testing crop countermeasures and control measures [1–4]. A variety of epidemiology models based upon those used mostly in animal or human epidemiology have been created to assess the population ecosystem of viral infections [5–10]. The delay differential equations can be used to define relatively different formulations of epidemic proliferation. The application of delayed differential equations in epidemiological studies extends back to Van Der Plank's pioneering work [11], when these models were first proposed to represent plant diseases. The work of Van Der Plank seemed to have a limited impact on epidemic models, owing to the model hypotheses being particularly specific to plant pathology. However, a version of the Van Der Plank model has been shown to be well-suited to characterize human/animal diseases [12]. Stella et al. investigated the dynamics of the plant epidemic model and the presence and stability of distinct model equilibria. In the absence of delay, the Routh-Hurwitz criterion is employed to assess the stability of the disease free and epidemic equilibrium. In the existence of delay, the stability of epidemic equilibrium is also studied [13]. The bifurcation modulation of a fractional mosaic virus infectious disease model of Jatropha curcas with agricultural understanding and an executing delay was examined by Liu et al. Hopf bifurcation generated by the executing delay is explored for the unconstrained system by examining the corresponding characteristic equation [5]. Basir et al. developed a mathematical model that included multiple time delays as well as a Holling type-II functioning responses. The basic reproductive number and delays in time are used to determine the presence and stability of the equilibria. The delayed system's cost-effectiveness was assessed using the optimal control theory [14]. Ray et al. proposed a mathematical model to analyze

TABLE 1 Description and default parameters setting of for non-linear PVPMV [25].

Parameters	Description	Value
N	Total density of plants	100
γ	Rate of infection of a susceptible plant by an infected vector	0.01
γ_1	Infection ratio of vectors by infected plants	0.01
υ	Plants' natural fatality rate	0.1
r	Vectors' natural fatality rate	0.2
Ω	Vector replenishment rate	10
c	Plants' increased fatality rate owing to illness	0.1
m	Plants' proliferation rate	5
δ	Time delay	2

TABLE 2 Scenarios for model A and model B of non-linear PVPMV.

	Model A	Model B
Scenario 1 for the rate of infection of a susceptible plant by an infected vector		
C-1	$\gamma = 0.001$	$\gamma = 0.001$
C-2	$\gamma = 0.004$	$\gamma = 0.004$
C-3	$\gamma = 0.006$	$\gamma = 0.006$
C-4	$\gamma = 0.007$	$\gamma = 0.007$
C-5	$\gamma = 0.009$	$\gamma = 0.009$
	Model A	**Model B**
Scenario 2 for the rate at which an infected plant infects a susceptible vector		
C-1	$\gamma_1 = 0.001$	$\gamma_1 = 0.001$
C-2	$\gamma_1 = 0.002$	$\gamma_1 = 0.002$
C-3	$\gamma_1 = 0.003$	$\gamma_1 = 0.003$
C-4	$\gamma_1 = 0.004$	$\gamma_1 = 0.004$
C-5	$\gamma_1 = 0.005$	$\gamma_1 = 0.005$
	Model A	**Model B**
Scenario 3 for disease's additional fatality rate		
C-1	$c = 0.1$	$c = 0.1$
C-2	$c = 0.2$	$c = 0.2$
C-3	$c = 0.3$	$c = 0.3$
C-4	$c = 0.4$	$c = 0.4$
C-5	$c = 0.5$	$c = 0.5$
	Model A	**Model B**
Scenario 4 for the plants' natural fatality rate		
C-1	$r = 0.1$	$r = 0.1$
C-2	$r = 0.2$	$r = 0.2$
C-3	$r = 0.3$	$r = 0.3$
C-4	$r = 0.4$	$r = 0.4$
C-5	$r = 0.6$	$r = 0.6$
	Model A	**Model B**
Scenario 5: υ plants' natural fatality rate for model A, Ω vector replenishment rate for model B		
C-1	$\upsilon = 0.1$	$\Omega = 10$
C-2	$\upsilon = 0.2$	$\Omega = 100$
C-3	$\upsilon = 0.3$	$\Omega = 110$
C-4	$\upsilon = 0.4$	$\Omega = 210$
C-5	$\upsilon = 0.5$	$\Omega = 250$

the dynamics that included the incubation period as a time delay component for the vector-borne plant epidemic. The occurrence and stability of equilibrium have been investigated based on the reproduction number. Hopf bifurcation causes stability variations in the delaying and non-delaying systems [15]. Abraha et al. studied a mathematical model that included two time delays in agricultural pest management as well as the effect of farmer awareness. They assumed that the number of healthy parasites in the particular crop is proportionate to the growth of self-aware individuals. A saturation term is used to model the effects of awareness. The basic reproductive number, as well as time delays, are used to determine the presence and stability of the equilibrium. Whenever time delays reach the optimum values, stability transitions occur due to Hopf-bifurcation. The delayed system's cost-effectiveness was analyzed using adaptive control theory [16]. Phan et al. designed a system of differential equations including delay to represent the cell-to-cell propagation of infection by cereal and barley yellow dwarf pathogens throughout the plant. The model may capture a broad range of biologically pertinent phenomena through disease-free, epidemic, bilateral mortality equilibria, and a persistent periodical orbit by including a ratio-dependent incident function and logistic proliferation of healthy cells [17]. Blyuss et al. developed and analyzed a mathematical model for controlling the mosaic disease with natural microbiological biostimulants that, in addition to promoting plant development, also protect plants from infection *via* an RNA interference mechanism. They revealed how characteristics of biostimulants affect disease dynamics, and in particular, how they determine whether the mosaic disease is eliminated or preserved at a consistent level, by measuring the resilience of the system's equilibria [18]. Alemneh et al. introduced and assessed/analyzed an eco-epidemiological model of maize streak virus infection dynamics in order to evaluate the optimal strategy for preserving maize populations from the disease. To obtain an optimum controlling strategy, they applied the Pontryagin's maximum criterion to derive the Hamiltonian, control characterization, adjoint variables and the optimization system [19]. Amelia et al. presented a mathematical model of the yellow virus's spread in red chili plants, using the logistical function to predict the increase of insects as disease vectors. By calculating the dominating eigenvalue of the next generational matrix, we may determine the value of the fundamental reproduction number namely R_0 of the model [20]. Kendig et al. investigated a mathematical model

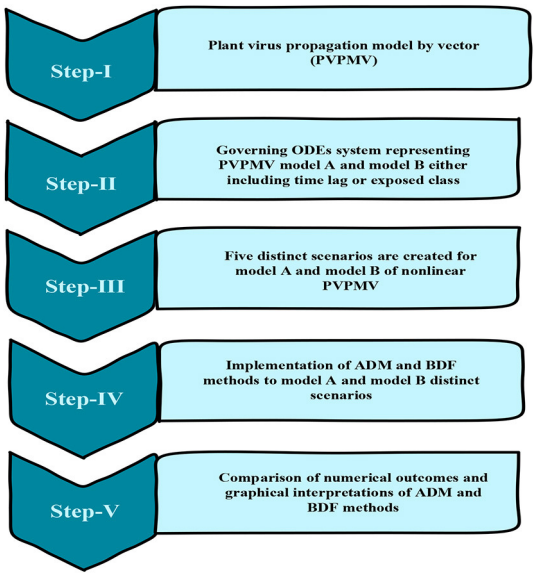

FIGURE 1
Working procedure of design approach for non-linear PVPMV.

TABLE 3 Numerical outcomes of non-linear PVPMV model A for case-1 of scenario 2.

Time (Days)	ADM Case 1				BDF Case 1			
	S	*I*	*X*	*Y*	*S*	*I*	*X*	*Y*
0	90.0000	10.0000	47.0000	47.0000	90.0000	10.0000	47.0000	47.0000
3	46.2099	53.7901	44.1326	30.5029	45.8928	54.1072	44.0134	30.1343
6	44.9054	55.0946	41.4564	22.0639	45.0189	54.9811	41.3998	21.8527
9	49.4698	50.5302	40.4576	16.9624	49.6415	50.3585	40.4446	16.8286
12	54.5650	45.4350	40.4169	13.6554	54.7283	45.2717	40.4251	13.5665
15	59.1522	40.8478	40.8143	11.4206	59.2932	40.7068	40.8314	11.3592
18	63.0405	36.9595	41.3740	9.8525	63.1582	36.8418	41.3936	9.8086
21	66.2645	33.7355	41.9611	8.7120	66.3616	33.6384	41.9803	8.6795
24	68.9206	31.0794	42.5148	7.8546	69.0006	30.9994	42.5323	7.8298
27	71.1121	28.8878	43.0115	7.1912	71.1783	28.8217	43.0270	7.1718
30	72.9859	27.0141	43.4595	6.6495	72.9307	27.0692	43.4460	6.6652

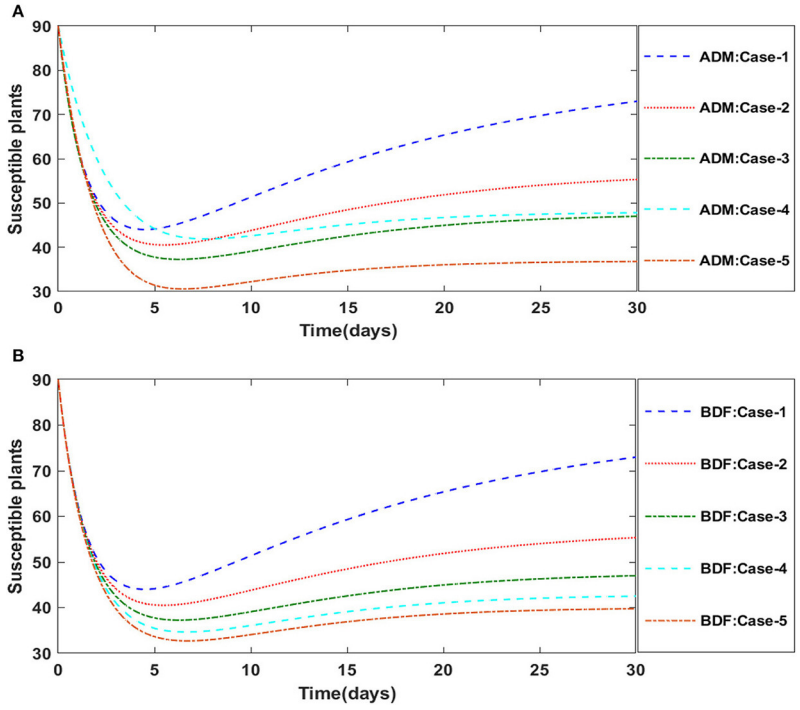

FIGURE 2
(A) Dynamics of susceptible plants for the varition in γ_1 using ADM for model A. **(B)** Dynamics of susceptible plants for the varition in γ_1 using BDF for model A.

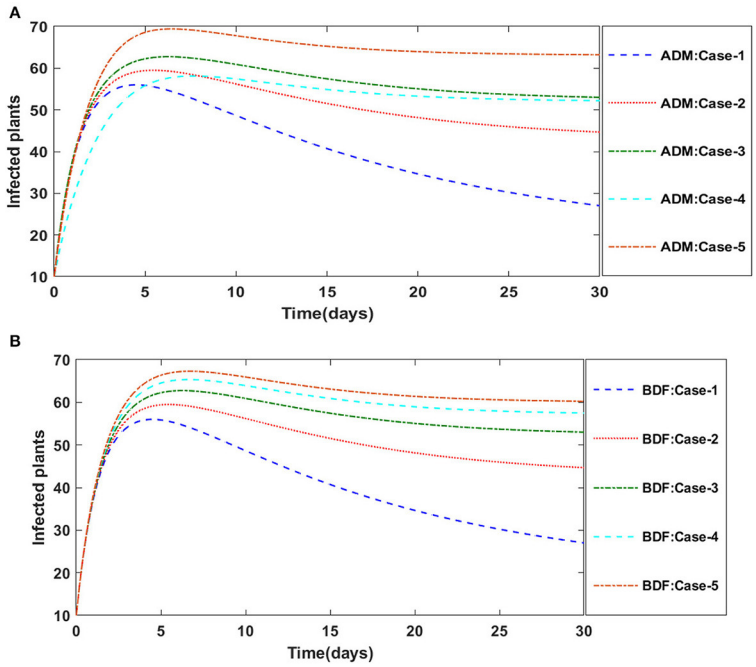

FIGURE 3
(A) Dynamics of infected plants for the varition in γ_1 using ADM for model A. **(B)** Dynamics of infected plants for the varition in γ_1 using BDF for model A.

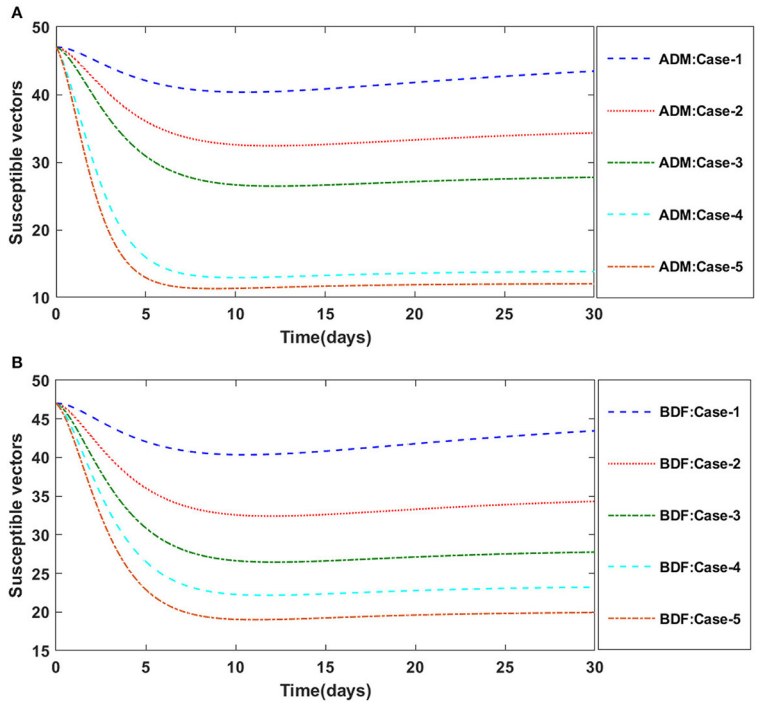

FIGURE 4
(A) Dynamics of susceptible vectors for the varition in γ_1 using ADM for model A. **(B)** Dynamics of susceptible vectors for the varition in γ_1 using BDF for model A.

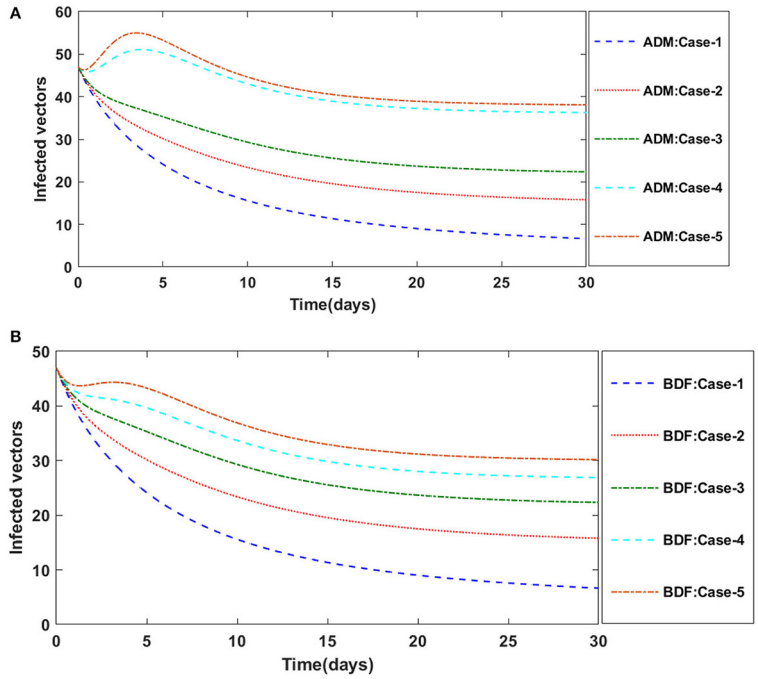

FIGURE 5
(A). Dynamics of infected vectors for the varition in γ_1 using ADM for model A. **(B)** Dynamics of infected vectors for the varition in γ_1 using BDF for model A.

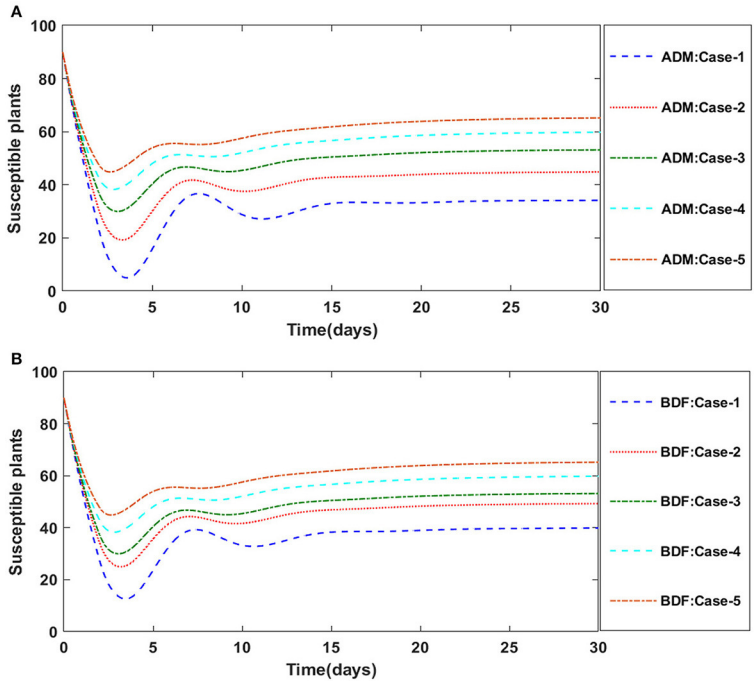

FIGURE 6
(A) Dynamics of susceptible plants for the varition in υ using ADM for model A1. **(B)** Dynamics of susceptible plants for the varition in υ using BDM for model A1.

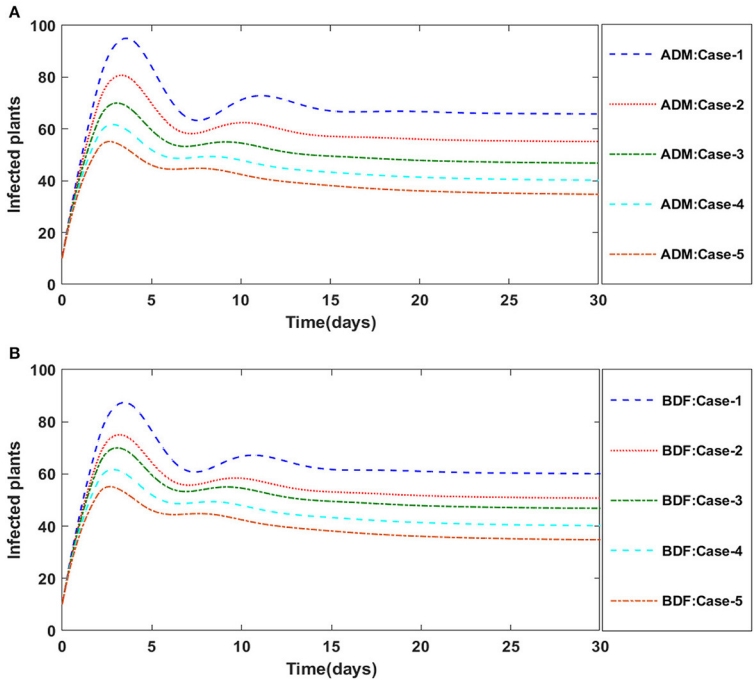

FIGURE 7
(A) Dynamics of infected plants for the varition in υ using ADM for model A1. **(B)** Dynamics of infected plants for the varition in υ using BDF for model A1.

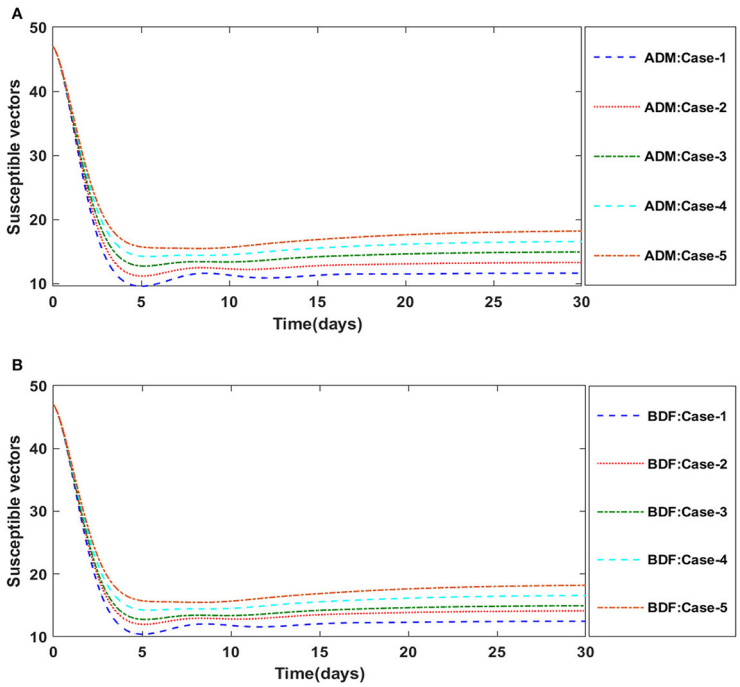

FIGURE 8
(A) Dynamics of infected plants for the varition in υ using ADM for model A1. **(B)** Dynamics of infected plants for the varition in υ using BDF for model A1.

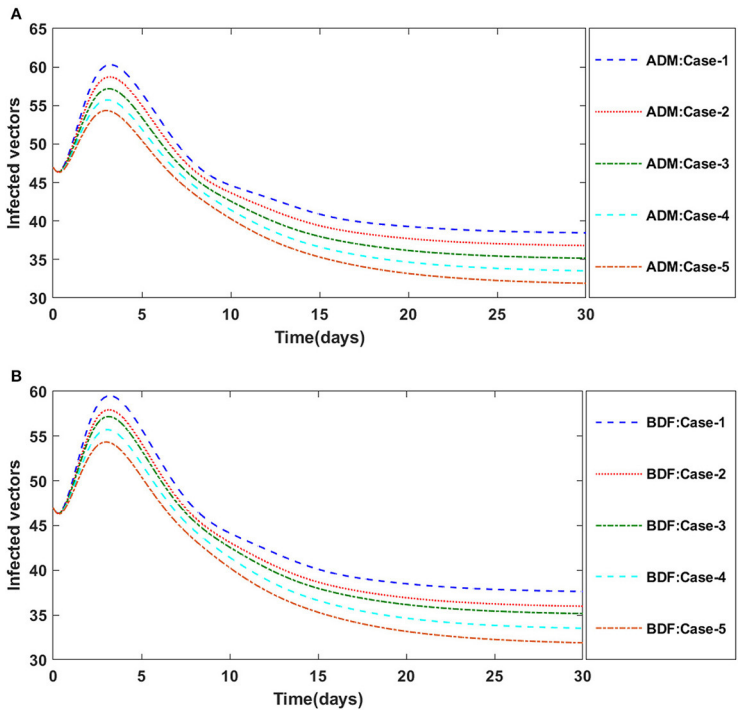

FIGURE 9
(A) Dynamics of susceptible vectors for the varition in r using ADM for model A1. **(B)** Dynamics of susceptible vectors for the varition in r using BDF for model A1.

depicting the propagation of two viruses in a plant density, parameterized assuming empirically determined transmitting values, and discovered that nutrient pathogen communication could influence disease transmission. Thus, epidemic dynamics were regulated by interactions that affected propagation through viral density-independent pathways [21]. Shaw et al. compared the model based on individual and ordinary differential equation mathematical models to investigate the impact of insect vector living cycle and behavioral factors on the transmission of vector borne plant viruses. They discovered that evacuating virus infected species proved more effective than removing vector-infested species in terms of reducing infection [22]. The interactions within the plants, vectors and predators were described by Charpentier et al. using a system of ordinary differential equations. They used direct and indirect approaches to find the controls that minimize the optimization function subjected to population factors [23]. Jittamai et al. presented a mathematical framework to analyze the dynamics for Cassava Mosaic Virus, which is accelerated by both contaminated cuttings plantings and whitefly propagation. The model was used by the authors to determine the optimal cost-effective disease control strategy [24]. Charpentier recently presented two plant virus propagation models to illustrate the two perspectives of incorporating the delays. He numerically studied the models' stability [25].

Numerical techniques are generally employed in science as well as engineering to solve mathematical problems where exact solutions are difficult or impossible to obtain. Analytical solutions are only possible for a limited differential equation. For solving ordinary differential equations, there are a variety of analytical approaches. Even though, there are many ordinary differential equations (ODEs) whose solutions can be obtained in closed form using known analytical techniques, necessitating the progression and application of numerical methods in order

TABLE 4 Numerical outcomes of non-linear PVPMV model A1 for case-1 of scenario 5.

Time (Days)	ADM Case 1				BDF Case 1			
	S	*I*	*X*	*Y*	*S*	*I*	*X*	*Y*
0	90.000	10.0000	47.0000	47.0000	90.0000	10.0000	47.0000	47.0000
3	7.253847	92.7462	13.9510	60.1967	13.8285	86.1715	14.7278	59.4199
6	28.1173	71.8826	10.0509	53.2016	33.6215	66.3785	10.7929	52.4597
9	32.5847	67.4153	11.5980	45.6751	35.5494	64.4506	12.0058	45.2673
12	27.8969	72.1031	10.8913	43.1003	34.2496	65.7504	11.5894	42.4022
15	32.9806	67.0194	11.3024	40.8883	38.2692	61.7308	12.0642	40.1265
18	33.1879	66.8121	11.5152	39.6871	38.5764	61.4236	12.2555	38.9467
21	33.4720	66.5280	11.5338	39.1260	39.1839	60.8161	12.3340	38.3258
24	33.9535	66.0464	11.6013	38.7608	39.5901	60.4099	12.4137	37.9484
27	34.0761	65.9239	11.6318	38.5669	39.7538	60.2462	12.4507	37.7480
30	34.1658	65.8342	11.6456	38.4635	39.8670	60.1330	12.4722	37.6369

TABLE 5 Numerical outcomes of non-linear PVPMV model A2 for case-1 of scenario 1.

Time (Days)	ADM Case 1				BDF Case 1			
	S	*I*	*X*	*Y*	*S*	*I*	*X*	*Y*
0	90.0000	10.0000	10.0000	47.0000	90.0000	10.0000	10.0000	47.0000
3	85.2381	17.0689	8.8230	39.7728	82.4143	20.0025	9.23605	39.4695
6	85.9571	18.0416	8.87925	36.8224	82.6595	21.6085	9.86141	36.1337
9	88.3295	16.933	8.82304	35.5548	85.0741	20.6993	10.1945	34.4088
12	90.7455	15.3976	8.47258	35.1839	87.6295	19.2833	10.0901	33.6603
15	92.7167	13.9604	7.9416	35.3571	89.7366	17.9531	9.71931	33.5382
18	94.2317	12.6973	7.3321	35.8644	91.3260	16.8256	9.24056	33.7840
21	95.2509	11.7055	6.7767	36.4903	92.4830	15.8834	8.7472	34.2194
24	96.00428	10.8327	6.2490	37.1941	93.3156	15.0854	8.28247	34.7336
27	96.5393	10.0799	5.7780	37.8979	93.9153	14.3967	7.8615	35.2635
30	96.9228	9.4206	5.36171	38.5714	94.3505	13.7927	7.4860	35.7768

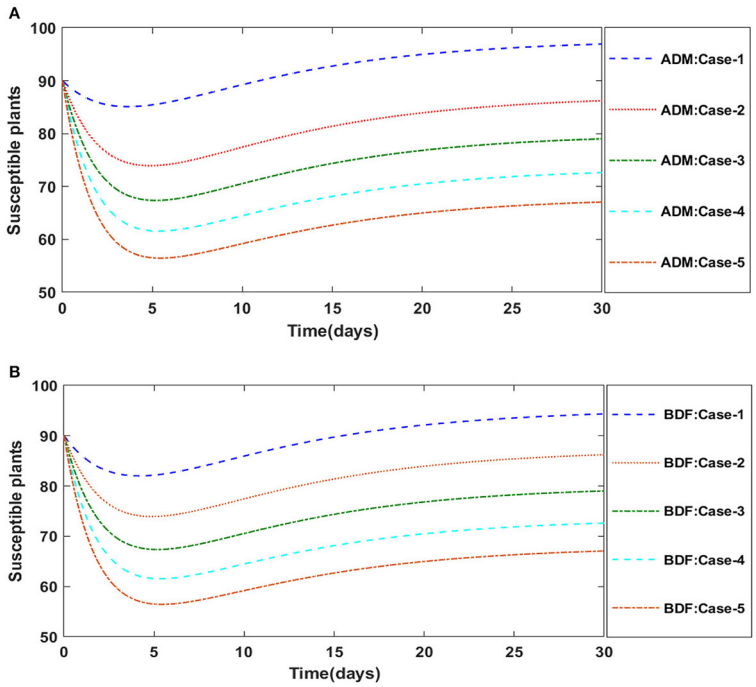

FIGURE 10
(A) Dynamics of susceptible plants for the varition in γ using ADM for model A2. **(B)** Dynamics of susceptible plants for the varition in γ using BDF for model A2.

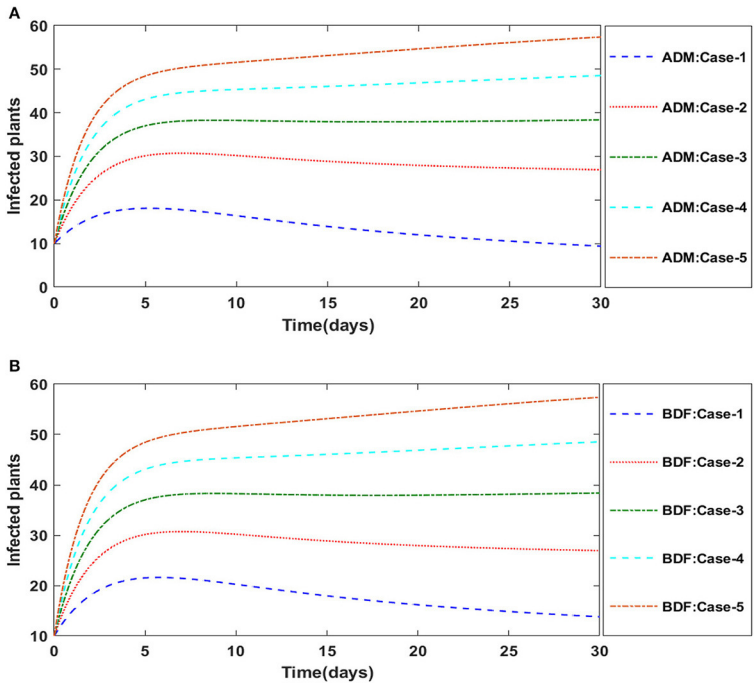

FIGURE 11
(A) Dynamics of infected plants for the varition in γ using ADM for model A2. **(B)** Dynamics of infected plants for the varition in γ using BDF for model A2.

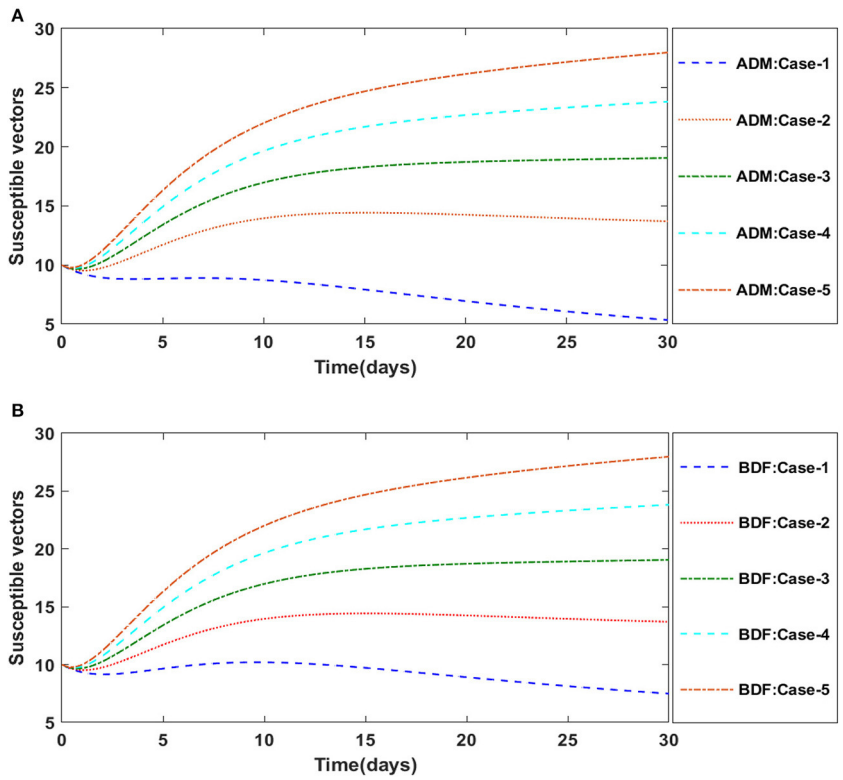

FIGURE 12
(A) Dynamics of susceptible vectors for the varition in γ using ADM for model A2. **(B)** Dynamics of susceptible vectors for the varition in γ using ADM for model A2.

to obtain the numerical solutions of a differential equation under the predefined initial condition. Various researchers have been intrigued by developing numerical techniques for solving initial value problems in ODEs in current years. Many researchers exploited various numerical techniques to approximate the solution of several mathematical models, yielding superior findings than a few of the existing ones in the literature, such as [26–30]. Recently research workers concentrated their efforts on numerically solving various mathematical models in the field of epidemiology such as COVID-19 [31], HIV model [32], tuberculosis transmission model [33], predator-prey mathematical model [34], mathematical model of cancer treatment [35]. Although the precision and stability of the aforementioned techniques are significant, they need a lot of memory and a long computation time. As a result, the numerical treatments for such approaches provide significant challenges that must be overcome in order to guarantee the precision and consistency of the solution. Therefore, ADM can be used to reliably confront one- and multi-dimensional stiff and non-stiff problems. The discrepancy between the predicted and corrected values might be used as one indicator of the error being made at each step. This gives a rather simple way to regulate the step size used in the integration. The widely used multistep ADM may approximate the solution of a first-order differential equation. In comparison to the equivalent-order Runge–Kutta method, these methods generally preserve reasonably good stability and accuracy properties while being more computationally efficient. When used with high order systems, this can significantly reduce computing time and effort. The most widely used techniques for treating stiff and non-stiff ODEs are implicit multistep techniques that utilize the BDF method. These methods were first used to confront a complex problem by Curtis and Hirschfelder [36]. Numerous implicit approaches have been created over time and are the subject of in-depth literature discussion; see [37–43]. To that end, the goal of this study is to apply the precise and stable ADM [44–48] and BDF methods to determine an initial value problem solution.

The paramount characteristics of this study are as follows: -

- The dynamics of two models of virus transmission in plants are investigated numerically to incorporate either a time lag or an exposed plant density into the system governed with non-linear delayed ODEs.
- The approximate solutions for classes $S(t)$, $I(t)$, $X(t)$, and $Y(t)$ are determined by the implementation of exhaustive

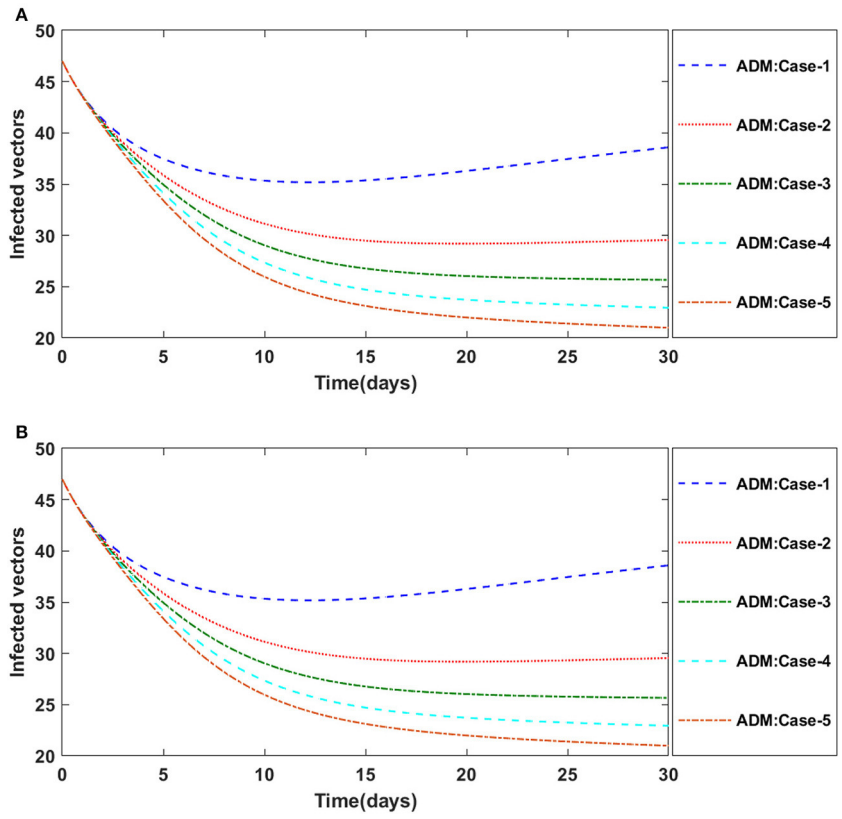

FIGURE 13
(A) Dynamics of infected vectors for the varition in γ using ADM for model A2. **(B)** Dynamics of infected vectors for the varition in γ using ADM for model A2.

TABLE 6 Numerical outcomes of nonlinear PVPMV model B for case-1 of scenario 3.

Time (Days)	ADM Case 1				BDF Case 1			
	S	*I*	*X*	*Y*	*S*	*I*	*X*	*Y*
0	30.0000	5.0000	42.0000	9.0000	30.0000	5.0000	42.0000	9.0000
3	81.2187	20.0001	34.8550	15.7049	80.6520	20.5766	34.4587	16.0901
6	64.5971	36.5518	23.2982	27.0091	64.1159	37.0125	22.9842	27.3170
9	54.1651	46.1322	16.9357	33.2329	53.9550	46.3141	16.8181	33.3472
12	50.4141	49.2806	14.8998	35.1928	87.6295	19.2833	10.0901	33.6603
15	49.4357	50.0592	14.3831	35.6677	49.4218	50.0701	14.3756	35.6742
18	49.2174	50.2283	14.2635	35.7644	49.2146	50.2304	14.2619	35.7655
21	49.1758	50.2592	14.2378	35.7775	49.1754	50.2595	14.2375	35.7775
24	49.1714	50.2617	14.2332	35.7752	49.1714	50.2616	14.2331	35.7751
27	49.1733	50.2597	14.2328	35.7718	49.1733	50.2596	14.2328	35.7717
30	49.1753	50.2578	14.2331	35.7694	49.1753	50.2577	14.2331	35.7693

scenarios with variation in the infection ratio of a susceptible plant by an infected vector, infection ratio of vectors by infected plants, plants' natural fatality rate, plants' increased fatality rate owing to illness, vectors' natural fatality rate, vector replenishment rate, and plants' proliferation rate.

- The approximate solutions of the non-linear plant virus propagation by a vector (PVPMV) are determined by

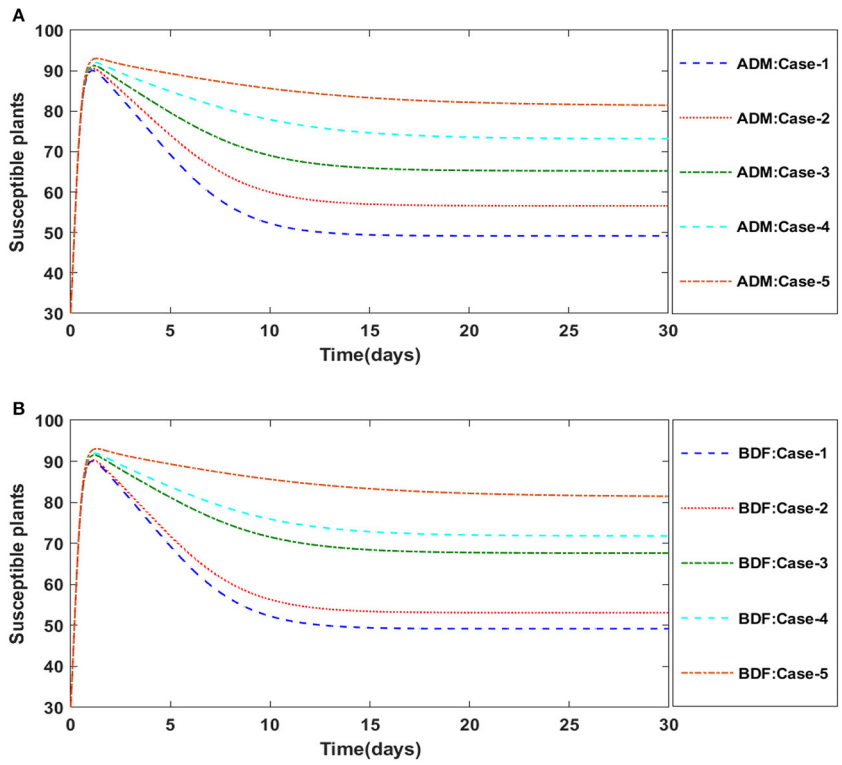

FIGURE 14
(A) Dynamics of susceptible plants for the varition in *c* using ADM for model B. **(B)** Dynamics of susceptible plants for the varition in *c* using BDF for model B.

TABLE 7 Numerical outcomes of non-linear PVPMV model B1 for case-1 of scenario 5.

Time (Days)	ADM Case 1				BDF Case 1			
	S	*I*	*X*	*Y*	*S*	*I*	*X*	*Y*
0	30.0000	5.0000	42.0000	9.0000	30.0000	5.0000	42.0000	9.0000
3	97.0808	2.6966	42.3118	8.23704	97.0728	2.70300	85.5535	10.1141
6	97.7627	2.0623	43.5322	6.7690	97.5514	2.24878	109.2329	10.9489
9	98.2168	1.6433	44.6376	5.52769	97.6434	2.15890	121.877	11.7585
12	98.5571	1.3297	45.5658	4.52489	97.5842	2.21071	128.3769	12.6420
15	98.8229	1.0848	46.3316	3.71820	97.4567	2.32606	131.4595	13.6115
18	99.0345	0.8898	46.9610	3.0663	97.2924	2.4755	132.6472	14.6478
21	99.2048	0.7329	47.4786	2.5363	97.1064	2.6450	132.7857	15.7296
24	99.3428	0.6057	47.9050	2.1033	96.9074	2.82649	132.3457	16.8395
27	99.4555	0.5019	48.2568	1.7477	96.7010	3.0148	131.5909	17.9620
30	99.5478	0.4168	48.5477	1.4548	96.4914	3.2060	130.6708	19.0838

exploiting the knacks of the Adams method (ADM) and backward differentiation formula (BDF) for sundry cases.

- Numerical and graphic interpretations of outcomes illustrate the significance/potential of these numerical methods as efficient, accurate, stable and viable computational procedures.

The remaining layout of the paper is as follows: Section Mathematical models presents mathematical models with relevant descriptions, Section Learning methodologies describes learning methodologies for the problem, Section Results and discussion provides results and discussion based on the numerical simulations,

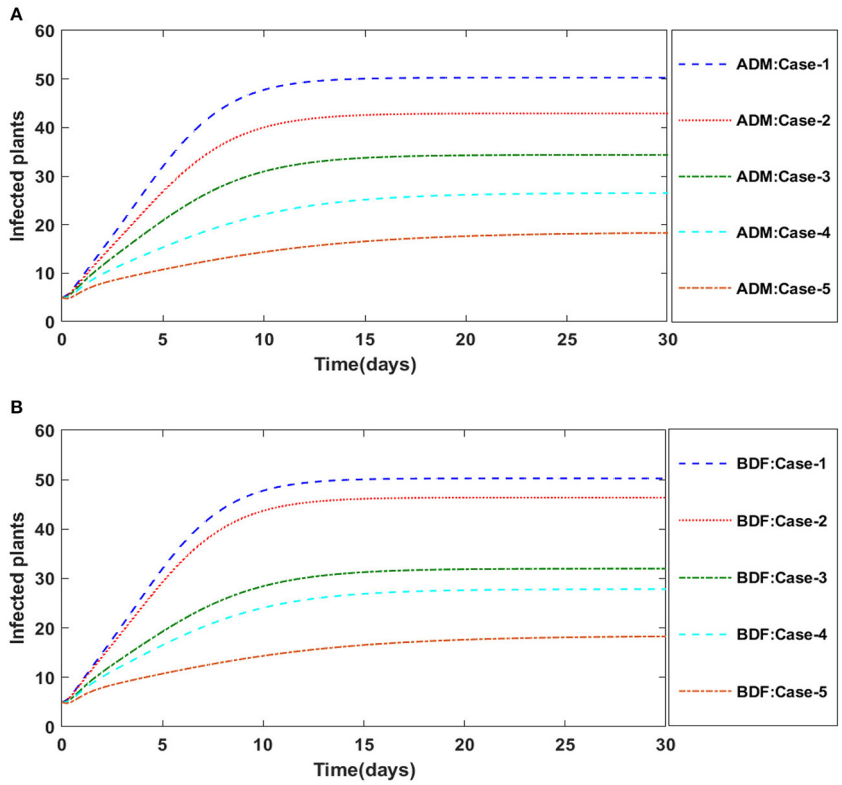

FIGURE 15
(A) Dynamics of infected plants for the varition in *d* using ADM for model B. **(B)** Dynamics of infected plants for the varition in *d* using BDF for model B.

and Section Conclusions concludes with future research recommendations.

Mathematical models

Two plant virus models are presented here in this section. The mathematical model of plant virus propagation by a vector with a constant plant density is first presented. Second, a saturated and non-constant plant density plant virus propagation model is presented.

Plant virus propagation model by a vector: Model A

We investigate two models of vector-borne plant virus transmission. Both of these are basic, and the objective is to explore how different techniques of introducing the delay affect the outcomes. There are two plant densities in the first, model A: susceptible [$S(t)$], healthier and susceptible to infection, and infectious [$I(t)$], previously infected. Because we assume that plants may not recover, we should not have a recovered class. There are also two vector populations: susceptible [$X(t)$] and infectious [$Y(t)$]. This model is a simplified form of the models provided in [49, 50].

Model A assumes that: plants as well as vectors that are new to this field, are susceptible, and the overall plant density remains stable at N because a farmer may replace any dead plants with healthy new ones, that the interaction among both the vector as well as plant is a mass movement, that the viruses decapitate plants but not the vectors who do not contract the disease, and the disease cannot be recovered from either plants or vectors. The model's parameters are the γ infection ratio of a susceptible plant by an infected vector, γ_1 infection ratio of vectors by infected plants, υ plants' natural fatality rate, c plants' increased fatality rate owing to illness, r vectors' natural fatality rate, and vector replenishment rate (according to birth or/and emigration).

Model A is represented by the system of ODEs as follows [25]:

$$S'(t) = \upsilon(N - S(t)) + cI(t) - \gamma Y(t) S(t), \quad (1)$$

$$I'(t) = \gamma Y(t) S(t) - (c + \upsilon) I(t), \quad (2)$$

$$X'(t) = \Omega - \gamma_1 I(t) X(t) - rX(t), \quad (3)$$

$$Y'(t) = \gamma_1 I(t) X(t) - rY(t). \quad (4)$$

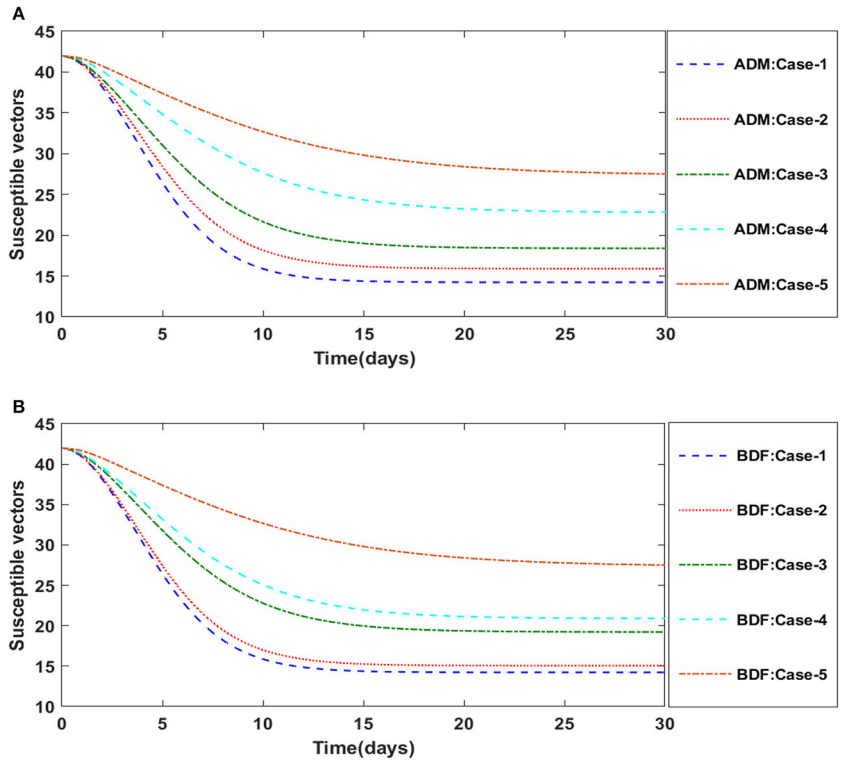

FIGURE 16
(A) Dynamics of susceptible vectors for the varition in *d* using ADM for model B. **(B)** Dynamics of susceptible vectors for the varition in *d* using BDF for model B.

There are two delays in virus transmission *via* a vector. One is being the time required for the virus to propagate throughout the plant after it has been infected. The other is the time required for the virus to propagate within the vector after it has been infected. Because the virus is not reproducing in the vector, the second is significantly smaller than the first. For the sake of simplicity, we'll assume that the second delay is zero.

We will incorporate the delays in two ways: the first is based on the premise that a susceptible needs the time delay to become infectious after coming into contact with an infectious [50, 51]. This is supposed to be model A1 [25]:

$$S'(t) = \upsilon(N - S(t)) + cI(t) - \gamma Y(t-\delta) S(t-\delta), \quad (5)$$
$$I'(t) = \gamma Y(t-\delta) S(t-\delta) - (c+\upsilon) I(t), \quad (6)$$
$$X'(t) = \Omega - \gamma_1 I(t) X(t) - rX(t), \quad (7)$$
$$Y'(t) = \gamma_1 I(t) X(t) - rY(t). \quad (8)$$

It would be possible to replace the exposed density $[E(t)]$ with a delay-accounting density. After coming into contact with an infectious, a susceptible become exposed or dormant, unable to infect. The exposed becomes infectious at the rate $\eta = 1/\delta$.

Then the model A2 will be:

$$S'(t) = \upsilon(N - S(t)) + cI(t) - \gamma Y(t) S(t) + \upsilon E(t), \quad (9)$$
$$E'(t) = \gamma Y(t) S(t) - \upsilon E(t) - \eta E(t), \quad (10)$$
$$I'(t) = \eta E(t) - (c+\upsilon) I(t), \quad (11)$$
$$X'(t) = \Omega - \gamma_1 I(t) X(t) - rX(t), \quad (12)$$
$$Y'(t) = \gamma_1 I(t) X(t) - rY(t). \quad (13)$$

Epidemic models involving an exposed class are widely known for plant virus propagation [52, 53]. Models containing exposed densities have the advantage of not requiring the initial/staring conditions to be presented at an interval equal to the delay, as delay differential equations (DDEs) require.

Plant virus propagation model by vector: Model B

We construct a further plant virus propagation model which is based on the models presented in [54, 55], but revised to include healthy vectors and mass response interactions for the disease. It takes into account four different densities:

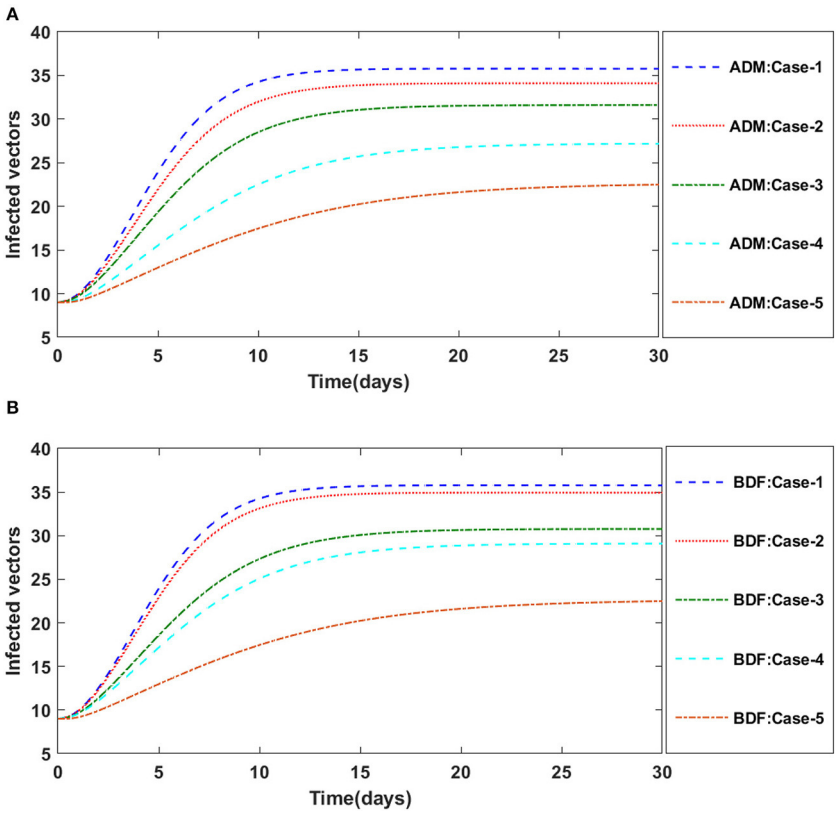

FIGURE 17
(A) Dynamics of infected vectors for the varition in *d* using ADM for model B. **(B)** Dynamics of infected vectors for the varition in *d* using BDF for model B.

susceptible plants [*S(t)*], infectious plants [*I(t)*], susceptible vectors [*X(t)*] and infectious vectors [*Y(t)*]. Because the plants grow in a logistical manner, the overall plant density does not remain constant. All emerging vectors are subject to susceptible, and their growth rate is continuously attributed to births as well as emigration. Plants are unable to recover and insects do not contract the disease, as it does in model A.

Model B, which propagates plant viruses is as follows [25]:

$$S'(t) = mS(t)\left(1 - \frac{S(t)+I(t)}{N}\right) - \frac{\gamma S(t) Y(t)}{1+\beta S(t)+aY(t)}, \quad (14)$$

$$I'(t) = \gamma S(t) Y(t) - (r+c) I(t), \quad (15)$$

$$X'(t) = \Omega - \gamma_1 I(t) X(t) - rX(t), \quad (16)$$

$$Y'(t) = \gamma_1 I(t) X(t) - rY(t). \quad (17)$$

Here, m represents the plants' proliferation rate, N their maximum capacity of carrying, and γ the rate of infection of a susceptible plant by an infected vector, r represents the plants' natural fatality rate, and c represents the virus's additional fatality rate. Ω represents the rate at which susceptible vectors are recruited, $\boldsymbol{\gamma_1}$ represents the rate at which an infected plant infects a susceptible vector, and r represents the vectors' natural fatality rate.

We will incorporate the delay in two different ways, just like we did with model A. The first assumes that a susceptible takes the time delay to get infected after coming into contact with an infected [50, 51]. Then model B* may be expressed in the form [25]:

$$S'(t) = mS(t)\left(1 - \frac{S(t)+I(t)}{N}\right) - \frac{\gamma S(t-\delta) Y(t-\delta)}{1+\beta S(t-\delta)+aY(t-\delta)}, \quad (18)$$

$$I'(t) = \frac{\gamma S(t-\delta) Y(t-\delta)}{1+\beta S(t-\delta)+aY(t-\delta)} - (r+c) I(t), \quad (19)$$

$$Y'(t) = \gamma I(t) - rY(t). \quad (20)$$

In the alternative version, we uphold [54, 55] in which the plant ceases being susceptible immediately after interaction with an infected insect, but it requires a delay period to become

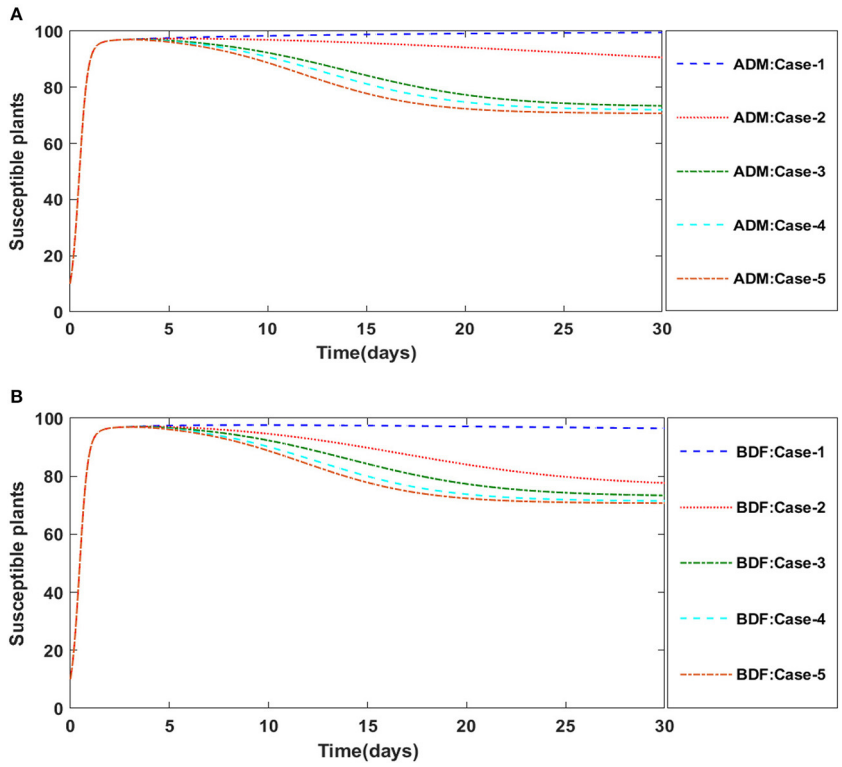

FIGURE 18
(A) Dynamics of susceptible plants for the varition in Ω using ADM for model B1. **(B)** Dynamics of susceptible plants for the varition in Ω using BDF for model B1.

infected. Because the plant could die at any time, the surviving rate is directly proportional $e^{-r\delta}$, where r is the plant's fatality rate and δ is the delay. Then model B1 will be of the form [25]:

$$\begin{aligned} S'(t) &= mS(t)\left(1-\frac{S(t)+I(t)}{N}\right) \\ &\quad -\frac{\gamma S(t)\,Y(t)}{1+\beta S(t)+aY(t)}, \qquad (21)\\ I'(t) &= e^{-r\delta}\frac{\gamma S(t-\delta)\,Y(t-\delta)}{1+\beta S(t-\delta)+aY(t-\delta)} \\ &\quad -(r+c)\,I(t), \qquad (22)\\ X'(t) &= \Omega-\gamma_1 I(t)\,X(t)-rX(t), \qquad (23)\\ Y'(t) &= \gamma_1 I(t)\,X(t)-rY(t). \qquad (24) \end{aligned}$$

A susceptible plant is infected by an infected vector at time $(t-\delta)$ in model B*, as well as the susceptible plant becomes infective at time t. A susceptible plant is infected by an infected vector that takes t to infect in model B1, with $e^{-r\delta}$ indicating the average rate of infectious susceptible who survived in time t.

Incorporating an exposed density $[E(t)]$, as before, is an alternate with the same boon and bane. The model B2 with exposed class is as follows [25]:

$$\begin{aligned} S'(t) &= mS(t)\left(1-\frac{S(t)+I(t)}{N}\right) \\ &\quad -\frac{\gamma S(t)\,Y(t)}{1+\beta S(t)+aY(t)}, \qquad (25)\\ E'(t) &= \gamma Y(t)\,S(t)-\upsilon E(t)-\eta E(t), \qquad (26)\\ I'(t) &= \eta E(t)-(c+\upsilon)\,I(t), \qquad (27)\\ X'(t) &= \Omega-\gamma_1 I(t)\,X(t)-rX(t), \qquad (28)\\ Y'(t) &= \gamma_1 I(t)\,X(t)-rY(t). \qquad (29) \end{aligned}$$

Learning methodologies

Adams method

The Adams method (ADM) is a two-step procedure for solving an ODE [56–61]. First, to use an explicit approach, the predictive step determines a crude approximation of the target number. The corrector step streamlines the preceding approximation using a different mechanism, usually an implicit one.

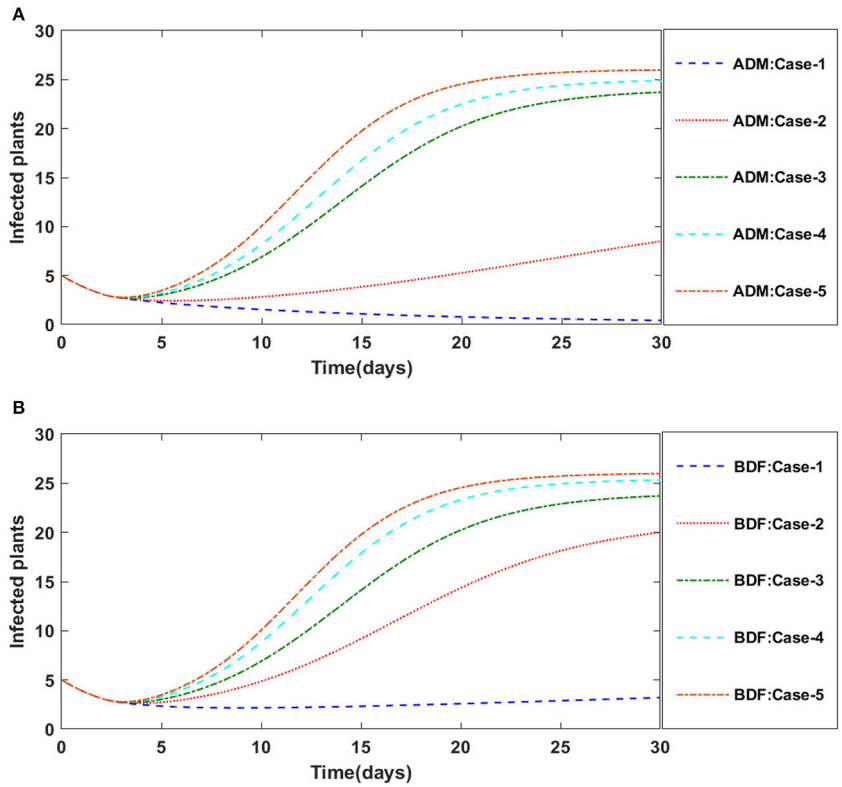

FIGURE 19
(A) Dynamics of infected plants for the varition in Ω using ADM for model B1. **(B)** Dynamics of infected plants for the varition in Ω using BDF for model B1.

The predictor-corrector technique, which is based on set of Equations (1)–(4), is represented as follows:

$$\begin{aligned}
\frac{dS}{dt} &= f\left(t, S, I, Y\right), \qquad S\left(t_0\right) = S\left(0\right), \\
\frac{dI}{dt} &= f\left(t, Y, S, I\right), \qquad I\left(t_0\right) = I\left(0\right), \\
\frac{dX}{dt} &= f\left(t, I, X\right), \qquad X\left(t_0\right) = X\left(0\right), \\
\frac{dY}{dt} &= f\left(t, I, X, Y\right), \qquad Y\left(t_0\right) = Y\left(0\right), \qquad (30)
\end{aligned}$$

To obtain a two-step predictor solution for first equation of set (30) for the non-linear plant virus propagation model by vector, use the following expression:

$$S_{k+1} = S_k + \frac{6}{4}hf\left(t_k, S_k\right) - \frac{1}{2}hf\left(t_{k-1}, S_{k-1}\right),$$

We have the following two-step corrector equation after evaluating the first equation in the nonlinear plant virus propagation model by vector:

$$S_{k+1} = S_k + \frac{1}{2}hf\left(t_{k+1}, S_{k+1}\right) + f\left(t_k, S_k\right),$$

Backward differentiation method

The backward differentiation formula (BDF) is a collection of implicit approaches for solving ordinary differential equations numerically [62–64]. They are linear multi-step algorithms that use information from previously determined time points to approximating the derivative of a function for a particular function and time, improving the precision of the approximations. These techniques are particularly useful for solving stiff differential equations [65]. In 1952, Charles F. Curtiss and Joseph O. Hirschfelder introduced the methods for the first time.

Consider the initial value problem as:

$$\frac{dz}{dt} = g\left(t, z\right), \quad z\left(t_0\right) = z_0,$$

BDF can be written in generic form as follows:

$$\sum_{m=0}^{l} c_m z_{n+m} = h\alpha g\left(t_{n+l}, z_{n+l}\right),$$

where the step size is denoted by h, g is being calculated for an unknown z_{n+l}. BDF techniques are implicit

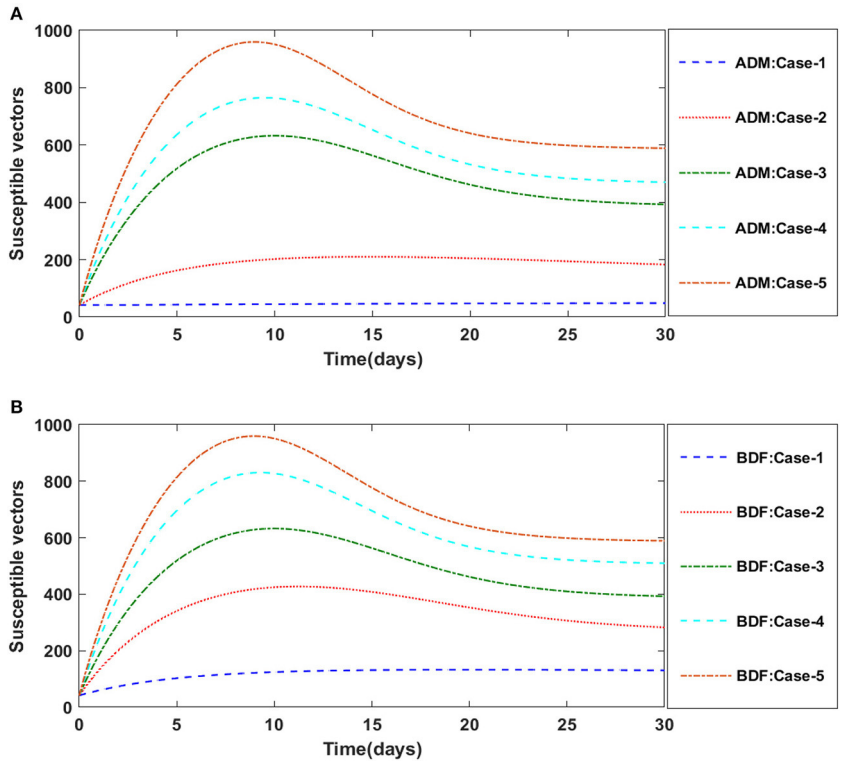

FIGURE 20
(A) Dynamics of susceptible vectors for the varition in Ω using ADM for model B1. **(B)** Dynamics of susceptible vectors for the varition in Ω using BDF for model B1.

and may require non-linear equations to be solved at each step. The coefficients c_m as well as α are considered to obtain order l, which is the highest feasible order.

Table 1 [25] lists the default settings for the non-linear PVPMV parameters, while the nomenclature describes the parameters. These default settings utilizing in all of the scenarios of non-linear PVPMV.

Results and discussion

The approximate numerical outcomes for model A [25] having a constant plant density and model B [25] having a non-constant plant density are presented in this study. The ADM and BDF methods are used to explore the dynamics of first order non-linear plant virus propagation models by a vector for three variants of models A and B, respectively with inputs from [0, 30] and step size 0.1 for cases 1–5 of each distinct scenarios of nonlinear PVPMV. As shown in Table 2, the approximate solution for the variants of model A is obtained by creating different scenarios with cases 1–5 and varying the γ infection ratio of a susceptible plant by an infected vector, γ_1 infection ratio of vectors by infected plants, υ plants' natural fatality rate, c plants' increased fatality rate owing to illness, r vectors' natural fatality rate, and Ω vector replenishment rate. Similarly, the approximate solution for the variants of model B is determined by using the impact of variation in m which represents the plants' proliferation rate, γ the rate of infection of a susceptible plant by an infected vector, r represents the plants' natural fatality rate, and c represents the disease's additional fatality rate. Ω represents the rate at which susceptible vectors are recruited, $\boldsymbol{\gamma_1}$ represents the rate at which an infected plant infects a susceptible vector, and r represents the vectors' natural fatality rate as shown in Table 2. Figure 1 depicts the working procedure of the designed approach for non-linear PVPMV.

Case study-I: Model A [25]

The three different models of plant virus propagation by a vector based on the system of ODEs without delay (model A), with delay (model A1), and without delay but including exposed class [$E(t)$] (model A2) as presented in Equations (1–4), (5–8), and (9–13) are numerically solved employing the ADM and BDF methods invoking he Mathematica routine with inputs [0, 30] and step size 0.1. Numerical outcomes and

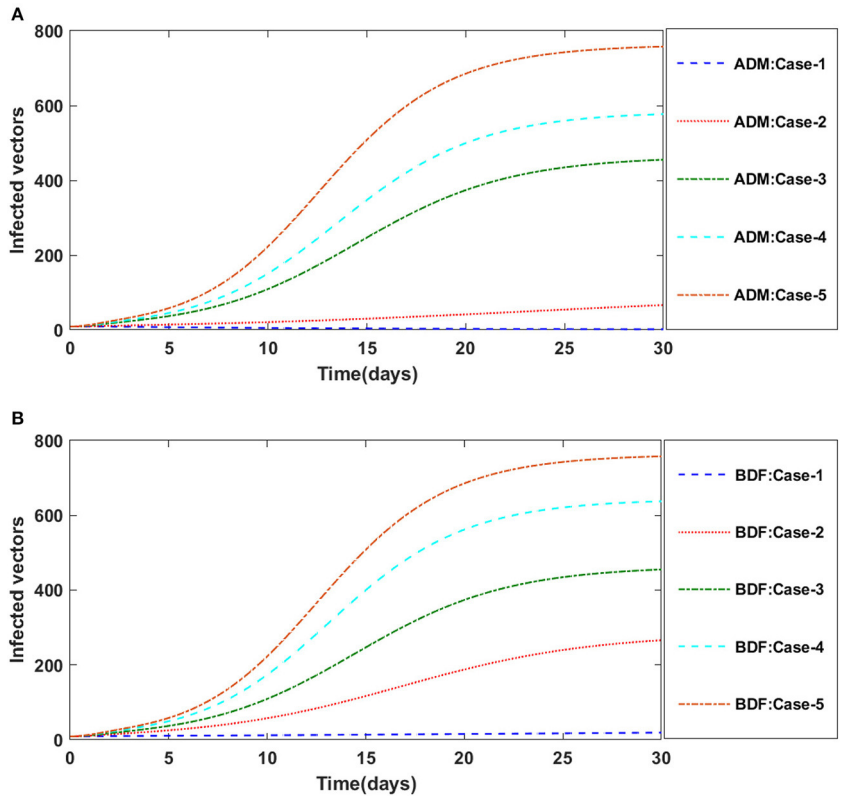

FIGURE 21
(A) Dynamics of infected vectors for the varition in Ω using ADM for model B1. **(B)** Dynamics of infected vectors for the varition in Ω using BDF for model B1.

TABLE 8 Numerical outcomes of nonlinear PVPMV model B2 for case-1 of scenario 4.

Time (Days)	ADM Case 1				BDF Case 1			
	S	*I*	*X*	*Y*	*S*	*I*	*X*	*Y*
0	30.0000	5.0000	42.0000	9.0000	30.0000	5.0000	42.0000	9.0000
3	86.3176	12.1709	12.3955	34.3073	86.6904	11.9595	12.0366	34.5894
6	73.7772	17.7705	24.1041	25.7580	74.2162	17.6038	23.6978	26.0241
9	61.1327	21.313	35.7658	19.2102	61.5174	21.2481	35.4136	19.3792
12	51.7536	21.8141	44.2058	15.5981	51.9920	21.8310	43.9967	15.6787
15	46.8476	20.9704	48.3739	14.0416	46.9494	21.0005	48.2913	14.0724
18	45.1048	20.2721	49.7273	13.5023	45.1322	20.2880	49.7077	13.5115
21	44.7574	19.9889	49.9509	13.3643	44.7596	19.9935	49.9503	13.3661
24	44.7835	19.9234	49.9091	13.3482	44.7814	19.9241	49.9111	13.3481
27	44.8401	19.9201	49.8597	13.3550	44.8386	19.9199	49.8609	13.3547
30	44.8703	19.9244	49.8356	13.3608	44.8697	19.9243	49.8361	13.3607

simulations are determined for five distinct scenarios of each model comprising cases 1–5 for non-linear PVPMV and selected random scenarios from each model for discussion. We first presented the dynamical behavior of *S(t)*, *I(t)*, *X(t)* and *Y(t)* classes of scenario 2 for model A of non-linear PVPMV. The numerical outcomes of non-linear PVPMV model A for case-1 of scenario 2 against the classes *S(t)*, *I(t)*, *X(t)* and *Y(t)* are listed in Table 3.

Figures 2A,B illustrate the dynamics of susceptible plants utilizing the ADM and BDF methods, respectively, for the

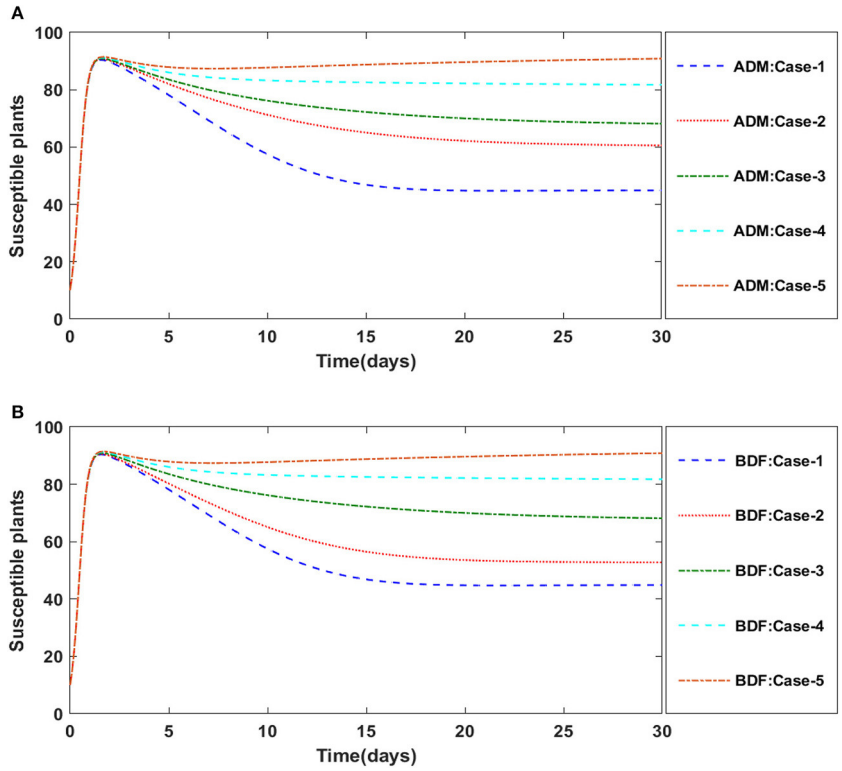

FIGURE 22
(A) Dynamics of susceptible plants for the varition in *r* using ADM for model B2. **(B)** Dynamics of susceptible plants for the varition in *r* using BDF for model B2.

variation in infection ratio of the vectors by infected plants, i.e., γ_1 for model A. It has been discovered that increasing the value of γ_1 causes the susceptible density of plants to drop. The impacts of infected plants are shown in Figures 3A,B for varied values of γ_1. As can be seen from the graph, increasing the value of γ_1 increases the density of infected plants. Figures 4A,B demonstrate that how the behavior of susceptible vectors changes as the value of γ_1 changes. For higher values of γ_1 there is an increase in the density of infected vectors. Figures 5A,B show the effects of infected vectors for various values of γ_1. Increasing the value of γ_1 increases the density of infected plants, as shown in the graphic.

The dynamics of plants' natural fatality rate i.e., υ is explored for all four classes *S(t)*, *I(t)*, *X(t)* and *Y(t)* using the strength of ADM and BDF methods for scenario 5 of the model A1. As seen in Figures 6A,B, raising the value of υ causes the density of susceptible plants to grow. The density of infected plants decreased as the value of υ increased, as seen in Figures 7A,B. Figures 8A,B show the effects of plants' natural mortality rate i.e., υ for class *X(t)* of model A1. As can be seen in the graphs, increasing the value of υ will increase the number of susceptible vectors. For class *Y(t)* of model A1, the influence of plants' natural fatality rate, i.e., υ is also computed. The rate of infected vectors reduces as the value of the infected vectors increases, as seen in Figures 9A,B. Table 4 shows the numerical outcomes of non-linear PVPMV model A1 for case-1 of scenario 5 against the classes *S(t)*, *I(t)*, *X(t)* and *Y(t)*.

Similarly, the dynamics for all four classes *S(t)*, *I(t)*, *X(t)* and *Y(t)*are analyzed by varying the infection ratio of a susceptible plant by an infected vector which is denoted by γ for scenario 1 of model A2 and graphical illustrations are presented in Figures 10–13, respectively. Numerical outcomes classes *S(t)*, *I(t)*, *X(t)* and *Y(t)* in model A2 for case-1 of scenario 1 are computed and provided in Table 5. Figures 10A,B depict the influence of the infection ratio of a susceptible plant by an infected vector on susceptible plants using the ADM and BDM methods, respectively. It is permissible to observe that when the value of γ rises, the density of susceptible plants decreases. Figures 11A,B describe the effects of the infection ratio of a susceptible plant by an infected vector on infected plants. One may observe that the density of infected plants increased in correlation with the value of γ. Figures 12A,B illustrate progressive increase in the density of susceptible vectors as the value of γ increases, whereas Figures 13A,B demonstrate the opposing behavior in the case of infected vectors.

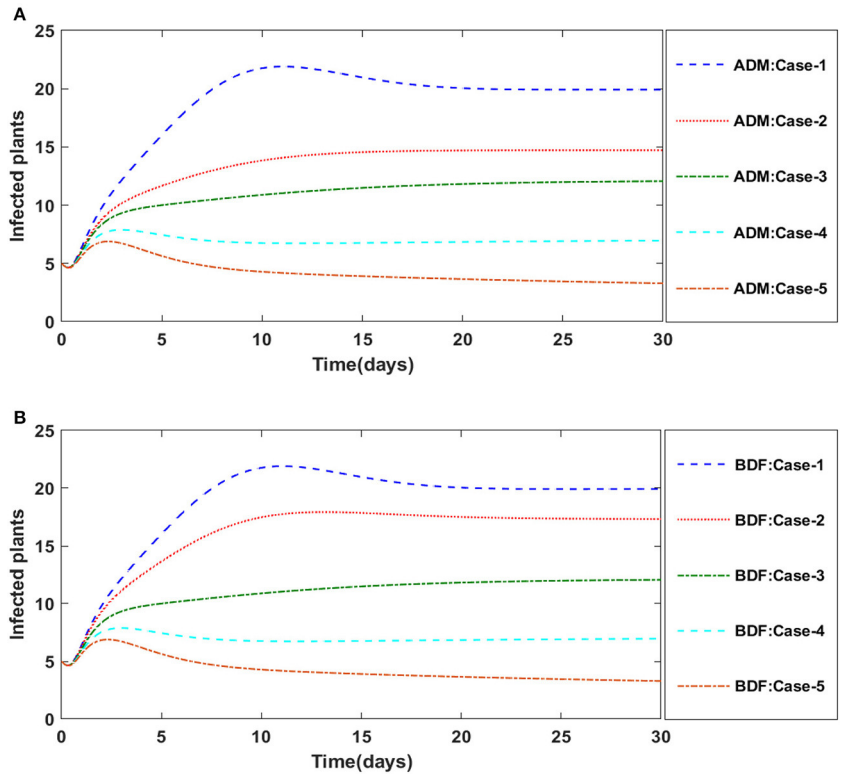

FIGURE 23
(A) Dynamics of infected plants for the varition in *r* using ADM for model B2. **(B)** Dynamics of infected plants for the varition in *r* using BDF for model B2.

Case study-II: Model B

The three segregated models of plant virus transmission by a vector, as described in Equations (14–17), (21–24), and (25–29), are numerically solved employing the ADM and BDF methods invoking the Mathematica routine. We construct five distinct scenarios incorporating cases 1–5 for non-linear PVPMV and chosen random scenarios from each model are used to determine numerical outcomes and simulations. For model B of non-linear PVPMV. We first described the dynamical behavior of the *S(t)*, *I(t)*, *X(t)*, and *Y(t)* classes in scenario 3 for the variation in disease's additional fatality rate i.e., *c*. for model B. For all four classes *S(t)*, *I(t)*, *X(t)*, and *Y(t)* numerical outcomes are determined and provided in Table 6 for case-1 of scenario 3 of model B. Figures 14A,B illustrate the dynamics of susceptible plants using the ADM and BDF methods for the variability in the disease's additional fatality rate i.e., *c*. It has been discovered that as the value of *c* is elevated, the susceptible density of plants increases. The impact of disease's additional fatality rate i.e., *c* on infected plants can be seen in Figures 15A,B. It is clear from Figures that increasing the value of *c* will result in reduction the density of infected plants. Figures 16A,B demonstrate the behavior of susceptible vectors for the variation in disease's additional fatality rate of model B. One may see that the density of susceptible vectors will increase as the value of c is increased. The influence of disease's additional fatality rate on infected vectors is presented in Figures 17A,B. It is observed from Figures that increasing the value of *c* causes the density of infected vectors to decrease.

Secondly, the dynamics of susceptible vectors' recruited rate i.e., Ω is investigated for all four classes *S(t)*, *I(t)*, *X(t)*, and *Y(t)* utilizing the strength of ADM and BDF methods for scenario 5 of the model B1 and numerical outcomes of all four classes *S(t)*, *I(t)*, *X(t)*, and *Y(t)* for the case-1 of scenario 5 is listed in Table 7. Figures 18A,B portrayed the behavior of susceptible plants density for the different values of Ω, and it is noticed that the number of susceptible plants decreases for the higher values of Ω. Figures 19A,B illustrated that as the value of Ω increases, the number of infected plants goes up. The dynmics of susceptible vectors for the variation in vectors' recruited rate i.e., *c* are presented in Figures 20A,B. One may witness that in Figures 20A,B the density of susceptible vectors goes in continous behavior for the first two cases and next three cases vectors density increased in the range of 0 to 10 days then steadily decreased and shows their steady behavior for next 20–30 days. As a result,

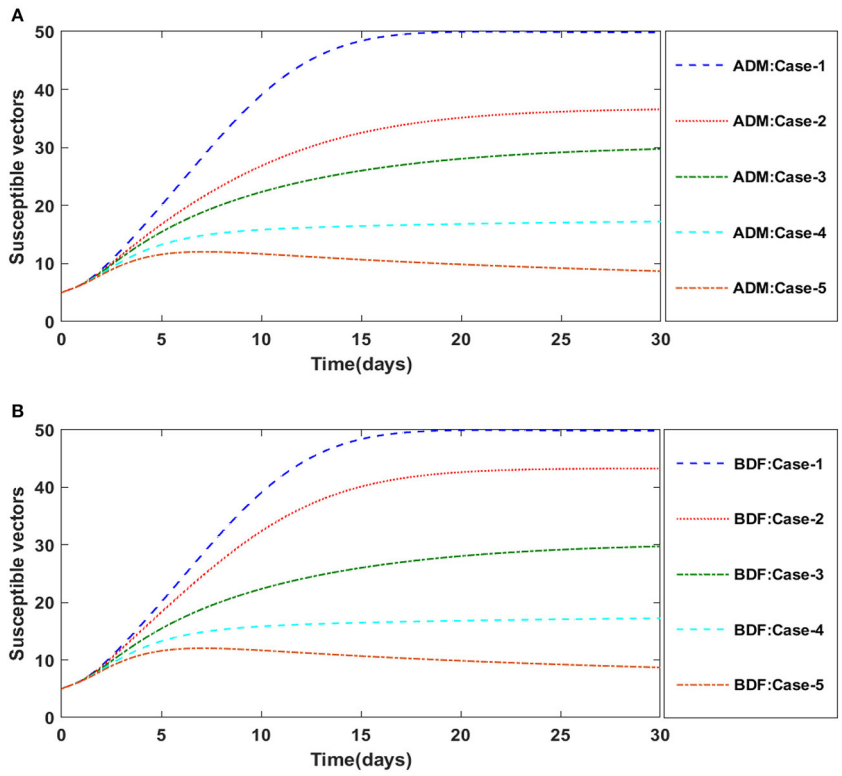

FIGURE 24
(A) Dynamics of susceptible vectors for the varition in *r* using ADM for model B2. **(B)** Dynamics of susceptible vectors for the varition in *r* using BDF for model B2.

for higher values of Ω, the density of susceptible vectors increases. Figures 21A,B portrayed the impact of susceptible vectors' recruited rate on infected vectors for model B1. The infected vectors show a steady behavior for the first two cases, also a steady behavior for the next three cases in 0–5 days, and then a gradual increase in 5–30 days, as shown in Figures 21A,B.

Finally, the dynamics of vectors' natural fatality rate i.e., *r* is investigated for all four classes *S(t)*, *I(t)*, *X(t)*, and *Y(t)* utilizing the strength of ADM and BDF methods for scenario 4 of the model B2. The respective numerical outcomes for case-1 of scenario 4 is provided in Table 8. The impact of vectors' natural fatality rate on susceptible plants is presented in Figures 22A,B As observed in graphical representation, the density of susceptible plants increased up to 90, then decreased between 3 and 10 days before returning to their steady state behavior. Also, the density of susceptible plants increased for the higher value of *r* as shown in Figures 22A,B, while the infected plants depicted reverse behavior as shown in Figures 23A,B. The influence of vectors' natural fatality rate *r* on susceptible vectors can be observed in Figures 24A,B for model B2. The number of susceptible vectors appears to decrease as the value of *r* increases. Similarly, the dynamics of infected vectors is portrayed in Figures 25A,B utilizing the ADM and BDF fro model B2, respectively. The number of infected vectors dropped as the natural fatality rate *r* of the vectors increased in model B2.

Conclusions

In this paper, we analyzed the dynamics of two models of virus transmission in plants to incorporate either a time lag or an exposed plant density into the system governed with non-linear delayed ODEs. The presented models may effectively predict susceptible plants [*S(t)*], infected plants *[I(t)*], susceptible vectors [*X(t)*], and infectious vectors [*Y(t)*]. Numerical analysis of the plant virus propagation model by a vector (PVPMV) is conducted through exhaustive scenarios with variation in different parameters used in the models. The approximate solution of the non-linear PVPMV is determined by exploiting the knacks of the Adams method (ADM) and backward differentiation formula (BDF) method We found delayed models to have a greater degree of realism since they account for the time between contact and infection. Processes are affected by delay

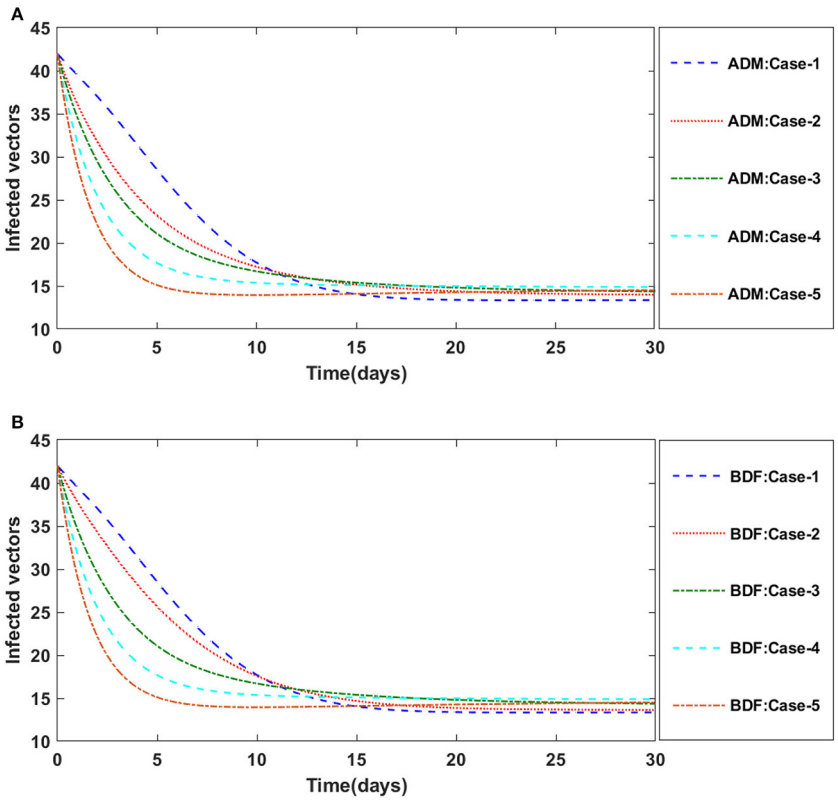

FIGURE 25
(A) Dynamics of infected vectors for the varition in *r* using ADM for model B2. **(B)** Dynamics of infected vectors for the varition in *r* using BDF for model B2.

and mathematically delay influences the dynamics along with stability. Moreover, the presented study proved to be extremely useful in controlling the plant outbreak in the subsequent seasons.

The dynamics of non-linear fluid dynamic models may be investigated in the future utilizing the strength of Adams predictor corrector method and BDF method [66–69].

Data availability statement

The original contributions presented in the study are included in the article/supplementary material, further inquiries can be directed to the corresponding author/s.

Author contributions

NA prepared methodology, results, and discussion. SN prepared introduction. MS prepared abstract and conclusion. All authors contributed to the article and approved the submitted version.

Conflict of interest

The authors declare that the research was conducted in the absence of any commercial or financial relationships that could be construed as a potential conflict of interest.

Publisher's note

All claims expressed in this article are solely those of the authors and do not necessarily represent those of their affiliated organizations, or those of the publisher, the editors and the reviewers. Any product that may be evaluated in this article, or claim that may be made by its manufacturer, is not guaranteed or endorsed by the publisher.

References

1. Rossi V, Sperandio G, Caffi T, Simonetto A, Gilioli G. Critical success factors for the adoption of decision tools in IPM. *Agronomy.* (2019) 9:710. doi: 10.3390/agronomy9110710

2. Shelton AM, Long SJ, Walker AS, Bolton M, Collins HL, Revuelta L, et al. First field release of a genetically engineered, self-limiting agricultural pest insect: evaluating its potential for future crop protection. *Front Bioeng Biotechnol.* (2020) 7:482. doi: 10.3389/fbioe.2019.00482

3. Chowdhury J, Al Basir F, Takeuchi Y, Ghosh M, Roy K. A mathematical model for pest management in Jatropha curcas with integrated pesticides-an optimal control approach. *Ecol Complex.* (2019) 37:24–31. doi: 10.1016/j.ecocom.2018.12.004

4. Pratiwi NP, Aldila D, Handari BD, Simorangkir GM. November. A mathematical model to control Mosaic disease of Jatropha curcas with insecticide and nutrition intervention. *AIP Conf Proc.* (2020) 2296:020096. doi: 10.1063/5.0030426

5. Liu S, Huang M, Wang J. Bifurcation control of a delayed fractional mosaic disease model for jatropha curcas with farming awareness. *Complexity.* (2020) 2020:2380451. doi: 10.1155/2020/2380451

6. Al Basir F, Ray S. Impact of farming awareness based roguing, insecticide spraying and optimal control on the dynamics of mosaic disease. *Ricerche Matematica.* (2020) 69:393–412. doi: 10.1007/s11587-020-00522-8

7. Wei X, Wang L, Jia Q, Xiao J, Zhu G. Assessing different interventions against Avian Influenza A (H7N9) infection by an epidemiological model. *One Health.* (2021) 13:100312. doi: 10.1016/j.onehlt.2021.100312

8. Ratchford, C. *Multi-scale and multi-group modeling techniques applied to Cholera and COVID-19 (Dissertation)*. The University of Tennessee at Chattanooga, Chattanooga, TN, United States. (2021).

9. Kwasi-Do Ohene Opoku N, Afriyie C. The role of control measures and the environment in the transmission dynamics of cholera. *Abstract Appl Anal.* (2020) 2020:2485979. doi: 10.1155/2020/2485979

10. Moore SE, Okyere E. Controlling the transmission dynamics of COVID-19. *arXiv[Preprint].arXiv:2004.00443*. (2020).

11. Van der Plank JE. Dynamics of epidemics of plant disease: Population bursts of fungi, bacteria, or viruses in field and forest make an interesting dynamical study. *Science.* (1965) 147:120–4. doi: 10.1126/science.147.3654.120

12. Noviello A, Romeo F, De Luca R. Time evolution of non-lethal infectious diseases: a semi-continuous approach. *Eur Phys J B Cond Matter Complex Syst.* (2006) 50:505–11. doi: 10.1140/epjb/e2006-00163-4

13. Stella IR, Srivastav AK, Ghosh M. May. Modeling and analysis of vector-borne plant disease with two delays. *J Phys Conf Series.* (2021) 1850:012125. doi: 10.1088/1742-6596/1850/1/012125

14. Al Basir F. A multi-delay model for pest control with awareness induced interventions—Hopf bifurcation and optimal control analysis. *Int J Biomath.* (2020) 13:2050047. doi: 10.1142/S1793524520500473

15. Ray S, Al Basir F. Impact of incubation delay in plant–vector interaction. *Math Comput Simul.* (2020) 170:16–31. doi: 10.1016/j.matcom.2019.09.001

16. Abraha T, Al Basir F, Obsu LL, Torres DF. Pest control using farming awareness: Impact of time delays and optimal use of biopesticides. *Chaos Solitons Fractals.* (2021) 146:110869. doi: 10.1016/j.chaos.2021.110869

17. Phan T, Pell B, Kendig AE, Borer ET, Kuang Y. Rich dynamics of a simple delay host-pathogen model of cell-to-cell infection for plant virus. *Discrete Continuous Dyn Syst B.* (2021) 26:515. doi: 10.3934/dcdsb.2020261

18. Blyuss KB, Al Basir F, Tsygankova VA, Biliavska LO, Iutynska GO, Kyrychko SN, et al. Control of mosaic disease using microbial biostimulants: insights from mathematical modelling. *Ricerche Matematica.* (2020) 69:437–55. doi: 10.1007/s11587-020-00508-6

19. Alemneh HT, Kassa AS, Godana AA. An optimal control model with cost effectiveness analysis of Maize streak virus disease in maize plant. *Infect Dis Modell.* (2021) 6:169–82. doi: 10.1016/j.idm.2020.12.001

20. Amelia R, Anggriani N, Istifadah N, Supriatna AK. Dynamic analysis of mathematical model of the spread of yellow virus in red chili plants through insect vectors with logistical functions. *AIP Conf Proc.* (2020) 2264:040006. doi: 10.1063/5.0023572

21. Kendig AE, Borer ET, Boak EN, Picard TC, Seabloom EW. Host nutrition mediates interactions between plant viruses, altering transmission and predicted disease spread. *Ecology.* (2020) 101:e03155. doi: 10.1002/ecy.3155

22. Shaw AK, Igoe M, Power AG, Bosque-Pérez NA, Peace A. Modeling approach influences dynamics of a vector-borne pathogen system. *Bull Math Biol.* (2019) 81:2011–28. doi: 10.1007/s11538-019-00595-z

23. Chen-Charpentier B, Jackson M. Optimal control of plant virus propagation. *Math Methods Appl Sci.* (2020) 43:8147–57. doi: 10.1002/mma.6244

24. Jittamai P, Chanlawong N, Atisattapong W, Anlamlert W, Buensanteai N. Reproduction number and sensitivity analysis of cassava mosaic disease spread for policy design. *Math Biosci Eng.* (2021) 18:5069–93. doi: 10.3934/mbe.2021258

25. Chen-Charpentier B. Delays in plant virus models and their stability. *Mathematics.* (2022) 10:603. doi: 10.3390/math10040603

26. Zaky MA. Existence, uniqueness and numerical analysis of solutions of tempered fractional boundary value problems. *Appl Num Math.* (2019) 145:429–57. doi: 10.1016/j.apnum.2019.05.008

27. Banu MS, Raju I, Mondal S. A comparative study on classical fourth order and butcher sixth order Runge-Kutta methods with initial and boundary value problems. *Int J Mat Math Sci.* (2021) 3:8–21. doi: 10.34104/ijmms.021.08021

28. Hossen M, Ahmed Z, Kabir R, Hossan Z. A comparative investigation on numerical solution of initial value problem by using modified Euler method and Runge Kutta method. *ISOR J Math.* (2019) 15:2278–5728. doi: 10.9790/5728-1504034045

29. Kafle J, Thakur BK, Acharya G. Formulative visualization of numerical methods for solving non-linear ordinary differential equations. *Nepal J Math Sci.* (2021) 2:79–88. doi: 10.3126/njmathsci.v2i2.40126

30. Koroche KA. Numerical solution of first order ordinary differential equation by using Runge-Kutta method. *Int J Syst Sci Appl Math.* (2021) 6:1–8. doi: 10.11648/j.ijssam.20210601.11

31. Olivares A, Staffetti E. Uncertainty quantification of a mathematical model of COVID-19 transmission dynamics with mass vaccination strategy. *Chaos Solitons Fractals.* (2021) 146:110895. doi: 10.1016/j.chaos.2021.110895

32. Campos C, Silva CJ, Torres DF. Numerical optimal control of HIV transmission in Octave/MATLAB. *Math Comput Applic.* (2019) 25:1. doi: 10.3390/mca25010001

33. Fatmawati MAK, Bonyah E, Hammouch Z, Shaiful EM. A mathematical model of tuberculosis (TB) transmission with children and adults groups: a fractional model. *Aims Math.* (2020) 5:2813–42. doi: 10.3934/math.2020181

34. Bürger R, Chowell G, Gavilán E, Mulet P, Villada LM. Numerical solution of a spatio-temporal predator-prey model with infected prey. *Math Biosci Eng.* (2019) 16:438–73. doi: 10.3934/mbe.2019021

35. Sweilam NH, Al-Mekhlafi SM, Assiri T, Atangana A. Optimal control for cancer treatment mathematical model using Atangana–Baleanu–Caputo fractional derivative. *Adv Diff Equat.* (2020) 2020:1–21. doi: 10.1186/s13662-020-02793-9

36. Curtiss CF, Hirschfelder JO. Integration of stiff equations. *Proc Natl Acad Sci.* (1952) 38:235–43. doi: 10.1073/pnas.38.3.235

37. Ebadi M, Gokhale MY. Hybrid BDF methods for the numerical solutions of ordinary differential equations. *Num Alg.* (2010) 55:1–17. doi: 10.1007/s11075-009-9354-4

38. Cash J. Efficient numerical methods for the solution of stiff initial-value problems and differential algebraic equations. *Proc R Soc Lond Ser A Math Phys Eng Sci.* (2003) 459:797–815. doi: 10.1098/rspa.2003.1130

39. Ogunrinde RB, Fadugba SE, Okunlola JT. On some numerical methods for solving initial value problems in ordinary differential equations. On Some Numerical Methods for Solving Initial Value Problems in Ordinary Differential Equations. (2012).

40. Lapidus L, Schiesser WE. *Numerical Methods for Differential Systems: Recent Developments in Algorithms, Software, and Applications.* (1976). doi: 10.1016/C2013-0-11041-0

41. Shampine LF. *Numerical Solution of Ordinary Differential Equations*. New York, NY: Routledge (2018). doi: 10.1201/9780203745328

42. Nasarudin AA, Ibrahim ZB, Rosali H. On the integration of stiff ODEs using block backward differentiation formulas of order six. *Symmetry.* (2020) 12:952. doi: 10.3390/sym12060952

43. Samson O, Victor JK. An application of second derivative ten step blended block linear multistep methods for the solutions of the holling tanner model and van der pol equations. *Covenant J Phys Life Sci.* (2019) 7:1–11. doi: 10.20370/s8gx-ft87

44. Qin G, Lou W, Wang H, Wu Z. *High Efficiency and Precision Approach to Milling Stability Prediction Based on Predictor-Corrector Linear Multi-Step Method.*

London: The International Journal of Advanced Manufacturing Technology (2022). doi: 10.21203/rs.3.rs-1456269/v1

45. Naz S, Raja MAZ, Mehmood A, Zameer A, Shoaib M. Neuro-intelligent networks for Bouc–Wen hysteresis model for piezostage actuator. *Eur Phys J Plus.* (2021) 136:1–20. doi: 10.1140/epjp/s13360-021-01382-3

46. Awan SE, Raja MAZ, Gul F, Khan ZA, Mehmood A, Shoaib M. Numerical computing paradigm for investigation of micropolar nanofluid flow between parallel plates system with impact of electrical MHD and Hall current. *Arabian J Sci Eng.* (2021) 46:645–62. doi: 10.1007/s13369-020-04736-8

47. Ghrist ML, Fornberg B, Reeger JA. Stability ordinates of Adams predictor-corrector methods. *BIT Num Math.* (2015) 55:733–50. doi: 10.1007/s10543-014-0528-7

48. Anwar N, Ahmad I, Raja MAZ, Naz S, Shoaib M, Kiani AK. Artificial intelligence knacks-based stochastic paradigm to study the dynamics of plant virus propagation model with impact of seasonality and delays. *Eur Phys J Plus.* (2022) 137:1–47. doi: 10.1140/epjp/s13360-021-02248-4

49. Shi R, Zhao H, Tang S. Global dynamic analysis of a vector-borne plant disease model. *Adv Diff Equat.* (2014) 2014:1–16. doi: 10.1186/1687-1847-2014-59

50. Jackson M, Chen-Charpentier BM. Modeling plant virus propagation with delays. *J Comput Appl Math.* (2017) 309:611–21. doi: 10.1016/j.cam.2016.04.024

51. Goel K. A mathematical and numerical study of a SIR epidemic model with time delay, nonlinear incidence and treatment rates. *Theory Biosci.* (2019) 138:203–13. doi: 10.1007/s12064-019-00275-5

52. Anggriani N, Amelia R, Istifadah N, Arumi D. October. Optimal control of plant disease model with roguing, replanting, curative, and preventive treatment. *J Phys Conf Series.* (2020) 1657:012050. doi: 10.1088/1742-6596/1657/1/012050

53. Janssen D, Ruiz L. Plant virus epidemiology. *Plants.* (2021) 10:1188. doi: 10.3390/plants10061188

54. Al Basir F, Takeuchi Y, Ray S. Dynamics of a delayed plant disease model with Beddington-DeAngelis disease transmission. *Math Biosci Eng.* (2021) 18:583–99. doi: 10.3934/mbe.2021032

55. Zhou X, Zhang L, Zheng T, Li HL, Teng Z. Global stability for a class of HIV virus-to-cell dynamical model with Beddington-DeAngelis functional response and distributed time delay. *Math Biosci Eng.* (2020) 17:4527–43. doi: 10.3934/mbe.2020250

56. Raja MAZ, Shah FH, Tariq M, Ahmad I. Design of artificial neural network models optimized with sequential quadratic programming to study the dynamics of nonlinear Troesch's problem arising in plasma physics. *Neural Comput Applic.* (2018) 29:83–109. doi: 10.1007/s00521-016-2530-2

57. Zahoor Raja MA, Shoaib M, El-Zahar ER, Hussain S, Li YM, Khan MI, et al. Heat transport in entropy-optimized flow of viscoelastic fluid due to Riga plate: analysis of artificial neural network. *Waves Random Complex Media.* (2022) 1–20. doi: 10.1080/17455030.2022.2028933

58. Ilyas H, Ahmad I, Raja MAZ, Shoaib M. A novel design of Gaussian WaveNets for rotational hybrid nanofluidic flow over a stretching sheet involving thermal radiation. *Int Commun Heat Mass Transfer.* (2021) 123:105196. doi: 10.1016/j.icheatmasstransfer.2021.105196

59. Soomro H, Zainuddin N, Daud H, Sunday J. Optimized hybrid block Adams method for solving first order ordinary differential equations. *Comput Mater Continua.* (2022) 72:2947–61. doi: 10.32604/cmc.2022.025933

60. Soomro H, Zainuddin N, Daud H, Sunday J, Jamaludin N, Abdullah A, et al. Variable step block hybrid method for stiff chemical kinetics problems. *Appl Sci.* (2022) 12:4484. doi: 10.3390/app12094484

61. Soomro H, Zainuddin N, Daud H. July. Convergence properties of 3-point block Adams method with one off-step point for ODEs. *J Phys Conf Series.* (2021) 1988:012038. doi: 10.1088/1742-6596/1988/1/012038

62. Abdi A, Hojjati G. Second derivative backward differentiation formulae for ODEs based on barycentric rational interpolants. *Num Alg.* (2021) 87:1577–91. doi: 10.1007/s11075-020-01020-6

63. Zhao J, Jiang X, Xu Y. A kind of generalized backward differentiation formulae for solving fractional differential equations. *Appl Math Comput.* (2022) 419:126872. doi: 10.1016/j.amc.2021.126872

64. Meyer T, Li P, Schweizer B. Backward differentiation formula and Newmark-type index-2 and index-1 integration schemes for constrained mechanical systems. *J Comput Nonlinear Dyn.* (2020) 15:021006. doi: 10.1115/1.4045505

65. Hu J, Shu R. On the uniform accuracy of implicit-explicit backward differentiation formulas (IMEX-BDF) for stiff hyperbolic relaxation systems and kinetic equations. *Math Comput.* (2021) 90:641–70. doi: 10.1090/mcom/3602

66. Wang R, Ding M, Wang Y, Xu W, Yan L. Field characterization of landslide-induced surge waves based on computational fluid dynamics. *Front Phys.* (2022) 9:813827. doi: 10.3389/fphy.2021.813827

67. Brenneisen J, Daub A, Gerach T, Kovacheva E, Huetter L, Frohnapfel B, et al. Sequential coupling shows minor effects of fluid dynamics on myocardial deformation in a realistic whole-heart model. *Front Cardiovasc Med.* (2021) 8:768548. doi: 10.3389/fcvm.2021.768548

68. Awan SE, Awais M, Raja MAZ, Parveen N, Ali HM, Khan WU, et al. Numerical treatment for dynamics of second law analysis and magnetic induction effects on ciliary induced peristaltic transport of hybrid nanomaterial. *Front Phys.* (2021) 9:631903. doi: 10.3389/fphy.2021.631903

69. Ferdian E, Suinesiaputra A, Dubowitz DJ, Zhao D, Wang A, Cowan B, et al. 4DFlowNet: super-resolution 4D flow MRI using deep learning and computational fluid dynamics. *Front Phys.* (2020) 8:138. doi: 10.3389/fphy.2020.00138

10.3389/fams.2022.1001392

Nomenclature

Symbols			
N	Total plant density	r	Plants' natural fatality rate
c	Plants' increased fatality rate	m	Plants' proliferation rate
$S(t)$	Susceptible plants	$X(t)$	Susceptible vectors
$I(t)$	Infected plants	$Y(t)$	Infectious plants
$S(t_0)$	Initial conditions for $S(t)$	$X(t_0)$	Initial conditions for $X(t)$
$I(t_0)$	Initial conditions for $I(t)$	$Y(t_0)$	Initial conditions for $Y(t)$
Greek Letters			
γ	Infection ratio of a susceptible plant by an infected vector,	γ_1	Infection ratio of vectors by infected plants
υ	Plants' natural fatality rate	Ω	Vector replenishment rate
δ	Time delay		
Abbreviations			
ODEs	Ordinary differential equations	ADM	Adams method
COVID-19	Coronavirus disease of 2019	BDF	Backward differentiation formula
HIV	Human immunodeficiency virus	PVPMV	Plant virus propagation by a vector
DDEs	Delay differential equations		

frontiers | Frontiers in Applied Mathematics and Statistics

TYPE Original Research
PUBLISHED 24 January 2023
DOI 10.3389/fams.2022.1086745

OPEN ACCESS

EDITED BY
Ramoshweu Solomon Lebelo,
Vaal University of Technology, South Africa

REVIEWED BY
Mahmoud Abdel-Aty,
Sohag University, Egypt
Anastasiia Panchuk,
Institute of Mathematics (NAN Ukraine), Ukraine

*CORRESPONDENCE
Stephen E. Moore
✉ stephen.moore@ucc.edu.gh

SPECIALTY SECTION
This article was submitted to Mathematical Biology, a section of the journal Frontiers in Applied Mathematics and Statistics

RECEIVED 01 November 2022
ACCEPTED 28 December 2022
PUBLISHED 24 January 2023

CITATION
Kwofie T, Dogbatsey M and Moore SE (2023) Curtailing crime dynamics: A mathematical approach. *Front. Appl. Math. Stat.* 8:1086745. doi: 10.3389/fams.2022.1086745

Curtailing crime dynamics: A mathematical approach

Theophilus Kwofie[1], Matthias Dogbatsey[2] and Stephen E. Moore[3,4]*

[1]School of Mathematical and Statistical Sciences, Arizona State University, Tempe, AZ, United States, [2]Department of Mathematics, The University of Alabama, Tuscaloosa, AL, United States, [3]Department of Mathematics, University of Cape Coast, Cape Coast, Ghana, [4]Africa Centre of Excellence, Regional Transport Research and Education Centre (TRECK), Kumasi, Ghana

Introduction: Crime and criminal activities have huge influences on society and societal development. The social makeup of the society has a significant impact on the propagation of crime within a population. It is a well-known reality that crime spreads across society like an infectious disease, despite the fact that there are many elements that might affect this dynamic. So, understanding crime and the factors influencing its spread are essential in formulating policies to reduce the prevalence and impacts of crime.

Methods: We formulate a deterministic mathematical model using a system of nonlinear ordinary differential equations incorporating education programs as tools to assess the population-level impact on the spread of crime. The model has a global asymptotically stable crime-free equilibrium whenever a certain criminological threshold, known as the effective reproduction number $\mathcal{R}_E$, is less than unity.

Results and discussion: The model is fitted with prison data reported from July 2021 to June 2022 by the State of Illinois in The United States. The simulations are carried out to assess the population-level impact of the widespread use of the intervention programs and the compliance rate in the State of Illinois. We hypothetically fixed the efficacy of the intervention programs at 25% while varying the compliance rate (by the general public). With no compliance, a high level of active criminal population was recorded. As the compliance rates were significantly improved, the active population level decreased. The global sensitivity analysis is performed primarily to determine the parameters with the most effect on the spread of crime in the State of Illinois. The results demonstrate that the effective community contact rate, β_C, for the criminally active individuals is the main driver of crime in the State of Illinois.

KEYWORDS

crime dynamics, effective reproduction number, stability analysis, sensitivity analysis, USA

1. Introduction

One of the illegal ways to undermine human civilized society is through crime. It is crucial to thoroughly handle this issue because it has existed for a very long time [1]. Crime is a significant sociological problem that has been researched extensively in the scientific literature [2]. It is difficult to provide a concrete definition of crime because every society has its own norms and values. However, what constitutes a crime is an illegal act or a perpetrator's deviant conduct, its effective punishment can be imposed by a criminal legislating institution [3, 4], and the victims of these acts. Crime mainly rises from the combination of three factors: a driven offender, a suitable target, and the absence of an able guardian [5–7]. In view of this, all crimes require opportunity but not every opportunity is followed by crime. The spread of crime usually happens as a result of coming into contact with criminally active groups of people. We may not realize the spread of crime until it becomes predominant. Consequently, it goes without saying that crime imposes costs on society.

Mathematical modeling is a powerful tool that has been employed to examine the spread of crime. One of its main goals is to understand the condition under which the spread of crime within a population will disappear or persist. For instance, the United States (U.S) government spends more on the criminal justice system than any other country. Public spending on its prison system has increased by six times the rate of government spending on higher education over the past two decades [8]. A statistical model of criminal behavior is demonstrated [10]. The role of technology in combating social crime is studied using a deterministic model [11]. Here, authors considered a deterministic compartment model and emphasized the need for technology to combat crime in society. A mathematical model considering serious and minor criminal activities are formulated and analyzed [12]. In González-Parra et al. [2], authors have studied a mathematical model by considering crime as a social epidemic. Here, authors have considered several compartments and have assumed that a judge or a police officer can also become a criminal if they come into contact with criminals. An interesting mathematical model for the dynamics of the spread of crime is formulated and analyzed [8], where authors have shown that if they relax the assumption that crime initiates only through contagion, then the crime-free equilibrium is no longer possible and the model system can tend to either lower the crime equilibrium or increase the crime equilibrium. For example, the epidemic spread of drug use has been modeled using differential equations [13–15]. In Gonzalez et al. [16], the authors constructed a model examining the dynamics of peer pressure on college-age bulimia, focusing on the effects of the intervention at two stages of the disease. The Optimal control for crime at its minimal level during festive periods such as Christmas and Valentine's day, and entertainment events, such as music awards, have also been studied and presented [17].

Introducing fear to combat crime, will reduce the expectation of a benefit, and consequently the intention to engage in crime after considering the cost. Similar research on mathematical models of crime stems from Becker's perspective of crime as a rational decision-making [18] mechanism whereby the individual compares the benefits and costs (punishment) associated with criminal activity against criminal alternatives. For example, Freedman et al. [19] developed a model that depicts that crime is concentrated in places where the possible monetary benefit from committing a crime (the probability of not being convicted due to the reward of the crime) exceeds the cost of criminal opportunity. Wang et al. [20] generalized this approach allowing for the cost of an opportunity to be heterogeneous across future criminals and depending on the level of crime in a given society and estimated the amount of group crime activity in equilibrium. Another study focused on sanction policies that reduce crime through general or specific deterrence [21, 22]. Recently, Durlauf and Nagin [23] reviewed this research and concluded that incarceration is not the optimal approach to combat crime. From several research studies, increase in prison sentence lengths are associated with weak to modest declines in crime, while micro-level studies suggest that experiencing incarceration does not seem to prevent reoffending. Their findings show that the most significant deterrent effects come from implementing tactics that increase the perceived risk of apprehension. Recidivism rates in the United States vary depending on the crime. In the case of property and drug-related offenses, the likelihood of rearrest within 3 years after release is about 70% [24].

The present study is a development of a new mathematical model for studying crime dynamics and incorporating education programs as a tool to curtailing the menace of crime and criminality in the United States of America (particularly in the State of Illinois). The model takes the form of Kermack-McKendrick, a compartmental, deterministic system of nonlinear differential equations [25]. We consider some relevant aspects of the crime dynamics, including incarceration, desistance by criminals, and how released criminals return to their previous crime life. It is worth mentioning that the model under study exhibits certain features as illustrated in Srivastav et al. [1]. The model parameterized using available crime data obtained from the Illinois Department of Corrections Prison Population Data Sets. In addition, the parameterization of the model provides an insight into the assessment of some of the education programs.

The rest of the article is organized as follows; In Section 2, we present the model formulation while the basic properties of the model are presented in Section 3. The local and global stability analysis of the Crime-free equilibrium is presented in Section 4. In Section 5, we present both the global and local sensitivity analysis of the model, and finally, we present numerical simulations and discussions in Section 6.

2. Model formulation

We present a model to assess the various education programs to curtail criminality in the State of Illinois. The total population denoted as $N(t)$ is subdivided into mutually exclusive compartments of susceptible individuals (i.e., individuals who are at risk of becoming criminals) $S(t)$, criminally active individuals (i.e., individuals who are actively involved in crime at any given time) $C(t)$, criminals in prison (i.e., individuals who are caught in the act of crime and are put in prison) $P(t)$, and reformed Individuals (i.e., individuals who have come out of prison and leading a normal life), $R(t)$. We consider the following assumptions: (a) a homogeneously-mixed population [i.e., all individuals (both susceptible and criminals)] in the community are assumed to have an equal probability of coming into contact with one another), (b) exponentially-distributed waiting time in each criminological compartment, and (c) human demographic processes (i.e., migration, births or deaths due to causes other than the crime being modeled). Susceptible individuals join the criminal group when there is effective interaction with either criminal or prison individuals. A standard incidence

$$\lambda = \frac{(1-\varepsilon\eta)\left(\beta_c C + \beta_p P\right)}{N},$$

measures the force of crime, where β_c and β_p are community contact rates for both active criminals and criminals in prison, respectively, $0 < \eta \leq 1$ is the proportion of community members who observe the education programs introduced, $0 < \varepsilon \leq 1$ is the efficacy of the education programs (low values of η imply limited compliance of the intervention programs by the public, whiles values of η near unity signify widespread observance of the intervention programs). Again, values of ε close to zero imply that the intervention programs may not

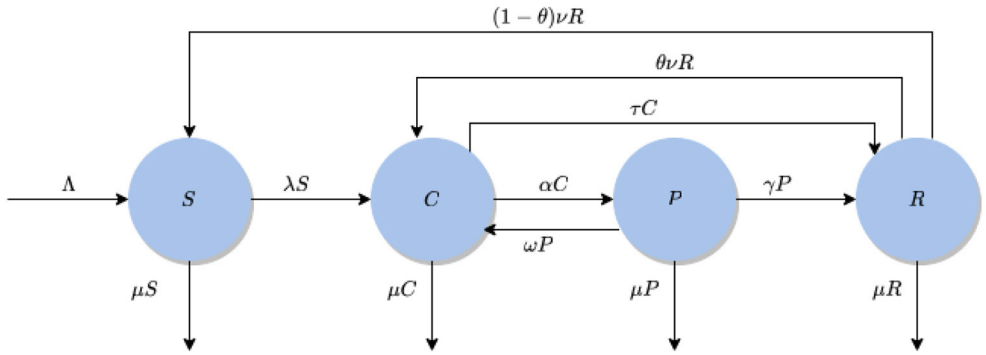

FIGURE 1
Flow diagram of the model (Equations 1–4).

TABLE 1 Description of state variables of the model (Equations 1–4).

State variables	Description
S	Susceptible individuals
C	Criminally active individuals
P	Criminals in prison
R	Reformed individuals

TABLE 2 Description of parameters of the model (Equations 1–4).

Parameter	Description
Λ	Recruitment rate
μ	Natural mortality rate
β_c	Community effective contact rate for criminally active individuals
β_p	Community effective contact rate for criminals in prison
ν	Rate of movement of individuals from the reformed class to either C or S
τ	Rate of desistance by criminals
ω	Rate at which incarcerated individuals go back to crime (recidivism)
α	Rate of incarceration
γ	Rate at which individuals move from P to R after completing their prison terms
ε	Efficacy of the intervention programs (education)
η	Proportion of community members who observe the education programs
θ	Fraction corresponding to movement of individuals from R to C

be a major tool to stop or reduce the spread of crime in the community.

Based on this fact (and noting the flow diagram in Figure 1), the basic model for the spread of crime dynamics in a community is given by the following deterministic system of nonlinear differential equations (where a dot represents differentiation with respect to time t):

$$\dot{S} = \Lambda - \lambda S + (1-\theta)\nu R - \mu S \tag{1}$$
$$\dot{C} = \lambda S + \omega P + \theta\nu R - (\mu + \alpha + \tau)C \tag{2}$$
$$\dot{P} = \alpha C - (\mu + \gamma + \omega)P \tag{3}$$
$$\dot{R} = \gamma P + \tau C - (\mu + \nu)R \tag{4}$$

Equation (1) describes the dynamics of the law-abiding individuals in the community $S(t)$. The first term Λ refers to a fixed number of individuals who join the susceptible population either through migration or birth. The term $(1-\theta)\nu R$ refers to the proportion of individuals who recover fully and return to the susceptible class. Equations (2) and (3) describe the dynamics within the active criminal population $C(t)$ and prison population $P(t)$, respectively, either through incarceration, desistance, recidivism, or proportion of individuals that return to their previous criminal life after they have been released from prison. Equation (4) highlights the modification in the reformed class $R(t)$, which describes the movement from $R(t)$ to $C(t)$ and $C(t)$ to $R(t)$. The term ν describes the rate at which reformed individuals recover fully and return to the susceptible class $S(t)$. We assume natural deaths occurrence in all compartments. The description of the variables and parameters are given in Tables 1, 2, respectively.

3. Basic properties of the model

Lemma 1. *(Positivity) Let $t > 0$. In this model, if the initial conditions satisfy $S(0) > 0, C(0) > 0, P(0) > 0, R(0) > 0$, then for all $t \in [0, t_0]$, $S(t), C(t), P(t)$, and $R(t)$ will remain positive in $\mathbb{R}^4_+$ for arbitrary t_0.*

Proof: With all the parameters used in the system being non-negative, we can thus place a lower bound on each of the equations making up the model. Thus,

$$\dot{S} = \Lambda + (1-\theta)\nu R - \left[\frac{(1-\varepsilon\eta)(\beta_c C + \beta_p P) + \mu N}{N}\right]$$
$$S \geq -\left[\frac{(1-\varepsilon\eta)(\beta_c C + \beta_p P) + \mu N}{N}\right] S \tag{5}$$
$$\dot{C} = \frac{(1-\varepsilon\eta)(\beta_c C + \beta_p P)}{N} S - (\mu + \alpha + \tau)C \geq -(\mu + \alpha + \tau)C \tag{6}$$
$$\dot{P} = \alpha C - (\mu + \gamma + \omega)P \geq -(\mu + \gamma + \omega)P \tag{7}$$
$$\dot{R} = \gamma P + \tau C - \nu R \geq -\nu R. \tag{8}$$

By applying basic differential equations method (separation of variables), we can resolve these inequalities to produce

$$\begin{aligned} S &\geq S_0 e^{-\Delta t} > 0, \\ C &\geq C_0 e^{-(\mu+\tau+\alpha)t} > 0, \\ P &\geq P_0 e^{-(\mu+\gamma+\omega)t} > 0, \\ R &\geq R_0 e^{-\nu t} > 0, \end{aligned}$$

where $\Delta = \dfrac{(1-\varepsilon\eta)(\beta_c C + \beta_p P) + \mu N}{N}$. Thus, for all $t \in [0, t_0]$, $S(t), C(t), P(t)$, and $R(t)$ will be positive and remain in $\mathbb{R}^4_+$.

Lemma 2. *(Boundedness) There exists an* $S_M, C_M, P_M, R_M > 0$ *such that for* $S(t), C(t), P(t), R(t)$ $\limsup_{t\to\infty}(S(t)) \leq S_M$, $\limsup_{t\to\infty}(C(t)) \leq C_M$, $\limsup_{t\to\infty}(P(t)) \leq P_M$, $\limsup_{t\to\infty}(R(t)) \leq R_M$ *for all* $t \in [0, t_0]$ *for arbitrary* t_0.

Proof: Since the model Equations (1)–(4) monitors human populations, all the associated parameters and state variables are positive, and adding the four equations of the model Equations (1)–(4) gives us

$$\dot{N} = \Lambda - \mu N. \tag{9}$$

Solving Equation (9) yields

$$N = \frac{\Lambda}{\mu} - \left(N_0 - \frac{\Lambda}{\mu}\right) e^{-\mu t}.$$

The upper bound can be found by taking the lim sup of both sides as $t \longrightarrow \infty$ to get $\dfrac{\Lambda}{\mu}$. So N is bounded below by 0 and above by $\dfrac{\Lambda}{\mu}$. Therefore for $t \in [0, t_0]$, $S(t), C(t), P(t), R(t)$ are bounded.

The model (Equations 1–4) is biologically and mathematically well-posed in the domain

$$\mathcal{D} = \left\{(S, C, P, R) \in \mathbb{R}^4_+ : 0 \leq N \leq \frac{\Lambda}{\mu}\right\}.$$

Thus, the domain, $\mathcal{D}$ is positively invariant.

4. Stability analysis of crime-free equilibrium

4.1. Crime-free equilibrium

The model has a crime-free equilibrium (*CFE*), obtained by setting the right-hand sides of Equations (1)–(4) to zero, given by

$$\mathcal{E}_0 := (S^*, C^*, P^*, R^*) = \left(\frac{\Lambda}{\mu}, 0, 0, 0\right), \tag{10}$$

with $N^* = S^* + C^* + P^* + R^* = \Lambda/\mu$.

4.2. Crime effective reproduction number

For infectious diseases, one of the most important threshold parameters is the basic reproduction number, denoted by $\mathcal{R}_0$, which is required to determine the transmission dynamics of an infectious disease in a population. However, in criminal dynamic models, $\mathcal{R}_0$, is a threshold parameter that measures the average number of new criminals produced by the relapse and interaction of the criminal population with the susceptible population [26].

The basic tool for examining epidemic thresholds in complex, structured models is the so-called next-generation matrix [27]. We use the next-generation method to compute the crime effective reproduction number $\mathcal{R}_E$ for our model. Here, we assumed that each function is at least twice continuously differentiable in each variable

$$f = \begin{pmatrix} \dfrac{(1-\varepsilon\eta)\left(\beta_c C + \beta_p P\right) S}{N} \\ 0 \end{pmatrix} \quad \text{and} \quad \nu = \begin{pmatrix} (\mu+\alpha+\tau)C - \omega P \\ (\mu+\gamma+\omega)P - \alpha C \end{pmatrix}, \tag{11}$$

where f is the rate of appearance of a new crime in a compartment and ν is the rate of transfer of individuals into and out of a compartment. We linearized the two expressions earlier with respect to C and P to obtain

$$\mathcal{F} = \begin{pmatrix} \beta_c\,(1-\varepsilon\,\eta) & \beta_p\,(1-\varepsilon\,\eta) \\ 0 & 0 \end{pmatrix} \quad \text{and}$$

$$\mathcal{V} = \begin{pmatrix} \alpha+\mu+\tau & -\omega \\ -\alpha & \gamma+\mu+\omega \end{pmatrix},$$

since $S^* = N^*$. The effective or control reproduction number, denoted by $\mathcal{R}_E$, is then given by $\mathcal{R}_E = \rho(\mathcal{F}\mathcal{V}^{-1})$ where $\rho(\cdot)$ denotes the spectral radius (dominant eigenvalue). It follows that

$$\mathcal{R}_E = \mathcal{R}_c + \mathcal{R}_p,$$

where

$$\begin{aligned} \mathcal{R}_c &= \frac{\beta_c(1-\eta\varepsilon)}{(\mu+\alpha+\tau)(1-\psi)} \quad \text{and} \\ \mathcal{R}_p &= \frac{\alpha\beta_p(1-\eta\varepsilon)}{(\mu+\alpha+\tau)(\mu+\gamma+\omega)(1-\psi)}. \end{aligned}$$

Thus by expressing $\mathcal{R}_E$ in terms of $\mathcal{R}_0$, we obtain $\mathcal{R}_E = (1-\eta\varepsilon)\mathcal{R}_0$.

In the absence of intervention strategies (*i.e.*, $\varepsilon = 0 = \eta$), the effective reproduction number is given by

$$\mathcal{R}_0 = \frac{\beta_c}{(\mu+\alpha+\tau)(1-\psi)} + \frac{\alpha\beta_p}{(\mu+\alpha+\tau)(\mu+\gamma+\omega)(1-\psi)},$$

where $\psi = \left(\dfrac{\alpha}{\mu+\alpha+\tau}\right)\left(\dfrac{\omega}{\mu+\gamma+\omega}\right)$.

Remark. *The expression* ψ *represents the proportion of active criminals incarcerated and reverted back to be criminals or the likelihood that a criminal will return to being a criminal again. The terms* $\dfrac{1}{(\mu+\alpha+\tau)}$ *and* $\dfrac{1}{(\mu+\gamma+\omega)}$ *are the duration of stay in compartments C and P, respectively. The expression* $\dfrac{\alpha}{(\mu+\alpha+\tau)}$ *is the proportion of active criminals that are imprisoned or the probability that a criminal will be sent to prison, and* $\dfrac{\omega}{(\mu+\gamma+\omega)}$ *is the proportion of prisoners that are released and go back into criminality.*

$\mathcal{R}_E$ is the number of individuals a criminal activist can influence during the period of successful criminal behavior where intervention programs are introduced into the community. The effective reproduction number $\mathcal{R}_E$ of the model (Equations 1–4) is expressed as the sum of two constituents reproduction numbers, namely the average number of new crimes generated by a typical active criminal in a community, denoted by $\mathcal{R}_c$, and the average number of crimes generated by a typical criminal in prison, denoted by $\mathcal{R}_p$.

4.3. Local stability analysis of crime-free equilibrium

Theorem 4.1. *The CFE ($\mathcal{E}_0$) of the model (Equations 1–4) is locally asymptotically stable (LAS) if $\mathcal{R}_E < 1$. If $\mathcal{R}_E > 1$, the crime rises to a peak and then eventually declines to zero.*

Proof: The local stability of the *CFE* ($\mathcal{E}_0$) is determined by using the eigenvalues of the Jacobian matrix at $\mathcal{E}_0$, given by

$$J^{\diamond}(\mathcal{E}_0) = \begin{pmatrix} -\mu & \beta_c(\varepsilon\,\eta - 1) & \beta_p(\varepsilon\,\eta - 1) & -\nu(\theta - 1) \\ 0 & -K_1 - \beta_c(\varepsilon\,\eta - 1) & \omega - \beta_p(\varepsilon\,\eta - 1) & \nu\,\theta \\ 0 & \alpha & -K_2 & 0 \\ 0 & \tau & \gamma & -K_3 \end{pmatrix}, \tag{12}$$

where $K_1 = (\mu + \alpha + \tau)$, $K_2 = (\mu + \gamma + \omega)$, and $K_3 = (\mu + \nu)$. It is easy to see that the first negative eigenvalue is $\lambda_1 = -\mu$. The remaining eigenvalues are obtained below:

$$J^{\star} = \begin{pmatrix} -K_1 - \beta_c(\varepsilon\,\eta - 1) & \omega - \beta_p(\varepsilon\,\eta - 1) & \nu\,\theta \\ \alpha & -K_2 & 0 \\ \tau & \gamma & -K_3 \end{pmatrix}.$$

The characteristic polynomial of the aforementioned matrix $J^{\star}$ is given by

$$\mathcal{P}(\lambda) = \lambda^3 + a_1\lambda^2 + a_2\lambda + a_3,$$

where

$$\begin{aligned} a_1 &= K_1 + K_2 + K_3 - \beta_c(1 - \varepsilon\,\eta), \\ a_2 &= K_1K_2 - K_3\beta_c - \alpha\beta_p - \alpha\omega - K_2\beta_c + K_1K_3 + K_2K_3 - \nu\tau\theta \\ &\quad + K_2\beta_c\varepsilon\,\eta + K_3\beta_c\varepsilon\,\eta + \alpha\beta_p\varepsilon\,\eta, \text{ and} \\ a_3 &= K_3(K_1K_2 - \alpha\omega)(1 - \mathcal{R}_E) + \nu\theta(K_2\tau + \alpha + \gamma). \end{aligned}$$

Applying the Routh-Hurwitz criterion [28], it is clear that $a_1 > 0$ if $K_1 + K_2 + K_3 > \beta_c(1 - \varepsilon\,\eta)$. It should be emphasized that $\mathcal{R}_E < 1$ makes $a_3 > 0$. Furthermore, if $\mathcal{R}_E > 1$, then $a_3 < 0$. The condition $\mathcal{R}_E < 1$, makes

$$K_1K_2 - \alpha\omega > \alpha\beta_pK_2\beta_c, \tag{13}$$

$$K_1K_3 + K_2K_3 - \nu\tau\theta > K_3\beta_c. \tag{14}$$

The two inequalities (Equations 13–14) imply that $a_2 > 0$. Finally, we need to show that $a_1a_2 > a_3$. After algebraic manipulations, we have that $a_1a_2 > a_3$. Thus, the crime-free equilibrium of the model (Equations 1–4) is locally asymptotically stable whenever $\mathcal{R}_E < 1$, otherwise unstable.

The criminological implication of Theorem 4.1 is that a small influx of active criminal individuals in the community will not generate an outbreak of crime in the community if $\mathcal{R}_E < 1$. That is, the spread of crime rapidly dies out (when $\mathcal{R}_E < 1$) if the initial number of active criminal individuals in the community are in the basin of attraction of the *CFE* ($\mathcal{E}_0$). For instance, when $\mathcal{R}_0 = 2$, one active criminal in the community will, on average, influence two other individuals during the duration of his/her successful criminal behavior. Hence, in this case, the crime will be spreading exponentially until intervention strategies are implemented in the community and/or a certain proportion of the public is educated. In this article, since intervention measures are put in place to help stop or reduce the spread of crime, the rate at which crime spreads will be minimized. In order for crime elimination to be independent of the initial size of the sub-populations of the model, it is necessary to show that the crime-free equilibrium ($\mathcal{E}_0$) is globally asymptotically stable.

4.4. Global asymptotic stability of the crime-free equilibrium

The global asymptotic stability of the crime-free equilibrium of the model (Equations 1–4) can be established for the special case, that is in the absence of re-committing the crime (i.e., $\theta = 0$).

Theorem 4.2. *Consider the special case of the model (Equations 1–4) in the absence of re-committing the crime (i.e., $\theta = 0$), the crime-free equilibrium ($\mathcal{E}_0$) of the model (Equations 1–4) is globally asymptotically stable in $\mathcal{D}$ whenever $\mathcal{R}_E < 1$.*

The proof of Theorem 4.2 is based on using a comparison theorem [29].

Proof: Consider the special case of the model (Equations 1–4) in the absence of re-committing the crime. Let us assume that $\mathcal{R}_E < 1$. The equations for the crime compartments for the special case of the model (Equations 1–4) can be re-written in terms of the next generation matrices ($\mathcal{F}$ and $\mathcal{V}$) as follows:

$$\frac{d}{dt}\begin{bmatrix} C(t) \\ P(t) \end{bmatrix} = (\mathcal{F} - \mathcal{V})\begin{bmatrix} C(t) \\ P(t) \end{bmatrix} - \mathcal{M}\begin{bmatrix} C(t) \\ P(t) \end{bmatrix}, \tag{15}$$

where (with S^* and N^* as defined in Section 11),

$$(\mathcal{F} - \mathcal{V}) = \begin{bmatrix} \frac{\beta_c(1-\epsilon\,\eta)S^*}{N^*} - (\alpha + \mu + \tau) & \frac{\beta_p(1-\epsilon\,\eta)S^*}{N^*} + \omega \\ \alpha & -(\gamma + \mu + \omega) \end{bmatrix},$$

and

$$\mathcal{M} = (1 - \varepsilon\,\eta)\left(1 - \frac{S}{N}\right)\begin{bmatrix} \beta_c & \beta_p \\ 0 & 0 \end{bmatrix}. \tag{16}$$

Since $S \leq N$ for all $t > 0$ in $\mathcal{D}$, it follows that the matrix $\mathcal{M}$, defined in Equation (16), is non-negative. Hence, the Equation (15) can be re-written in terms of the following inequality:

$$\frac{d}{dt}\begin{bmatrix} C(t) \\ P(t) \end{bmatrix} \leq (\mathcal{F} - \mathcal{V})\begin{bmatrix} C(t) \\ P(t) \end{bmatrix}. \tag{17}$$

If $\mathcal{R}_E < 1$, this implies that all eigenvalues of the next generation matrix $\mathcal{F}\mathcal{V}^{-1}$ are negative. Equivalently, we can claim that $\mathcal{F} - \mathcal{V}$

is a stable matrix [27]. Thus, it can be concluded that the linearized differential inequality system (Equation 17) is stable whenever $\mathcal{R}_E < 1$. Hence, it follows from aforementioned analysis that

$$(C(t), P(t)) \to (0, 0), \text{ as } t \to \infty.$$

Eventually after substituting $C(t) = P(t) = 0$ into the differential equations for the rate of change of the $R(t)$ and $S(t)$ compartments shows that

$$R(t) \to 0 \text{ and } S(t) \to S^* \text{ as } t \to \infty.$$

Hence, we can finally claim that the CFE (given in Section 11) for the special case of the model (Equations 1–4) (with $\theta = 0$) is globally asymptotically stable in $\mathcal{D}$ whenever $\mathcal{R}_E < 1$.

The criminological implication of Theorem 4.2 shows that, for the special case of the model (Equations 1–4) with $\theta = 0$, the overall crime can be eliminated from the community if $\mathcal{R}_E$ is brought to and maintained to a value less than unity.

5. Sensitivity analysis

We use sensitivity analysis to determine the robustness of model predictions to parameter values since there usually are errors in data collection and presumed parameter values [30]. Sensitivity indices also enable us to quantify the change in the state variables that results from changes in the parameters [9]. Sensitivity analysis is used to discover parameters that have a high impact on the crime reproductive number and should be targeted by intervention strategies. We define the normalized forward sensitivity index (NFSI) of the effective crime reproduction number as the relative change in $\mathcal{R}_0$ occasioned by the relative change in each of the parameters. The normalized forward sensitivity index of a variable to a parameter is the ratio of the relative change in the variable to the relative change in the parameter. Since the effective crime reproduction number $\mathcal{R}_0$ is differentiable with respect to all the parameters, we define the sensitivity index as follows:

Definition 1. *For an effective crime reproduction number, $\mathcal{R}_0$, differentiable with respect to the parameter q, the normalized forward sensitivity index (NFSI) is defined as*

$$\Upsilon_q^{\mathcal{R}_0} = \frac{\partial \mathcal{R}_0}{\partial q} \times \frac{q}{\mathcal{R}_0}. \tag{18}$$

Using this definition, we estimate the sensitivity indices of the parameters of the effective crime reproduction number as follows:

$$\Upsilon_{\beta_c}^{\mathcal{R}_0} = \frac{\beta_c\,(\gamma + \mu + \omega)}{\alpha\beta_p + \beta_c\,(\gamma + \mu + \omega)}$$

$$\Upsilon_{\beta_p}^{\mathcal{R}_0} = \frac{\alpha\beta_p}{\alpha\beta_p + \beta_c\,(\gamma + \mu + \omega)}$$

$$\Upsilon_{\tau}^{\mathcal{R}_0} = -\frac{\tau(\gamma + \mu + \omega)}{(\gamma + \omega)(\alpha + \mu + \tau) + \mu(\mu + \tau)}$$

$$\Upsilon_{\gamma}^{\mathcal{R}_0} = -\frac{\alpha\gamma(\beta_c\mu + \alpha + \mu + \tau)(\gamma + \mu + \omega)))}{(\alpha\beta_p + \beta_c(\gamma + \mu + \omega))(\alpha(\gamma + \omega) + (\mu + \tau)(\gamma + \mu + \omega))(\gamma + \mu + \omega)}$$

$$\Upsilon_{\omega}^{\mathcal{R}_0} = -\frac{\alpha\omega(\beta_c\mu + \alpha + \mu + \tau)(\gamma + \mu + \omega)))}{(\alpha\beta_p + \beta_c(\gamma + \mu + \omega))(\alpha(\gamma + \omega) + (\mu + \tau)(\gamma + \mu + \omega))(\gamma + \mu + \omega)}$$

$$\Upsilon_{\alpha}^{\mathcal{R}_0} = -\frac{\alpha\,(\gamma + \mu + \omega)\,\big(\beta_c(\gamma + \omega) - \beta_p(\mu + \tau)\big)}{\big(\alpha\,\beta_p + \beta_c\,\gamma + \beta_c\,\mu + \beta_c\,\omega\big)\,\big(\alpha\,\gamma + \alpha\,\omega + \gamma\,\mu + \gamma\,\tau + \mu\,\omega + \mu\,\tau + \omega\,\tau + \mu^2\big)}$$

TABLE 3 Baseline values of the fixed parameters of the model (Equations 1–4).

Parameter	Value	Source
N	2,746,388	[31]
μ	$1/(74.7 \times 52)$ week^{-1}	[32]
Λ	707.0302 week^{-1}	Estimated
α	0.005 week^{-1}	[33]
γ	0.0159 week^{-1}	[34]
ε	0.43 (dimensionless)	[35]
η	0.52 (dimensionless)	[36]
θ	0.7 (dimensionless)	[22]
ν	0.003 week^{-1}	[34]

TABLE 4 Baseline values of fitted (estimated) parameters of the model (Equations 1–4), obtained by fitting the model with the weekly crime data for Illinois for the period July 1st, 2021 to June 30th, 2022.

Parameter	Estimated value	Parameter	Estimated value
β_c	0.1543 week^{-1}	β_p	0.0010 week^{-1}
τ	0.0100 week^{-1}	ω	0.1067 week^{-1}

The simulations of the model were Equations (1–4) were carried out using the parameters estimated from the weekly crime data for the State of Illinois.

The final sign of the last index is dependent on the value of the numerator. It is easily verifiable that all the index values are less than 1. Since the effective crime reproductive number plays a critical role in the spread of crime, it is important to identify the most effective approach in bringing down our $\mathcal{R}_0$. To this end, we perform numerical simulations using the baseline parameter values given in Tables 3, 4 to identify which parameters are sensitive to the effective reproductive number.

Parameter	Sensitivity index	Parameter	Sensitivity index
β_c	0.999736	β_p	0.000264
τ	−0.160078	γ	−0.000251
ω	−0.001686	α	−0.798448
μ	−0.039537		

We observe that community contact rate for active criminals β_c has nearly one to one corresponding relationship with the crime reproductive number $\mathcal{R}_0$ such that a 10% change in β_c results in

a 9.9% change in $\mathcal{R}_0$. So the crime reproductive number is most sensitive to β_c. The crime reproductive number also has a direct proportional relationship with the parameter β_p. However, the effect is much lower, a 100% change in β_p only leads to 0.26% change in the crime reproductive number. The crime reproductive number $\mathcal{R}_0$ has an inverse proportional relationship with parameters $\tau, \omega, \gamma, \alpha, \mu$; an increase in any of them will bring about a decrease in crime reproductive number $\mathcal{R}_0$.

5.1. Data fitting and parameter estimation

In this section, we have fitted the observed weekly cumulative crime data for Illinois from the period of 1 July 2021 to 30 June 2022 [37]. The time series illustration of the least squares fit of the model (Equations 1–4) is depicted in Figure 2, showing the model estimation (i.e., blue curve which is plotted for the criminals in prisons as formulated in Equation 3) represents the cumulative weekly crimes compared to the observed cumulative weekly crime data (i.e., red dots) for the aforementioned time period.

The developed model has a total of 13 different parameters, out of which 8 parameters are known from the existing literature which is shown in Table 3. We have calculated the daily recruitment rate (Λ) as a product of the total population (N) of Illinois, which is based on the projections of the latest U.S. census [31] and the weekly natural mortality rate (μ). The developed model was fitted using a standard nonlinear least squares approach, which involved using the inbuilt Matlab R2022a optimizer function "lsqcurvefit," which will be used to obtain the best values of the remaining four unknown parameters. SSE minimizes the sum of the squared differences between each observed cumulative crime data points and the corresponding cumulative crime points obtained from the model (Equations 1–4). The estimated values of the unknown parameters which are obtained from the fitting are shown in Table 4. The effective reproduction number for the set of the fixed and fitted parameters for the model (Equations 1–4) is $\mathcal{R}_E = 11.4223$.

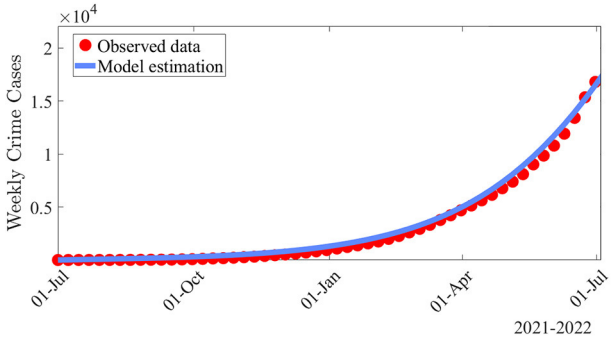

FIGURE 2
Data fitting of the model (Equations 1–4) using weekly crime data for Illinois from 1 July 2021 to 30 June 2022. The simulations of the model (Equations 1–4) carried out using the parameters estimated from the weekly crime data for the Illinois. The values of the fixed and fitted parameters used for the purpose of the data fitting and parameter estimation are shown in Tables 3, 4, respectively.

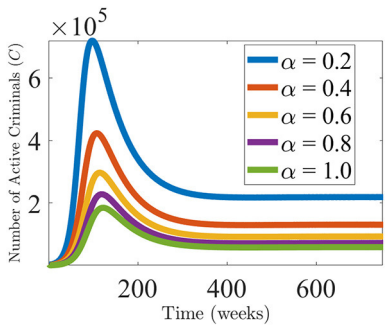

FIGURE 3
Effect of varying the incarceration rate α on the criminal population. Simulation displaying the active criminal population, as a function of time. The values of the parameters are used from Tables 3, 4 with the values of α being varied.

6. Numerical simulations and discussions

To demonstrate some of the various theoretical results contained in this paper, the model (Equations 1–3) is simulated using the baseline values shown in Table 3 (unless otherwise stated), to assess the population-level impact of the interventions programs (in a form of education) against crime level in Illinois. It is worth noting that throughout the simulations, Matlab R 2022a was used, and the initial conditions considered are $S(0) = 2,742,386, C(0) = 3,950, P(0) = 2, and\ R(0) = 50$. We also simulated the model (Equations 1–3) using the calibrated parameters in Table 4, coupled with other estimated parameters in Table 3 to assess the population-level impact of mitigation strategies. First of all, we simulated the model to assess the population-level impact of the incarceration on the active criminal population. The population-level impact of incarceration is measured by the reduction of the active criminal population.

One thing that is important in the fight against crime is the rate of uptake into correctional facilities of criminals. We varied the rate of uptake into rehabilitation (α) and we found that as the rate of incarceration increases, the number of criminals in the population reduces as a result. Thus, the more criminals are incarcerated and put in rehabilitation programs, the more crime reduces. This can be seen in Figure 3. This observation is consistent with the conclusion from similar studies done by Nyabadza et al. [9] and Berenji et al. [38]. Liedka et al. [39] observed that there exists a negative relationship between prison(incarceration) and crime. Rose et al. [40] observed that within 3 years of incarceration, the risk of committing new assault crimes, property crimes, and drug crimes reduced by 38%, 24%, and 30%, respectively.

In Figure 4, the simulations are carried out to assess the population-level impact of the widespread use of the intervention programs and the compliance rate in the Illinois. This Figure shows a marked decrease in the active criminal population with varying efficacy and compliance rates. For (a), we hypothetically fixed the efficacy of the intervention programs at 25% while varying the compliance rate (by the general public). With no compliance, a high level of the active criminal population (approximately 2,020,650)

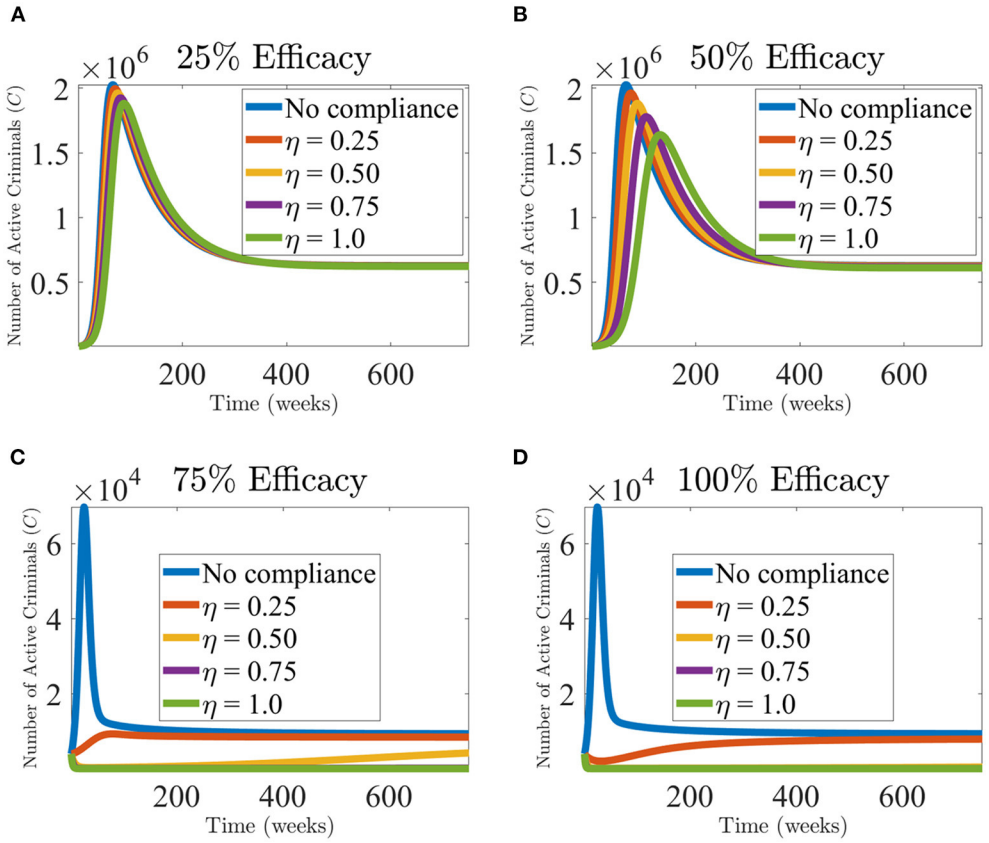

FIGURE 4
Effect of intervention programs in the Illinois community. The simulation of the model (Equations 1–3), showing the weekly crime levels, as a function of time, for the assessment of the impact of the intervention programs (ε) and the compliance rate (η); **(A)** 25% efficacy of intervention programs, **(B)** 50% efficacy of intervention programs, **(C)** 75% efficacy of intervention programs, and **(D)** 100% efficacy of intervention programs for Illinois. Allowing for the assessment of the combined effect of the intervention strategies and how the masses comply with the policies. The improvement in the intervention strategies and compliance rate are measured in terms of the percentage reduction of crime levels in Illinois. The other parameter values used are given in Tables 3, 4.

was recorded. As the compliance rates were significantly improved, the active population level decreased. For (b), we hypothetically improved the efficacy rate by fixing it at 50% and realized that increasing the compliance rates by 25% dramatically flattens the active criminal population curves. However, with such an efficacy level coupled with the varying compliance rates, the crime level in the community may still persist. Even though the use of intervention programs with low-level of efficacy rates may not lead to the elimination of crime in the community, they have the potential of reducing the burden of crime in the community (Figure 4B). An interesting observation was made when the efficacy and compliance were 75 and 25%, respectively. The burden of active criminal populations reduces, almost leading to the eventual eradication of crime in the population. In order to effectively measure the impact of the intervention programs, it is imperative to consider further increasing the efficacy levels while varying the compliance rates. For a case where 100% of the populace in Illinois complies with the intervention programs with a low-efficacy rate of 50%, the number of active criminals in the community will be reduced. As it is clear that it will be impossible to have everyone comply with the education programs. However, with the right set of strategies, many of the populace may understand the message and eventually comply with it.

Authors in Zitko [41] made a comparison of state-level education data and crime and incarceration rates, and they realized that states that have focused the most on education (in general, financial support) tend to have lower rates of violent crime and incarceration. Although education cannot be seen as a "cures all" or a panacea that will ensure declines in criminal behavior or crime rates, research indicates that increased spending on high-quality education can have a favorable impact on public safety. Many trends have been supported by contemporary research that has examined possible connections between education and criminal behavior. Both the idea that people with learning difficulties are more likely to engage in violent behavior and the idea that education levels (both greater and lower) are important in the manifestation of criminal behavior have empirical backing. Numerous criminologists have examined the connection between intelligence and crime in their writings, frequently discovering an inverse link between the two. In other words, criminologists have discovered that those with lower IQs are more likely to commit a crime than people with higher IQs [42]. However, James Oleson's "Criminal Genius" sheds light on the offenses–drawn from self-reports and interviews–committed by high-IQ individuals, a group understudied in the field of criminology [42].

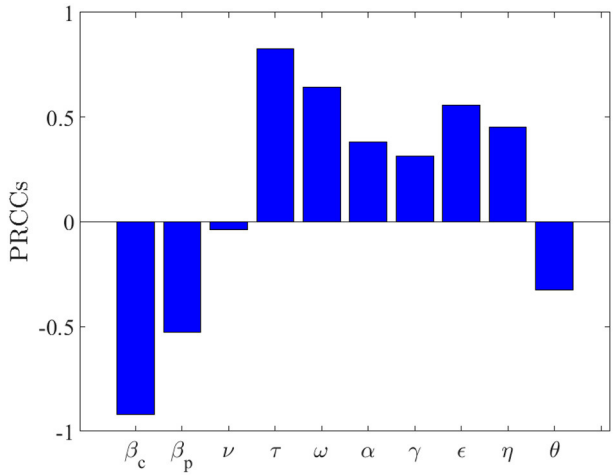

FIGURE 5
Partial rank correlation coefficients (PRCCs) showing the effects of the model parameters on the response variable (which in our case is the crime population as a function of time). The baseline values of the parameters used are given in Tables 3, 4.

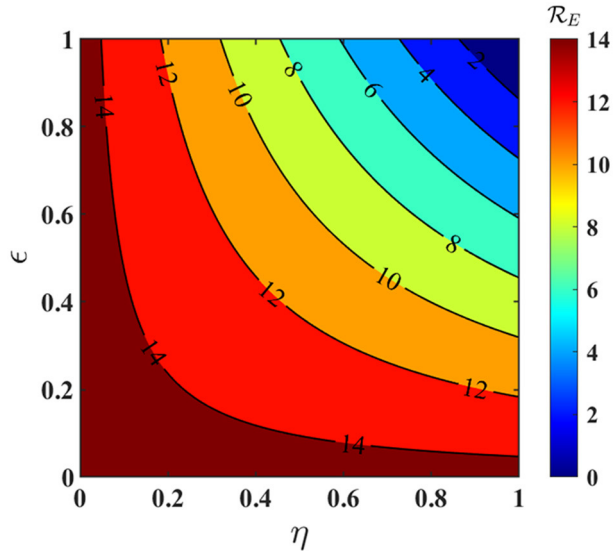

FIGURE 6
The contour plot of the effective (or control) reproduction number $\mathcal{R}_E$, as a function of the intervention programs (ϵ) and the compliance rate (η). The other parameter values used for the contour plot are given in Tables 3, 4, respectively.

6.1. Global sensitivity analysis

The model (Equations 1–3) has 12 parameters and the purpose of the sensitivity analysis is to measure the impact of the sensitivities of the parameters on the outcome of the numerical simulation results (with respect to a particular response function). The standard uncertainty and sensitivity analysis, using the Latin Hypercube Sampling technique and partial rank correlation coefficients (PRCCs) were applied to ascertain the sensitivities of the parameters against the crime compartment which is a function of time (as a response function) [43]. Other response functions, such as the crime effective reproduction number ($\mathcal{R}_E$), could have been used to measure such sensitivities of the parameters. To do the sensitivity analysis, each model parameter's range (lower and upper bound) and distribution must first be defined, followed by the division of each range into 1,000 equal sub-intervals. A 1,000 × 12 matrix is created by randomly selecting parameter sets from this space without replacing them [44, 45]. The values of the response function (crime compartment which is a function of time) are obtained for each row of this matrix, and then PRCCs are computed to analyze the contributions of uncertainty and variability in specific parameters to uncertainty and variability in the response function. High PRCC values near 1 or -1 are seen as significantly correlated with the response function, whereas low PRCC values are regarded as negatively (or positively) correlated with the response function. We assume, for simplicity, that each of the 12 parameters of the model (Equations 1–3) obeys a uniform distribution, and the range for each parameter is obtained by taking 20% to the left, and then 20% to the right, of its baseline value (given in Tables 3, 4) [43].

In Figure 5, the parameters that have a great impact on the response variable are the community effective contact rate for criminally active individuals (β_c), the rate of desistance by criminals (τ), and the recidivism rate (ω). This explains that the effective community contact rate for criminally active individuals is the main driver of crime in our society.

We depict the contour plots of the effective reproduction number $\mathcal{R}_E$ as a function of the intervention programs (ϵ) and the compliance rate (η) at steady-state in Figure 6. As expected, the increment in the efficacy of the intervention programs along with the increment in the proportion of community members who observe the education program (i.e., the compliance rate) has a significant impact on the reduction of $\mathcal{R}_E$. Furthermore, it is notable from Figure 6 that to keep and maintain $\mathcal{R}_E$ to a value less than unity, we need to keep the intervention programs and the compliance rate above 95%. On the contrary, if due to any reasons, the intervention programs and the compliance rate both drop down drastically to 20% or even much lower than it, so for this scenario, we could observe that the value of $\mathcal{R}_E$ increases dramatically to 14 or even above. Overall, our study shows that to effectively control crime in the community, it is necessary and sufficient to keep the efficacy of the intervention programs and the compliance rate of the education programs above 95%. Thus, a strategy that emphasizes the significant increments in ϵ and η would notably enhance the prospects of crime elimination in the state of Illinois.

7. Conclusion

In this paper, we developed a mathematical model that incorporates programs in curtailing crime dynamics. The deterministic model was fitted with crime data from Illinois [37] in the United States (U.S.) by means of a least squares method. We present both local and global asymptotic analysis for the crime free equilibrium. We observed globally asymptotically stable crime-free equilibrium whenever the effective crime reproduction number $\mathcal{R}_E$ is less than one, i.e., $\mathcal{R}_E < 1$. By using the partial rank correlation coefficients (PRCCs) method, we are able to estimate the parameters that have a significant influence on the model. We observed that the community effective contact rate

for criminally active individuals (β_c), the rate of desistance by criminals (τ), and the recidivism rate (ω) tend to have a great impact on the spread of crime, see, Figure 5. The numerical simulation shows that with an efficacy level of 75% with varying compliance levels (0 − 100%), the burden of crime will be reduced drastically.

Data availability statement

Publicly available datasets were analyzed in this study. This data can be found at: https://www2.illinois.gov/idoc/reportsandstatistics/Pages/Prison-Population-Data-Sets.aspx.

Author contributions

TK, MD, and SM: conceptualization, methodology, formal analysis, writing—original draft, writing—review, and editing. All authors contributed to the article and approved the submitted version.

Funding

SM was supported by a grant from UNESCO-TWAS and the Swedish International Development Cooperation Agency (SIDA).

Acknowledgments

Thanks to the reviewers whose comments helped improve the article.

Conflict of interest

The authors declare that the research was conducted in the absence of any commercial or financial relationships that could be construed as a potential conflict of interest.

Publisher's note

All claims expressed in this article are solely those of the authors and do not necessarily represent those of their affiliated organizations, or those of the publisher, the editors and the reviewers. Any product that may be evaluated in this article, or claim that may be made by its manufacturer, is not guaranteed or endorsed by the publisher.

Author disclaimer

The views expressed herein do not necessarily represent those of UNESCO-TWAS, SIDA or its Board of Governor.

References

1. Srivastav AK, Ghosh M, Chandra P. Modeling dynamics of the spread of crime in a society. *Stochastic Anal Appl*. (2019) 37:991–1011. doi: 10.1080/07362994.2019.1636658

2. González-Parra G, Chen-Charpentier B, Kojouharov HV. Mathematical modeling of crime as a social epidemic. *J Interdisc Math*. (2018) 21:623–43. doi: 10.1080/09720502.2015.1132574

3. Block CR, Block RL. Crime definition, crime measurement, and victim surveys. *J Soc Issues*. (1984) 40:137–59. doi: 10.1111/j.1540-4560.1984.tb01086.x

4. Garside R. Criminal justice since 2010. What happened, and why? Richard Garside considers the divergent policy developments within the three jurisdictions. *Crim Justice Matters*. (2015) 100:4–8. doi: 10.1080/0268117X.2015.1061331

5. Ajayi J, Adefolaju T. Crime prevention and the emergence of self-help security outfits in South-western Nigeria. *Int J Humanities Soc Sci*. (2013) 3:287–99.

6. Ayodele JO. Crime-reporting practices among market women in oyo, nigeria. *SAGE Open*. (2015) 5:940. doi: 10.1177/2158244015579940

7. Squires P, Grimshaw R, Solomon E. (2008). *English 'Gun crime': A Review of Evidence and Policy*. Whose Justice? (Centre for Crime and Justice Studies). © Centre for Crime and Justice Studies (2008).

8. McMillon D, Simon CP, Morenoff J. Modeling the underlying dynamics of the spread of crime. *PLoS ONE*. (2014) 9:e88923. doi: 10.1371/journal.pone.0088923

9. Nyabadza F, Ogbogbo C, Mushanyu J. Modelling the role of correctional services on gangs: insights through a mathematical model. *R Soc Open Sci*. (2017) 4:170511. doi: 10.1098/rsos.170511

10. Pasour V, Tita G, Brantingham P, Bertozzi A, Short M, D'Orsogna M, et al. A statistical model of crime behavior. *Math Methods Appl Sci*. (2008) 107:1249–67. doi: 10.1142/S0218202508003029

11. Shukla JB, Goyal A, Agrawal K, Kushwah H, Shukla A. Role of technology in combating social crimes: a modeling study. *Eur J Appl Math*. (2013) 24:501–14. doi: 10.1017/S0956792513000065

12. Lacey A, Tsardakas M. A mathematical model of serious and minor criminal activity. *Eur J Appl Math*. (2016) 1:1–19. doi: 10.1017/S0956792516000139

13. Behrens D, Caulkins J, Tragler G, Haunschmied J, Feichtinger G. A dynamic model of drug initiation: implications for treatment and drug control. *Math Biosci*. (1999) 159:1–20. doi: 10.1016/S0025-5564(99)00016-4

14. Song B, Castillo-Garsow M, Rios-Soto K, Mejran M, Henso L, Castillo-Chávez C. Raves, clubs and ecstasy: the impact of peer pressure. *Math Biosci Eng*. (2006) 3:249. doi: 10.3934/mbe.2006.3.249

15. White E, Comiskey C. Heroin epidemics, treatment and ODE modelling. *Math Biosci*. (2007) 208:312–24. doi: 10.1016/j.mbs.2006.10.008

16. Gonzalez B, Huerta-Sánchez E, Ortiz-Nieves A, Vázquez-Alvarez T, Kribs-Zaleta C. Am I too fat? Bulimia as an epidemic. *J Math Psychol*. (2003) 47:515–26. doi: 10.1016/j.jmp.2003.08.002

17. Ohene Opoku NKD, Bader G, Fiatsonu E. Controlling crime with its associated cost during festive periods using mathematical techniques. *Chaos Solitons Fractals*. (2021) 145:110801. doi: 10.1016/j.chaos.2021.110801

18. Becker GS. Crime and punishment: an economic approach. *J Political Econ*. (1968) 76:169–217. doi: 10.1086/259394

19. Freeman S, Grogger J, Sonstelie J. The spatial concentration of crime. *J Urban Econ*. (1996) 40:216–31. doi: 10.1006/juec.1996.0030

20. Wang SJ, Batta R, Rump C. Stability of a crime level equilibrium. *Soc Econ Plann Sci*. (2005) 39:229–44. doi: 10.1016/j.seps.2004.01.001

21. Nagin DS. Deterrence in the twenty-first century. *Crime Justice*. (2013) 42:199–263. doi: 10.1086/670398

22. Nagin D. Deterrence: a review of the evidence by a criminologist for economists. *Ann Rev Econ*. (2012) 5:1310. doi: 10.1146/annurev-economics-072412-131310

23. Durlauf S, Nagin D. Overview of imprisonment and crime: can both be reduced?". *Criminol Public Policy*. (2011) 10:9–12. doi: 10.1111/j.1745-9133.2010.00681.x

24. Nagin DS, Cullen FT, Jonson CL. Imprisonment and reoffending. *Crime Justice*. (2009) 38:115–200. doi: 10.1086/599202

25. Kermack WO, McKendrick AG. A contribution to the mathematical theory of epidemics. *Proc R Soc Lond A*. (1927) 115:700–21. doi: 10.1098/rspa.1927.0118

26. van den Driessche P, Watmough J. *Further Notes on the Basic Reproduction Number*. Berlin; Heidelberg: Springer Berlin Heidelberg (2008).

27. Van den Driessche P, Watmough J. Reproduction numbers and sub-threshold endemic equilibria for compartmental models of disease transmission. *Math Biosci*. (2002) 180:29–48. doi: 10.1016/S0025-5564(02)00108-6

28. Allen LJ. *Introduction to Mathematical Biology*. Pearson; Prentice Hall (2007).

29. Lakshmikantham V, Leela S, Martynyuk AA. *Stability Analysis of Nonlinear Systems*. Springer (1989).

30. Chitnis N, Hyman JM, Cushing JM. Determining important parameters in the spread of malaria through the sensitivity analysis of a mathematical model. *Bull Math Biol.* (2008) 70:1272–96. doi: 10.1007/s11538-008-9299-0

31. Chicago IP. *020 US Census Updated* (2022). Available online at: https://worldpopulationreview.com/us-cities/chicago-il-population (accessed August 11, 2022).

32. Kekatos M. *Life Expectancy in Chicago Declined During 1st Year of COVID Pandemic, Especially for People of Color* (2022). Available online at: https://abcnews.go.com/Health/life-expectancy-chicago-declined-1st-year-covid-pandemic/story?id=84314520 (accessed August 11, 2022).

33. Initiative PP. *Illinois Incarceration Rate* (2022). Available online at: https://www.prisonpolicy.org/profiles/IL.html (accessed August 11, 2022).

34. Chicago L. *A Plan to Help Returning Citizens Succeed in Chicago* (2022). Available online at: http://www.lightfootforchicago.com/wp-content/uploads/2019/02/LL_ReturningCitizens_policy.pdf (accessed August 11, 2022).

35. Zitko PA. *The Efficacy of Correctional Education* (2022). Available online at: http://www.zitko.net/efficacy-of-prison-education (accessed August 11, 2022).

36. Harlow CW. *Education and Correctional Populations* (2022). Available online at: http://bjs.ojp.gov/content/pub/pdf/ecp.pdf (accessed August 11, 2022).

37. Illinois State U. *Prison Population Data Sets-Report* (2022). Available online at: https://www2.illinois.gov/idoc/reportsandstatistics/Pages/Prison-Population-Data-Sets.aspx

38. Berenji B, Chou T, D'Orsogna MR. Recidivism and rehabilitation of criminal offenders: a carrot and stick evolutionary game. *PLoS ONE.* (2014) 9:e85531. doi: 10.1371/journal.pone.0085531

39. Liedka RV, Piehl AM, Useem B. The crime-control effect of incarceration: does scale matter? *Criminol Public Policy*. (2006) 5:245–76. doi: 10.1111/j.1745-9133.2006.00376.x

40. Rose EK, Shem-Tov Y. *Does Incarceration Increase Crime*? Available at SSRN 3205613 (2018).

41. Education and Crime (2022). Available online at: https://criminal-justice.iresearchnet.com/crime/education-and-crime/4/

42. Oleson JC. *Criminal Genius: A Portrait of High-IQ Offenders*. Berkeley, CA: University of California Press (2016).

43. Gumel AB, Iboi EA, Ngonghala CN, Elbasha EH. A primer on using mathematics to understand COVID-19 dynamics: modeling, analysis and simulations. *Infect Dis Model.* (2021) 6:148–68. doi: 10.1016/j.idm.2020.11.005

44. Marino S, Hogue IB, Ray CJ, Kirschner DE. A methodology for performing global uncertainty and sensitivity analysis in systems biology. *J Theor Biol.* (2008) 254:178–96. doi: 10.1016/j.jtbi.2008.04.011

45. McLeod RG, Brewster JF, Gumel AB, Slonowsky DA. Sensitivity and uncertainty analyses for a SARS model with time-varying inputs and outputs. *Math Biosci Eng.* (2006) 3:527. doi: 10.3934/mbe.2006.3.527

Frontiers in
Applied Mathematics and Statistics

Investigates both applied and applicable mathematics and statistical techniques

Explores how the application of mathematics and statistics can drive scientific developments across data science, engineering, finance, physics, biology, ecology, business, medicine, and beyond

---

Discover the latest Research Topics

See more →

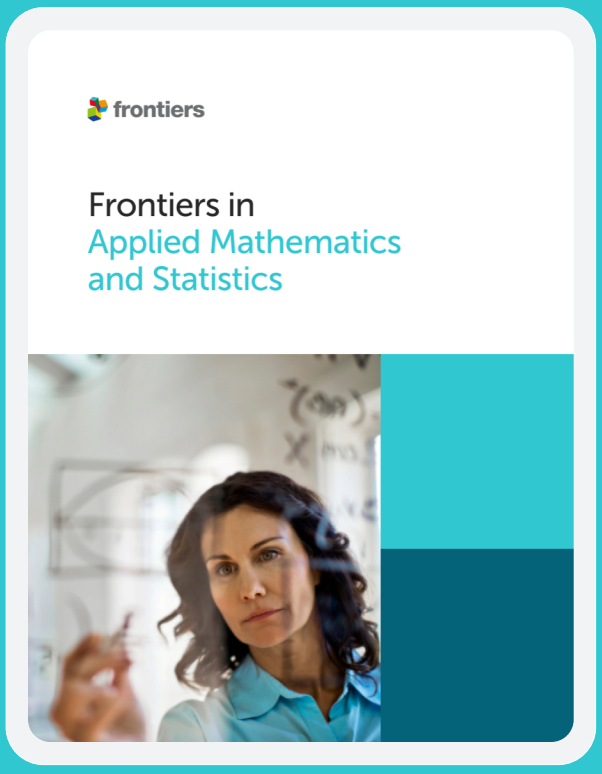

Frontiers

Avenue du Tribunal-Fédéral 34
1005 Lausanne, Switzerland
frontiersin.org

Contact us

+41 (0)21 510 17 00
frontiersin.org/about/contact